



Copyright

By

Andrea Lynn Kotys

2003

**Durability Examination of Bonded Tendons in Concrete Beams  
Under an Aggressive Corrosive Environment**

**by**

**Andrea Lynn Kotys, B.S.C.E**

**Thesis**

Presented to the Faculty of the Graduate School of  
The University of Texas at Austin  
in Partial Fulfillment  
of the Requirements  
for the Degree of

**Master of Science in Engineering**

**The University of Texas at Austin**

**May 2003**

**Durability Examination of Bonded Tendons in Concrete Beams**  
**Under an Aggressive Corrosive Environment**

**Approved by  
Supervising Committee:**

---

**John E. Breen, Co-Supervisor**

---

**Michael E. Kreger, Co-Supervisor**

*To my parents,  
For your unconditional love, support and encouragement*

## **Acknowledgements**

I would like to thank the Texas Department of Transportation for the financial support of this project.

My deepest gratitude goes to my advisor, Dr. John Breen, who has made this an unforgettable experience. The continuous guidance, support and encouragement I received from Dr. Breen are invaluable. He has shown and taught me things, both in the field of engineering and in the philosophy of life that I will carry with me always. I can only hope to make such an impact on someone's life as he has on mine.

I would also like to thank the staff at the Ferguson Lab for all of their help: Blake, Mike, Dennis, Hortensia, Regina and Mary Jo. I would not have been able to accomplish this without each individual's specialized knowledge and assistance.

A sincere thanks goes to the other graduate students (past and present) that worked on this project. Without Andrea Schokker and Jeff West's thorough literature review and strategic program design, this project would not have been such a huge success. I never would have understood the depth of this project without Ruben's guidance and help. We were faced with many obstacles throughout the project, yet somehow we were able to overcome them all.

I cannot thank the undergraduate students who worked on this project enough. Juan was so helpful in helping me get acquainted with the project when I began and always showed so much dedication. To Art and Chris, who were

present during the most difficult and stressful times. They were such hard workers and always kept a smile on my face. Without them, I don't know how I would have accomplished most of the physical tasks required for the project and remained sane during the times that it seemed the obstacles encountered throughout the project would never end.

I am forever indebted to my parents, who have always pushed me to achieve as much as I could and supported me every step of the way. Without their encouragement, I would not have had the confidence that I was capable of this achievement. I want to thank my sisters, Valerie and Melanie, who were also always there with support, love and encouragement.

I also want to send my love and thanks to Carter, who constantly reminds me of the value of my accomplishments. Without his support and amazing ability to listen, I would not have made it through this.

April 27, 2003

## TABLE OF CONTENTS

<b>LIST OF TABLES</b>	<b>xii</b>
<b>LIST OF FIGURES</b>	<b>xiv</b>
<b>CHAPTER 1: INTRODUCTION</b>	<b>1</b>
1.1 Background.....	1
1.2 Post-Tensioning.....	3
1.3 Mixed Reinforcement.....	4
1.4 Problem Statement.....	5
1.5 Research Project.....	6
1.5.1 Objectives.....	8
1.5.2 Scope.....	8
1.6 Thesis.....	9
1.6.1 Objectives.....	9
1.6.2 Scope.....	10
<b>CHAPTER 2: BEAM LONG TERM EXPOSURE CORROSION SPECIMENS</b>	<b>11</b>
2.1 Specimen Test Concept.....	11
2.2 Specimen Design.....	12
2.2.1 Beam Test Specimens.....	12
2.2.2 Reaction Beams.....	15
2.3 Variable Selection.....	16
2.3.1 Control Variables.....	16
2.3.2 Phase I Variables.....	17
2.3.2.1 Level of Prestress, Loading and Crack Width.....	17
2.3.2.2 Duct Splice Type and Condition.....	19
2.3.2.3 Grout Type.....	21
2.3.3 Phase II Variables.....	21
2.3.3.1 Level of Prestress, Loading and Crack Width.....	22
2.3.3.2 Concrete Type.....	22
2.3.3.3 Duct Type.....	23
2.3.3.4 Duct Splice Type and Condition.....	23
2.3.3.5 Grout Type.....	24
2.3.3.6 Grouting Procedure.....	25
2.3.3.7 Strand Type.....	25
2.3.3.8 End Anchorage Protection.....	25



2.4	Materials .....	26
2.5	Fabrication .....	27
2.5.1	Beam Fabrication .....	27
2.5.2	Post-Tensioning .....	29
2.5.3	Grouting .....	30
2.5.4	Anchorage Protection .....	32
2.6	Beam Specimen Loading .....	33
2.7	Beam Specimen Notation .....	34

**CHAPTER 3: EXPERIMENTAL PROGRAM 37**

3.1	Experimental Set-Up .....	37
3.1.1	Beam Specimen Setup .....	37
3.1.2	Block Specimen Setup .....	40
3.1.3	Beam Dripper System Setup .....	41
3.2	Measurements Taken During Exposure Testing .....	41
3.2.1	Visual Inspection .....	42
3.2.2	Crack Width Measurements .....	42
3.2.2.1	Theory .....	42
3.2.2.2	Procedure .....	43
3.2.2.3	Application to Experiment .....	43
3.2.3	Half-Cell Readings .....	44
3.2.3.1	Theory .....	44
3.2.3.2	Procedure .....	46
3.2.3.3	Application to Experiment .....	47
3.2.4	Corrosion Rate Readings .....	49
3.2.4.1	Theory .....	49
3.2.4.2	Procedure .....	50
3.2.4.3	Application to Experiment .....	52
3.2.5	Chloride Penetration Measurements .....	56
3.2.5.1	Theory .....	56
3.2.5.2	Ponding Block Procedure .....	57
3.2.5.3	Beam Specimen Procedure .....	57
3.2.6	Limited Autopsy .....	60

**CHAPTER 4: LONG TERM EXPOSURE TEST RESULTS AND ANALYSIS 62**

4.1	Crack Width Measurements .....	62
4.1.1	Initial Measurements .....	62
4.1.2	Final Measurements .....	66

4.2	Half-Cell Readings .....	71
4.2.1	Phase I Beams .....	74
4.2.2	Phase II Beams .....	83
4.3	Corrosion Rate Readings .....	92
4.3.1	Phase I Beams .....	93
4.3.1.1	Differences Between 3LP and PR Monitor Corrosion Rates .....	96
4.3.2	Phase II Beams .....	98
4.4	Chloride Penetration Measurements .....	99
4.4.1	Phase I Block Specimens .....	100
4.4.2	Phase II Block Specimens .....	102
4.4.3	Phase I Autopsy Beam Specimens .....	104
4.4.4	Phase II Autopsy Beam Specimens .....	110

## **CHAPTER 5: FORENSIC EXAMINATION 115**

5.1	Forensic Examination .....	115
5.2	Selection of Autopsy Beams .....	116
5.3	Beam Autopsy Procedure .....	120
5.3.1	Visual Inspection .....	120
5.3.2	Crack Width Measurements .....	120
5.3.3	Concrete Samples for Chloride Analysis .....	120
5.3.4	Saw Cuts .....	120
5.3.5	Exposure and Removal of Post-Tensioning System .....	122
5.3.6	Exposure and Removal Mild Steel .....	123
5.3.7	Exposure, Examination and Removal of Grout .....	124
5.3.8	Examination of Elements .....	125
5.4	Corrosion Rating System .....	125
5.4.1	Mild Steel Reinforcement .....	126
5.4.2	Galvanized Steel Duct/Splice .....	129
5.4.3	Prestressing Strand .....	131
5.4.4	Duct Splice .....	133
5.5	Specimen Examination and Data – Phase I Specimens .....	134
5.5.1	Beams Specimen 1.1 – Non-PS, Unloaded .....	134
5.5.2	Beams Specimen 1.3 – Non-PS, Service Load .....	138
5.5.3	Beams Specimen 2.3 – 2/3 PS, Service Load .....	140
5.5.4	Beams Specimen 2.11 – 2/3 PS, Service Load, Fly Ash Grout .....	145
5.5.5	Beams Specimen 3.1 – 100%U PS, Unloaded .....	150
5.5.6	Beams Specimen 3.2 – 100%U PS, Service Load .....	155
5.5.7	Beams Specimen 3.3 – 100%U PS, Overload .....	160
5.5.8	Beams Specimen 4.2 – 100%S PS, Service Load .....	165

5.6	Specimen Examination and Data – Phase II Specimens .....	170
5.6.1	Beams Specimen 1.5 – Non-PS, Fly Ash Concrete.....	170
5.6.2	Beams Specimen 1.6 – Non-PS, High Performance Concrete.....	173
5.6.3	Beams Specimen 2.5 – 2/3 PS, Fly Ash Concrete.....	176
5.6.4	Beams Specimen 2.6 – 2/3 PS, High Performance Concrete .	181
5.6.5	Beams Specimen 3.6 – 100%U PS, Fly Ash Concrete.....	186
5.6.6	Beams Specimen 3.7 – 100%U PS, High Performance Concrete.....	191
5.7	Corrosion Rating Summary .....	196
5.7.1	Stirrup Ratings.....	197
5.7.2	Longitudinal Bar Ratings.....	199
5.7.3	Galvanized Steel Duct Ratings .....	201
5.7.4	Prestressing Strand Ratings .....	203
 <b>CHAPTER 6: ANALYSIS OF EXPOSURE TEST MEASUREMENTS AND FORENSIC EXAMINATION FINDINGS</b>		 <b>205</b>
6.1	Forensic Examination vs. Exposure Testing Measurements .....	205
6.1.1	Forensic Examination vs. Half-Cell Potential Readings .....	205
6.1.2	Forensic Examination vs. Corrosion Rate Readings .....	209
6.1.3	Forensic Examination vs. Chloride Penetration Measurements.....	212
 <b>CHAPTER 7: SUMMARY OF RESULTS, CONCLUSIONS AND RECOMMENDATIONS</b>		 <b>215</b>
7.1	Summary of Results.....	215
7.2	Conclusions .....	218
7.2.1	Variable Performance .....	218
7.2.2	Exposure Test Measurements.....	220
7.3	Future Testing Recommendations .....	221
 <b>APPENDIX A: BEAM SPECIMENS AND CORRESPONDING VARIABLES</b>		 <b>222</b>
 <b>APPENDIX B: BEAM SPECIMEN TIMELINE</b>		 <b>225</b>
 <b>APPENDIX C: FINAL SURFACE CRACK PATTERNS AND MEASUREMENTS OF AUTOPSY BEAMS</b>		 <b>227</b>

<b>APPENDIX D: ADDITIONAL EXPOSURE TEST BEAM DATA</b>	<b>239</b>
D.1 Half-Cell Potential Readings .....	239
D.2 Half-Cell Potential Reading Contour Maps.....	247
D.3 Half-Cell Potential Reading Outliers.....	248
D.4 Corrosion Rate Readings .....	249
D.5 Block Chloride Penetration .....	252
D.6 Beam Chloride Penetration.....	255
<b>APPENDIX E: BEAM SPECIMEN RATINGS</b>	<b>262</b>
<b>REFERENCES</b>	<b>264</b>
<b>VITA</b>	<b>267</b>

## LIST OF TABLES

Table 1.1: Project Tasks and Contributions of Graduate Students.....	6
Table 2.1: Summary of Section Details.....	14
Table 2.2: Details of Control Variables.....	17
Table 2.3: Planned Crack Widths, Prestress Amounts and Loading.....	19
Table 2.4: Initial Prestress, Prestress Losses and Jacking Forces .....	30
Table 2.5: Specimen Designation.....	36
Table 3.1: Common Reference Electrode Potentials versus SHE.....	45
Table 3.2: Interpretation of Half-Cell Potentials for Uncoated Reinforcing Steel.....	46
Table 3.3: PR Monitor Corrosion Severity Based on Current Density .....	54
Table 3.4: Procedure for Chloride Penetration Concrete Samples.....	59
Table 4.1: Half-Cell Potential Map Designations.....	73
Table 4.2: Phase I Autopsy Beam Corrosion Current Density Measurements....	96
Table 4.3: Phase II Autopsy Beam Corrosion Current Density Measurements ...	99
Table 4.4: Phase I Ponded Block Chloride Penetration Measurements .....	102
Table 4.5: Phase II Ponded Block Chloride Penetration Measurements.....	104
Table 4.6: Phase I Autopsy Beam Chloride Penetration Measurements.....	109
Table 4.7: Phase II Autopsy Beam Chloride Penetration Measurements.....	114
Table 5.1: Phase I Beams Selected for Forensic Examination.....	118
Table 5.2: Phase II Beams Selected for Forensic Examination.....	119
Table 5.3: Evaluation and Rating System for Corrosion Found on Mild Steel Bars.....	128
Table 5.4: Evaluation and Rating System for Corrosion Found on Galvanized Steel Duct/Duct Splice .....	130
Table 5.5: Evaluation and Rating System for Corrosion Found on Prestressing Strand.....	132
Table 5.6: Corrosion Rating Scenarios for Analysis .....	197
Table 7.1: Summary of Exposure Test Results .....	216

Table 7.2: Summary of Forensic Examination Corrosion Rating Results.....	217
Table D1: Half-Cell Outliers – Phase I Beams.....	248
Table D2: Half-Cell Outliers – Phase II Beams .....	248
Table E1: Phase I Beam Ratings .....	263
Table E2: Phase II Beam Ratings .....	263

## LIST OF FIGURES

Figure 1.1: Levels of Corrosion Protection for Bonded Post-Tensioning Tendons .....	2
Figure 1.2: Basic Principles of Post-Tensioning .....	3
Figure 2.1: Specimen Setup .....	13
Figure 2.2: Beam Exposure Specimen .....	13
Figure 2.3: Specimen Cross-Section Details .....	15
Figure 2.4: Phase I Beam s- Duct Splice Configuration.....	20
Figure 2.5: Duct Splices .....	21
Figure 2.6: Phase II Beams – Duct Splice Configuration.....	24
Figure 2.7: VSLAB+™ System.....	26
Figure 2.8: Beam Fabrication .....	28
Figure 2.9: Post-Tensioning Setup .....	29
Figure 2.10: Grouting Setup .....	31
Figure 2.11: Loading Apparatus .....	33
Figure 3.1: Beam Specimen Test Setup.....	38
Figure 3.2: Beam Specimen Outside of Ferguson Laboratory .....	38
Figure 3.3: Beam Specimen Arrangement .....	39
Figure 3.4: Ponding Blocks for Beam Specimens .....	40
Figure 3.5: Beam End Dripper System.....	41
Figure 3.6: Crack Width Measurement Setup .....	43
Figure 3.7: Wire Connections to Post-Tensioning Tendons.....	47
Figure 3.8: Half-Cell Reading Locations .....	48
Figure 3.9: 2/3 PS Specimen Half-Cell Potential Reading Grid .....	48
Figure 3.10: Non-PS Specimen Half-Cell Potential Reading Grid .....	48
Figure 3.11: Applied Current Linear Polarization Curve .....	49
Figure 3.12: Polarization Resistance Apparatus .....	52
Figure 3.13: 3LP Equipment and Setup.....	56

Figure 3.14: Non-PS Beam Concrete Sample Locations .....	59
Figure 3.15: 100%U PS Beam Concrete Sample Locations .....	60
Figure 2.12: Beam Specimen Arrangement .....	34
Figure 2.13: Besm Specimens Outside of Ferguson Laboratory.....	35
Figure 2.14: Ponding Block for Beam Specimens .....	36
Figure 2.15: Loading Apparatus.....	37
Figure 4.1: Typical Crack Patterns for Each Section Type .....	63
Figure 4.2: Measured Maximum Crack Widths .....	65
Figure 4.3: Non-PS Section – Crack Patterns and Measurements .....	67
Figure 4.4: 2/3 PS Section – Crack Patterns and Measurements.....	68
Figure 4.5: 100%U PS Section – Crack Patterns and Measurements .....	69
Figure 4.6: Crack Widths – Phase I Beams .....	70
Figure 4.7: Crack Widths – Phase I Beams .....	71
Figure 4.8: Half-Cell Potential Readings (Phase I Autopsy Beams).....	75
Figure 4.9: Half-Cell Potential Readings (Phase I Autopsy Beams – Non-PS)...	76
Figure 4.10: Half-Cell Potential Readings (Phase I Autopsy Beams – 2/3 PS) ....	77
Figure 4.11: Half-Cell Potential Readings (Phase I Autopsy Beams – 100%U PS) .....	78
Figure 4.12: Half-Cell Potential Readings (Phase I Autopsy Beams – Unloaded) .....	79
Figure 4.13: Half-Cell Potential Readings (Phase I Autopsy Beams – Service Load).....	80
Figure 4.14: Highest Average Half-Cell Potential Reading at 1594 Days (Phase I Autopsy Beams) .....	81
Figure 4.15: Half-Cell Potential Contour Plots at 1594 Days (All Phase I Beams).....	82
Figure 4.16: Time to Initiation of Corrosion (Phase I Beams).....	83
Figure 4.17: Half-Cell Potential Readings (Phase II Autopsy Beams) .....	84
Figure 4.18: Half-Cell Potential Readings (Phase II Autopsy Beams – Non- PS) .....	85
Figure 4.19: Half-Cell Potential Readings (Phase II Autopsy Beams – 2/3 PS)...	86



Figure 4.20: Half-Cell Potential Readings (Phase II Autopsy Beams – 100%U PS) .....	87
Figure 4.21: Half-Cell Potential Readings (Phase II Autopsy Beams – Fly Ash Concrete) .....	88
Figure 4.22: Half-Cell Potential Readings (Phase I Autopsy Beams – High Performance Concrete) .....	89
Figure 4.23: Highest Average Half-Cell Potential Reading at 1235 Days (Phase II Autopsy Beams) .....	90
Figure 4.24: Half-Cell Potential Contour Plots at 1235 Days (All Phase II Beams) .....	91
Figure 4.25: Time to Initiation of Corrosion (Phase II Beams).....	92
Figure 4.26: Maximum Corrosion Rate Readings Using PR Monitor (Phase I Autopsy Beams) .....	94
Figure 4.27: Maximum Corrosion Rate Readings Using 3LP (Phase I Autopsy Beams) .....	95
Figure 4.28: Comparison of Corrosion Rate Measurement Equipment .....	97
Figure 4.29: Corrosion Rate Readings Using 3LP (Phase II Autopsy Beams) .....	98
Figure 4.30: Chloride Penetration (Phase I Ponded Block Specimens) .....	101
Figure 4.31: Chloride Penetration (Phase II Ponded Block Specimens).....	103
Figure 4.32: Beam and Block Chloride Penetration at 54 Months (Phase I – Ponded Region on Beams) .....	105
Figure 4.33: Beam and Block Chloride Penetration at 54 Months (Phase I – Unponded Region on Beams).....	107
Figure 4.34: Chloride Content at Bar and Top-of-Duct Level (Phase I Beams) .	108
Figure 4.35: Beams and Block Chloride Penetration at 42 Months (Phase II Autopsy Beams – Ponded Region and Beams) .....	111
Figure 4.36: Beams and Block Chloride Penetration at 42 Months (Phase II Autopsy Beams – Unponded Region and Beams).....	112
Figure 4.37: Chloride Content at Bar and Top-of-Duct Level (Phase II Beams)	113
Figure 5.1: Beam Specimens Selected for Forensic Examination.....	117
Figure 5.2: Section Removed from Beams for Analysis .....	121
Figure 5.3: Concrete Saw Used in Autopsy .....	122
Figure 5.4: Concrete Removal and Reinforcement Exposure .....	123

Figure 5.5: Mild Steel Reinforcement Cage.....	124
Figure 5.6: Intervals for Corrosion Ratings on Mild Steel.....	126
Figure 5.7: Intervals for Corrosion Ratings on Galvanized Steel Duct/Splice...	130
Figure 5.8: Specimen 1.1 – Condition Prior to Autopsy .....	135
Figure 5.9: Specimen 1.1 – Mild Steel Bar and Stirrup .....	136
Figure 5.10: Specimen 1.1 – Crack Pattern and Specimen Corrosion Rating Graphs.....	137
Figure 5.11: Specimen 1.3 – Condition Prior to Autopsy .....	138
Figure 5.12: Specimen 1.3 – Mild Steel Bar and Stirrup .....	139
Figure 5.13: Specimen 1.3 – Crack Pattern and Specimen Corrosion Rating Graphs.....	139
Figure 5.14: Specimen 2.3 – Condition Prior to Autopsy .....	140
Figure 5.15: Specimen 2.3 – Duct Splices.....	142
Figure 5.16: Specimen 2.3 – Reinforcing Elements.....	143
Figure 5.17: Specimen 2.3 – Crack Pattern and Specimen Corrosion Rating Graphs.....	144
Figure 5.18: Specimen 2.11 – Condition Prior to Autopsy .....	145
Figure 5.19: Specimen 2.11 – Duct Splices.....	147
Figure 5.20: Specimen 2.11 – Reinforcing Elements.....	148
Figure 5.21: Specimen 2.11 – Crack Pattern and Specimen Corrosion Rating Graphs.....	149
Figure 5.22: Specimen 3.1 – Condition Prior to Autopsy .....	150
Figure 5.23: Specimen 3.1 – Duct Splices.....	152
Figure 5.24: Specimen 3.1 – Reinforcing Elements.....	153
Figure 5.25: Specimen 3.1 – Crack Pattern and Specimen Corrosion Rating Graphs.....	154
Figure 5.26: Specimen 3.2 – Condition Prior to Autopsy .....	155
Figure 5.27: Specimen 3.2 – Grouted Duct .....	157
Figure 5.28: Specimen 3.2 – Duct Splices.....	157
Figure 5.29: Specimen 3.2 – Reinforcing Elements.....	158

Figure 5.30: Specimen 3.2 – Crack Pattern and Specimen Corrosion Rating Graphs.....	159
Figure 5.31: Specimen 3.3 – Condition Prior to Autopsy .....	160
Figure 5.32: Specimen 3.3 – North Duct Splice.....	162
Figure 5.33: Specimen 3.3 – Reinforcing Elements.....	163
Figure 5.34: Specimen 3.3 – Crack Pattern and Specimen Corrosion Rating Graphs.....	164
Figure 5.35: Specimen 4.2 – Condition Prior to Autopsy .....	165
Figure 5.36: Specimen 4.2 – Duct Splices.....	167
Figure 5.37: Specimen 4.2 – Reinforcing Elements.....	168
Figure 5.38: Specimen 4.2 – Crack Pattern and Specimen Corrosion Rating Graphs.....	169
Figure 5.39: Specimen 1.5 – Condition Prior to Autopsy .....	170
Figure 5.40: Specimen 1.5 – Mild Steel Bar and Stirrup .....	171
Figure 5.41: Specimen 1.5 – Crack Pattern and Specimen Corrosion Rating Graphs.....	172
Figure 5.42: Specimen 1.6 – Condition Prior to Autopsy .....	173
Figure 5.43: Specimen 1.6 – Mild Steel Bar and Stirrup .....	174
Figure 5.44: Specimen 1.6 – Crack Pattern and Specimen Corrosion Rating Graphs.....	175
Figure 5.45: Specimen 2.5 – Condition Prior to Autopsy .....	176
Figure 5.46: Specimen 2.5 – Duct Splices.....	178
Figure 5.47: Specimen 2.5 – Reinforcing Elements.....	179
Figure 5.48: Specimen 2.5 – Crack Pattern and Specimen Corrosion Rating Graphs.....	180
Figure 5.49: Specimen 2.6 – Condition Prior to Autopsy .....	181
Figure 5.50: Specimen 2.6 – Duct Splices.....	183
Figure 5.51: Specimen 2.6 – Reinforcing Elements.....	184
Figure 5.52: Specimen 2.6– Crack Pattern and Specimen Corrosion Rating Graphs.....	185
Figure 5.53: Specimen 3.6 – Condition Prior to Autopsy .....	186

Figure 5.54: Specimen 3.6 – Duct Splices.....	188
Figure 5.55: Specimen 3.6 – Reinforcing Elements.....	189
Figure 5.56: Specimen 3.6 – Crack Pattern and Specimen Corrosion Rating Graphs.....	190
Figure 5.57: Specimen 3.7 – Condition Prior to Autopsy .....	191
Figure 5.58: Specimen 3.7 – Duct Splices.....	193
Figure 5.59: Specimen 3.7 – Reinforcing Elements.....	194
Figure 5.60: Specimen 3.7 – Crack Pattern and Specimen Corrosion Rating Graphs.....	195
Figure 5.61: Generalized Stirrup Corrosion Ratings.....	198
Figure 5.62: Localized Stirrup Corrosion Ratings.....	198
Figure 5.63 Generalized Bar Corrosion Ratings .....	200
Figure 5.64: Localized Bar Corrosion Ratings.....	200
Figure 5.65: Generalized Duct Corrosion Ratings .....	202
Figure 5.66: Localized Duct Corrosion Ratings.....	202
Figure 5.67: Generalized Strand Corrosion Ratings.....	204
Figure 5.68: Localized Strand Corrosion Ratings .....	204
Figure 6.1: Corrosion Ratings vs. Half-Cell Potential Readings – Phase I Beams .....	207
Figure 6.2: Corrosion Ratings vs. Half-Cell Potential Reading – Phase II Beams .....	208
Figure 6.3: Corrosion Ratings vs. Corrosion Rate Readings – Phase I Beams ..	210
Figure 6.4: Corrosion Ratings vs. Corrosion Rate Readings – Phase II Beams.	211
Figure 6.5: Corrosion Ratings vs. Chloride Content Measurements – Phase I Beams .....	213
Figure 6.6: Corrosion Ratings vs. Chloride Content Measurements – Phase II Beams .....	214
Figure A1: Phase I Beam Specimens and Variables .....	223
Figure A2: Phase II Beam Specimens and Variables.....	224
Figure B1: Beam Specimen Timeline .....	226
Figure C1: Final Crack Pattern and Measurements – Beam 1.3 .....	227

Figure C2: Final Crack Pattern and Measurements – Beam 2.3 .....	228
Figure C3: Final Crack Pattern and Measurements – Beam 2.11 .....	229
Figure C4: Final Crack Pattern and Measurements – Beam 3.2 .....	230
Figure C5: Final Crack Pattern and Measurements – Beam 3.3 .....	231
Figure C6: Final Crack Pattern and Measurements – Beam 4.2 .....	232
Figure C7: Final Crack Pattern and Measurements – Beam 1.5 .....	233
Figure C8: Final Crack Pattern and Measurements – Beam 1.6 .....	234
Figure C9: Final Crack Pattern and Measurements – Beam 2.5 .....	235
Figure C10: Final Crack Pattern and Measurements – Beam 2.6 .....	236
Figure C11: Final Crack Pattern and Measurements – Beam 3.6 .....	237
Figure C12: Final Crack Pattern and Measurements – Beam 3.7 .....	238
Figure D1: Half-Cell Potential Readings (All Phase I Beams) .....	239
Figure D2: Half-Cell Potential Readings (All Phase I Beams – Non-PS).....	240
Figure D3: Half-Cell Potential Readings (All Phase I Beams – 2/3 PS).....	240
Figure D4: Half-Cell Potential Readings (All Phase I Beams – 100%U PS).....	241
Figure D5: Half-Cell Potential Readings (All Phase I Beams – 100%S PS) .....	241
Figure D6: Half-Cell Potential Readings (All Phase I Beams - Unloaded) .....	242
Figure D7: Half-Cell Potential Readings (All Phase I Beams – Service Load) .....	242
Figure D8: Half-Cell Potential Readings (All Phase I Beams - Overload) .....	243
Figure D9: Half-Cell Potential Readings (All Phase II Beams).....	243
Figure D10: Half-Cell Potential Readings (All Phase II Beams – 2/3 PS) .....	244
Figure D11: Half-Cell Potential Readings (All Phase II Beams – Fly Ash Concrete) .....	244
Figure D12: Half-Cell Potential Readings (All Phase II Beams – High Performance Concrete) .....	245
Figure D13: Half-Cell Potential Readings (All Phase II Beams – Varying Strand Type) .....	245
Figure D14: Half-Cell Potential Readings (All Phase II Beams – Varying Grout Type) .....	246
Figure D15: Half-Cell Potential Readings (All Phase II Beams – Varying Duct Type) .....	246

Figure D16: Contour Plots of Half-Cell Potential Readings at 498 Days .....	247
Figure D17: Phase I Beams – Measured Corrosion Rates (Seven Month Exposure Duration – PR Monitor Equipment) .....	249
Figure D18: Phase I Beams – Measured Corrosion Rates (Twelve Month Exposure Duration – 3LP Equipment) .....	249
Figure D19: Phase I Beams – Measured Corrosion Rates (Fifteen Month Exposure Duration – PR Monitor Equipment) .....	250
Figure D20: Phase I Beams – Measured Corrosion Rates (Fifteen Month Exposure Duration – 3LP Equipment) .....	250
Figure D21: Phase I Beams – Measured Corrosion Rates (47 Month Exposure Duration – 3LP Equipment) .....	251
Figure D22: Phase II Beams – Measured Corrosion Rates (35 Month Exposure Duration – 3LP Equipment) .....	251
Figure D23: Block Chloride Penetration at 7 Months (Phase I Poned Block Specimens).....	252
Figure D24: Block Chloride Penetration at 14 Months (Phase I Poned Block Specimens).....	252
Figure D25: Block Chloride Penetration at 41 Months (Phase I Poned Block Specimens).....	253
Figure D26: Block Chloride Penetration at 54 Months (Phase I Poned Block Specimens).....	253
Figure D27: Block Chloride Penetration at 29 Months (Phase II Poned Block Specimens) .....	254
Figure D28: Block Chloride Penetration at 42 Months (Phase II Poned Block Specimens) .....	254
Figure D29: Chloride Penetration at 54 Months – Beam 1.1 .....	255
Figure D30: Chloride Penetration at 54 Months – Beam 1.3 .....	255
Figure D31: Chloride Penetration at 54 Months – Beam 2.3 .....	256
Figure D32: Chloride Penetration at 54 Months – Beam 2.11 .....	256
Figure D33: Chloride Penetration at 54 Months – Beam 3.1 .....	257
Figure D34: Chloride Penetration at 54 Months – Beam 3.2 .....	257
Figure D35: Chloride Penetration at 54 Months – Beam 3.3 .....	258
Figure D36: Chloride Penetration at 54 Months – Beam 4.2 .....	258

Figure D37: Chloride Penetration at 42 Months – Beam 1.5 .....	259
Figure D38: Chloride Penetration at 42 Months – Beam 1.6 .....	259
Figure D39: Chloride Penetration at 42 Months – Beam 2.5 .....	260
Figure D40: Chloride Penetration at 42 Months – Beam 2.6 .....	260
Figure D41: Chloride Penetration at 42 Months – Beam 3.6 .....	261
Figure D42: Chloride Penetration at 42 Months – Beam 3.7 .....	261

# CHAPTER 1

## Introduction

### 1.1 BACKGROUND

Durability is defined as the ability of a structure to withstand various forms of attack from the environment.<sup>1</sup> Three of the most common concerns with respect to the durability of concrete bridge substructures include sulfate attack, freeze-thaw damage and alkali-aggregate reactions, all of which involve the attack of the concrete. The fourth major concern is the corrosion of the steel reinforcement. Much study and research has been devoted to the three previously mentioned concerns involving concrete attack, and solutions for new structures have been found. This is not true of the attack of the steel reinforcement. Currently, research in this area for post-tensioned bridges is limited due to the long-term nature of durability studies.

Post-tensioning is becoming more widely used in bridge substructures due to structural and economical benefits. Some of the possible benefits of post-tensioning include:

- Control of Deflections
- Increased Stiffness
- Improved Crack Control
- Reduced Reinforcement Congestion
- Continuity of Reinforcement

Although usually considered for its structural and construction benefits, post-tensioning also improves the durability of the structure. It reduces the



number and size of cracks in the concrete, limiting the paths available for chloride ions to reach the reinforcement. Post-tensioning requires less reinforcement and the reinforcement is continuous, resulting in less congestion during construction, which allows the concrete to be placed and compacted more easily to reduce the number of voids. It can also be electrically separated from the other reinforcement. Finally, depending on the choice of the system, it can create more layers of corrosion protection for the tendons, as shown in Figure 1.1. A non post-tensioned concrete member only provides protection through a surface treatment, the concrete and any coating that may be applied to the reinforcing steel or prestressing strand. A post-tensioning system can introduce two additional layers of protection through the duct and the grout.

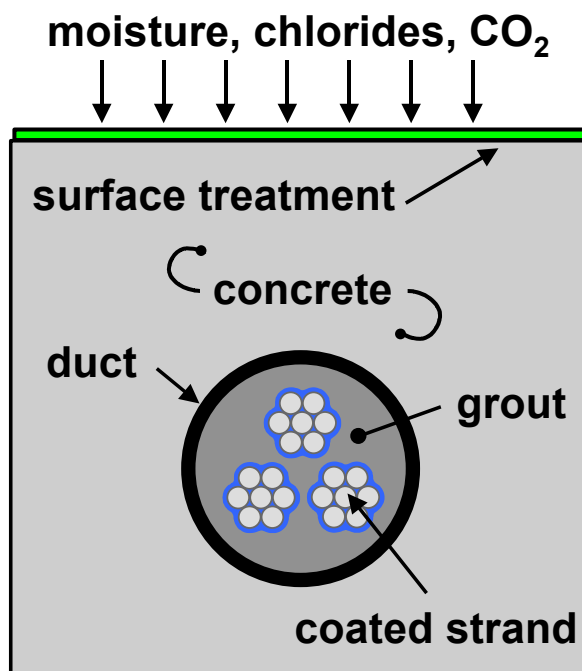


*Figure 1.1 - Levels of Corrosion Protection for Bonded Post-Tensioning Tendons*

## 1.2 POST-TENSIONING

Concrete is a material that has much more desirable behavior in compression than in tension; for this reason it is beneficial to start with a certain amount of precompression in the concrete to counteract tensile stresses introduced in the members during loading. This prestressing can be performed in two ways. One of these ways is to cast the fresh concrete around pretensioned high strength steel strands and then allow the concrete to harden before releasing the pretensioned strands. In this type of prestressing the strands are anchored by the bond formed with the concrete. It does not require an end-anchorage system. In the second form of prestressing the members are cast with a hollow duct that leaves space for steel tendons to be run through the member after curing. The steel tendon is then tensioned and secured with some form of end anchorage. During the tensioning process, the concrete is put into compression. This type of prestressing is known as post-tensioning. The basic principles are illustrated in Figure 1.2. The current research focuses on bonded post-tensioning, which includes injecting cement grout into the duct after stressing the steel. The grout develops the bond between the steel tendon and concrete under higher loading and contributes to the corrosion protection of the prestressing steel.<sup>2</sup>

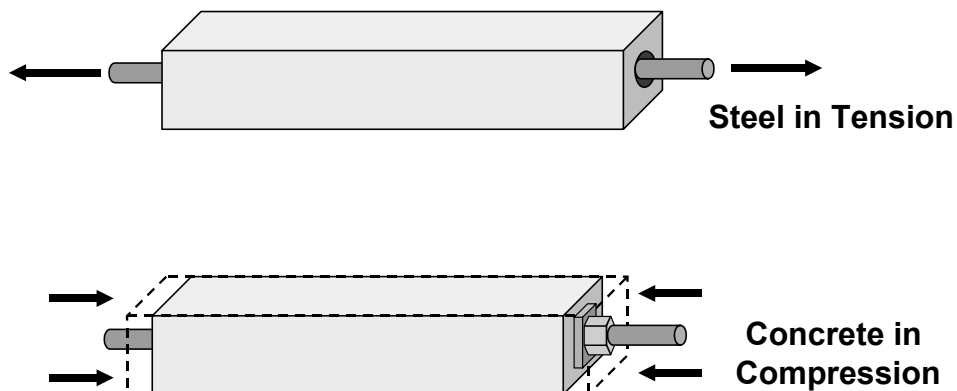


*Figure 1.2 – Basic Principles of Post-Tensioning*

### 1.3 MIXED REINFORCEMENT

The concept and implementation of mixed reinforcement (sometimes referred to as partial prestressing) is a fairly recent development. The concept uses a combination of non-prestressed mild steel reinforcement mixed with high strength prestressing steel to provide the required flexural strength of the member. A portion of the tensile reinforcement (the high strength steel) is prestressed while the remaining tensile reinforcement (the mild steel) is non-prestressed. The amount of mild steel reinforcement and the level of prestress in the high strength prestressing steel are varied from case to case.

In fully prestressed concrete elements, the prestressed tensile reinforcement is designed to keep service level concrete tensile stresses below the cracking limit thus eliminating cracking under service load levels. Though good for durability, this design requires high levels of prestressing and can provide an overly conservative design and problems due to excessive creep and camber. The use of mixed reinforcement offers many advantages over reinforced concrete and fully prestressed concrete:<sup>3,4</sup>

- Mixed reinforcing designs can be based on the strength limit state or the nominal capacity of the member, leading to more efficient designs than allowable stress methods.
- The amount of prestressed reinforcement can be altered to cater to each individual design situation. Examples include determining the necessary amount of prestress to:
  - Balance any desired load combination to zero deflections
  - Increase the cracking moment to a desired value
  - Control the number and width of cracks
- In comparison to fully prestressed concrete, the reduced level of prestress leads to fewer creep and excessive camber problems.

- In comparison to reinforced concrete, mixed reinforcement reduces the volume of steel alleviating reinforcement congestion, provides better detailing, and requires fewer splices.

#### **1.4 PROBLEM STATEMENT**

Currently there are no durability guidelines for post-tensioned concrete structures available for bridge engineers to follow. These guidelines are needed to inform designers of precautionary measures that should be incorporated in their design to improve durability, to provide ways to detect durability issues in existing structures and to insure that new durability problems are not introduced. A considerable amount of research has focused on the design of bridge decks to improve durability, but insufficient attention has been given to bridge substructures, which often see aggressive corrosive attack. Although the concept of post-tensioning is not new, its application in bridge substructures is relatively recent, therefore there is a need to study the materials and construction practices to improve the durability of post-tensioned bridge substructures.

The durability of structures using mixed reinforcement is a topic of concern due to the fact that they can develop cracking under service loads. There is a possibility that these cracks can affect the durability of the structure by providing pathways for chlorides to reach the reinforcement, thus accelerating the rate of corrosion of the steel. This question has not been adequately studied and therefore needs investigation. The belief that prestressing steel is more susceptible to corrosion, and the heightened consequences of its failure as opposed to mild reinforcement have also contributed to the desire for further investigation as to whether mixed reinforcement is ultimately beneficial when considering both the strength and durability of the structure.

## 1.5 RESEARCH PROJECT

The Texas Department of Transportation Project 0-1405 began approximately 10 years ago in August of 1993 under the supervision of Dr. John Breen and Dr. Michael Kreger, and will continue until August 31, 2003. Six graduate students have worked on this research project to date: Brad Koester, Chuck Larosche, Andrea Schokker, Jeff West, Ruben Salas and the author. The segmental joint macrocell specimens were developed and constructed by Rene Vignos<sup>5</sup> under TxDOT Project 0-1264 and transferred to Project 0-1405 in 1995 for long term testing. The contributions of each individual are summarized in Table 1.1.

*Table 1.1: Project Tasks and Contributions of Graduate Students*

<b>Project Tasks</b>	<b>Participants</b>
Literature Review	West, Koester, Larosche, Schokker
Identification of Substructure Post-Tensioning Applications and Systems	West, Koester
Identification of Protection System Variables	West, Koester
Survey of Existing Structures	Larosche
<b><u>Testing Program Design:</u></b>	
Long Term Beam Exposure Tests	West
Long Term Column Exposure Tests	Larosche, West
Segmental Macrocell Corrosion Tests	Vignos
Evaluation of Improved Grouts for Post-Tensioning	Koester, Schokker, West
<b><u>Fabrication of Test Specimens:</u></b>	
Long Term Beam Exposure Tests	West, Schokker
Long Term Column Exposure Tests	Larosche, West
Segmental Macrocell Corrosion Tests	Vignos
Evaluation of Improved Grouts for Post-Tensioning	Koester, Schokker

<b><u>Initial Exposure Testing:</u></b>	
Long Term Beam Exposure Tests	West, Schokker
Long Term Column Exposure Tests	West, Schokker
Segmental Macrocell Corrosion Tests	Vignos, West
Evaluation of Improved Grouts for Post-Tensioning	Koester, Schokker
<b><u>Limited Specimen Autopsies:</u></b>	
Long Term Beam Exposure Tests	Schokker
Long Term Column Exposure Tests	Schokker
Segmental Macrocell Corrosion Tests	West
Preliminary Design Guidelines	West, Schokker
<b><u>Continued Exposure Testing and Data Collection:</u></b>	
Long Term Beam Exposure Tests	Salas, Kotys
Long Term Column Exposure Tests	Salas, Kotys
Segmental Macrocell Corrosion Tests	Salas
<b><u>Final Autopsy and Analysis:</u></b>	
Long Term Beam Exposure Tests	Salas, Kotys
Long Term Column Exposure Tests	Salas, Kotys
Segmental Macrocell Corrosion Tests	Salas, Kotys
<b><u>Updated Design Guidelines:</u></b>	
Long Term Beam Exposure Tests	Salas
Long Term Column Exposure Tests	Salas
Segmental Macrocell Corrosion Tests	Salas
Continued Exposure Testing and Data Collection	Salas, Kotys

All tasks of project 0-1405 will not be completed this year, as monitoring, exposure testing and data collection will continue on the portion of the long-term beam specimens not chosen for final analysis. The remaining specimens will be

transferred to TxDOT Project 0-4562 and accelerated exposure testing will continue for several more years before their final autopsies and analyses.

### **1.5.1 Objectives**

The research objectives for the Texas Department of Transportation Project 0-1405 are as follows:<sup>1</sup>

1. To examine the use of post-tensioning in bridge substructures,
2. To identify durability concerns for bridge substructures,
3. To identify existing technology to ensure durability or improve durability,
4. To develop experimental testing programs to evaluate protection measures for improving the durability of post-tensioned bridge substructures, and
5. To develop durability design guidelines and recommendations for post-tensioned bridge substructures.

### **1.5.2 Scope**

The subject of durability is a very broad topic and was therefore narrowed down after an extensive literature review was conducted. Much detailed information on sulfate attack, freeze-thaw damage and alkali-aggregate reaction was found during the literature review and substantial recommendations for preventing such attacks exist. Thus these subjects were not covered in this project. However, absence of comprehensive information on corrosion of tendons established the need for the focus of this project to be on the corrosion of reinforcement in post-tensioned concrete. To achieve the ultimate objective of this project, which is to develop durability design guidelines for post-tensioned bridge substructures, the following components of the project were established:

- Extensive Literature Review

- Survey of Existing Bridge Substructures
- Long-Term Corrosion Tests with Large-Scale Post-Tensioned Beam and Column Elements
- Investigation of Corrosion Protection for Internal Prestressing Tendons in Precast Segmental Bridges
- Development of Improved Grouts for Post-Tensioning

Due to the long-term nature of durability testing, a combination of electrically accelerated corrosion tests and accelerated exposure tests with varying degrees of severity were used to provide the desired results in a timely manner. There is no recognized way that the results can be related to actual service lives. Only comparative trends can be used to determine relative effectiveness of various measures.

## **1.6 THESIS**

This thesis covers the contribution of the author to TxDOT Research Project 0-1405: “Durability Design of Post-Tensioned Bridge Substructure Elements.”

### **1.6.1 Objectives**

The objectives of this thesis are:

- To evaluate the extent and severity of corrosion found in all reinforcement of non-prestressed, fully prestressed and mixed reinforcement concrete beam specimens
- To evaluate the effect of mixed reinforcement on corrosion protection through comparison with non-prestressed and fully prestressed members



- To evaluate the corrosion protection performance of a number of variables related to post-tensioned structures, including:
  - Unloaded vs. Loaded
  - Level of Prestress and Crack Width
  - Concrete Type
  - Grout Type
  - Splice Type
  - Splice Damage and Repair Measures
- To evaluate the accuracy of non-destructive measurements taken during exposure testing
- To use results obtained from long term beam exposure testing and autopsy to develop durability design guidelines for bridge substructures

### **1.6.2 Scope**

The scope of this thesis includes:

- Exposure testing, maintenance and data collection of all beam specimens until the autopsy date
- Exposure testing, maintenance and data collection of remaining beam specimens after selective autopsy
- Autopsy and analysis of 14 of the 27 large-scale beam specimens under accelerated exposure testing

## **CHAPTER 2**

### **Beam Long Term Exposure Corrosion Specimens**

#### **2.1 SPECIMEN TEST CONCEPT**

The use of post-tensioning in concrete elements can improve their durability against corrosion. First, the precompression in the concrete due to post-tensioning reduces the number and width of surface cracks, thus reducing the direct routes for the chlorides to reach the reinforcement and post-tensioning system. Secondly, the use of a post-tensioning system introduces more layers of corrosion protection with the addition of a duct, grout, grout corrosion inhibitors and strand coatings. Each level of protection is available in several varieties, with the extent of protection provided by each type depending on its quality and the type of material used. Therefore it is necessary to investigate each variety to determine the most beneficial variables for the post-tensioning system and establish the most effective durability design guidelines.

Fully prestressed members are designed to remain in the elastic stress range under service load levels, keeping the most extreme tensile stress below the modulus of rupture, and thus able to resist cracking. As discussed in Chapter 1, this method of design is not always the most efficient, for in certain cases it can result in an overly conservative design. This has prompted the application of mixed reinforcement. However, mixed reinforcement usually does not provide enough precompression in the concrete to maintain stress levels below the modulus of rupture. Therefore, cracking under service load levels will occur. The effect of this cracking on corrosion is uncertain. This issue prompted the creation

of multiple large-scale concrete beam specimens typical of bridge substructures with varying levels of prestressing and mixed reinforcement for long term testing and evaluation of the corrosion protection provided by each type.

The experimental program uses large-scale linear elements, designed as beams. The beams are subjected to combined structural loading and an aggressive corrosive environment. The specimens are tested outside the Ferguson Structural Engineering Laboratory, and are exposed to cyclic wetting and drying with a 3.5% NaCl solution to promote accelerated corrosion. The majority of the specimens are continually subjected to service load conditions. The effect of post-tensioning is investigated for a range of prestressing, from non-prestressed (reinforced concrete) to mixed reinforcement to fully prestressed. Variables investigated include the influence of prestress level, crack width, high performance concrete, duct type, duct splice type and condition, high performance grout, prestressing strand coatings, and encapsulated end anchorage systems.<sup>1</sup>

The experimental program was implemented in two phases. The first phase was developed by Jeff West<sup>1</sup> and contained beam specimens designed to investigate the influence of prestress level, cracking, high performance grout and post-tensioning duct splices. The second phase was developed by Andrea Schokker<sup>2</sup> and contained beam specimens designed to investigate high performance concrete, high performance grout, prestressing strand coatings and an encapsulated end anchorage system. The beam detailing, loading and exposure testing is identical in both phases.

## **2.2 SPECIMEN DESIGN**

### **2.2.1 Beam Test Specimens**

The test specimens in this experimental program are beams with a rectangular cross-section. The specimen dimensions and details were chosen to

allow for the investigation of a large range of variables and to simulate elements in practical applications, while facilitating construction and loading in the laboratory. A cross-section of 18" x 24" (450 mm x 600 mm) was chosen to provide the most flexibility in the design of mixed reinforcement sections, and a length of 15'2" (4.6 m) for practical handling and loading of the specimens.<sup>1,2</sup> A diagram of the specimen setup is shown in Figure 2.1, with the experimental beam on top and the reaction beam, used for loading, on the bottom. A photo of one of the specimens outside of the laboratory is shown in Figure 2.2.

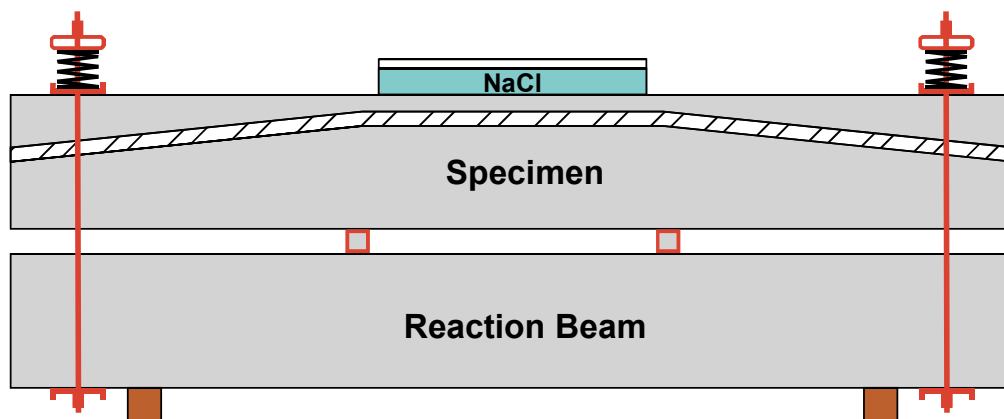


*Figure 2.1: Specimen Setup<sup>2</sup>*



*Figure 2.2: Beam Exposure Specimen*

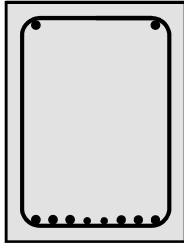
The specimens used in the experimental program are not patterned after a prototype bridge element; therefore no specified design loading is available. Reinforcement was proportioned based on the total allowable service load moment (dead plus live) computed for the 100%S PS section (fully prestressed, service load design). Assuming a ratio of dead load to live load of 1.5, the calculated permissible total service load moment was used to compute the dead and live load moments. The factored moment was then computed and used to proportion the reinforcement for the remaining sections.<sup>1</sup> A thorough description and calculations of the design loading, section reinforcement design and section analysis of the specimens can be found in Reference 1. The specimen details are summarized in Table 2.1 and diagrams of the specimen cross-sections are shown in Figure 2.3.

*Table 2.1: Summary of Section Details<sup>1</sup>*

<b>Section</b>	<b>Prestressing Strands</b>	<b>Effective Prestress (after all losses)</b>	<b>Mild Steel Bars (tension)</b>	<b>Nominal Capacity</b>
Non-PS	None	n/a	6 - #6 and 2 - #4	4682 k-in
2/3 PS	4 - 0.5 in	$0.60f_{pu}=161.9$ ksi	4 - #4 and 4 - #3	4744 k-in
100%U PS	6 - 0.5 in	$0.60f_{pu}=161.9$ ksi	2 - #3	4682 k-in
100%S PS	8 - 0.5 in	$0.56f_{pu}=151.1$ ksi	2 - #3	5930 k-in

Bar Sizes: #6 – 0.75 in. dia.      Conversion Factors: 1 in. = 25.4 mm  
 #4 – 0.5 in. dia.                      1 ksi = 6.895 MPa  
 #3 – 0.375 in. dia.                    1 k-in. = 0.11298 kN-m

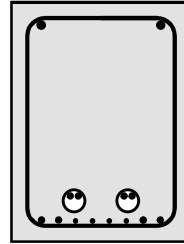
### **Non-Prestressed**



Compression Steel:  
2 - #5's (15.9 mm dia.)

Tension Steel:  
6 - #6's (19 mm dia.) and  
2 - #4's (12.7 mm dia.)

### **2/3 Prestressed**

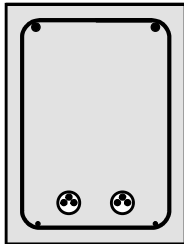


Compression Steel:  
2 - #5's (15.9 mm dia.)

Tension Steel:  
4 - #3's (9.5 mm dia.) and  
4 - #4's (12.7 mm dia.)

Prestressing Steel:  
4 - 12.7 mm dia. strands

### **100% Prestressed Strength Design**

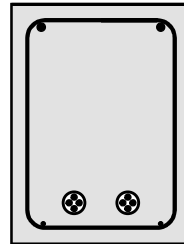


Compression Steel:  
2 - #5's (15.9 mm dia.)

Tension Steel:  
2 - #3's (9.5 mm dia.)  
(not required by design)

Prestressing Steel:  
6 - 12.7 mm dia. strands

### **100% Prestressed Allowable Stress Design**



Compression Steel:  
2 - #5's (15.9 mm dia.)

Tension Steel:  
2 - #3's (9.5 mm dia.)  
(not required by design)

Prestressing Steel:  
8 - 12.7 mm dia. strands

*Figure 2.3: Specimen Cross-Section Details<sup>1</sup>*

## **2.2.2 Reaction Beams**

Reaction beams were needed to apply the desired load to the test specimens. They were designed as reinforced concrete. The decision to use non-prestressed beams, as opposed to prestressed concrete beams or steel beams, was made based on cost and construction time. The dimensions of the reaction beams were identical to the test specimens. Reinforcement for the reaction beams was proportioned to provide excess strength in comparison to the test specimens and to limit crack widths at service load levels. The nominal strength of a reaction beam was 6180 k-in. (700 kN-m).<sup>1</sup> Additional details and drawings can be found in Reference 1. The reaction beams are not directly subjected to the aggressive corrosive environment of the saltwater exposure.

## **2.3 VARIABLE SELECTION**

A wide range of variables was selected for evaluation after an extensive literature review, conducted by West<sup>1</sup>. These variables included the level of prestress and crack width, applied load, concrete type, duct type, duct splice type and imposed damage, grout type, grouting procedure, strand type and end anchorage protection. It was determined that a total of 27 beam specimens were needed to address all of the variables under investigation. The specimens were fabricated in two separate phases. There were 16 beam specimens in Phase I, designed to investigate the level of prestress, crack width, applied load, grout type, duct splice type and imposed damage. Phase II consisted of an additional 11 identical beam specimens that investigated the level of prestress, concrete type, duct type, duct splice type, grout type, grouting procedure, strand type and end anchorage protection. A list of all of the specimens and their corresponding variables is shown in Appendix A. The first half of the number assigned to each specimen corresponds to the level of prestress in that specimen (1 = Non-PS, 2 = 2/3 PS, 3 = 100%U PS and 4 = 100%S PS), whereas the latter part of the number is arbitrary. A more detailed notation for the specimens can be found in Section 2.7.

### **2.3.1 Control Variables**

Control variables typical of current practice were used for comparison of the test variables. The Texas Department of Transportation standards for concrete mix design, concrete clear cover, cement grout, duct and anchorage protection were chosen as the control variables. Descriptions of each are given in Table 2.2.

**Table 2.2: Details of Control Variables<sup>1,2</sup>**

<b>Control Variable</b>	<b>Description</b>
Concrete	TxDOT Class C concrete for bridge substructure: Maximum w/c=0.53 (typically 0.45 for a 4" slump) Type I cement 4" (100 mm) slump Maximum coarse aggregate size = 3/4" (19 mm) Retarder (Rheocrete 300-R) Air entrainment admixture (Master Builders AE-90) 2" (50 mm) clear cover
Cement Grout	TxDOT Grout w/c ratio = 0.44 Type I cement Expanding admixture (Intraplast-N)
Post-Tensioning Duct	Galvanized steel duct
Anchorage Protection	TxDOT Type V State epoxy bonding compound Non-shrink grout patch (Euclid NS grout)

### **2.3.2 Phase I Variables**

The following sections contain a brief description of the variables investigated in Phase I of this experimental program. A more detailed description of each variable can be found in Reference 1.

#### **2.3.2.1 Level of Prestress, Loading and Crack Width**

The purpose of the variables in this section was to evaluate the effect of post-tensioning and crack width on the corrosion performance of the system. In the past, some have argued that crack widths become less important than concrete permeability for preventing corrosion during the later service life of the structure. With today's high performance concretes, permeability is very low, leaving cracks as the critical route for chloride ingress to the steel.<sup>2</sup> For this reason, the



effects of these variables, which are all inter-related, were given considerable emphasis in this experimental program.

In order to examine a broad range of prestressing, section reinforcement was proportioned for the following levels of prestress:<sup>1</sup>

- Non-prestressed (Non-PS)
- 100% prestress based on service load/allowable stress design (100%S PS)
- 100% prestress based on ultimate (nominal) strength (100%U PS)
- intermediate level of mixed reinforcement with a nominal prestress amount between 50% and 75% (2/3 PS)

The four types of sections used are shown above in Figure 2.3. Full design details and drawings are given in References 1 and 2.

The effect of cracking is primarily investigated using standard variables and the three sections that would be expected to crack under service loads (Non-PS, 2/3 PS and 100%U PS). The range of crack widths investigated in this program is based on a survey of relevant literature regarding critical crack widths for corrosion and recommended allowable crack widths. A broad range of crack widths was selected to provide a suitable evaluation of the effect of cracking on corrosion. The selected crack widths are 0.002 in. (0.05 mm), 0.004 in. (0.1 mm), 0.008 in. (0.2 mm), 0.012 in. (0.3 mm) and uncracked. To obtain this crack width range, the four loading cases shown in Table 2.3 were developed. Due to the large number of variables and uncertain nature of cracking, deviation from the planned crack width and loading combinations occurred.<sup>1</sup>

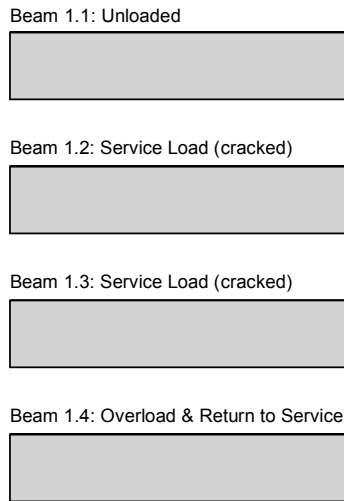
**Table 2.3: Planned Crack Widths, Prestress Amounts and Loading<sup>1</sup>**

<b>Loading Case</b>	<b>Crack Widths</b>	<b>Applicable Sections</b>	<b>Loading</b>
1) Constant Service Load	uncracked 0.004 in. 0.008 in. 0.012 in.	100%S PS 100%U PS 2/3 PS Non-PS	service load service load service load service load
2) Very Small Crack	0.002 in.	2/3 PS & 100%U PS	as needed & hold
3) Unloaded	uncracked	Non-PS & 100%U PS	none
4) Overload & Return to Service	as measured	Non-PS, 2/3 PS & 100%U PS	up to 1.33 x service load, then return to service

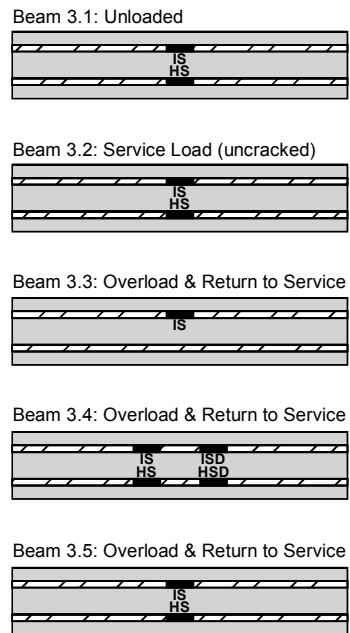
### **2.3.2.2 Duct Splice Type and Condition**

In most practical applications, the post-tensioning ducts must be spliced at some location. It was decided to compare industry standard splices to heat shrink splices and unspliced ducts. The effect of damaged splices was also examined. A diagram of the splice configuration for each specimen in Phase I is given in Figure 2.4 and a photograph of the two splice types is shown in Figure 2.5. The industry standard splice consists of a 1 ft (300 mm) length of oversized duct. Concrete is prevented from entering the splice by wrapping the ends with duct tape. The heat shrink splice consists of an 8 in. (100 mm) length of heat shrink tubing. The original diameter of the heat shrink tubing is 4 in. (100 mm). No mechanical connection was made between the two ducts being connected. For the damaged condition, poor or incomplete duct taping was used on the industry standard splice. For the damaged heat shrink splice, a 1 in. (25 mm) cut was made in the heat shrink tubing at the location where the ducts meet.

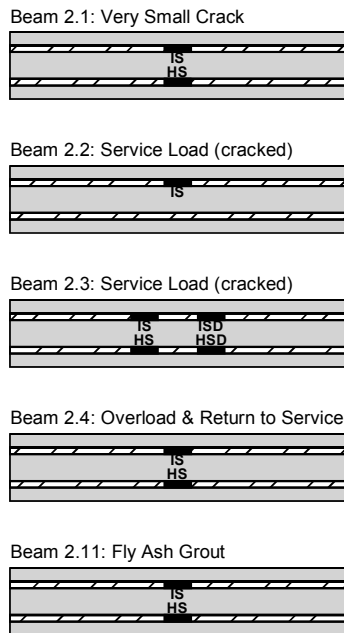
**Non-Prestressed Beams**



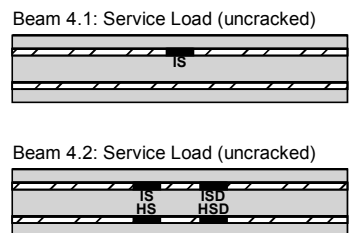
**100%U Prestressed Beams**



**2/3 Prestressed Beams**



**100%S Prestressed Beams**



**Splice Descriptions:**  
 IS - Industry Standard  
 HS - Heat Shrink  
 ISD - Industry Standard w/ Damage  
 HSD - Heat Shrink w/ Damage

*Figure 2.4: Phase I Beams-Duct Splice Configuration<sup>2</sup>*

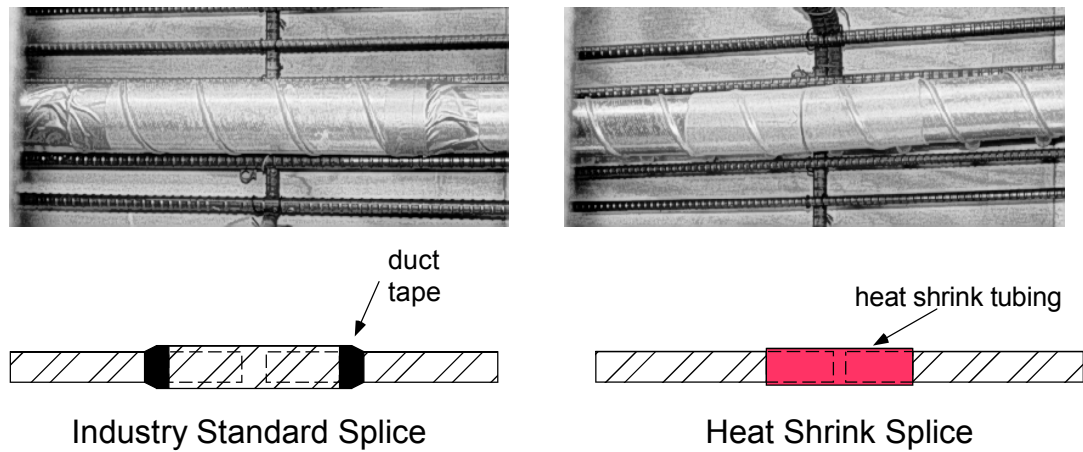


**Figure 2.5: Duct Splices<sup>1</sup>**

### **2.3.2.3 Grout Type**

The use of high performance grouts for corrosion protection of the prestressing strands is investigated in this experimental program. The grout used in Phase I of the testing program was selected based on fresh property tests and accelerated corrosion tests performed by Schokker.<sup>2</sup> The fly ash grout selected contained 30% fly ash by weight, and has a low water-cement material ratio of 0.35. This grout had the best corrosion protection of all grouts investigated, and possessed excellent fresh properties with good resistance to bleed.<sup>1</sup>

### **2.3.3 Phase II Variables**

The following sections contain a brief description of the variables investigated in Phase II of this experimental program. A more detailed description of each variable can be found in Reference 2.

### ***2.3.3.1 Level of Prestress, Loading and Crack Width***

The levels of prestress, loading and crack widths for the Phase II specimens are identical to those in Phase I. See Section 2.3.2.1 for a detailed description.

### ***2.3.3.2 Concrete Type***

In addition to the TxDOT standard concrete for bridge substructures, two other concrete designs were tested. Lowered permeability can significantly increase corrosion protection, thus it was desirable to test additional mix designs with lowered water-cement ratios and pozzolan addition. Fly ash is commonly used in Texas bridge substructures, as opposed to silica fume. For this reason, a TxDOT Class C concrete with 25% cement replacement fly ash was chosen as one variable for investigating concrete durability.<sup>2</sup>

High performance concretes are quickly gaining popularity for use in Texas bridges. Concretes rated as high performance for durability have very low permeability and make an interesting comparison with the standard TxDOT concretes. Concretes rated as high performance for strength may not give better corrosion protection alone, but may give rise to favorable situations for corrosion protection such as the absence of cracking at service loads for post-tensioned members. Higher strength concrete may also allow a higher level of post-tensioning and more slender members, both of which may help to justify the additional cost of these mixes. A mix classified as high performance for both strength (around 10,000 psi [68.9 MPa]) and durability was chosen. The mix contained 25% cement weight replacement fly ash (water-cement ratio around 0.29) batched to a slump of 1-2 in. (25-50 mm) with additional superplasticizer added on site to reach a slump of about 8 in. (200 mm) and a maximum aggregate size of  $\frac{3}{4}$  in. (19 mm). Details of both mix designs can be found in Reference 2.<sup>2</sup>

### ***2.3.3.3 Duct Type***

Duct types investigated in this experimental program included the control type, a galvanized steel duct, and a plastic duct. Plastic ducts have been found to increase durability for post-tensioned structures as both a barrier for chloride penetration as well as by resisting duct corrosion, which may cause further chloride ingress due to concrete cracking and spalling from corrosion product buildup. The plastic duct chosen for testing was a polyethylene duct that is part of VSL Corporation's VSLAB+™ system. The duct is oval in cross-section and can accommodate two strands. The smallest round plastic duct commercially available was intended for 5-12 strands and was too large for the beam specimens. Therefore, the two-strand slab system was chosen.<sup>2</sup>

### ***2.3.3.4 Duct Splice Type and Condition***

The duct splice types investigated in the Phase II specimens are identical to those in Phase I. See Section 2.3.2.2 for a detailed description. The effect of splice damage was not examined in Phase II. A schematic of the splice configuration for each specimen in Phase II is given in Figure 2.6.

### Non-Prestressed Beams

Beam 1.5: Fly Ash Concrete

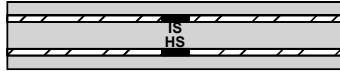


Beam 1.6: High Performance Concrete

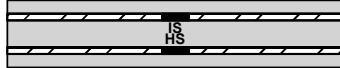


### 100%U Prestressed Beams

Beam 3.6: Fly Ash Concrete



Beam 3.7: High Performance Concrete

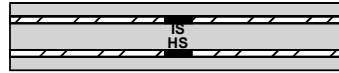


#### **Splice Descriptions:**

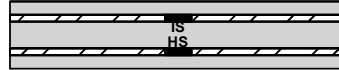
IS - Industry Standard  
HS - Heat Shrink

### 2/3 Prestressed Beams

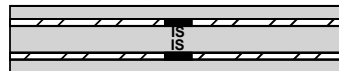
Beam 2.5: Fly Ash Concrete



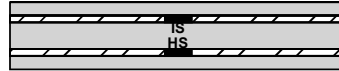
Beam 2.6: High Performance Concrete



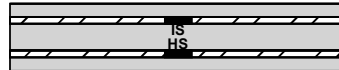
Beam 2.7: Epoxy Coated Strand



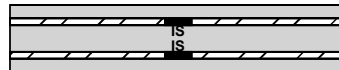
Beam 2.8: Galvanized Strand



Beam 2.9: Poor Grouting Procedures



Beam 2.10: Anti-Bleed Grout



Beam 2.12: Enc. System / Plastic Duct



**Figure 2.6: Phase II Beams-Duct Splice Configuration<sup>2</sup>**

#### 2.3.3.5 Grout Type

The second high performance grout chosen to be investigated in Phase II of this experimental program was an anti-bleed grout. The anti-bleed grout has a water-cement ratio of 0.33 with 2% cement weight of anti-bleed admixture.<sup>2</sup> Details of the grout mixtures can be found in Reference 2.

#### **2.3.3.6 Grouting Procedure**

Specimen 2.9 was used to investigate poor grouting procedures. This specimen had one tendon grouted by the standard method and one tendon poorly grouted. Both procedures are explained in Section 2.5.3.

#### **2.3.3.7 Strand Type**

The two types of corrosion resistant strands considered in this experimental program are an epoxy-coated strand and a galvanized strand. Both strand types were 0.5 in. (13 mm) diameter, 270 ksi (1860 MPa) stress relieved strands. The epoxy-coated strand had grit impregnated coating for improved bond (Flo-Bond™ strand).<sup>2</sup>

When examining coated steel for corrosion resistance, it is important to also consider the effect of damaged coating. To examine this effect, the specimen with an epoxy coated strand contains one damaged tendon and one undamaged tendon. The damaged tendon had small squares of epoxy removed at five selected locations along the length of each strand. Three of the damage locations coincide with the centerline crack and the cracks located at 1-ft. (300 mm) offsets on each side of the centerline. The remaining two damage locations coincide with the bends in the parabolic duct. One strand in the damaged tendon was repaired with an epoxy patch repair kit provided by Florida Wire and Cable and the other strand was left damaged.<sup>2</sup>

#### **2.3.3.8 End Anchorage Protection**

All anchorage systems were VSL Type E5-3 or VSL Type E5-4, with the exception of two specimens. Specimen 2.7 required special wedges due to the presence of the epoxy coated strand, and specimen 2.12 used an encapsulated system. The PT-Plus system utilized in specimen 2.12, due to its use of a plastic duct, also allowed for the investigation of an encapsulated system for end



anchorage protection. Figure 2.7 shows the end protection provided by the system. The end trumpet with the bearing plate clips directly onto the duct and a cap and gasket is provided that screws on over the end anchor head. A grout inlet is prefabricated into the end trumpet. This system is basically air and water tight.<sup>2</sup>

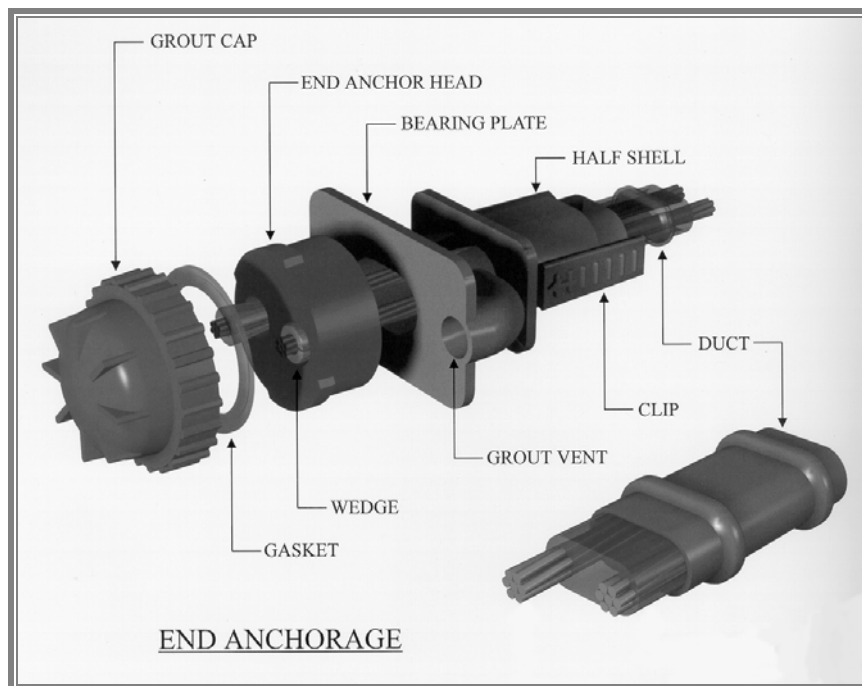


**Figure 2.7: VSLAB+™ System<sup>2</sup>**

## 2.4 MATERIALS

Where applicable, materials and proportions were selected to match TxDOT Standard Specification.<sup>6,7</sup> A local ready-mix concrete producer supplied the concrete. Grouts for post-tensioning were batched using a medium sized mortar mixer. Non-shrink grout for capping post-tensioning anchorages was mixed in a 5 gal. (18.9 liter) bucket using a paddle mixer mounted to a large hand-held drill. Mild steel reinforcement was supplied and fabricated according to design drawings by a local steel fabricator. Mild steel reinforcement was

uncoated. This was found to have been an unfortunate decision. Post-tensioning hardware was fabricated by the supplier<sup>1</sup>.

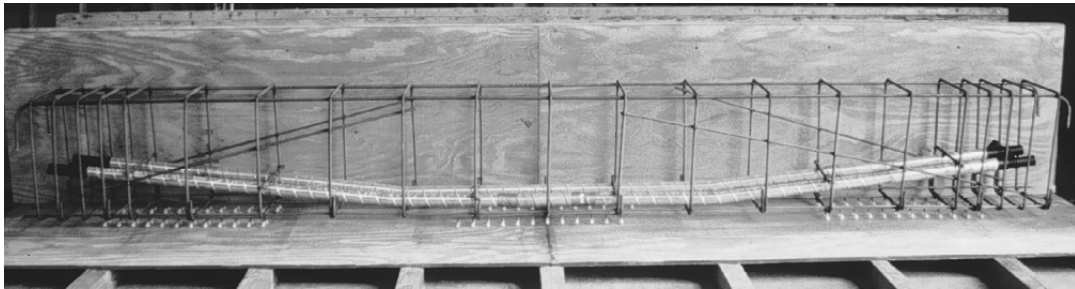
Typical concrete cylinder strength tests were conducted for the beam specimen concrete and reaction beam concrete, and grouts for post-tensioning were sampled according to PTI Specifications<sup>8</sup>. Testing procedures, concrete strength results, grout strength tests and details of materials used for Phase I and Phase II beams can be found in References 1 and 2.

## **2.5 FABRICATION**

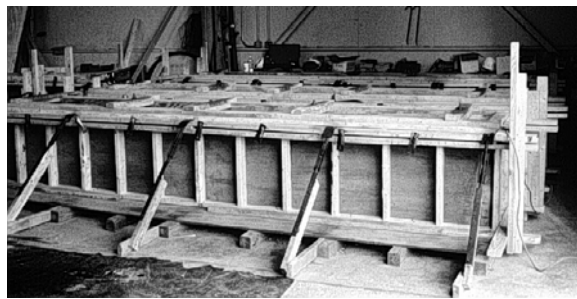
All beam specimens and reaction beams were fabricated at the Ferguson Structural Engineering Laboratory. The following sections cover the highlights of the fabrication of the beam test specimens. A detailed description of the procedures for each step of fabrication can be found in References 1 and 2.

### **2.5.1 Beam Fabrication**

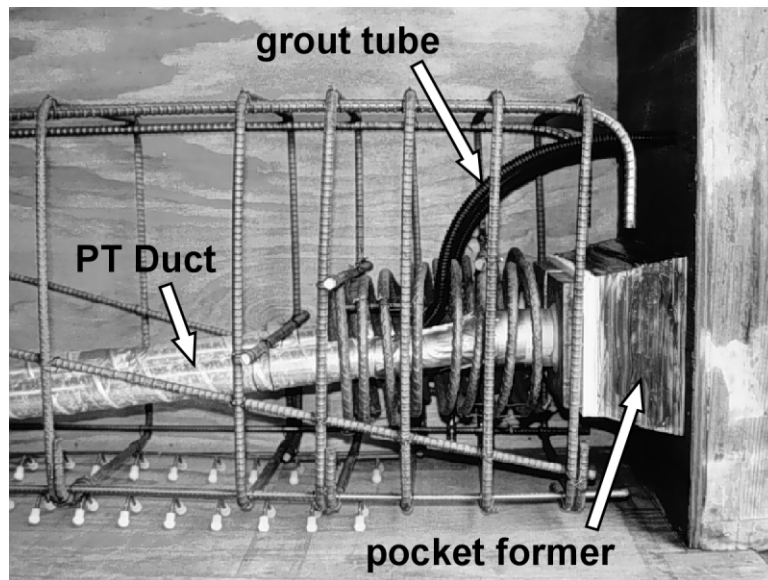
Reinforcement cages were prepared following typical construction practices. All flexural reinforcement was cleaned prior to construction using a wire brush wheel on an angle grinder. Post-tensioning anchorage hardware and confinement reinforcement were sandblasted to remove visible rust. This was done so that any corrosion occurring from exposure testing would be clearly identifiable. Reusable wooden forms were constructed for casting the beams. Concrete was supplied by a local ready-mix producer, and placed using a concrete bucket on an overhead crane. Concrete was placed and vibrated following typical practice and allowed to wet cure for a minimum of three days.<sup>1</sup> Several photographs of beam specimens taken during the construction process are shown in Figure 2.8. Additional details and photographs can be found in References 1 and 2.



**Reinforcement Cage with Ducts for Post-Tensioning**



**Formwork**



**Anchorage Zone Details**

**Figure 2.8: Beam Fabrication**

### 2.5.2 Post-Tensioning

All equipment for post-tensioning was adapted from Ferguson Laboratory hydraulic equipment. Several different sized hydraulic rams were used to stress the tendons, depending on the post-tensioned beam type. A system of two small rams and a transfer bracket was used to power seat the anchorage wedges<sup>1</sup>. An example of the setup for a 100%S PS beam can be seen in Figure 2.9.

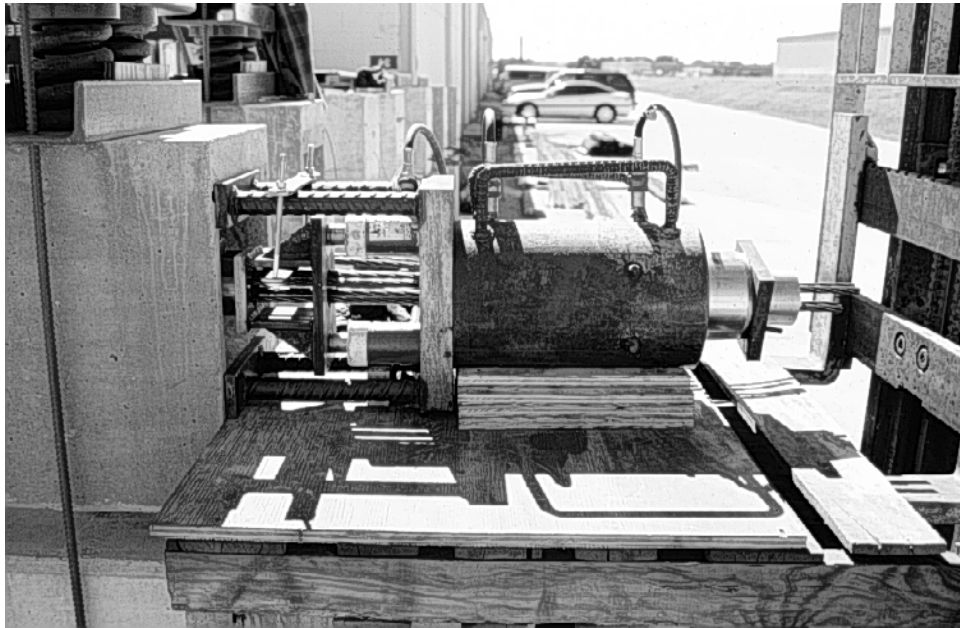


*Figure 2.9: Post-Tensioning Setup*

Prestress losses due to elastic shortening, friction and anchorage seating had to be considered when calculating required post-tensioning jacking forces for each section type. Staged post-tensioning was used to minimize losses due to elastic shortening. Losses due to friction, equaling 2.5% of the jacking force, were small due to the short length of the beams and limited variation in tendon path. Due to the short length of the beam, losses due to anchorage seating were critical, therefore it was necessary to power seat the wedges<sup>1</sup>. A summary of the prestress

losses, jacking forces and initial prestress for each of the post-tensioned beam types is shown in Table 2.4. Again, further details of calculations and procedures conducted during the post-tensioning of the specimens, including special consideration for the epoxy-coated strands, can be found in References 1 and 2.

**Table 2.4: Initial Prestress, Prestress Losses and Jacking Forces<sup>1</sup>**

<b>Item</b>	<b>2/3 PS Section: 2 strand tendon</b>	<b>100%U Section: 3 strand tendon</b>	<b>100%S Section: 4 strand tendon</b>
<b>Initial Prestress, <math>f_{pi}</math></b>	162 ksi	162 ksi	151 ksi
<b>Elastic Shortening Loss</b>	0.68 ksi	1.04 ksi	1.28 ksi
<b>Friction Loss</b>	4.05 ksi	4.05 ksi	3.77 ksi
<b>Anchorage Seat Loss</b>	18.9 ksi	18.9 ksi	18.9 ksi
<b>Jacking Stress, <math>f_{pj}</math></b>	187 ksi	187 ksi	176 ksi
<b>Jacking Force</b>	57.2 kips	87.2 kips	108 kips

Conversion Factor: 1 ksi = 6.895 MPa  
1 kip = 4.448 kN

### 2.5.3 Grouting

Grouting procedures followed those recommended by the Post-Tensioning Institute<sup>10</sup> and TxDOT Specifications.<sup>8</sup> Tendons were normally grouted within three days after post-tensioning. During this period the anchorage pockets were sealed using a plywood cover and silicone to prevent moisture entry. This duration is within PTI limits,<sup>10</sup> and temporary corrosion protections were not required. All post-tensioned beams were grouted with the TxDOT standard grout except the two specimens containing high performance grouts.<sup>1,2</sup>

Grouts were mixed in a mortar mixer and pumped immediately using an electric grout pump. The grouting setup is shown in Figure 2.10. The inlet and vent 2 were provided using a 0.75 in. (19 mm) grout tube with shut off valves.

Vent 1 was provided by drilling from the tension face of the beam to the duct with a 0.5 in. (12.7 mm) diameter rotary hammer. Drilling was performed before the stands were placed and tensioned, and the duct was blown clean using compressed air. Vent 1 was closed using a dowel plug. Vent 1 was not required by the PTI Specifications,<sup>10</sup> but was included to ensure that the crest of the duct profile was completely filled during grouting.<sup>1</sup>

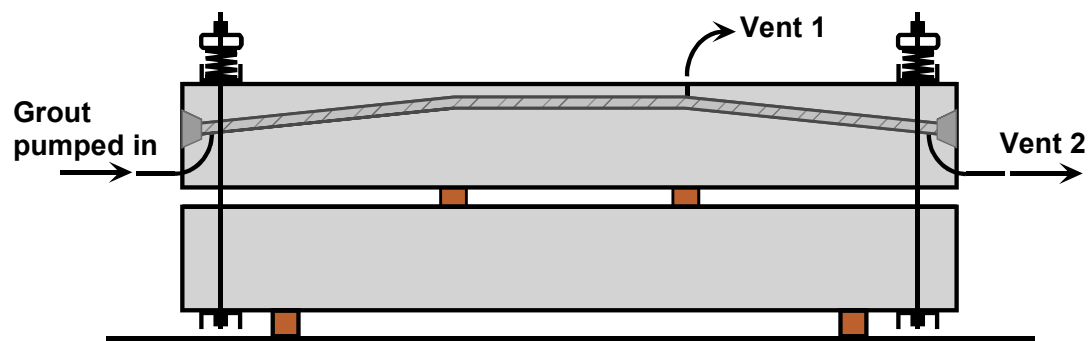


*Figure 2.10: Grouting Setup<sup>1</sup>*

Grouting began as soon as the grout was sufficiently mixed. Grout was transferred from the mixer using buckets, and poured into the pump reservoir through a screen to remove lumps, if any. The grout was continuously stirred in the reservoir to prevent segregation. Grout was pumped into each duct without stoppage. In all cases, the flow of grout filled the duct completely as it progressed along the duct length, and grout exited Vent 1 before reaching Vent 2. Once a continuous flow of grout was exiting Vent 1 with no slugs of air or water, Vent 1 was closed using a dowel. Pumping continued until a steady flow of grout was exiting Vent 2. At this time, Vent 2 was closed and the pump stopped. The pump was then restarted for a period of two or three seconds before closing the valve on the inlet tube. Grout bleed water was normally observed exiting from around the anchorage wedges immediately after the grouting operation had concluded.<sup>1</sup>

One specimen was used to investigate poor grouting procedures. One tendon of the specimen was grouted using standard procedures, but during grouting of the other tendon the pump was turned off twice during pumping to allow possible pockets of air in the line. The pump was left off for approximately 10 minutes at one point during grouting to allow the grout already pumped into the tendon to reach a different consistency than that of the grout in the pumping chamber that was continuously agitated. The far end grout tube was closed at the first appearance of grout instead of letting the grout flow reach a continuous stream.<sup>2</sup>

#### **2.5.4 Anchorage Protection**

Corrosion protection for the anchorage and strand ends was achieved by following procedures and using materials based on TxDOT Specifications.<sup>8</sup> After grouting was completed, all exposed surfaces including the anchorage heads, bearing plates and sides of the pockets were cleaned with a wire brush to remove grout and rust. All exposed surfaces were coated with an epoxy-bonding compound immediately prior to capping. After epoxy application, the end pockets were closed in with plywood. Silicone sealant was used to prevent leakage around the plywood. The pockets were filled with Euclid non-shrink grout using a funnel through a hole in the end form. The premixed grout contained a silica sand and a non-shrink admixture. After the grout had hardened, the plywood was removed. In some cases, a small void remained at the top of the pocket. The entire beam end was rubbed with a mixture of cement, sand and latex bonding agent to provide a uniform finish and fill any voids in the end pocket.<sup>1</sup>

## 2.6 BEAM SPECIMEN LOADING

To achieve the goal of this experiment, it was necessary to subject the test specimens to a sustained structural loading. A constant load of 50 kips (225 kN) applied at the end of each beam combined with two supports located at third points along the length of the beam created a constant negative moment region along the center 1/3 of the beam. The beams were loaded through a system of triple coil railroad springs and post-tensioning bars. The desired load was achieved by applying a load through this system at the ends of each beam and the reactions produced by the supports located at the third points along the length of the beam.

The beam specimens were loaded using two 120 kip (535 kN) hydraulic rams, one at each end of the beam. An air driven pump was used to apply loading by causing the ram to react against a steel spreader beam, compressing the springs. Load levels were monitored using a pressure gauge on the pump. Once the desired level of loading was attained, the force was locked in by tightening the nuts on the post-tensioning bars. The loading apparatus is shown in Figure 2.11<sup>1</sup>.

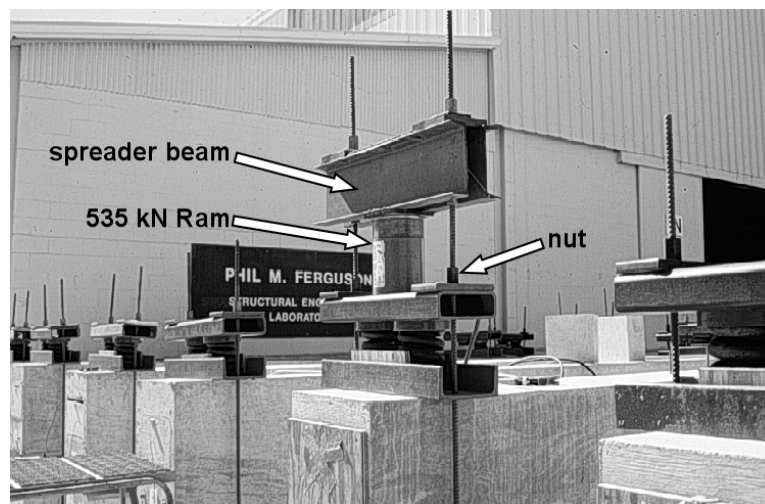


*Figure 2.11: Loading Apparatus*



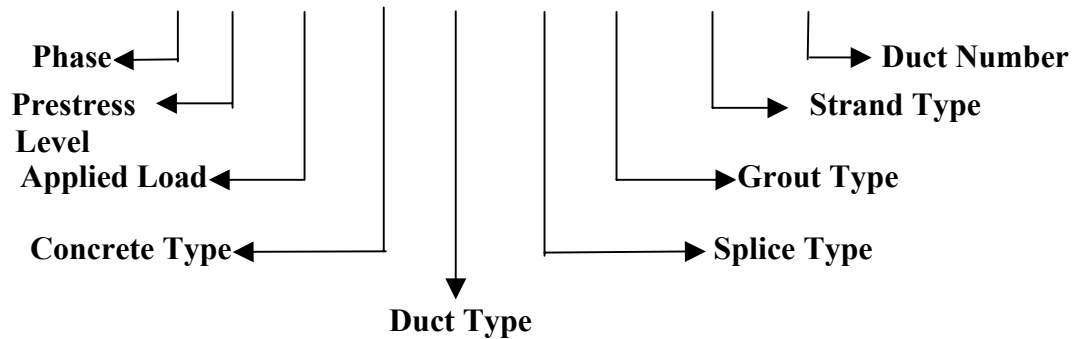
The initial load applied to each specimen varied depending on whether or not surface cracking of the concrete was desired and the load level required to cause cracking. Planned loading cases were determined prior to loading. However, deviations from the plan occurred due to variations in the concrete modulus of rupture and crack predictions. Details of the planned loading methodology, the actual loading, problems encountered during loading and deviations from the loading plan can be found in References 1 and 2.

It was decided not to use traditional methods to monitor the force in the loading system due to the cost of using load cells and the questionable long-term reliability of strain gauges in an exterior exposure<sup>1</sup>. Periodic reloading of the beams was conducted to ensure load levels remained within expected limits. A timeline showing the initial fabrication and loading of the beams in each Phase, the beginning and end of exposure testing, measurements taken during exposure testing and subsequent re-loading of the beams can be found in Appendix B.

## **2.7 BEAM SPECIMEN NOTATION**

A total of 27 beam specimen types were designed and fabricated to address all of the variables under investigation. A notation scheme, comprised of variable abbreviations, was used to develop an abbreviation for each test specimen for ease of identification and reference. Although the scope of this document does not evaluate all tested variables, they were still included in the notation for ease of comparison in the future when the remaining specimens undergo final autopsy and analysis. For the sake of simplicity, each specimen's assigned number, found in Table 2.5, will be used for reference throughout the remainder of this document. The notation used in the specimen designations is as follows:

# 1 - X - XL - C - SD - IS - NG - NS - D1



## Phase:

- 1 = Phase I
- 2 = Phase II

## Prestress Level:

- X = Non Prestressed
- P = 2/3 Prestressed
- U = 100% Ultimate Prestressed
- S = 100 % Service Prestressed

## Applied Load:

- XL = No Load
- SL = Service Load
- OL = Overload (124%)

## Concrete Type:

- C = TxDOT Class C
- F = 25% Fly Ash
- H = High Performance

## Duct Type:

- SD = Steel Duct
- PD = Plastic Duct

## Splice Type:

- IS = Industry Standard
- ISD = IS Damaged
- HS = Heat Shrinked
- HSD = HS Damaged
- XS = No Splice

## Grout Type:

- NG = Normal Grout
- FA = 30% Fly Ash Grout
- AB = Anti-Bleed Grout

## Strand Type:

- NS = Normal Strand
- GS = Galvanized Strand
- ES = Epoxy Coated Strand

## Duct Number:

- D1 = Duct 1
- D2 = Duct 2

*Table 2.5: Specimen Designation*

PHASE I		PHASE II	
Specimen Number	Specimen Notation	Specimen Number	Specimen Notation
1.1	1-X-XL-C	1.5	2-X-CS-FA
1.3	1-X-SL-C	1.6	2-X-CS-HP
2.3(1)	1-P-SL-C-SD-IS/ISD-NG-NS-D1	2.5(1)	2-P-SL-F-SD-HS-NG-NS-D1
2.3(2)	1-P-SL-C-SD-HS/HSD-NG-NS-D2	2.5(2)	2-P-SL-F-SD-IS-NG-NS-D2
2.11(1)	1-P-SL-C-SD-IS-FA-NS-D1	2.6(1)	2-P-SL-H-SD-HS-NG-NS-D1
2.11(2)	1-P-SL-C-SD-HS-FA-NS-D2	2.6(2)	2-P-SL-H-SD-IS-NG-NS-D2
3.1(1)	1-U-XL-C-SD-HS-NG-NS-D1	3.6(1)	2-U-SL-F-SD-IS-NG-NS-D1
3.1(2)	1-U-XL-C-SD-IS-NG-NS-D2	3.6(2)	2-U-SL-F-SD-HS-NG-NS-D2
3.2(1)	1-U-SL-C-SD-HS-NG-NS-D1	3.7(1)	2-U-SL-H-SD-IS-NG-NS-D1
3.2(2)	1-U-SL-C-SD-IS-NG-NS-D2	3.7(2)	2-U-SL-H-SD-HS-NG-NS-D2
3.3(1)	1-U-OL-C-SD-IS-NG-NS-D1		
3.3(2)	1-U-OL-C-SD-XS-NG-NS-D2		
4.2(1)	1-S-SL-C-SD-HS/HSD-NG-NS-D1		
4.2(2)	1-S-SL-C-SD-IS/ISD-NG-NS-D2		

## **CHAPTER 3**

### **Experimental Program**

#### **3.1 EXPERIMENTAL SET-UP**

##### **3.1.1 Beam Specimen Setup**

In addition to subjecting the test specimens to a sustained structural loading, to achieve the goal of this experimental program it was also necessary to expose them to an accelerated corrosive environment. A Plexiglas barrier, fastened to the concrete surface using a marine sealant/adhesive, was constructed on top of the center four feet of each test specimen (the constant moment and cracked section) to create a ponded region. This ponded region was filled with a 3.5% salt (NaCl) solution. The salt concentration was determined based on the recommendations of ASTM G109<sup>9</sup> to achieve the most aggressive exposure. The specimens were placed on a two-week wet-dry cycle to accelerate the corrosive effects. The cycle consisted of the ponded region of each beam being filled with the salt solution for a period of two weeks followed by a two-week dry period. The ponded region was covered during the wet interval to prevent contamination of the salt solution and limit evaporation. The wet-dry cycling of the specimens continued until their final autopsy and analysis. The duration of exposure testing for the beams examined in this document was four and a half years for the Phase I specimens and three and a half years for Phase II. (See Appendix B for timeline) A diagram of the test setup is shown in Figure 3.1.

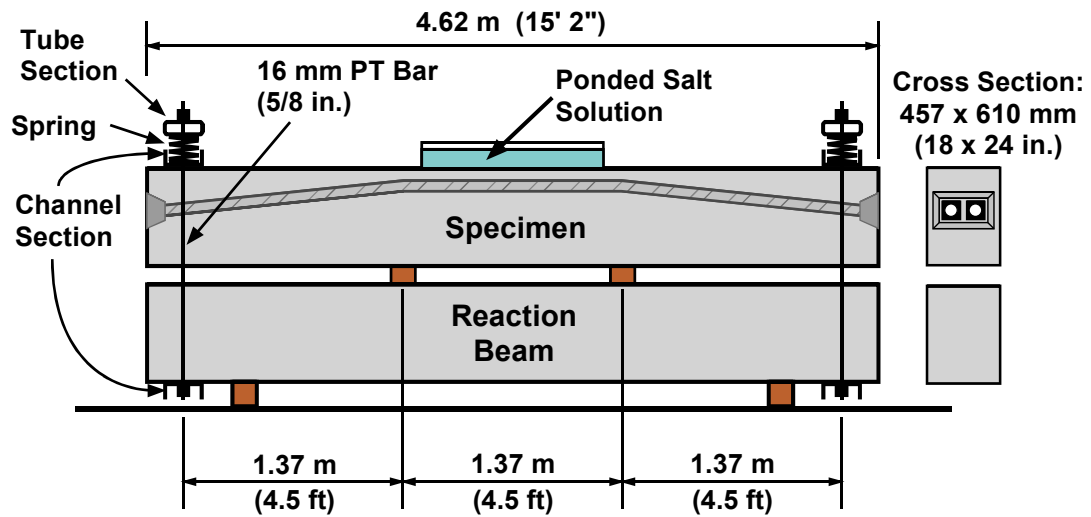


*Figure 3.1: Beam Specimen Test Setup<sup>1</sup>*

Due to the number and large size of the specimens, and the testing system and duration, a large outdoor area was needed for storage and testing of the specimens. A location outside of the Ferguson Structural Engineering Laboratory was chosen.<sup>1</sup> A photograph and a diagram of the arrangement of the beams are shown in Figures 3.2 and 3.3.



*Figure 3.2: Beam Specimens Outside of Ferguson Laboratory*

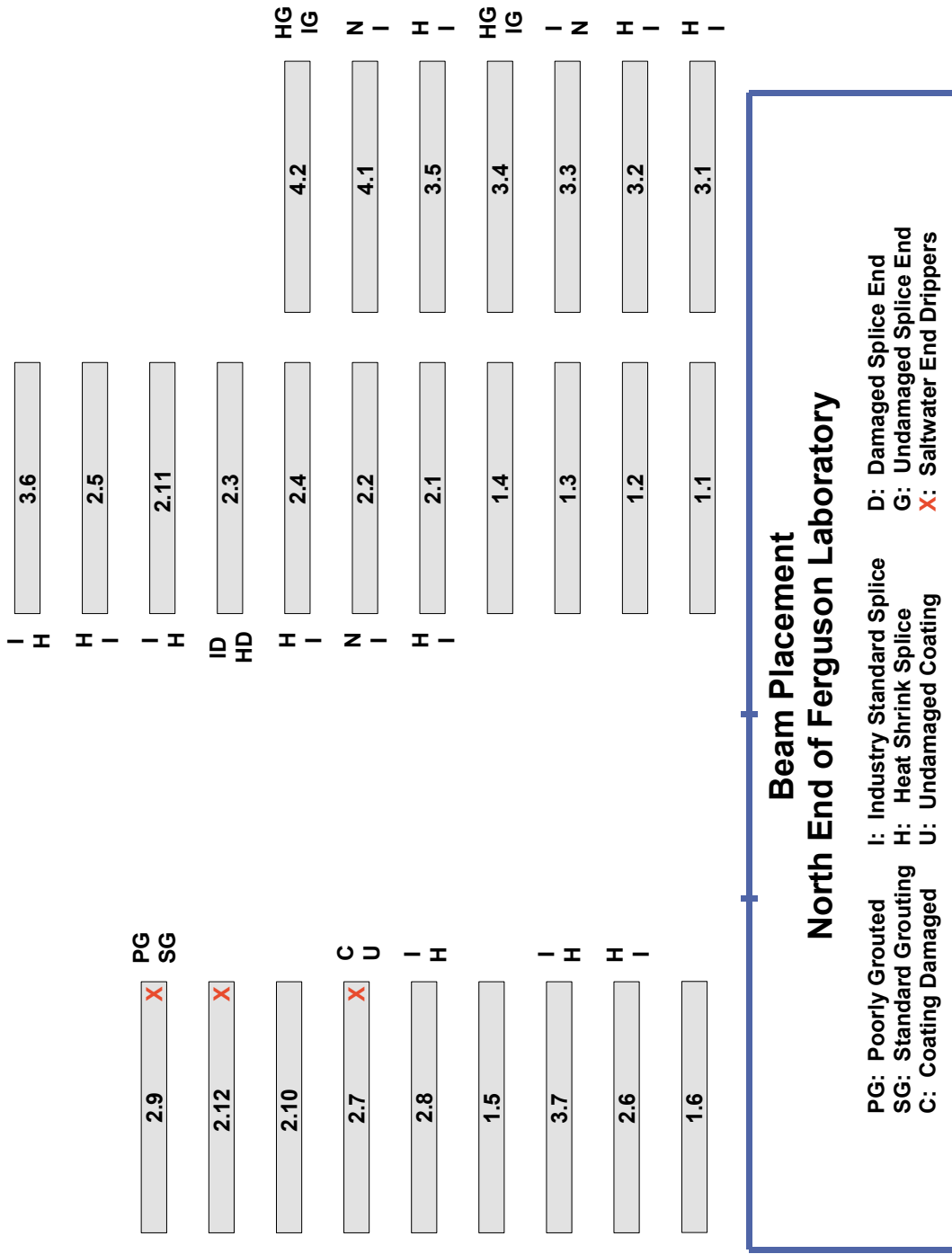
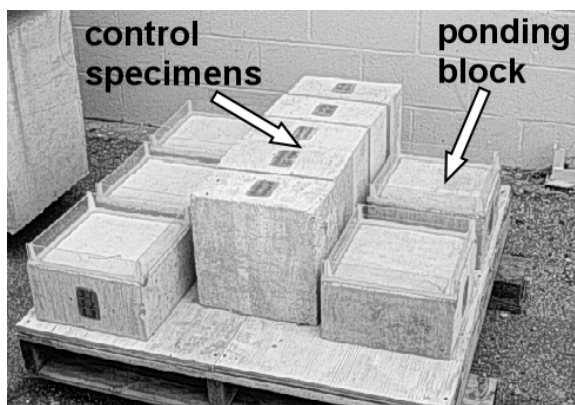


Figure 3.3: Beam Specimen Arrangement<sup>2</sup>

### 3.1.2 Block Specimen Setup

Concrete ponding blocks were used in this testing program to monitor chloride penetration in the beam specimens. The use of ponding blocks avoids drilling into the test area of the beam specimens, which could possibly affect later results. The ponding blocks have dimensions of 12 x 12 x 6 in. (300 x 300 x 150 mm), and were based on the AASHTO test method for evaluating chloride ion permeability of concrete.<sup>10</sup> The specified block thickness was increased to 6 in. (150 mm) to allow sample collection at larger depths. Two blocks were cast during each specimen pour. One block was fitted with a Plexiglas ponded region and subjected to the same exposure regimen as the beams. The ponded region was placed on the bottom surface of the block since the beam ponded area was also on a formed surface. The second block was used as a control specimen and was not subjected to saltwater exposure. The control specimens were used to indicate the base level of chlorides in the concrete. The blocks, shown in Figure 3.4, were stored outdoors with the beams<sup>1</sup>.



*Figure 3.4: Ponding Blocks for Beam Specimens*

### **3.1.3 Beam Dripper System Setup**

In addition to saltwater ponding, three specimens were selected to investigate the effects of chloride ingress at the end anchorage area. Specimen 2.12 (encapsulated system / plastic duct), Specimen 2.7 (epoxy-coated strand) and Specimen 2.9 (poorly grouted) were chosen for the end exposure testing. Specimen 2.9 contains one tendon grouted with standard procedures that can be used as a control. A dripper system was used to trickle saltwater over one end of the beams as shown in Figure 3.5. The drippers were run for a duration of eight hours at two week intervals.<sup>2</sup>



*Figure 3.5: Beam End Dripper System*

## **3.2 MEASUREMENTS TAKEN DURING EXPOSURE TESTING**

Determination of the presence and severity of corrosion in the specimens can only be concluded through complete destruction of the beams. Therefore,



multiple non-destructive forms of data collection were taken periodically during exposure testing in an attempt to monitor the corrosion activity of the beam specimens. Many of the measurements have limitations due to their non-destructive behavior and are therefore used to determine probabilities and trends of corrosion activity as opposed to quantitative values. A timeline showing each instance of data collection is given in Appendix B. The types of data gathered included visual inspection, crack width measurements, half-cell potential readings, corrosion rate readings and chloride penetration measurements. The following sections give a brief overview of the theory and procedure for each form of data collection. Additional detailed information can be found in References 1 and 2.

### **3.2.1 Visual Inspection**

The appearance of the specimens can indicate corrosion activity or distress. The beam specimens were regularly examined for signs of spalling, rust staining, changes in cracking and any other indication of distress.<sup>1</sup>

### **3.2.2 Crack Width Measurements**

#### ***3.2.2.1 Theory***

The effect of crack widths on corrosion protection is an area of great emphasis in this experimental program, as described in Section 2.3.2.1. Therefore, knowledge of the location and width of surface cracks on each specimen was essential.

### 3.2.2.2 Procedure

Surface crack widths were measured on the tension face of each specimen using a crack scope. Five reference lines were drawn on the face of the beams as shown in Figure 3.6. Crack widths were measured and recorded where each crack crossed the five reference lines. The five crack widths for a given crack were averaged to give a single crack width measurement for each crack location. The crack location was measured relative to the center of load application at one end of the beam.<sup>1,2</sup>

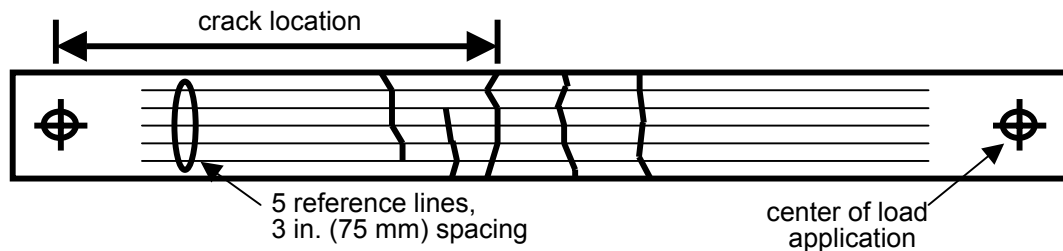


**Figure 3.6: Crack Width Measurement Setup**

### 3.2.2.3 Application to Experiment

Crack width measurements were taken on two separate occasions. Measurements of all of the specimens were recorded during the initial loading of the beams. Crack widths were measured at each loading stage until the desired crack width was achieved, then the loading was returned to the planned sustained load level. The second measurement of surface crack widths was only taken of the specimens selected in May 2002 for final autopsy and analysis. (See Section 5.2 for list of specimens and explanation.) The procedure took place immediately prior to the autopsy and was conducted in the same manner described in Section 3.2.2.2 and shown in Figure 3.6.

### **3.2.3 Half-Cell Readings**

A thorough explanation of the process and types of corrosion of steel embedded in concrete, and the significance of obtaining half-cell potential readings to detect corrosion activity can be found in References 1 and 2.

#### **3.2.3.1 Theory**

Electrical potential measurements are useful to monitor the corrosion of the steel embedded in the concrete. Electrical half-cell potential measurements are often used for this purpose. Because it is impossible to measure the absolute value of a half-cell potential, measurements of two half-cell potentials must be made with one used as a reference potential value. For convenience, the hydrogen half-cell reaction at standard state is arbitrarily defined as having a potential value of +0. Potentials may be reported in terms of the primary reference electrode, known as the Standard Hydrogen Electrode (SHE), or directly in terms of the secondary reference electrode used during half-cell potential measurements. For half-cell potentials measured in concrete specimens, common secondary reference electrodes used include the Copper-Copper Sulfate Electrode (CSE) and the Saturated Calomel Electrode (SCE). Table 3.1 gives the potential versus SHE for these reference electrodes. The secondary reference electrode used in this experiment was the SCE, therefore half-cell potentials throughout this document will be reported as millivolts versus SCE. To change these values to compare with results from CSE, simply add +77 mV to the values.<sup>1,2</sup>

**Table 3.1: Common Reference Electrode Potentials versus SHE<sup>11</sup>**

<b>Reference Electrode</b>	<b>Half-Cell Reaction</b>	<b>Potential (V vs. SHE)</b>
Copper-Copper Sulfate (CSE)	$\text{CuSO}_4 + 2e^- = \text{Cu} + \text{SO}_4^{2-}$	+0.318
Saturated Calomel Electrode (SCE)	$\text{Hg}_2\text{Cl}_2 = 2e^- = 2\text{Hg} + 2\text{Cl}^-$	+0.241
Standard Hydrogen Electrode (SHE)	$2\text{H} + 2e^- = \text{H}_2$	+0.000

Half-cell potential readings can provide two forms of information regarding the condition of the beam specimens:

- The magnitude of half-cell potential readings indicates the probability of corrosion at a given location.
- The time at which corrosion initiation occurred can be determined from regular potential readings taken during testing.

The numerical significance of the half-cell potential readings (Saturated Calomel Electrode) is shown in Table 3.2. The values reported in Table 3.2 were developed for uncoated reinforcing steel in concrete and may not necessarily be appropriate for post-tensioned concrete. In general, half-cell potential readings are not an effective method for monitoring corrosion activity in bonded post-tensioned structures. In structures with galvanized steel ducts, the prestressing tendon will be in contact with the duct in most cases and half-cell potentials taken on the prestressing tendon may reflect the potential of the zinc on the galvanized steel duct. Because the potential of the zinc will be more negative than that of the tendon, this could lead to erroneous results and conclusions. However, due to the lack of other non-destructive methods for monitoring corrosion activity in post-tensioned concrete, it was decided to use regular half-cell potentials to monitor specimen condition. By considering both the magnitude and variation of the

readings during testing it still may be possible to detect the onset of corrosion activity.<sup>1</sup> Since the specimens would be autopsied at a later date, the applicability of the half-cell method as a corrosion indicator could then be evaluated.

***Table 3.2: Interpretation of Half-Cell Potentials for Uncoated Reinforcing Steel<sup>1,2</sup>***

<b>Measured Potential (vs. SCE)</b>	<b>Probability of Corrosion</b>
more positive than -130 mV	less than 10% probability of corrosion
between -130 mV and -280 mV	corrosion activity uncertain
more negative than -280 mV	greater than 90% probability of corrosion

### ***3.2.3.2 Procedure***

Half-cell potential readings require a reference electrode, voltmeter and electrical connection to the reinforcement. As previously mentioned, the reference electrode used in this testing program was the Saturated Calomel Electrode (SCE). Ground clamps were used to attach a wire to the prestressing tendons before capping the anchorages as shown in Figure 3.7. In addition, two ground wires were attached to the reinforcement for each beam before placing concrete. The entire system of the reinforcement cage, ducts and prestressing tendons was found to be electrically continuous, and half-cell potential measurements using any of the lead wires should produce the same results.<sup>1</sup>

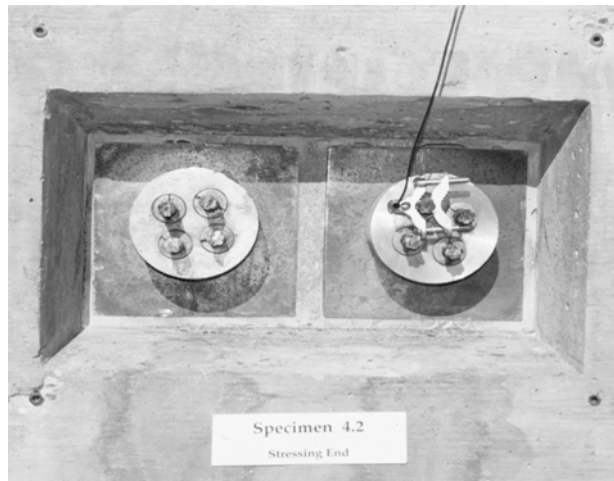


**Figure 3.7: Wire Connections to Post-Tensioning Tendons**

### **3.2.3.3 Application to Experiment**

Half-cell potential readings are taken at one month intervals, at the conclusion of the wet portion of the wet-dry exposure cycle. All measurements are performed according to ASTM C876.<sup>12</sup> Half-cell potential measurements are taken on a grid over the tension surface of beams. The grid spacing is 6 in. (150 mm) along the length of the beam. The grid spacing across the width of the beam is dependent on the section reinforcement. Three evenly spaced rows are used for the Non-PS sections. Two additional rows along the line of the ducts are added in the 2/3 PS section. A total of four rows are used in the 100%U PS and 100%S PS sections: two along the line of the ducts, and two along the two mild steel reinforcing bars. A diagram of the measurement locations in accordance with each specimen type's cross-section is shown in Figure 3.8. A photograph of a 2/3 PS section and the grid for the Non-PS beams are shown in Figures 3.9 and 3.10. Initially, measurements were performed before the saltwater solution was removed from the ponded area, at the conclusion of the wet portion of the exposure cycle.<sup>1</sup> It was later determined that more accurate readings could be taken if the saltwater solution was removed first and readings were taken

immediately after removal of the solution. This procedure eliminated the presence of standing water, yet the surface of the specimen remained saturated to provide a good electrical connection. For readings outside of the ponded area, a wetting solution was used according to the requirements of ASTM C876.<sup>12</sup>

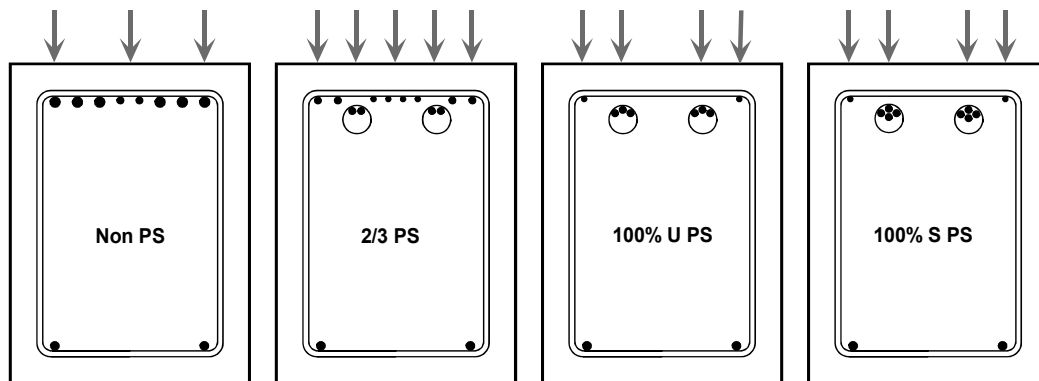


*Figure 3.8: Half-Cell Reading Locations<sup>2</sup>*

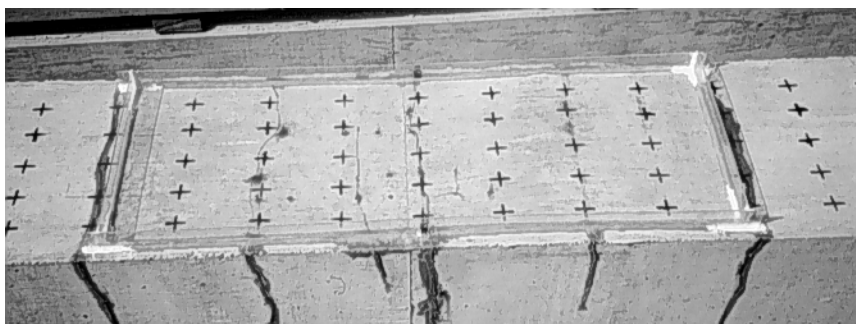


*Figure 3.9: 2/3 PS Specimen Half-Cell Potential Reading Grid*

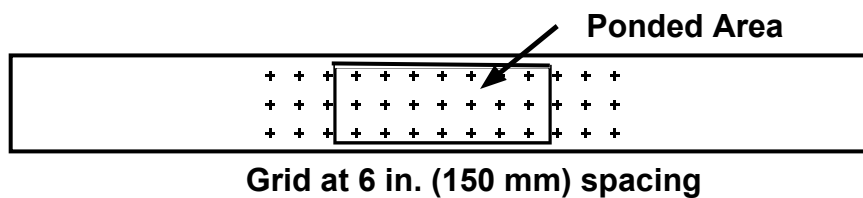


*Figure 3.10: Non-PS Specimen Half-Cell Potential Reading Grid*

### 3.2.4 Corrosion Rate Readings

A thorough explanation of the polarization resistance method, and the procedure for obtaining and analyzing corrosion rate measurements can be found in Reference 1.

#### 3.2.4.1 Theory

Polarization resistance is a useful technique for measuring instantaneous corrosion rates under laboratory and field conditions. Polarization measurements are rapid, highly sensitive, non-destructive and can be performed repeatedly. The theory behind this technique is detailed in many references.<sup>13,14,15,16</sup> The theory states that within a small range of over voltage ( $\pm 10$  to  $15$  mV from the free corrosion potential), there is a linear relationship between applied current and electrode potential. The slope of the curve of  $\Delta E$  versus  $\Delta I_{\text{applied}}$  at the origin is defined as the polarization resistance,  $R_p$  (see Figure 3.11).<sup>1</sup>

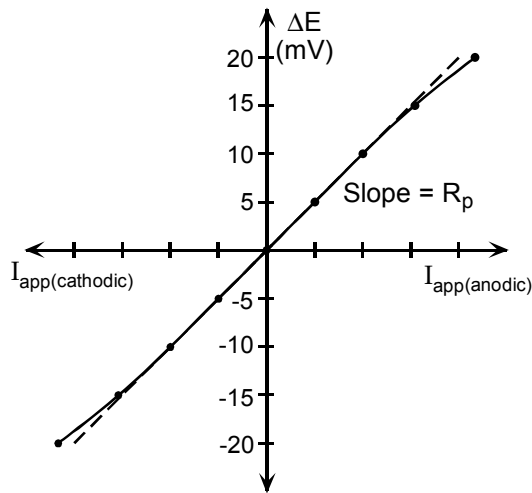


**Figure 3.11: Applied Current Linear Polarization Curve<sup>1</sup>**



The polarization resistance is inversely proportional to corrosion current by the Stern-Geary equation shown below.<sup>13,14</sup>

$$i_{\text{corr}} = \frac{\beta_a \beta_c}{2.3(\beta_a + \beta_c)} \times \frac{1}{R_p} \quad \text{Eq. 3.1}$$

where

$i_{\text{corr}}$  = corrosion current, mA

$\beta_a$  = anodic Tafel constant, mV

$\beta_c$  = cathodic Tafel constant, mV

$R_p$  = polarization resistance, Ohms

The corrosion current is in turn directly proportional to the rate of corrosion, in terms of corrosion current density, as shown below.

$$i = \frac{i_{\text{corr}}}{A_p} \quad \text{Eq. 3.2}$$

where

$i_{\text{corr}}$  = corrosion current, mA

$A_p$  = area of polarized steel, cm<sup>2</sup>

$i$  = corrosion current density, mA/cm<sup>2</sup>

The computed corrosion rate, in terms of corrosion current density, can be compared to the established guidelines to relate corrosion rate to corrosion damage. This method for corrosion rate measurements is often referred to as linear polarization or the polarization resistance method.<sup>1</sup>

#### **3.2.4.2 Procedure**

The polarization resistance,  $R_p$ , can be measured using several different techniques.<sup>14,15</sup> The two most common methods used for reinforced concrete are the three electrode procedure, and electrochemical impedance spectroscopy

(sometimes referred to as AC impedance). The three-electrode method is most common due to its simplicity and low equipment cost.<sup>1</sup>

The basic components of the equipment for the three-electrode method are shown in Figure 3.12. The working electrode is the steel reinforcement for which the corrosion rate is to be measured. The counter electrode is used to apply the polarizing current to the steel. The reference electrode measures the free corrosion potential of the working electrode and the change in potential of the working electrode due to the applied current from the counter electrode. The process of measuring the polarization resistance begins with measuring the free corrosion potential or open-circuit potential of the tested area of steel reinforcement (working electrode). The working electrode is then polarized in uniform increments from the free corrosion potential and the associated current is measured. The polarization resistance is taken as the slope of the curve when  $\Delta E$  versus  $\Delta I_{\text{applied}}$  is plotted (see Figure 3.11). This relationship is normally linear for a range of up to +/- 10 mV from the free corrosion potential.<sup>13</sup> When corrosion activity is low, small changes in applied current will produce a large change in potential and the polarization resistance will be large. When corrosion activity is high, large changes in applied current are needed to produce the desired potential increment, resulting in a low polarization resistance.<sup>1</sup>

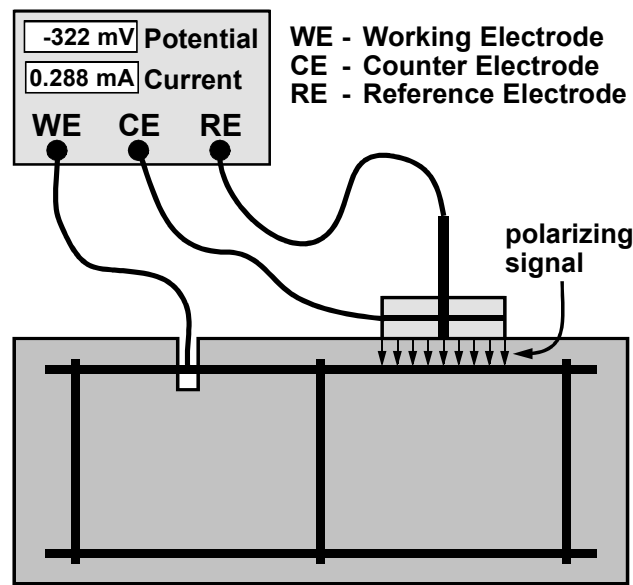


**Figure 3.12: Polarization Resistance Apparatus<sup>1</sup>**

### 3.2.4.3 Application to Experiment

At the beginning of this experiment there was no published work on using polarization resistance to monitor corrosion rates in pretensioned or post-tensioned concrete. Some of the factors that could cause errors in the corrosion rate measurements, which are discussed in Reference 1, may have a significant influence on the usefulness of the technique in prestressed concrete. In spite of these potential limitations, it was decided to use polarization resistance as an evaluation method in this testing program since qualitative information and comparisons may still be possible. Relative corrosion rate measurements can provide an indication of relative corrosion rates between specimens with different variables. For example, the relative effectiveness of different corrosion protection measures may be evaluated by comparing corrosion rates with those from “control” specimens. Also, regular measurements may indicate the onset of corrosion through increases in corrosion rate.<sup>1</sup>

This program used two different types of equipment to take corrosion rate measurements: the CORRTEST PR-Monitor Model IN-4500 and the 3LP Equipment. Both types of equipment use the three-electrode technique. Two corrosion rate measurements were taken on each beam, one at midspan and one at a 1 ft. (305 mm) offset from midspan. The polarization resistance technique requires a direct electrical connection to the steel for which the corrosion rate is being measured. This connection was provided by the ground wires attached to the mild steel reinforcement and prestressing tendons during construction. Corrosion rate measurements require the concrete to be initially dry. A wetting solution is used to moisten the concrete surface immediately prior to testing.<sup>1</sup>

The PR-Monitor device uses a portable computer to control the corrosion rate measurement process. The PR-Monitor compensates for the concrete resistance and has a guard electrode to confine the polarization signal. The default polarization scan uses six steps of 5 mV, starting at -15 mV from the free corrosion potential and ending at +15 mV. The starting and ending potentials and voltage increment may be adjusted by the user in situations where the solution resistance is large in comparison to the polarization resistance. The increased potential range for the polarization scan can improve the accuracy of the measured polarization resistance when the solution resistance is high. At the end of the polarization scan, the concrete resistance or solution resistance is measured using AC impedance. A high frequency, low voltage AC signal is used to isolate the solution resistance. The computer performs a linear regression analysis on the polarization scan data and computes the total resistance,  $R_{tot}$ , as the slope of  $\Delta E$  versus  $\Delta I_{applied}$ . The solution resistance,  $R_s$ , is subtracted from the total resistance to obtain the polarization resistance,  $R_p$  as shown below.

$$R_p = R_{tot} - R_s \qquad \text{Eq. 3.3}$$

The corrosion current is calculated assuming a proportionality constant, B, of 26 mV, a typical value for actively corroding steel reinforcement in concrete.<sup>17</sup>

$$i_{\text{corr}} = \frac{B}{R_p} \quad \text{Eq. 3.4}$$

where,

$$B = \frac{\beta_a \beta_c}{2.3(\beta_a + \beta_c)} \quad \text{Eq. 3.5}$$

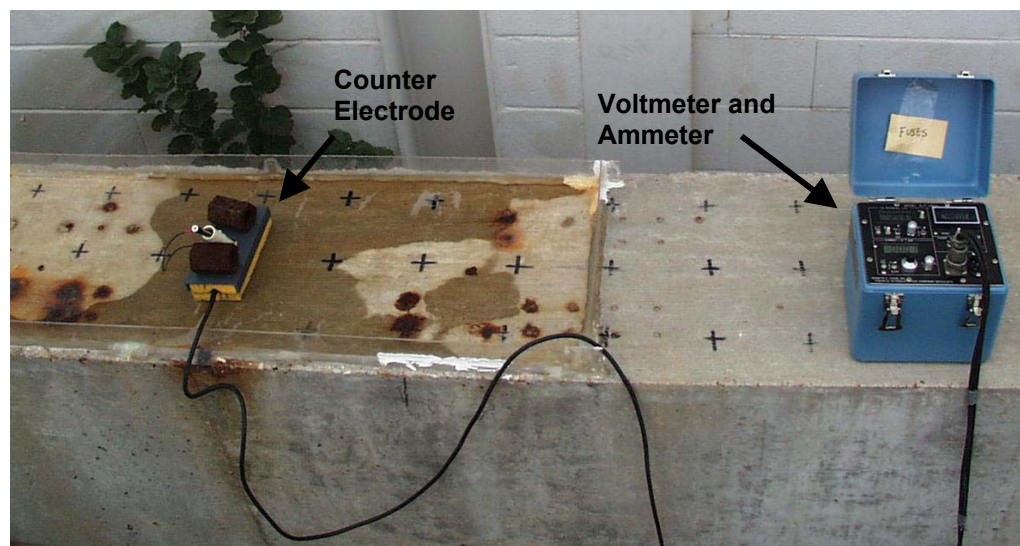
When all measurements and calculations are complete, the computer displays the free corrosion potential, polarization resistance, concrete resistance and corrosion rate in mils per year. This information and the polarization scan data are also written to an output file. The corrosion rate can be converted to current density by dividing the corrosion rate in mils per year by 0.4568.<sup>18</sup> The corrosion current density can also be calculated using the measured polarization resistance and assumed polarized area. (See Equations 3.1 and 3.2) The corrosion severity is assigned based on the ranges listed in Table 3.3.<sup>1</sup>

**Table 3.3: PR Monitor Corrosion Severity Based on Current Density<sup>18</sup>**

<b>Corrosion Current Density (<math>\mu\text{A}/\text{cm}^2</math>)</b>	<b>Corrosion Severity</b>
Less than 0.1	Passive
Between 0.1 and 0.5	Low
Between 0.5 and 1.0	Moderate
Greater than 1.0	High

The 3LP Equipment was developed by Kenneth C. Clear, Inc., USA. A photograph of the equipment and setup is shown in Figure 3.13. The 3LP device is manually operated, and polarization scan data are recorded by hand. The counter electrode is rectangular and current confinement is not provided. The

equipment measures the half-cell potential of the reinforcement (working electrode) and the applied polarization current. The polarization scan uses three steps of 4 mV, starting at the free corrosion potential and ending at +12 mV. The concrete resistance is not measured by the 3LP device. The linear regression analysis on the polarization scan data must be performed using a hand calculator or computer to determine the total resistance,  $R_{tot}$ , as the slope of  $\Delta E$  versus  $\Delta I_{applied}$ . No correction is made for the concrete resistance, and the polarization resistance,  $R_p$ , is simply taken as equal to the total resistance. The manufacturer recommends a proportionality constant,  $B$ , of 40.76 mV for calculating corrosion current. The manufacturer also provides guidance for relating corrosion current densities to expected corrosion damage. The SHRP Procedure Manual for Condition Evaluation of Bridges<sup>19</sup> indicates a proportionality constant,  $B$ , of 26 mV can be used with the 3LP device. The interpretation guidelines listed in Table 3.3 are appropriate for the 3LP device if  $B = 26$  mV is used.<sup>1</sup>



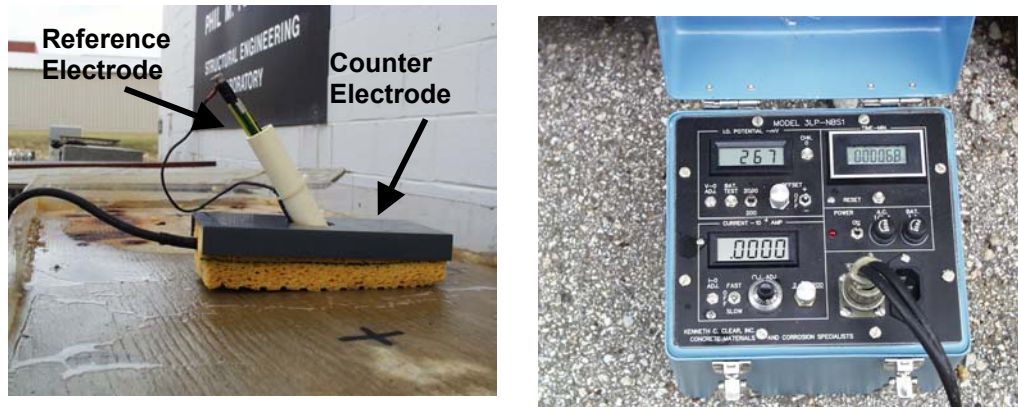


*Figure 3.13: 3LP Equipment and Setup*

### 3.2.5 Chloride Penetration Measurements

#### 3.2.5.1 Theory

By regularly monitoring the penetration of chlorides into the concrete, it is possible to determine when chloride concentrations at the level of the steel reinforcement exceed the threshold for corrosion activity. Although this is not an absolute measurement of corrosion activity, it can be used in conjunction with other data to estimate whether corrosion initiation had occurred.<sup>1</sup>

Chloride penetration is normally measured by collecting and testing samples from the concrete at varied depths. The most common method for obtaining samples is to use a rotary hammer (hammer drill). Holes are drilled in the concrete to the desired depth and the powder is collected for analysis. Samples were analyzed for acid soluble chloride content using a specific ion probe (CL Test System by James Instruments).<sup>1</sup> All sample collection and analysis procedures were based on AASHTO T260-94.<sup>20</sup>

### ***3.2.5.2 Ponding Block Procedure***

The concrete ponding blocks described in Section 3.1.2 were used in this testing program as a non-destructive method of monitoring chloride penetration in the beam specimens during exposure testing. Powder samples were taken periodically from two locations on each block at three depths: 0.5 in. (13 mm), 1 in. (25 mm) and 2 in. (50 mm). The 2 in. depth data represents the chloride concentration at the bar level. The two powder samples per block were combined to give a representative sample at each depth, several acid-soluble chloride tests were run and the results were averaged. After chloride sampling, the drill holes were filled with epoxy.<sup>2</sup>

### ***3.2.5.3 Beam Specimen Procedure***

Concrete powder samples were taken from Specimens 1.3 and 3.3 during the partial autopsy described in Section 3.2.6, and from the beam specimens chosen for final autopsy and analysis at the cessation of exposure testing. During the partial autopsy, samples were taken from three locations: the centerline crack in the ponded region, an uncracked area in the ponded region and 6 in. outside the ponded region. Two holes were drilled at each location and samples were collected at depths of 0.5 in. (13 mm) and 1 in. (25 mm). Samples were not taken at the 2 in. (50 mm) depth so that the reinforcing bars and post-tensioning ducts were not damaged. Analysis of the powder was conducted in the same manner as with the blocks. The samples were combined, tested and the results were averaged.

The procedure used on the beams chosen for final autopsy and analysis was similar to that previously mentioned with only a few minor modifications. It was possible to take samples at the third depth of 2 in. (50 mm) during this procedure since damage to the reinforcing bars or post-tensioning ducts would no



longer affect the corrosion activity of the specimens given that their exposure testing was complete and final autopsy was to immediately follow. Any instance that damage was inflicted on the reinforcing bars or post-tensioning ducts during drilling was recorded and acknowledged during final autopsy and analysis.

The locations and number of samples taken from each beam varied depending on the level of prestress of the specimen and its corresponding reinforcement. While developing the procedure for the autopsy beams, the following topics of investigation were taken into consideration:

- Vertical penetration of chlorides through concrete
- Horizontal penetration of chlorides through concrete
- Ponded versus non-ponded region
- Effect of surface cracking on chloride ingress

Details of the procedure developed to collect concrete samples for the autopsy beams are in Table 3.4. Photographs and diagrams illustrating the sampling locations for the Non-PS and 100%U PS specimens are shown in Figures 3.14 and 3.15. It was determined that only one sample would be taken from the Non-PS and 2/3 PS specimens due to the congestion of reinforcing bars. Minor adjustments in the locations had to be made during sampling due to the uncertainty of the exact positioning of the reinforcement.

**Table 3.4: Procedure for Chloride Penetration Concrete Samples**

Level of PS	Number of Samples	Centerline Offset Along the Length of the Beam	Centerline Offset Along the Width of the Beam	Depths
Non- PS & 2/3 PS	1	2 in. 18 in. 26 in. 32 in.	0 in.	0.5 in. 1 in. 2 in.
100%U PS 100%S PS	2	2 in. 18 in. 26 in. 32 in.	1.75 in. 2.25 in.	0.5 in. 1 in. 2 in.

Conversion Factors: 1 in. = 25.4 mm

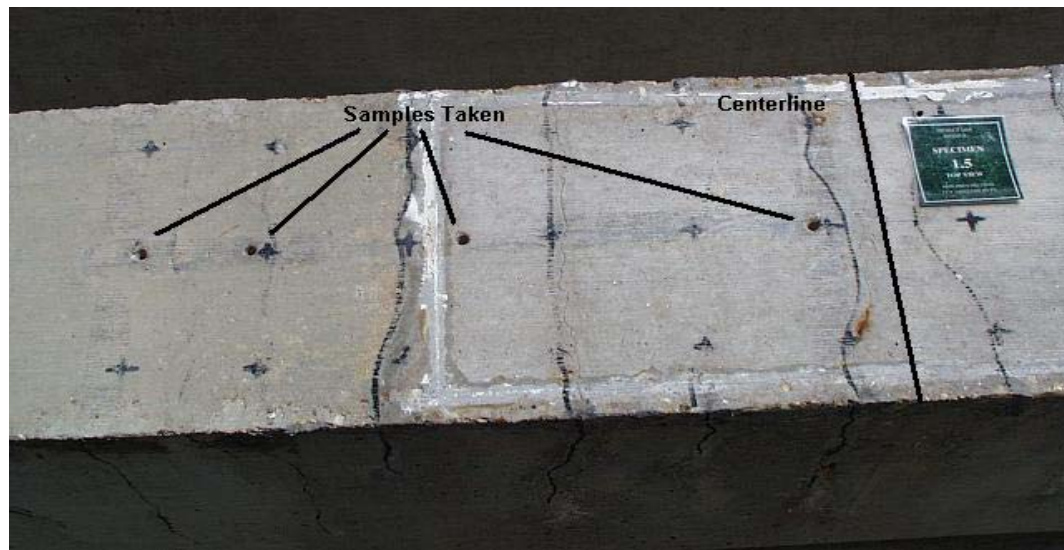
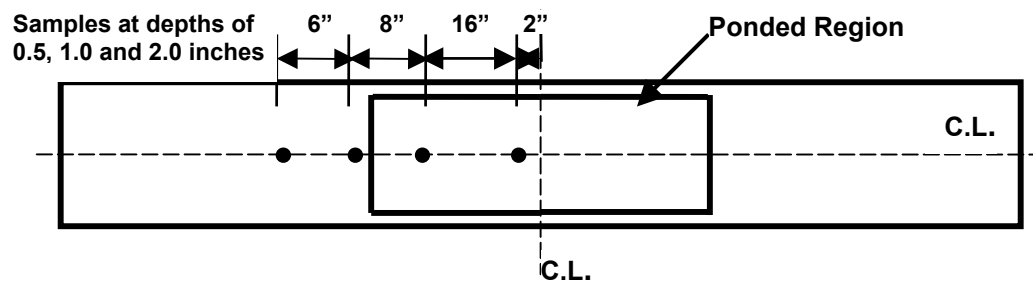


**Figure 3.14: Non-PS Beam Concrete Sample Locations**

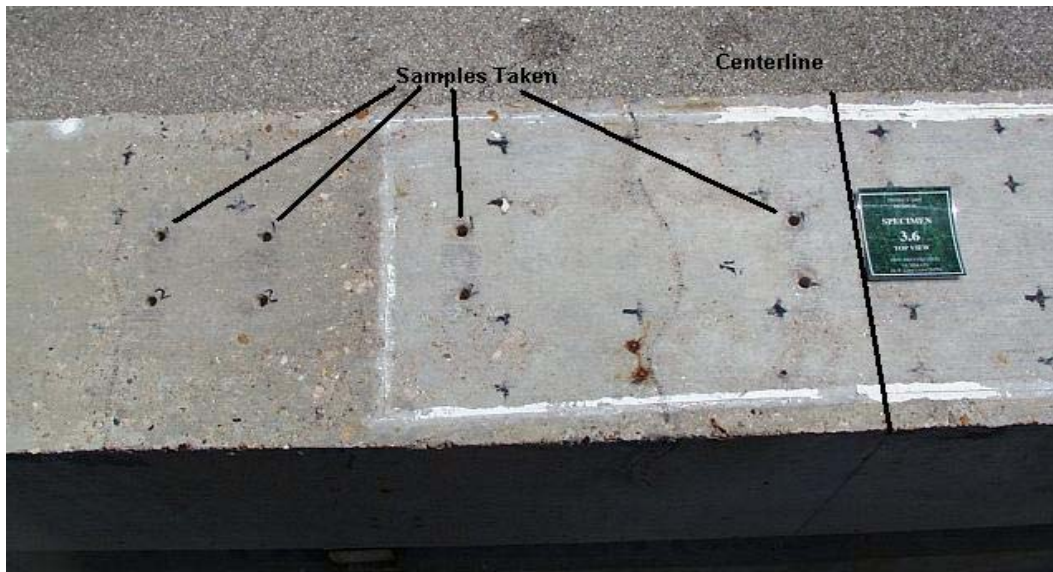
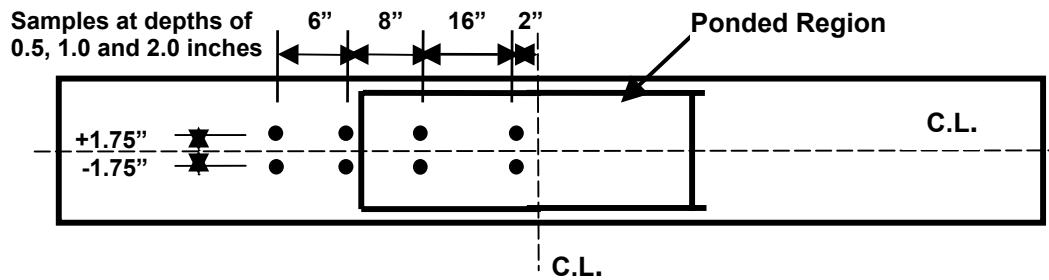


*Figure 3.15: 100%U PS Beam Concrete Sample Locations*

### 3.2.6 Limited Autopsy

In order to monitor the progression of corrosion without completely removing specimens from the testing program, selected beams were chosen for an invasive inspection by limited autopsy. Specimens 1.3 and 3.3 were chosen for invasive inspections. Specimen 3.4 was also inspected at one location where heavy surface staining was evident.<sup>2</sup>

The procedures used in the limited autopsy included concrete sampling for chloride content analysis, as described in Section 3.2.5.3, and a visual inspection of the reinforcement. The latter of the two was accomplished by drilling and hand chipping down to the reinforcement, after which the condition of the steel was examined. The holes were coated with epoxy and filled with a non-shrink grout following completion of the inspection. The data from this inspection was used to check the condition of the beams and to correlate the half-cell potential readings with actual reinforcement condition. Details and results of the partial autopsy and conclusions drawn can be found in Reference 2.

## **CHAPTER 4**

### **Long Term Exposure Test Results and Analysis**

#### **4.1 CRACK WIDTH MEASUREMENTS**

The procedure for taking surface crack width measurements of the beams described in Section 3.2.2 was conducted on two occasions. All of the beams were measured during initial loading of the specimens, and the beams selected for final autopsy and analysis were measured immediately prior to the autopsy. Crack widths were measured using a crack comparator and the unaided eye.

##### **4.1.1 Initial Measurements**

Crack width measurements were taken of all the specimens during initial loading. Note that initial crack width data do not exist for Specimens 1.1 and 3.1 since they are not loaded, and Specimens 3.2, 4.1 and 4.2 since they remained uncracked at service load levels. Figure 4.1 shows typical crack patterns for each of the cracked section types. The cracks are traced in the photographs so that they can be clearly seen. The Non-PS Section shows a textbook type cracking pattern for a reinforced concrete beam in flexure and a large number of cracks. The 2/3 PS section has fewer cracks that are more confined toward the maximum moment region. The 100%U PS section has only three cracks that are confined to the maximum moment region, and the 100%S PS section remains uncracked.<sup>2</sup> Diagrams of initial crack patterns and plots of maximum and minimum measured crack widths at each crack location for each specimen can be found in Reference 1.

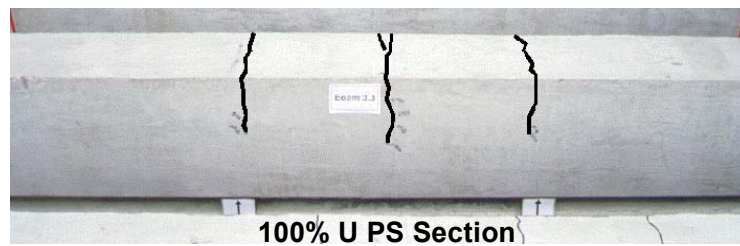
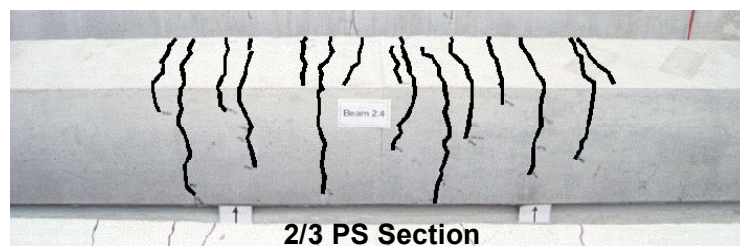
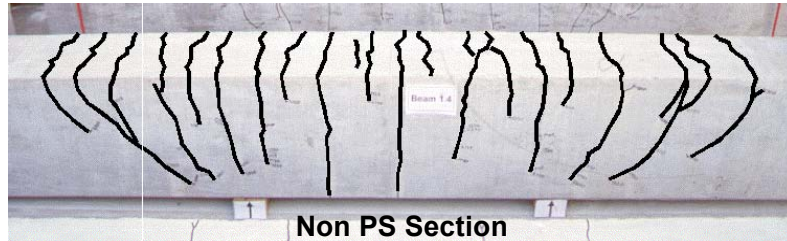


*Figure 4.1: Typical Crack Patterns for Each Section Type<sup>2</sup>*

Plots of measured maximum crack width versus moment for each cracked specimen are shown in Figure 4.2. The plots corresponding to the specimens with TxDOT standard concrete and control variables show excellent agreement with the estimated crack width values calculated prior to loading, using the Gergely-Lutz method. As expected, plots of specimens with variables such as high performance concrete, high performance grout and epoxy-coated strand slightly deviated from the estimated crack width plots.<sup>2</sup> The plots show that as the level of prestress increases, so does the cracking moment. Additionally, as the level of prestress increases, the rate of crack width growth also increases.

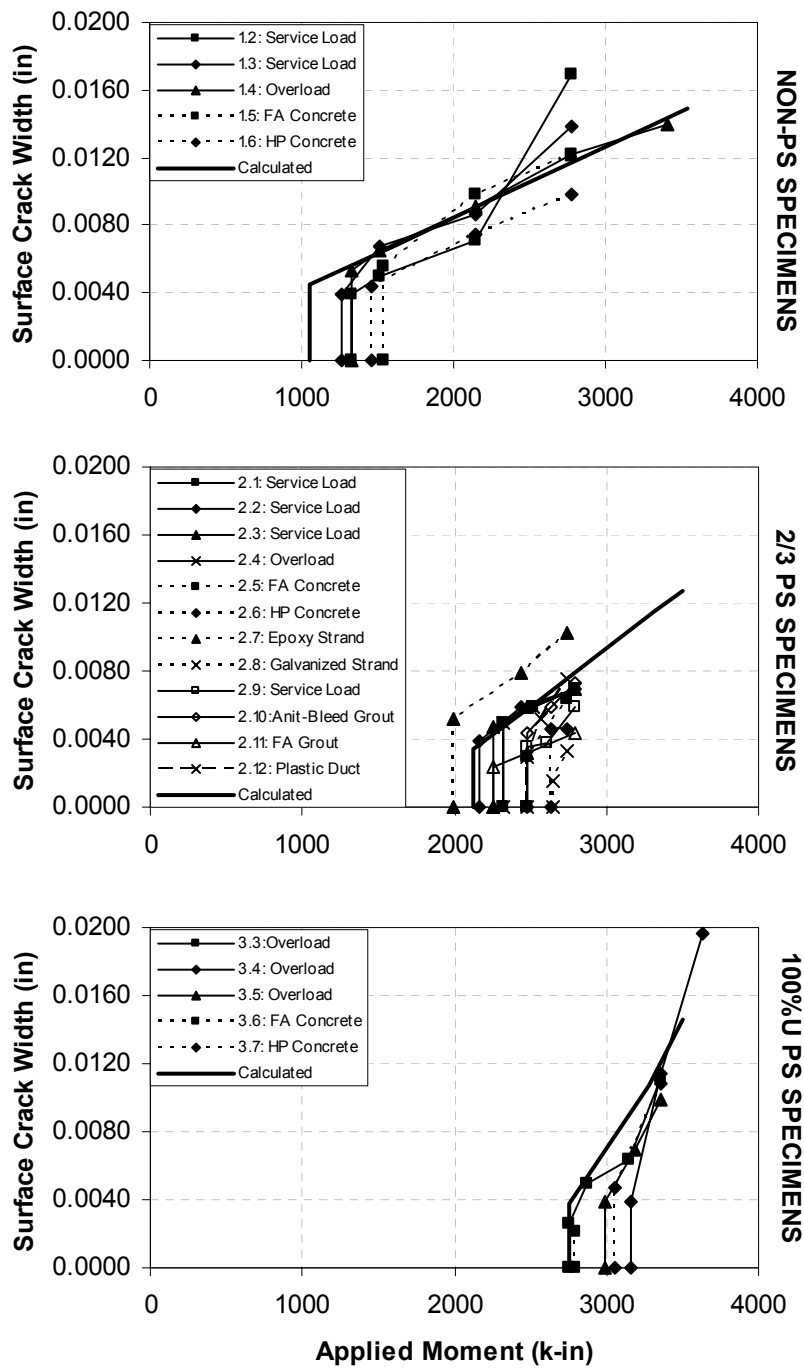


Figure 4.2: Measured Maximum Crack Widths<sup>2</sup>



#### **4.1.2 Final Measurements**

Final crack width measurements were taken of the beams selected for final autopsy and analysis, immediately prior to the autopsy. These measurements were required in order to determine possible correlations between surface cracks and any localized corrosion found during the forensic examination. It is interesting to note those surface cracks present during the final measurements that were not there in the initial measurements. New surface cracks can be associated with the buildup of corrosion products. They typically form parallel to the reinforcement, appearing as horizontal cracks on the tension surface of the specimen. The origin of new surface cracks can be determined from the forensic examination. It is also possible that any increase in crack width from the initial measurements could be due to creep.

Crack patterns on the tension face and side face of the beam, and a plot of the maximum and minimum crack width measurements at each crack location are shown in Figures 4.3-4.5. An example of each beam type from Phase II was chosen for these Figures. A diagram and plot for each autopsy specimen can be found in Appendix C. The same figures from the initial crack width measurement can be found in West.<sup>1</sup> Figures 4.3-4.5 follow the typical cracking patterns described above. Note that initial crack width data did not exist for Specimens 3.2 and 4.2, since they remained uncracked under service load levels. However, although minimal, final crack width data does exist for these two specimens. The cracking of these specimens could be due to one of the previously mentioned reasons. The exact cause for additional cracks or increased crack widths in any of the beams can be determined after the forensic examination.

**Beam 1.5: Non-PS - Constant Service Load**

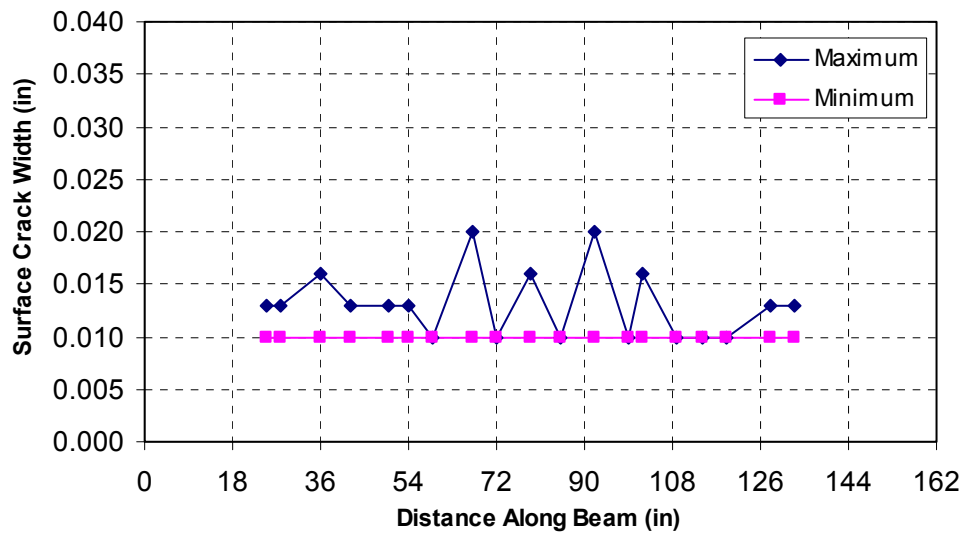
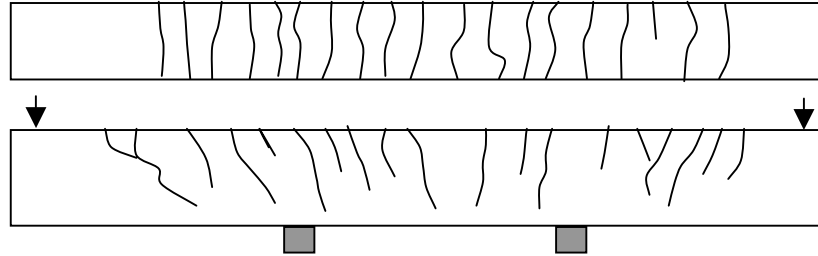


**Figure 4.3: Non-PS Section – Crack Patterns and Measurements**

**Beam 2.5: 2/3 PS - Constant Service Load**

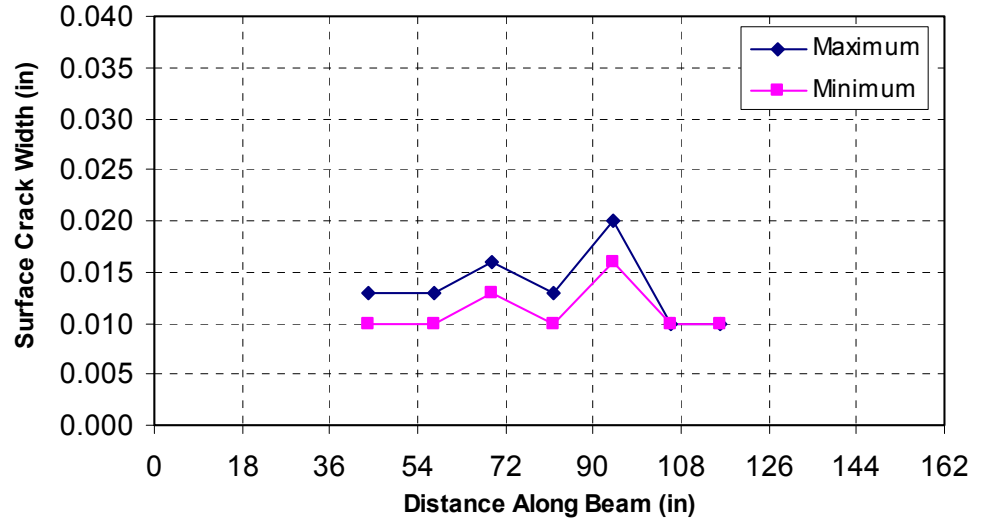
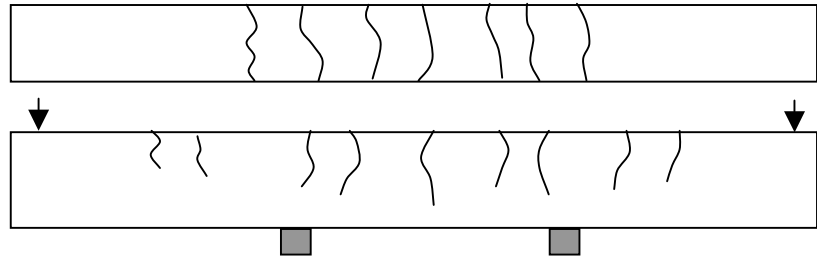


**Figure 4.4: 2/3 PS Section – Crack Patterns and Measurements**

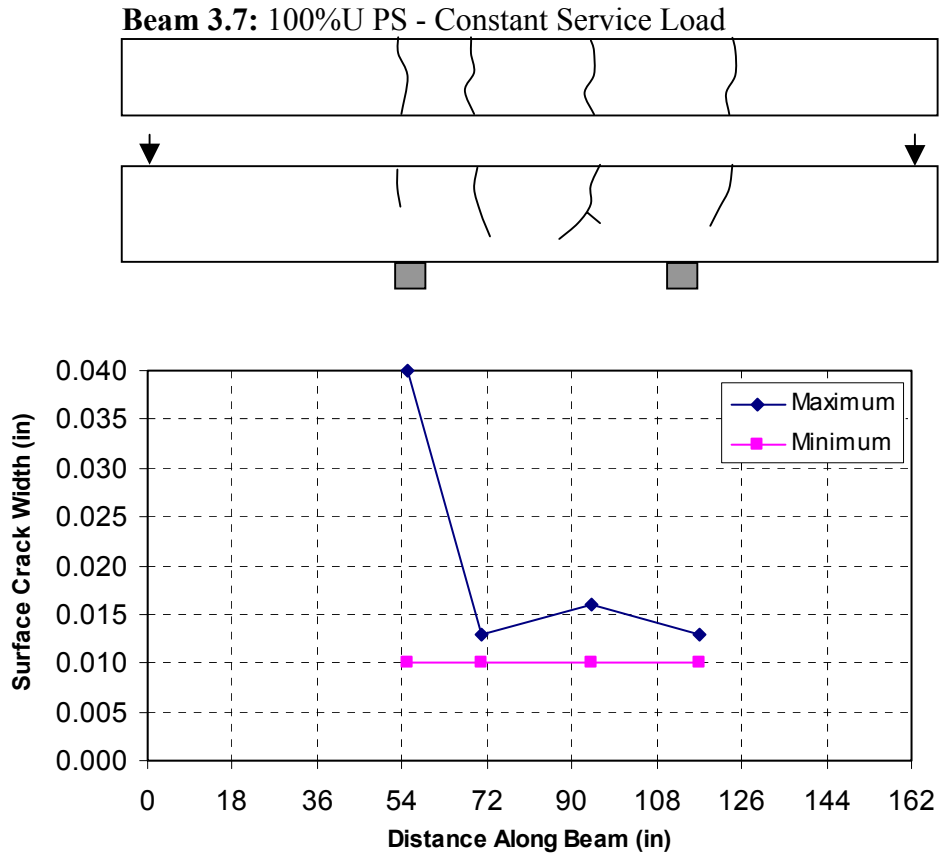


**Figure 4.5: 100%U PS Section – Crack Patterns and Measurements**

Figure 4.6 is a graph of the maximum measured crack width and the average of the maximum crack widths from each crack for the Phase I beams. Comparison of the maximum crack widths shows no difference between the Non-PS and 2/3 PS beams, but illustrates a small decrease in the 100% PS beams. The average maximum crack widths of the Phase I beams are almost identical, with Specimen 2.3 standing out as having the largest average maximum crack width. Figure 4.6 shows a slight trend of decreasing maximum crack widths as the level

of prestress increases. However, the variation in the maximum and average maximum crack widths among the Phase I beams is small and could be considered insignificant. The similarity of the crack widths are most likely due to the lack of precision of the crack comparator and unaided eye used to take the measurements.

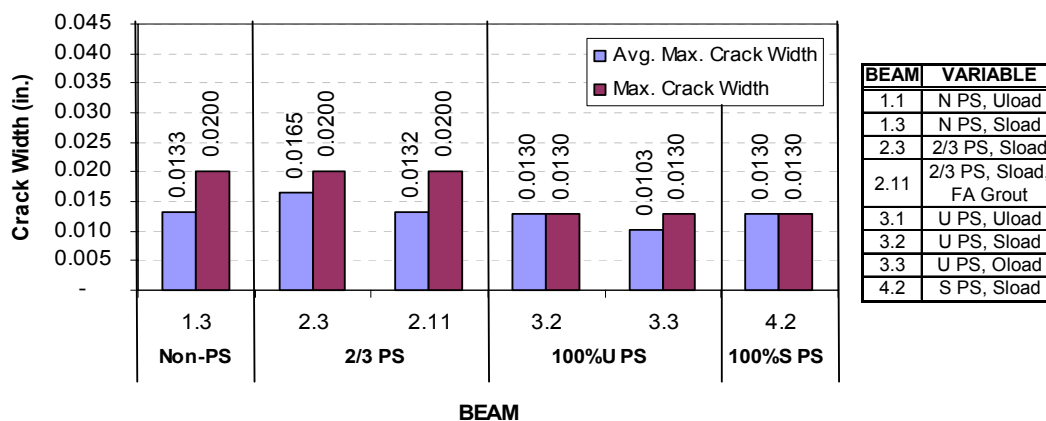


**Figure 4.6: Crack Widths – Phase I Beams**

Figure 4.7 is a graph of the maximum measured crack width and the average of the maximum crack width from each crack for the Phase II beams. Comparison of the maximum crack widths does not show a direct correlation between the crack width and level of prestress, or a consistent one between the crack width and type of concrete. Note the significant difference in the maximum for Specimen 3.7. The maximum initial crack width for this specimen was 0.018 inches. This could be of great interest when compared to the results of the forensic examination to determine the cause of the increased crack width. The average maximum crack widths of the Phase II beams show an increase in crack width as the level of prestress increases. Again, the differences in the maximum

and average maximum crack widths among the Phase II beams are also small and could be considered insignificant.

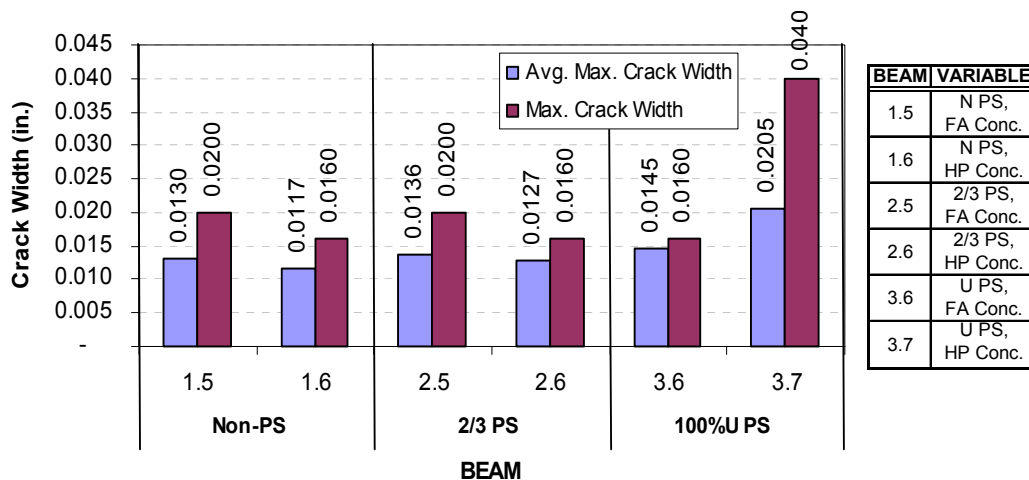


*Figure 4.7: Crack Widths – Phase II Beams*

## 4.2 HALF-CELL READINGS

The procedure for taking half-cell potential readings is explained in Section 3.2.3. Readings were taken of each beam specimen once every four weeks at the end of the wet interval of the cyclic wet-dry exposure regimen. The graphs presented in this section include readings of the specimens beginning at their initiation of exposure testing through May 2002. This is when exposure testing

ceased for the specimens chosen for the forensic examination. Because specimens from Phase I and Phase II have significantly different exposure durations, attempting to compare their data would produce erroneous results. Therefore, data from each Phase will always be presented separately.

The potentials plotted in this section are the highest value for a given specimen on a given day. The average half-cell potentials from the ponded region and the highest values follow the same trend, thus it was decided to plot the highest values.<sup>2</sup> The ASTM guidelines for interpreting half-cell potentials<sup>12</sup> (see Table 3.2) are indicated on the figures.

Readings were not available over a period of approximately seven months due to maintenance necessities of the specimens. The gap in each plot is a result of these missing readings. Over the course of exposure testing complications with the equipment used to take half-cell readings commonly arose. Although measures to correct these problems were taken when they occurred, there was always some uncertainty of the accuracy of the readings. This is why it was necessary to examine each specimen's plot and determine the outliers. The outliers are simply readings that obviously do not follow the trend of the rest of the plot. Due to each outlier's significant deviation from the trend, it was decided to replace the reading with an interpolation between the two adjacent readings. It is important to emphasize that any reading labeled as an outlier was done so only due to the unreliability of the equipment. A list of the each outlier and its initial and altered reading can be found in Appendix D.

Half-cell potential maps showing the readings as a contour plot over the specimen grid area were created for the beams. By ASTM standards,<sup>12</sup> potential ranges have been developed to assign each area a probability of corrosion. Each potential range was assigned a color to easily illustrate the probabilities as a map

on the tension face of the specimen. Table 4.1 lists the potential ranges, and the color and probability of corrosion activity assigned to each range.

**Table 4.1: Half-Cell Potential Map Designations**

<b>Potential Range</b>	<b>Color</b>	<b>Probability</b>
> -580 V <sub>SCE</sub>	Purple	Extremely High
-430 to -580 V <sub>SCE</sub>	Red	Very High
-280 to -430 V <sub>SCE</sub>	Orange	High
-130 to -280 V <sub>SCE</sub>	Yellow	Uncertain
+20 to -130 V <sub>SCE</sub>	Light Blue	Low

It is important to emphasize that half-cell potentials are only an indicator of corrosion activity, and a correlation with corrosion rate cannot be made. The ASTM C876 guidelines only indicate the probability of corrosion. Very negative potentials can be used to suggest a higher probability of corrosion activity, but not necessarily a higher corrosion rate. Many factors can influence measured half-cell potentials, including concrete cover thickness, concrete resistivity, concrete moisture content, different metals and availability of oxygen. In some cases, these factors can lead to very negative half-cell potentials with little or no corrosion activity. For this reason, it is important to consider the variation of half-cell potential measurements over an extended period of time in addition to the magnitude of the readings.<sup>1</sup>

A common trait observed in corrosion research is the length of time prior to the onset of corrosion activity. This can be determined based on the either of the following:

1. A sudden and significant change (more negative) in half-cell potential
2. Half-cell potential measurements more negative than -280 mV

The half-cell potential plot for each beam specimen was examined so that a time to initiation of corrosion could be determined. When it is concluded that corrosion



activity is highly probable during exposure testing, it is difficult to determine which element (stirrups, rebars, ducts or prestressing strands) is corroding because they are all electrically connected. This uncertainty can be resolved during the forensic examination.

#### **4.2.1 Phase I Beams**

This section discusses the half-cell potential readings of the Phase I autopsy beams only. Half-cell potential plots for all of the Phase I beams can be found in Appendix D. The Phase I autopsy specimens began exposure testing in December of 1997 and concluded in May 2002 after 1594 days of testing. Figure 4.8 is a plot of the Phase I autopsy beams. It shows that after 1594 days of exposure, all of the Phase I beams, with the exception of Specimen 3.1, have a greater than 90% probability of corrosion. It is difficult to determine additional trends among the specimens from this plot. Therefore, plots separating the autopsy specimens according to the main variables examined in Phase I of the experimental program are given in Figures 4.9-4.13 for ease of analysis.

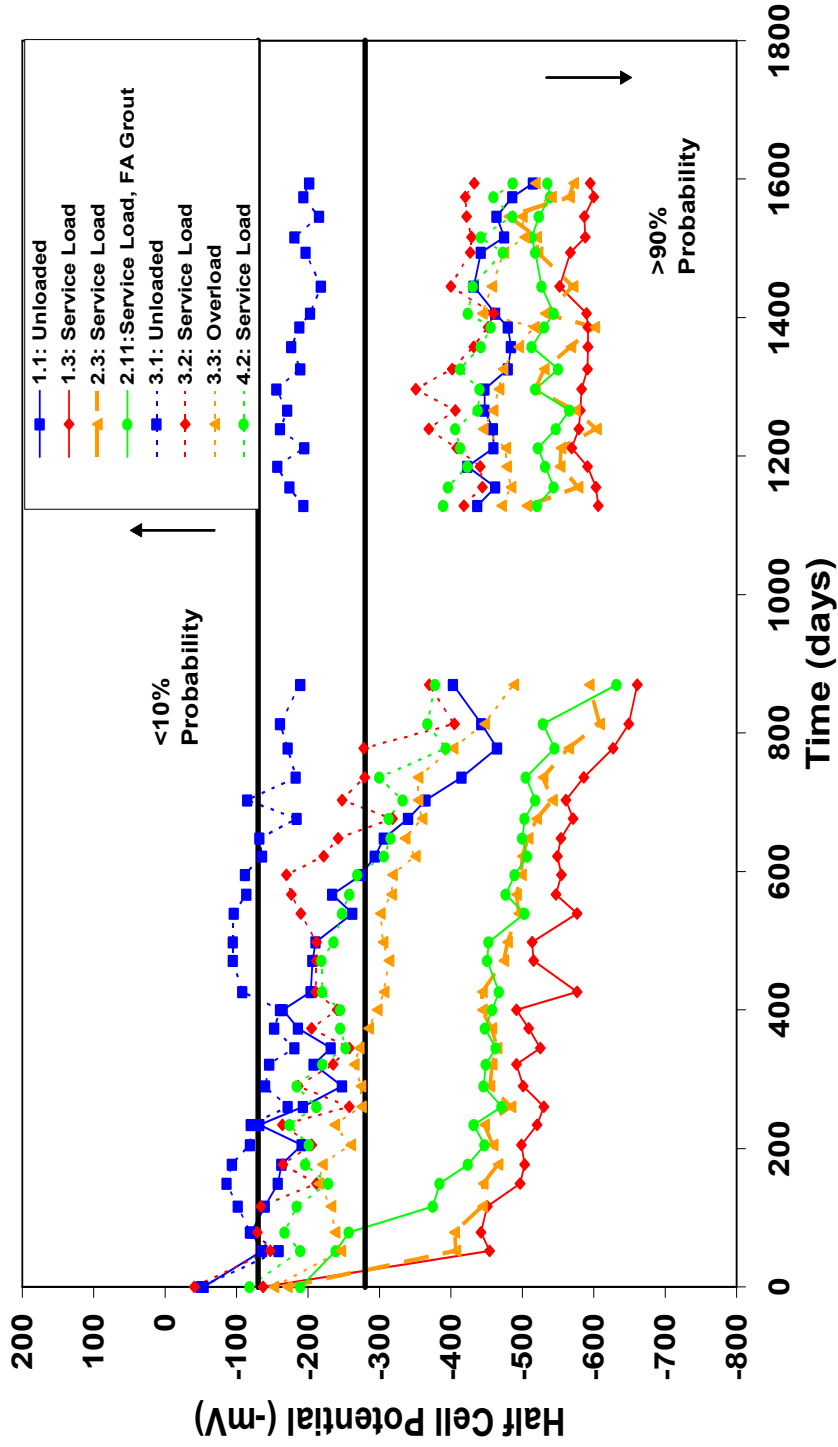
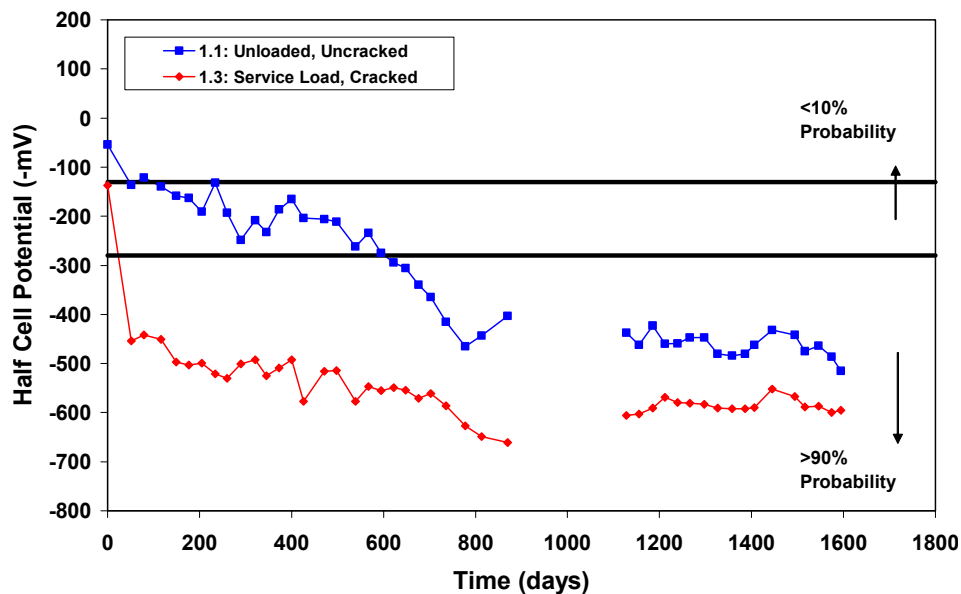


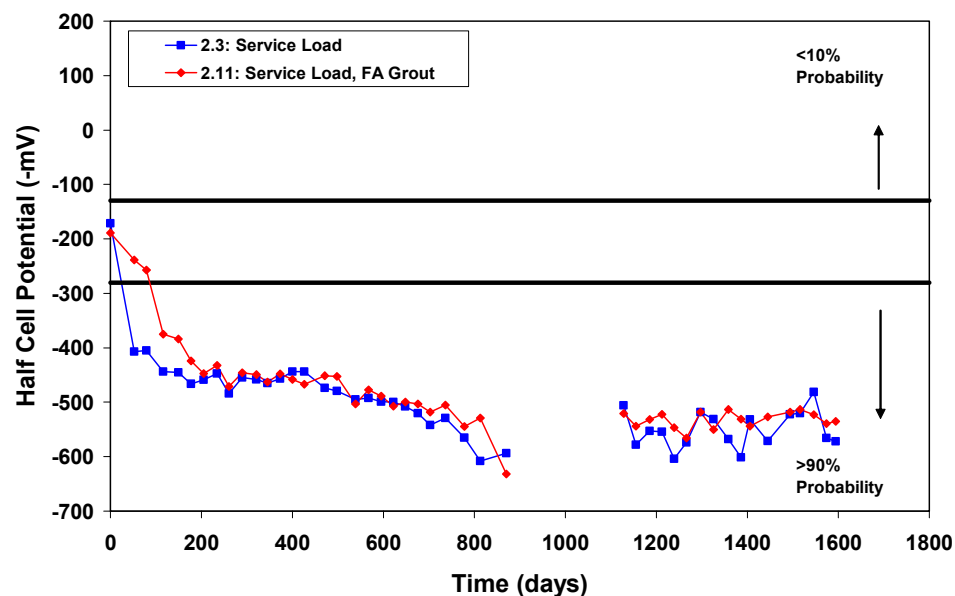
Figure 4.8: Half-Cell Potential Readings  
(Phase I Autopsy Beams)

Figure 4.9 shows a plot of the Non-PS beams in Phase I. All the details of Specimens 1.1 and 1.3 are identical, with the exception of the applied load and cracking. It clearly shows a decrease in corrosion protection performance when the beam is loaded through the significant difference in time to initiation of corrosion and final half-cell potentials. It is impractical to assume any structural element would be completely unloaded. Specimen 1.1 was only used to illustrate the effect of cracking on corrosion protection in comparison to an identical loaded specimen.



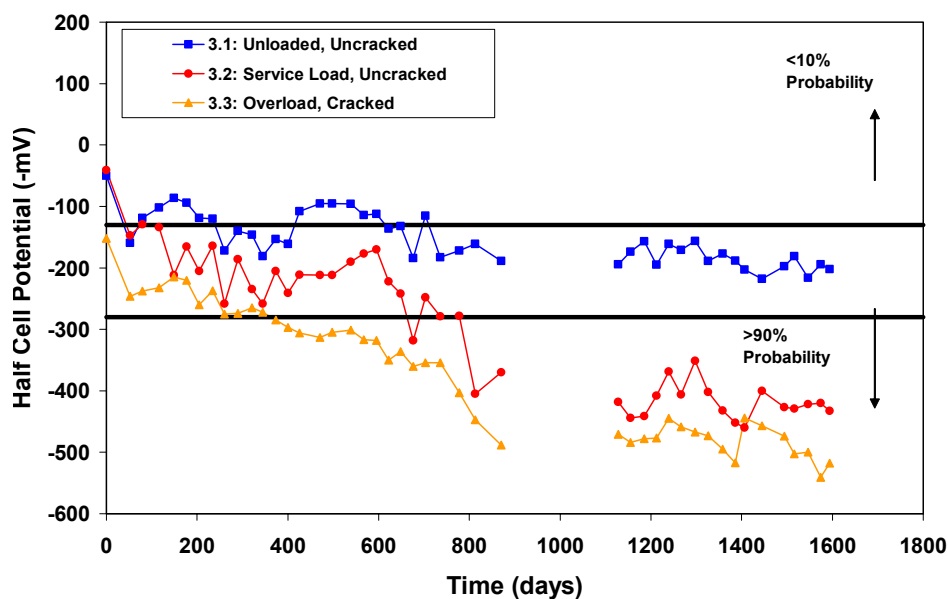
**Figure 4.9: Half-Cell Potential Readings  
(Phase I Autopsy Beams – Non-PS)**

Figure 4.10 shows a plot of the 2/3 PS beams in Phase I. All the details of Specimens 2.3 and 2.11 are identical, with the exception of the grout type. It does not show that the grout type has any effect on corrosion protection. While this may be true, it is also possible that the readings were measuring the potential of the mild steel reinforcement. If this is the case, then it would be expected that the specimens perform similarly since the grout type does not effect the protection of the mild steel. The results from the forensic examination will either confirm or disprove this conclusion.



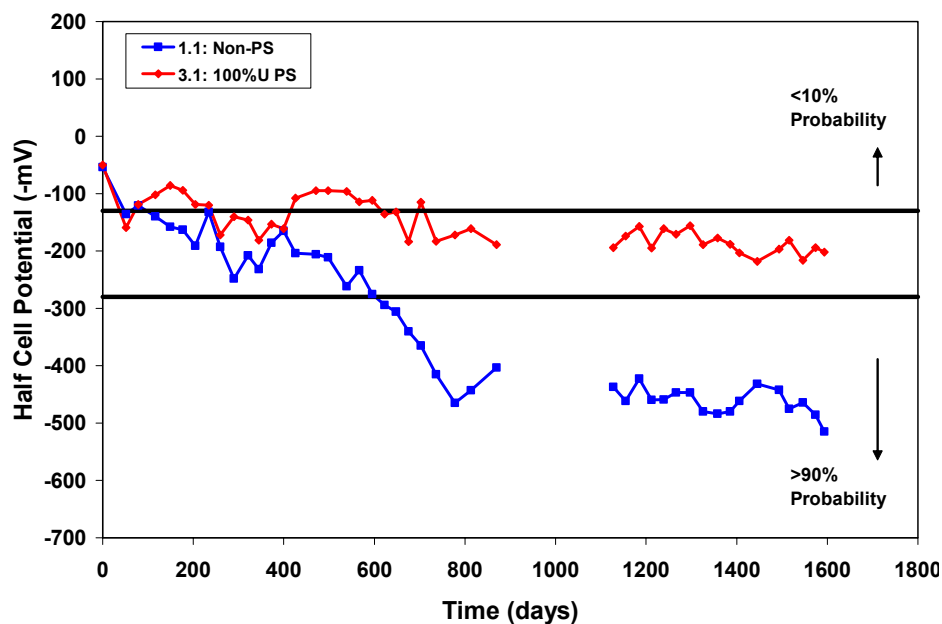
**Figure 4.10: Half-Cell Potential Readings  
(Phase I Autopsy Beams – 2/3 PS)**

Figure 4.11 shows a plot of the 100%U PS beams in Phase I. All the details of Specimens 3.1, 3.2 and 3.3 are identical, with the exception of the applied load and cracking. As expected, the performance of the specimens decreases as the load applied increases. Specimen 3.1 never crosses the greater than 90% probability of corrosion threshold. Comparison of Specimens 3.2 and 3.3 again shows an increase in corrosion protection when the specimen is uncracked through both time to initiation of corrosion and final potential readings. Note that, although Specimen 3.2 was designed to be uncracked, final crack width measurements found one crack on the specimen. The possible effect of this one crack on the corrosion protection of the specimen will be determined from the forensic examination.



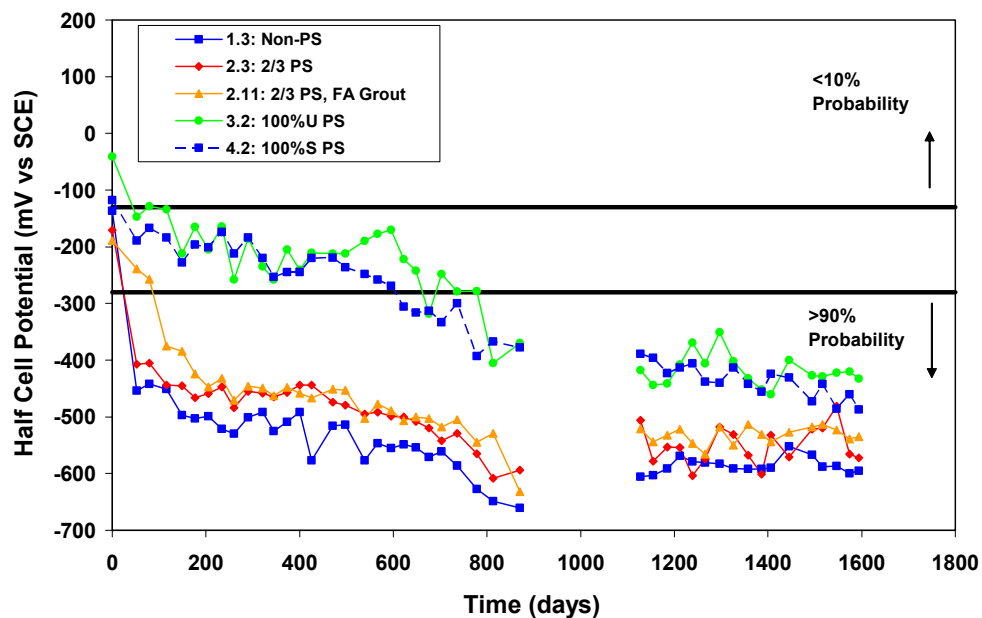
**Figure 4.11: Half-Cell Potential Readings (Phase I Autopsy Beams – 100%U PS)**

Figure 4.12 shows a plot of the unloaded beams in Phase I. All the details of Specimens 1.1 and 3.1 are identical, with the exception of the level of prestress. As expected, the 100%U PS beam performed better than the Non-PS beam as it did not even cross the greater than 90% probability of corrosion threshold. It is interesting to note the significantly high potential readings for Specimen 1.1 since it is unloaded and uncracked. This could suggest importance of concrete permeability and the effect of increased compressive stresses in the concrete prestressing since the only possible form of chloride ingress for this specimen is through the concrete.



**Figure 4.12: Half-Cell Potential Readings  
(Phase I Autopsy Beams – Unloaded)**

Figure 4.13 shows a plot of the service load beams in Phase I. All the details of Specimens 1.3, 2.3, 3.2 and 4.2 are identical, with the exception of the level of prestress. As expected, performance increases as the level of prestress increases. The difference in the time to the initiation of corrosion for the 2/3 PS and 100%U and S PS is significant. The trend shows that a 2/3 PS beam performs more similarly to a Non-PS beam than a 100% PS beam. Comparison of Specimens 3.2 and 4.2 shows a slightly better performance of the 100%S PS design as opposed to the 100%U PS through the final potential reading. However, both designs have the same time to initiation of corrosion.



**Figure 4.13: Half-Cell Potential Readings (Phase I Autopsy Beams – Service Load)**

Figure 4.14 is a graph of the highest half-cell potential for the final readings of the Phase I autopsy specimen. Figure 4.15 shows the half-cell potential contour maps for all the Phase I beams after 1594 days of exposure

testing. (Additional contour plots of all the Phase I specimens after 498 days of exposure can be found in Appendix D) Figure 4.16 is a plot of the time to initiation of corrosion activity determined for each Phase I autopsy specimen. The length of time for each beam was designated as the day the half-cell potential reading was more negative than -280 mV, indicating a probability of corrosion greater than 90%. Figures 4.14, 4.15 and 4.16 are just another way of illustrating the following conclusion drawn from the half-cell potential plots:

- Specimen performance increases as the applied load decreases
- Specimen performance is worse when cracking is present
- Specimen performance increases as the level of prestress increases
- Performance of a 2/3 PS specimen is more similar to that of a Non-PS specimen as opposed to a 100% PS specimen
- No significant difference in performance of 100%U and S PS specimens

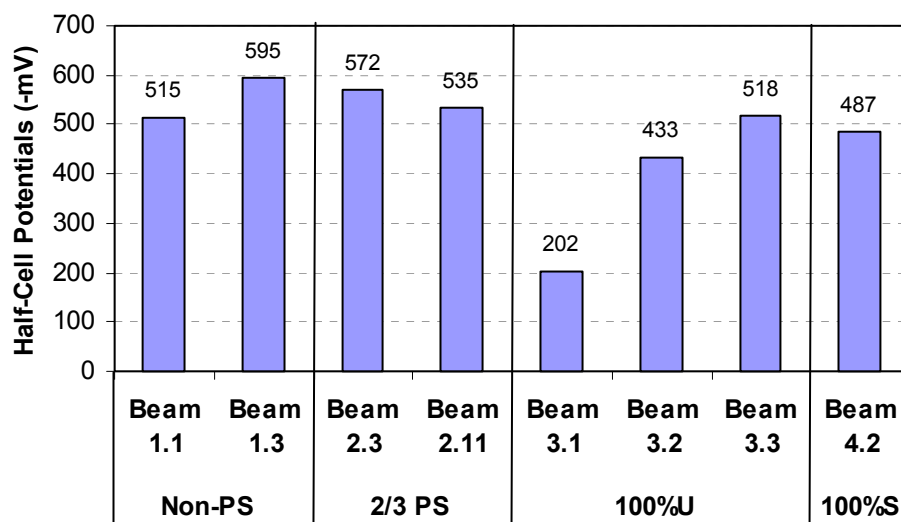


**Figure 4.14: Highest Average Half-Cell Potential Reading at 1594 Days (Phase I Autopsy Beams)**



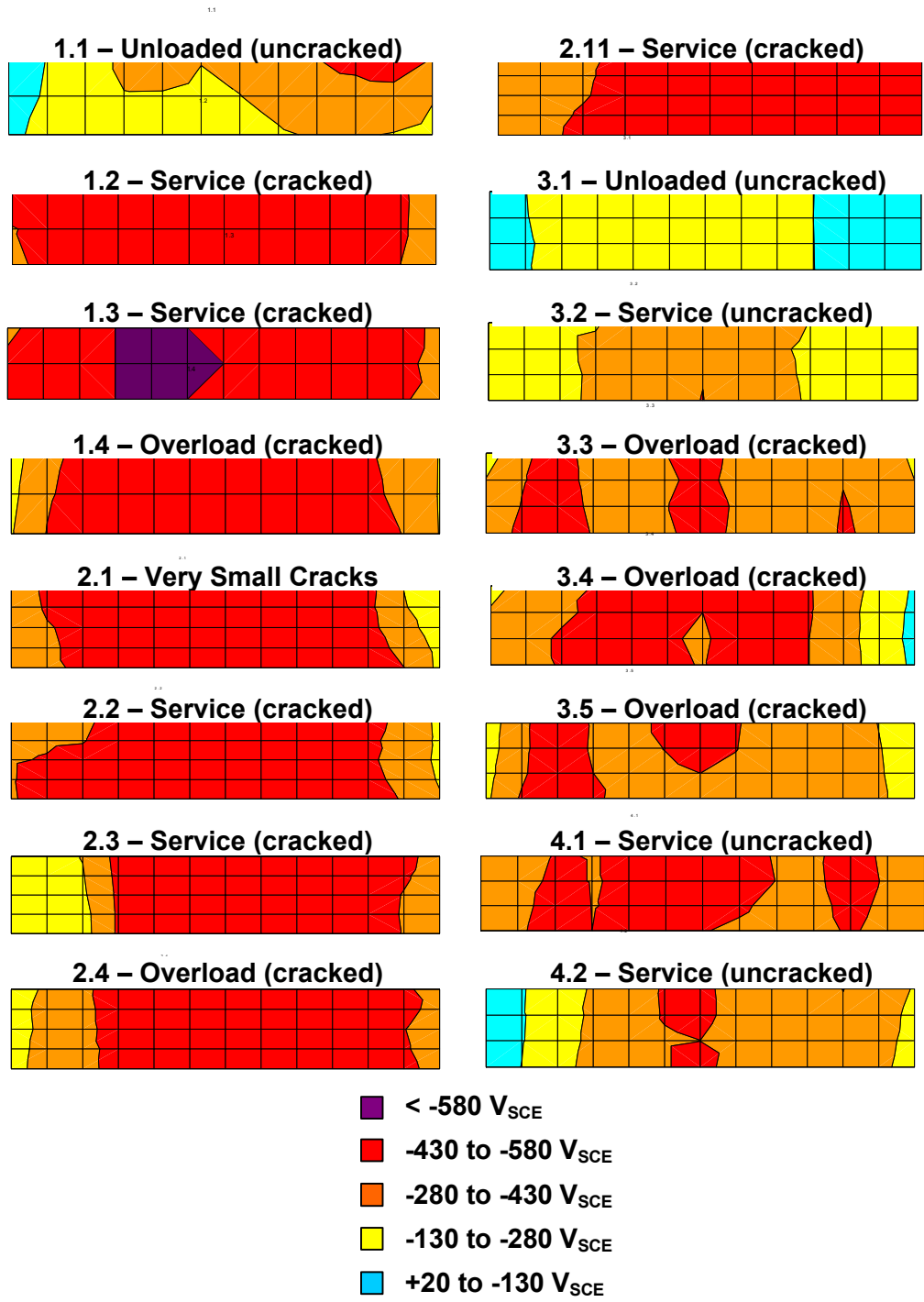


*Figure 4.15: Half-Cell Potential Contour Plots at 1594 Days  
(All Phase I Beams)*

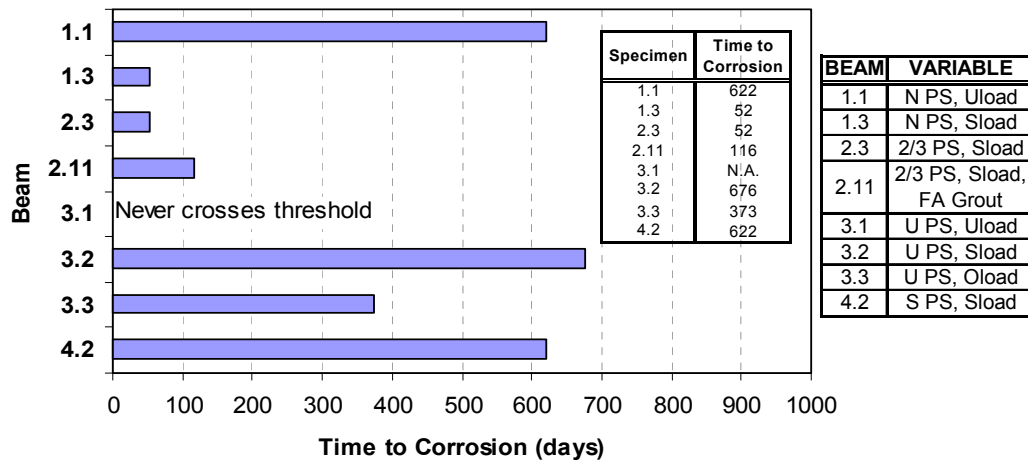


**Figure 4.16: Time to Initiation of Corrosion (Phase I Beams)**

#### 4.2.2 Phase II Beams

This section discusses the half-cell potential readings of the Phase II autopsy beams only. Half-cell potential plots for all of the Phase II beams can be found in Appendix D. The Phase II autopsy specimens began exposure testing in December of 1998 and concluded in May 2002 after 1235 days of testing. Figure 4.17 is a plot of all of the Phase II autopsy beams. It shows that after 1235 days of exposure, all of the Phase II beams have a greater than 90% probability of corrosion. It is difficult to determine additional trends among the specimens from this plot. Therefore, plots separating the autopsy specimens according to the main variables examined in Phase II of the experimental program are given in Figures 4.18-4.22 for ease of analysis.

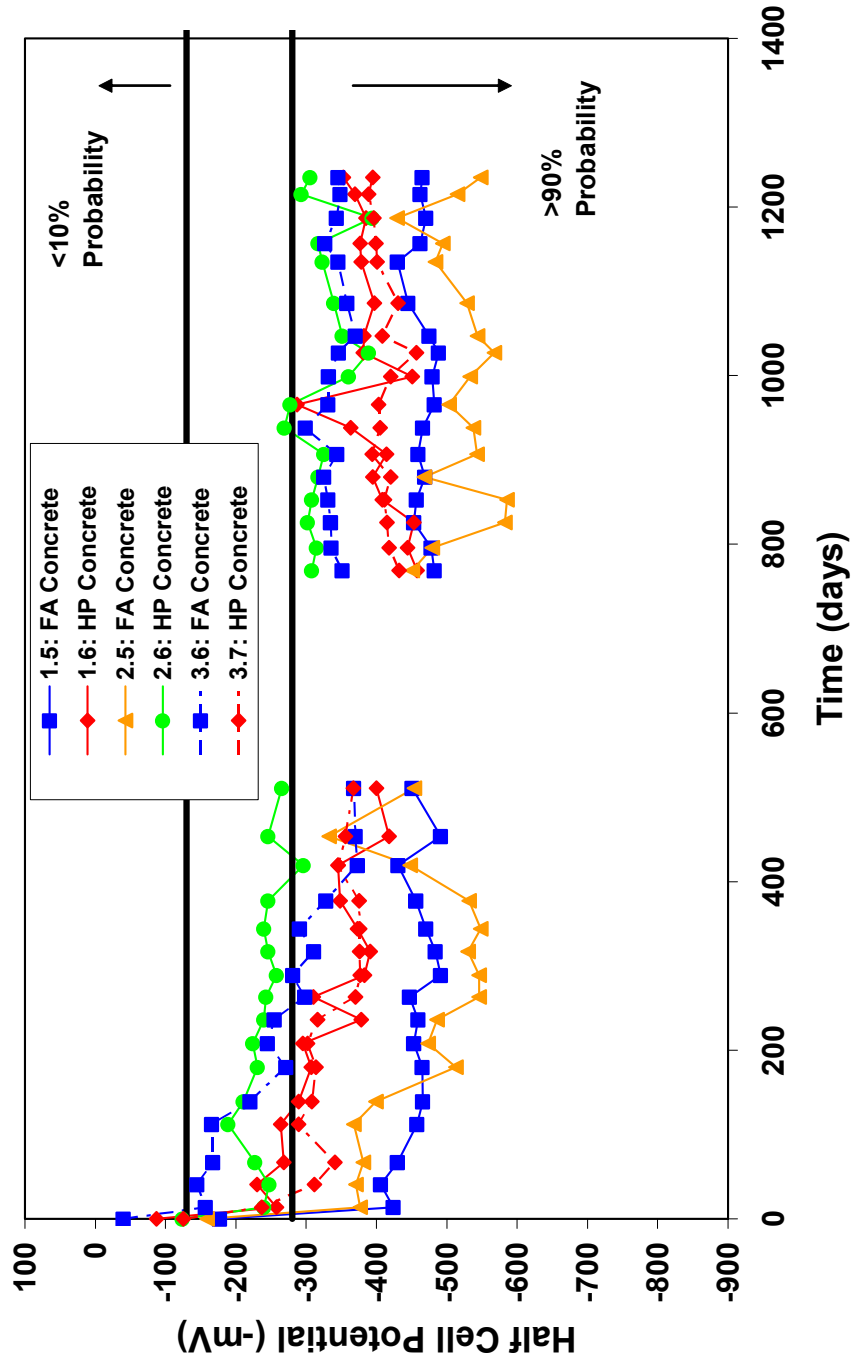
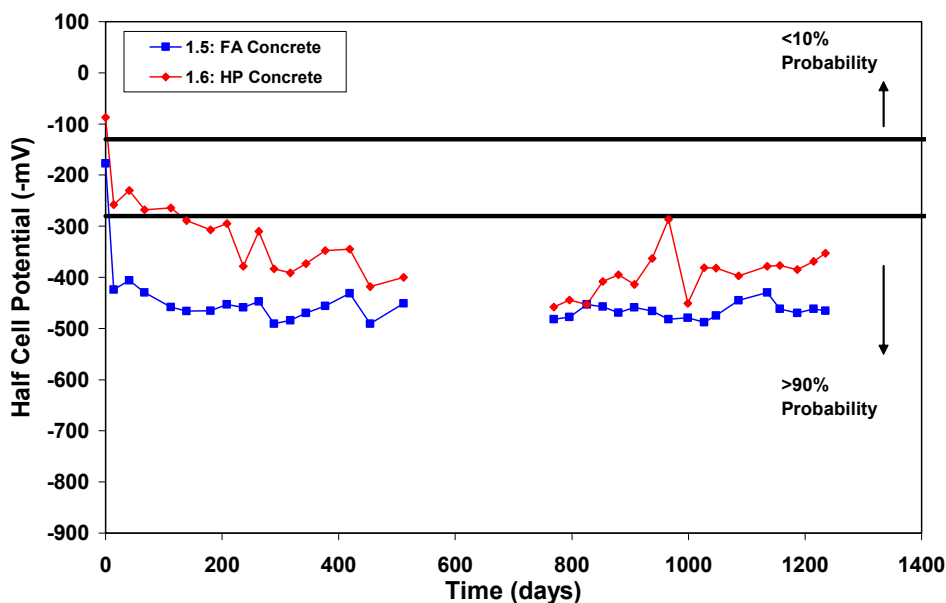


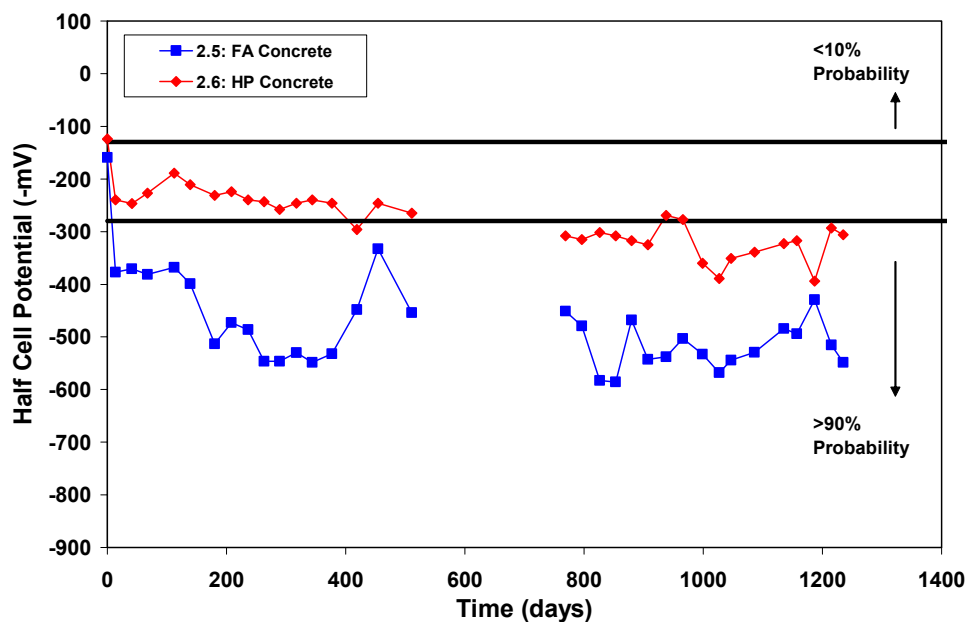
Figure 4.17: Half-Cell Potential Readings  
(Phase II Autopsy Beams)

Figure 4.18 shows a plot of the Non-PS beams in Phase II. All the details of Specimens 1.5 and 1.6 are identical, with the exception of the concrete type. According to the potential readings and time to initiation of corrosion, the high performance concrete performed better than the fly ash concrete. However, it appears that over time they begin to merge to follow the same trend.



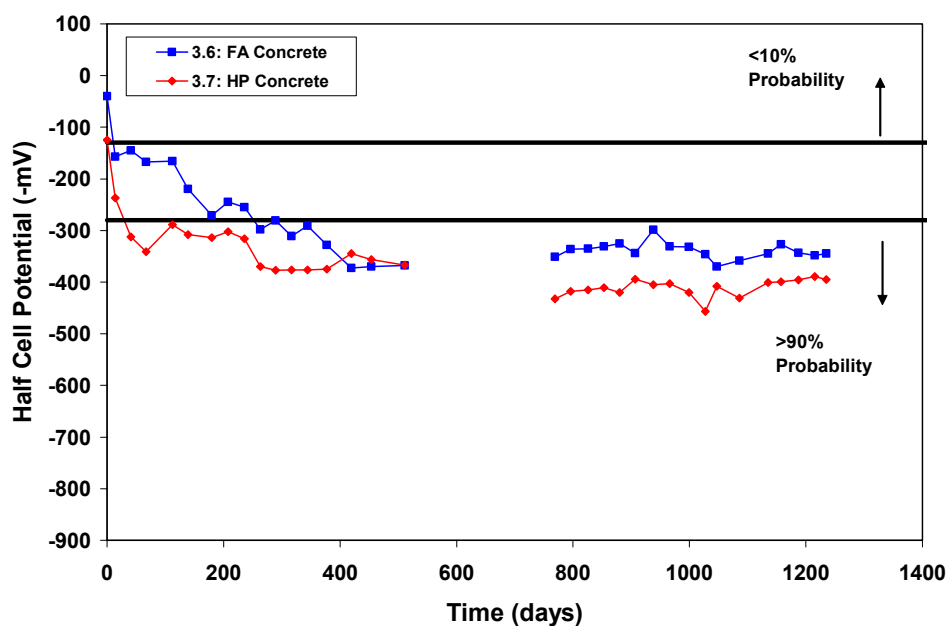
**Figure 4.18: Half-Cell Potential Readings (Phase II Autopsy Beams – Non-PS)**

Figure 4.19 shows a plot of the 2/3 PS beams in Phase II. All the details of Specimens 2.5 and 2.6 are identical, with the exception of the concrete type. According to the potential readings and time to initiation of corrosion, the high performance concrete performed better than the fly ash concrete. These specimens do not appear to be merging together as much as in the previous plot. (Readings taken at 1187 days appear to be outliers since they do not follow the trend of the rest of the plot.)



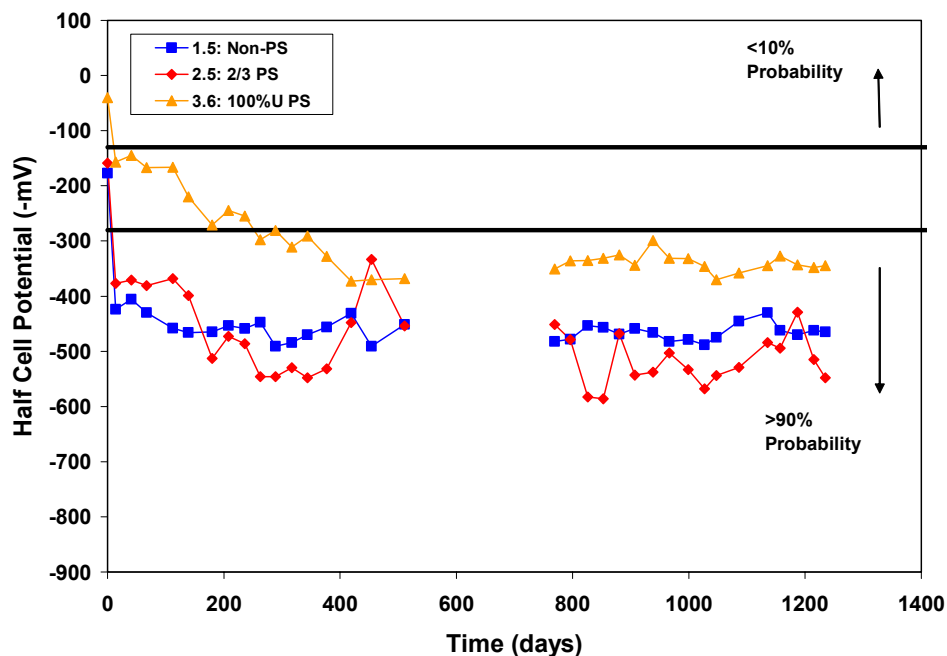
**Figure 4.19: Half-Cell Potential Readings  
(Phase II Autopsy Beams – 2/3 PS)**

Figure 4.20 shows a plot of the 100%U PS beams in Phase II. All the details of Specimens 3.6 and 3.7 are identical, with the exception of the concrete type. The results of the comparison of these two specimens differs from the previous two. According to the potential readings and time to initiation of corrosion, the fly ash concrete performed better than the high performance concrete. However, the difference between them is not significant and they appear to be merging together.



**Figure 4.20: Half-Cell Potential Readings (Phase II Autopsy Beams – 100%U PS)**

Figure 4.21 shows a plot of the fly ash concrete beams in Phase II. All the details of Specimens 1.5, 2.5 and 3.6 are identical, with the exception of the level of prestress. According to the potential readings and time to initiation of corrosion, the 100%U PS beam performed much better than the Non-PS and 2/3 PS beams. Both the Non-PS and 2/3 PS beams have the same time to initiation of corrosion. Although the final potential reading of the 2/3 PS beam is more negative than that of the Non-PS beam, the difference between the potentials is minimal and the superior level of prestress between the two varies with time.



**Figure 4.21: Half-Cell Potential Readings (Phase Autopsy II Beams – Fly Ash Concrete)**

Figure 4.22 shows a plot of the high performance concrete beams in Phase II. All the details of Specimens 1.6, 2.6 and 3.7 are identical, with the exception of the level of prestress. According to the final potential readings and time to initiation of corrosion, the 100%U PS beam performed the worst and the 2/3 PS beam performed the best. However, the difference among the final potential readings is minimal.

A comparison of Figures 4.21 and 4.22 implies that the overall performance of the high performance concrete was slightly better than the fly ash concrete, as the final potential readings of the high performance concrete beams was close to or less negative than the least negative final reading of the fly ash concrete beams.

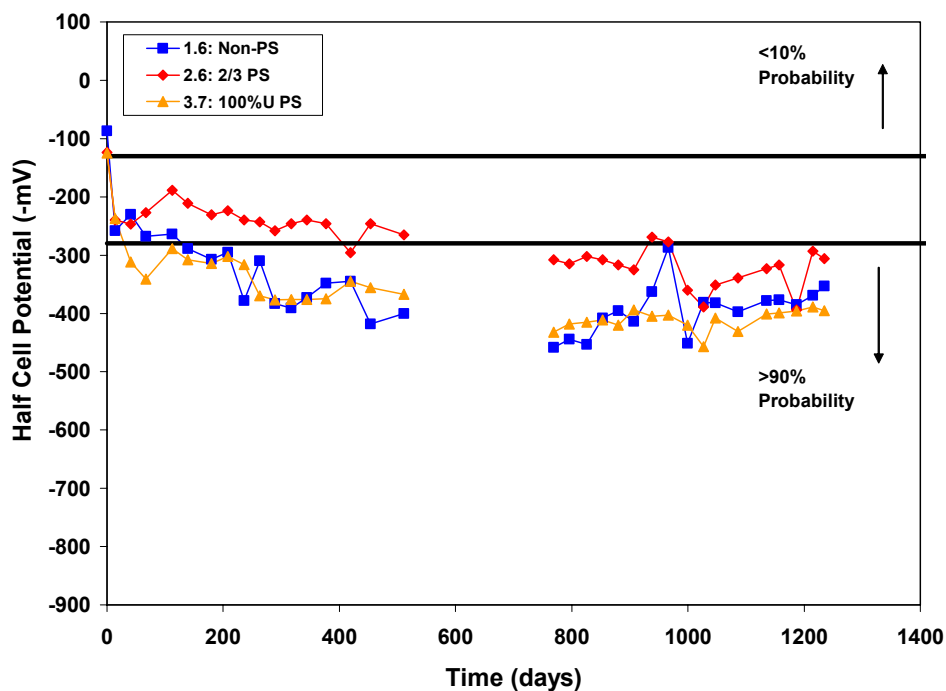
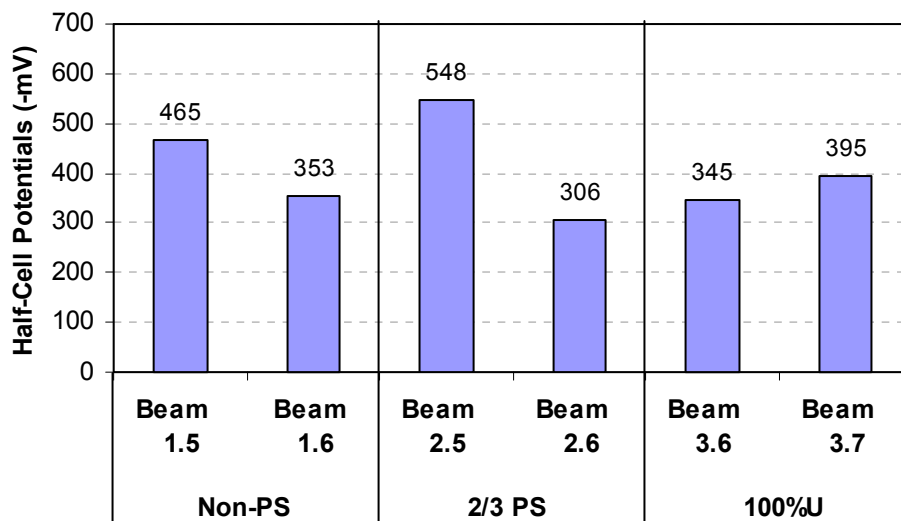


**Figure 4.22: Half-Cell Potential Readings  
(Phase II Autopsy Beams – High Performance Concrete)**

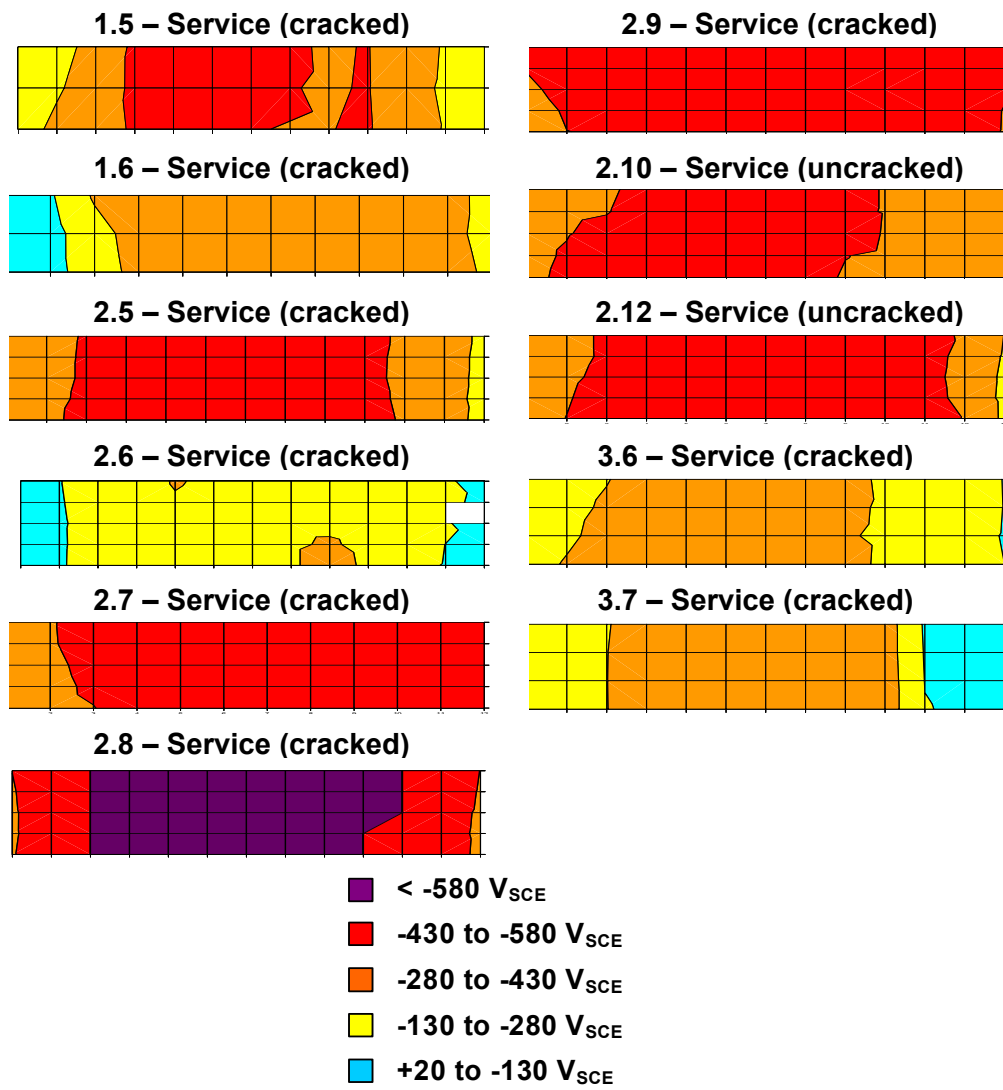


Figure 4.23 is a graph of the highest half-cell potential for the final readings of the Phase II autopsy specimens. Figure 4.24 shows the half-cell potential contour maps for all the Phase II beams after 1235 days of exposure testing. Figure 4.25 is a plot of the time to initiation of corrosion activity determined for each Phase II autopsy specimen. The length of time for each beam was designated as the day the half-cell potential reading was more negative than -280 mV, indicating a probability of corrosion greater than 90%. Figures 4.23, 4.24 and 4.25 are just another way of illustrating the following conclusions drawn from the half-cell potential plots:

- Performance of a 2/3 PS specimen is more similar to that of a Non-PS specimen as opposed to a 100% PS specimen
- High performance concrete appears to perform better than fly ash concrete, however the difference between the two is not significant



**Figure 4.23: Highest Average Half-Cell Potential Reading at 1235 Days (Phase II Beams)**



*Figure 4.24: Half-Cell Potential Contour Plots at 1235 Days  
(All Phase II Beams)*

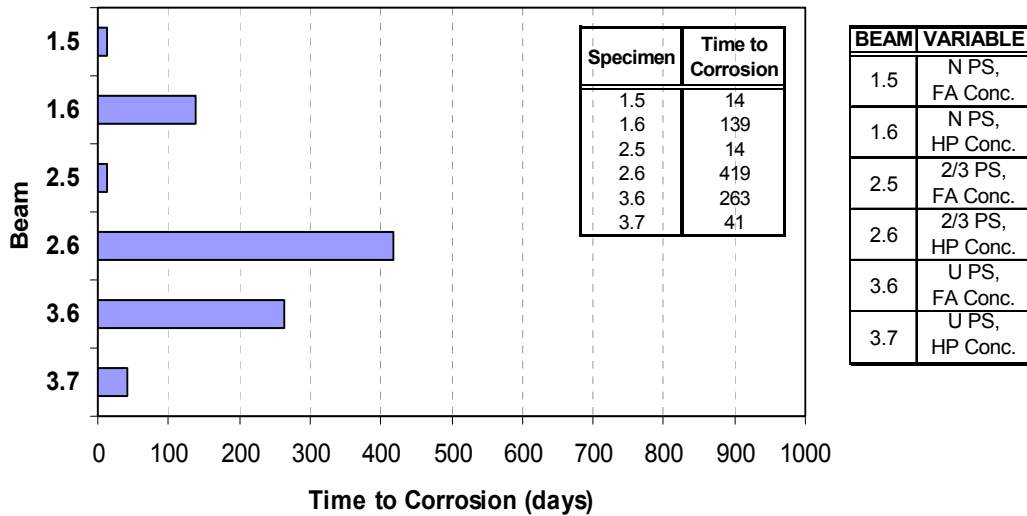


**Figure 4.25: Time to Initiation of Corrosion (Phase II Beams)**

### 4.3 CORROSION RATE READINGS

Corrosion rate measurements have been taken four times to date. The procedure for taking the measurements is explained in Section 3.2.4. The two types of equipment used in this experimental program, the PR Monitor and the 3LP, are described in Sections 3.2.4.3 and 3.2.4.4. Measurements of the Phase I beams were taken after seven, twelve, fifteen and forty-seven months of exposure. Measurements of the Phase II beams were taken after 37 months of exposure (See Appendix B for timeline). A final attempt to take corrosion rate measurements of all the beams was made immediately prior to the forensic examination. This attempt was unsuccessful due to complications with the 3LP equipment.

#### 4.3.1 Phase I Beams

Corrosion rate measurements of all the Phase I beams were performed after seven months of exposure testing using the PR Monitor equipment. Readings were taken midway (one week) through the dry portion of the exposure cycle. Corrosion rate measurements were performed after twelve months of exposure testing using the 3LP equipment. Readings were taken on day five of the two week dry portion of the exposure cycle. The next measurements were performed after fifteen months of exposure testing using both the PR Monitor and 3LP equipment. Readings were taken sixteen days after the start of the dry portion of the exposure cycle (the dry period was extended beyond the normal two weeks because work was being performed on the beams). The final successful corrosion rate measurements of the Phase I beams were performed after 47 months of exposure testing using the 3LP equipment.

As recommended in the SHRP Procedure Manual for Condition Evaluation of Bridges,<sup>19</sup> a proportionality constant, B, of 26 mV was used in the calculation of the corrosion current when the 3LP equipment was used. This assumption was made so the interpretation guidelines in Table 3.3 (shown on each graph) could be used to rank the corrosion severity according to the measurements.

Corrosion rate readings, in terms of corrosion current density, for the Phase I autopsy beams are shown in Figures 4.26 and 4.27, and are listed in Table 4.2. Graphs of the corrosion rate readings of all the Phase I beams can be found in Appendix D.

Figure 4.26 is a graph of the maximum corrosion rate readings taken of the Phase I autopsy beams using the PR Monitor equipment. The graph shows a consistent trend that the corrosion rate decreased over time. This does not make practical sense. Therefore, further investigation of the corrosion rate readings will

be made after the forensic examination to determine the reliability of the use of the PR Monitor equipment as a means of assessing corrosion rate. Through comparison of the three 100%U PS beams, both sets of readings show that the corrosion rate increases as the applied load, and thus crack width increases.

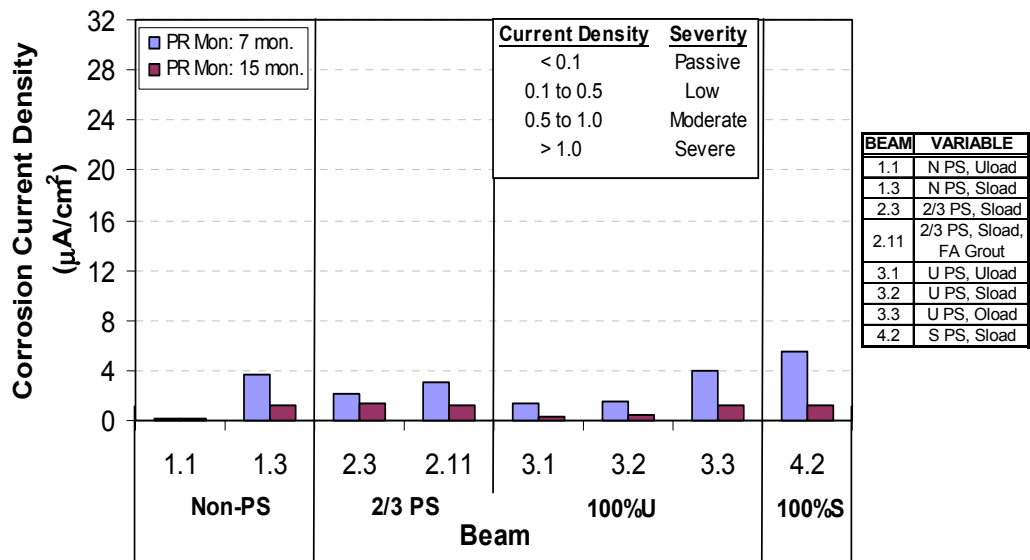


**Figure 4.26: Maximum Corrosion Rate Readings Using PR Monitor (Phase I Autopsy Beams)**

Figure 4.27 is a graph of all the maximum corrosion rate readings taken of the Phase I autopsy beams using the 3LP equipment. The graph shows a consistent trend that the corrosion rate increased over time, with the exception of Specimen 3.1. Again, comparison of the 100%U PS sections show increasing corrosion rates with increasing applied load. There is a significant increase from Specimen 3.2 (uncracked) to Specimen 3.3 (cracked).

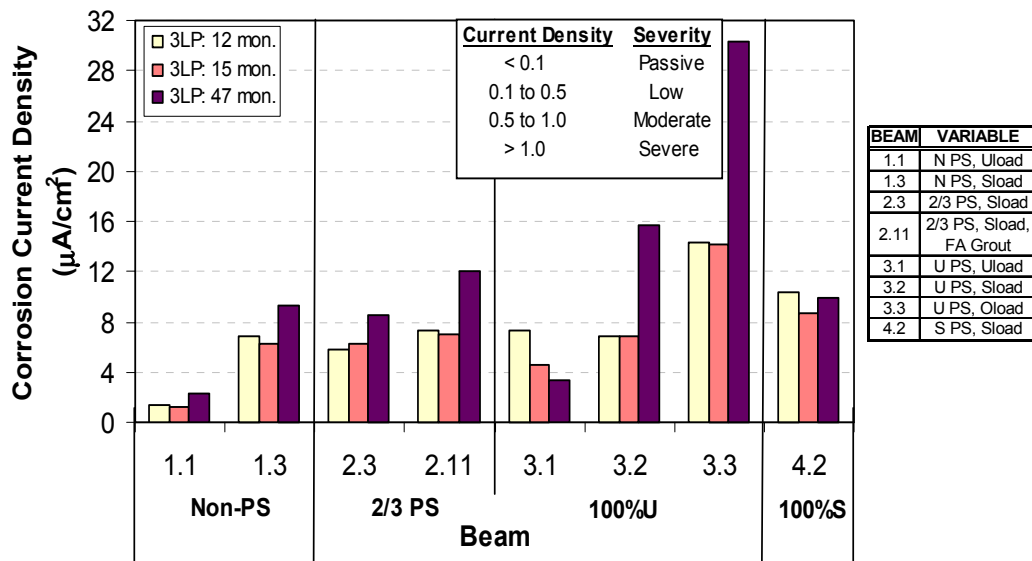


**Figure 4.27: Maximum Corrosion Rate Readings Using 3LP (Phase I Autopsy Beams)**

The corrosion severities determined in Table 4.2 are based on the last corrosion rate readings taken with the PR Monitor equipment. All readings taken with the 3LP equipment are extremely high, showing severe corrosion for all measurements. This indicates that, although they can be used to make relative comparisons and identify trends, readings using the 3LP are not reliable for determining actual corrosion rates and severities. For this reason, the corrosion severities assigned were based on the most recent reading taken with the PR Monitor.

**Table 4.2: Phase I Autopsy Beam Corrosion Current Density Measurements**

Beam & Location	7 months	12 months	15 months		47 months	Corrosion Severity at 15 Months
	PR Monitor $\mu\text{A}/\text{cm}^2$	3LP $\mu\text{A}/\text{cm}^2$	PR Monitor $\mu\text{A}/\text{cm}^2$	3LP $\mu\text{A}/\text{cm}^2$	3LP $\mu\text{A}/\text{cm}^2$	
1.1: Offset	0.18	1.31	0.19	1.15	2.32	Low
Midspan	0.20	1.09	0.12	0.76	1.21	Low
1.3: Offset	3.70	6.83	1.29	6.29	9.27	Severe
Midspan	1.07	4.64	1.06	3.50	8.03	Severe
2.3: Offset	2.17	5.85	1.43	4.79	8.02	Severe
Midspan	1.53	4.93	0.47	6.32	8.52	Low
2.11: Offset	1.90	7.39	1.16	7.08	11.28	Severe
Midspan	3.09	6.61	1.26	6.70	12.07	Severe
3.1: Offset	1.29	7.06	0.31	4.62	3.03	Low
Midspan	1.34	7.37	0.14	4.44	3.30	Low
3.2: Offset	1.42	6.33	0.42	6.83	15.74	Low
Midspan	1.49	6.84	0.31	5.43	7.46	Low
3.3: Offset	0.99	7.50	0.45	6.56	5.62	Low
Midspan	3.92	14.27	1.21	14.14	30.32	Severe
4.2: Offset	4.95	10.31	1.21	8.75	9.43	Severe
Midspan	5.58	9.47	1.06	7.16	9.86	Severe

#### **4.3.1.1 Differences Between 3LP and PR Monitor Corrosion Rates**

The PR Monitor and 3LP equipment both use the three electrode technique for measuring polarization resistance. However, several differences exist between the two pieces of equipment. The 3LP equipment represents the first generation of polarization resistance equipment for measuring corrosion rates of steel in concrete. The PR Monitor reflects several advancements, including the use of a guard ring electrode to confine the polarizing signal of the counter electrode, and measurement of the concrete resistance to compensate for solution resistance. The possible effects of these differences are discussed in West.<sup>1</sup>

Figure 4.28 is a graph of maximum corrosion rate readings taken after 15 months of exposure. The purpose of this graph is to compare the two types of

equipment used for taking the readings over the duration of this experimental program. The 3LP corrosion rates measured after fifteen months of testing are significantly higher than the PR Monitor corrosion rates. Other research and field experience with various devices for corrosion rate measurement have consistently shown that the 3LP equipment indicates higher corrosion rates than other devices.<sup>1</sup> Although there is a large difference in the readings from the two types of equipment, the trends in corrosion activity are similar. This suggests that the large discrepancy in magnitude is likely due to inherent differences between the two devices. Although the magnitude measured by the 3LP equipment may not be reliable, it is a good method for determining corrosion trends of individual specimens and comparing these trends among multiple specimens.

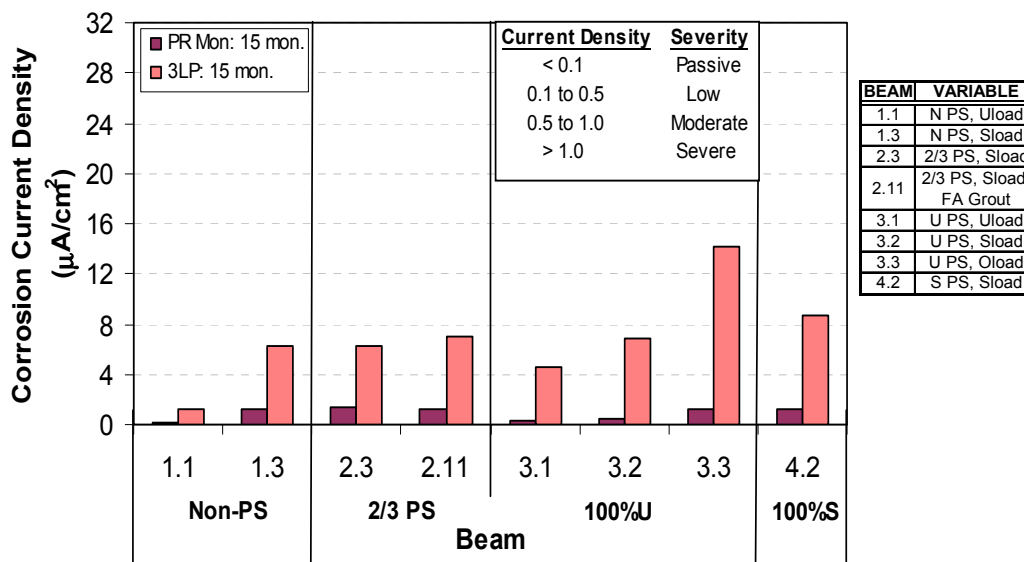


**Figure 4.28: Comparison of Corrosion Rate Measurement Equipment**



### 4.3.2 Phase II Beams

Only one successful set of corrosion rate readings was obtained for the Phase II beams. They were performed after 35 months of exposure testing using the 3LP equipment. As with the measurements of the Phase I beams, a proportionality constant, B, of 26 mV was used in the corrosion current calculations. Corrosion rate readings, in terms of corrosion current density, for the Phase II autopsy beams are plotted in Figure 4.29 and listed in Table 4.3. A graph of the corrosion rate readings for all Phase II beams can be found in Appendix D.

Figure 4.29 shows higher corrosion rates in the 100%U PS than the 2/3 PS beams for both concrete types. Specimen 3.7 is significantly higher than all the other readings. The reason for this will be determined after the forensic examination. The readings do not show a consistently better concrete type. Since only one set of measurements was obtained, comparisons among readings over time or between equipment cannot be made for the Phase II specimens.

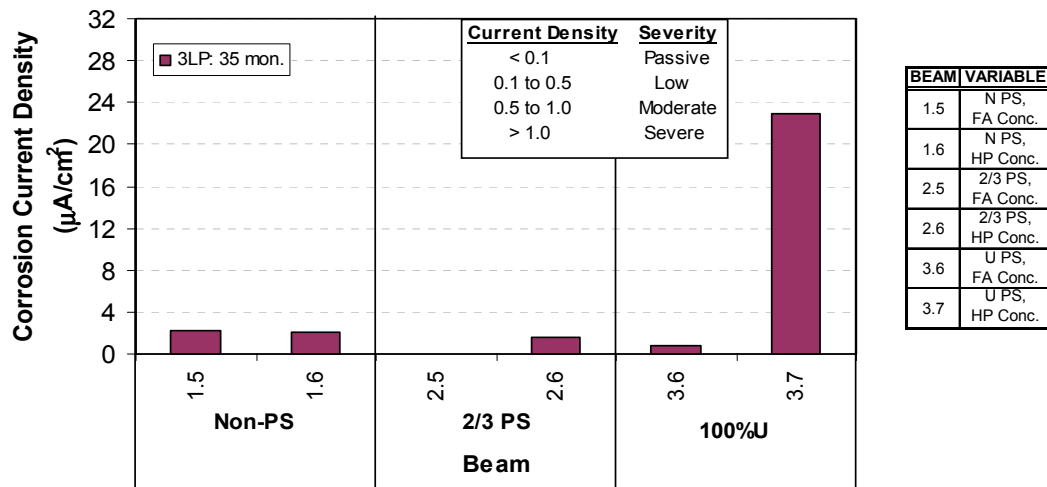


**Figure 4.29: Corrosion Rate Readings Using 3LP (Phase II Autopsy Beams)**

Because corrosion severities were only assigned according to readings taken with the PR Monitor, and no readings of the Phase II beams were taken using this equipment, corrosion severities could not be assigned to the Phase II beams in Table 4.3.

**Table 4.3: Phase II Autopsy Beam Corrosion Current Density Measurements**

<b>Beam &amp; Location</b>	<b>35 months 3LP <math>\mu\text{A}/\text{cm}^2</math></b>
1.5: Offset	2.17
Midspan	2.01
1.6: Offset	1.86
Midspan	2.05
2.5: Offset	0.06
Midspan	0.07
2.6: Offset	1.45
Midspan	1.55
3.6: Offset	no reading
Midspan	0.78
3.7: Offset	9.66
Midspan	22.90

#### **4.4 CHLORIDE PENETRATION MEASUREMENTS**

All concrete samples were taken and analyzed following the procedure described in Section 3.2.5. Samples were taken from all the Phase I block specimens after seven, fourteen, forty-one and fifty-four months of exposure testing. Samples were taken from the Phase II saltwater ponding blocks and from the non-exposed control blocks after twenty-nine and forty-two months of exposure testing. Concrete samples were also taken from the beam specimens chosen for final autopsy and analysis immediately prior to the forensic examination.

The chloride threshold for corrosion is indicated on each plot at 0.030% by weight of concrete. This value is intended as a guideline only, and is based on a chloride threshold value of 0.2% of weight of cement.<sup>21</sup> For ease of reference, the representative beam specimens are listed for each series in the plots instead of a single block number.

#### **4.4.1 Phase I Block Specimens**

The concrete type was not a variable in Phase I of this experimental program, therefore all the Phase I block specimens are Standard TxDOT Class C concrete. The results of the chloride analysis for the Phase I ponding blocks corresponding to the autopsy beams are shown in Figure 4.30 and listed in Table 4.4. Results from the Phase I control blocks showed negligible chloride content at all depths.

Figure 4.30 shows the plots of results from the ponding blocks corresponding to the autopsy beams only. Each block may have also represented non-autopsy beams. These beams were not included on the list for each plot for the sake of simplicity. Plots of the chloride content results for all the blocks can be found in Appendix D.

The plots in Figure 4.30 show the trends that the chloride content progressively increases over time and decreases with depth, as expected. All chloride contents at the bar level are below the threshold for corrosion, with the exception of the samples taken from Specimen 1.1 and 1.3 after 54 months. Although all specimens were made of TxDOT Class C concrete, the actual concrete mixtures varied a little, which was the purpose of casting and testing the block specimens. The TxDOT Class C concrete mix used in Beam 4.2 consistently shows the highest permeability, and that used in Beams 2.3 and 2.11 consistently show the lowest permeability.

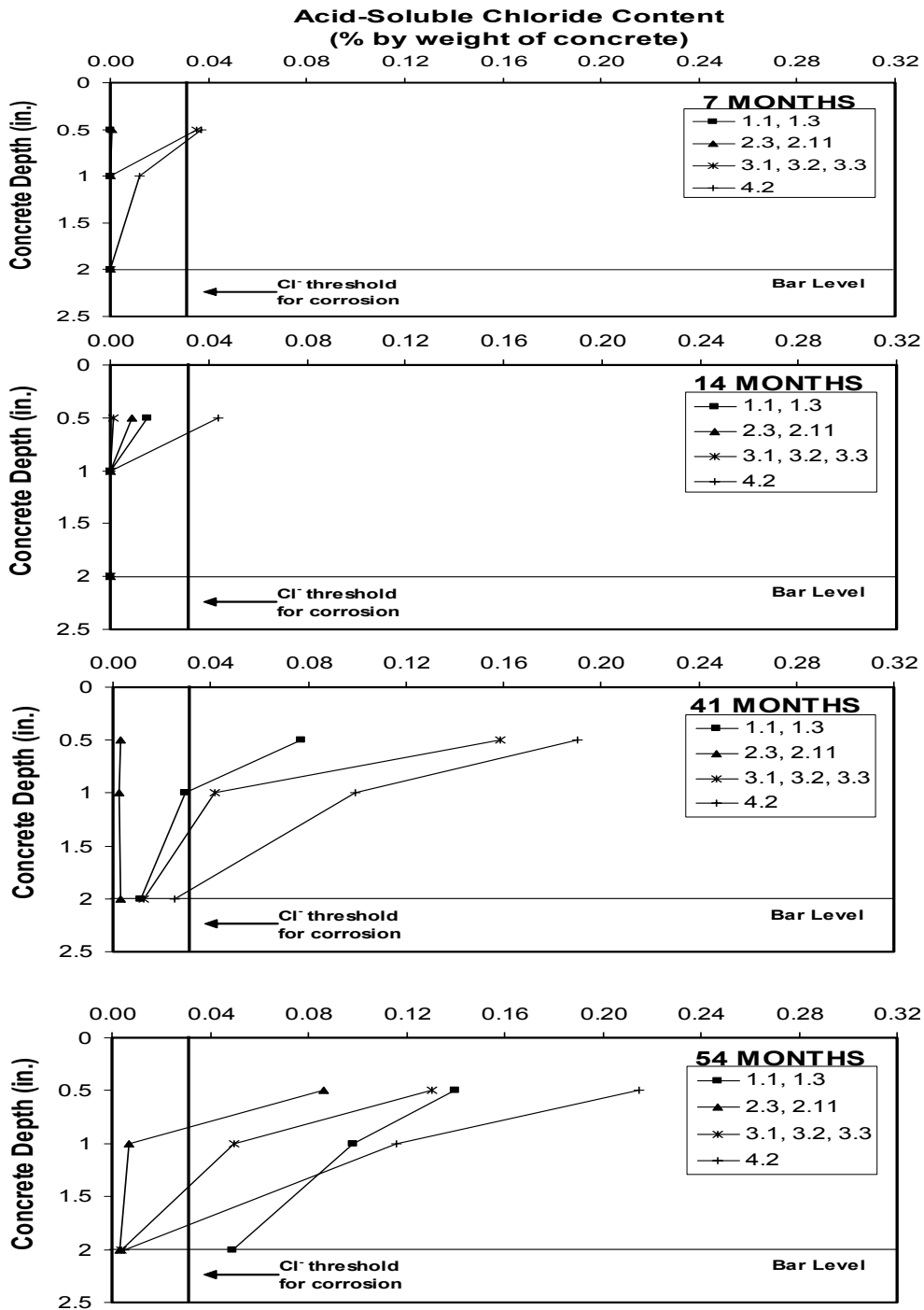


**Figure 4.30: Chloride Penetration (Phase I Poned Block Specimens)**

**Table 4.4: Phase I Poned Block Chloride Penetration Measurements**

Beams Represented	Depth (inches)	Chloride Content (% by weight of concrete)			
		7 months	14 months	41 months	54 months
1.1, 1.3	0.5	0.0000	0.0152	0.0774	0.1399
	1.0	0.0000	0.0000	0.0300	0.0982
	2.0	0.0000	0.0000	0.0112	0.0490
2.3, 2.11	0.5	0.0000	0.0086	0.0029	0.0862
	1.0	0.0000	0.0000	0.0027	0.0068
	2.0	0.0000	0.0000	0.0035	0.0031
3.1, 3.2, 3.3	0.5	0.0004	0.0013	0.1586	0.1303
	1.0	0.0000	0.0000	0.0417	0.0501
	2.0	0.0000	0.0000	0.0125	0.0039
4.2	0.5	0.0004	0.0440	0.1904	0.2149
	1.0	0.0001	0.0000	0.0994	0.1162
	2.0	0.0000	0.0000	0.0250	0.0048

#### **4.4.2 Phase II Block Specimens**

The concrete type was a main variable in Phase II of this experimental program. The results of the chloride analysis for the Phase II ponding blocks corresponding to the autopsy beams are shown in Figure 4.31 and listed in Table 4.5. Results from the Phase II control blocks showed negligible chloride content at all depths.

Figure 4.31 shows the plots of the ponding blocks corresponding to the autopsy beams only. Again, each block may have also represented non-autopsy beams. These beams were not included on the list for each plot for the sake of simplicity. Plots of the chloride content results for all the blocks can be found in Appendix D.

The plots in Figure 4.31 show the trends that the chloride content progressively increases over time and decreases with depth, as expected. All chloride contents at the one-inch and two-inch (bar level) depths are well below

the threshold for corrosion and show little variation between the concrete types. Samples taken at a depth of 0.5 inches after 29 and 42 months of exposure both show that the high performance concrete was less permeable.

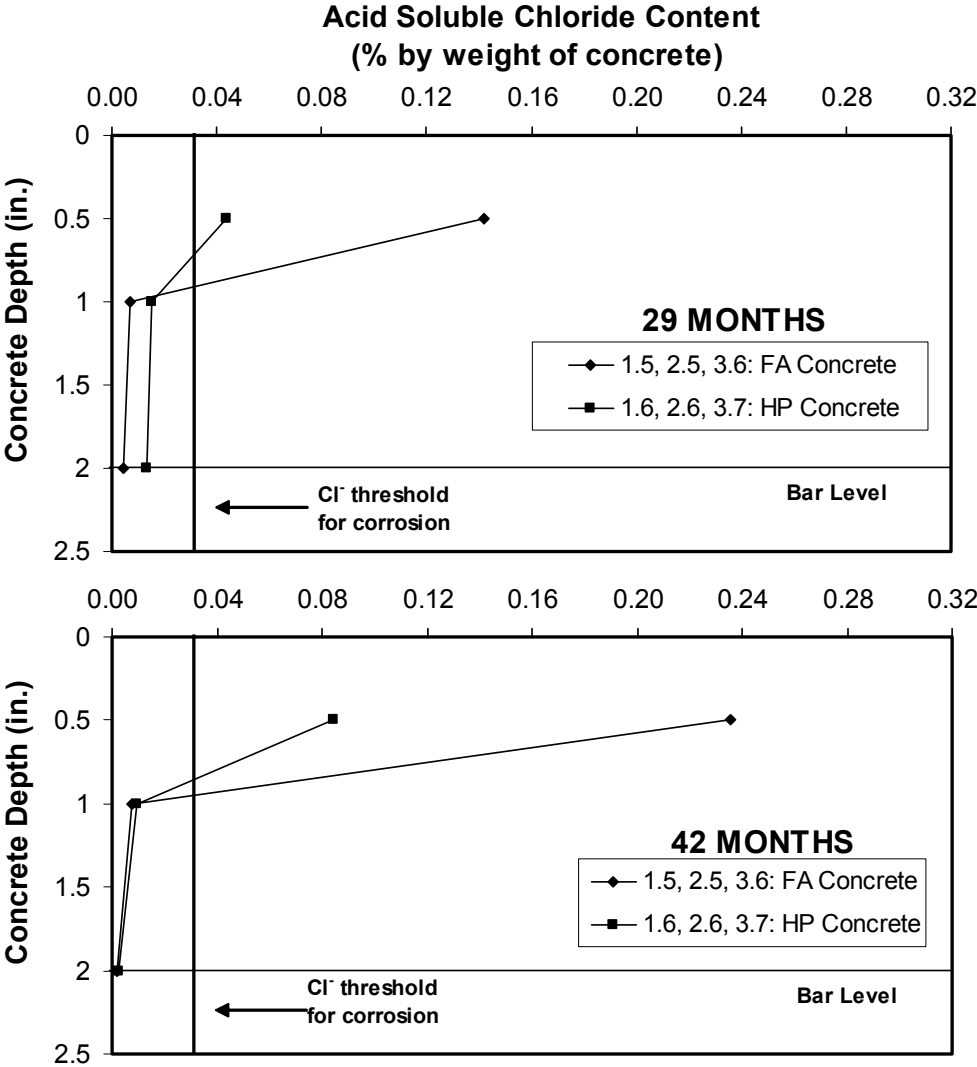


*Figure 4.31: Chloride Penetration (Phase II Ponded Block Specimens)*

**Table 4.5: Phase II Ponded Block Chloride Penetration Measurements**

<b>Beams Represented</b>	<b>Depths (inches)</b>	<b>Chloride Content (% by weight of concrete)</b>	
		<b>29 months</b>	<b>42 months</b>
1.5, 2.5, 3.6	0.5	0.1422	0.2359
	1.0	0.0072	0.0078
	2.0	0.0046	0.0017
1.6, 2.6, 3.7	0.5	0.0439	0.0846
	1.0	0.0151	0.0097
	2.0	0.0133	0.0025

#### **4.4.3 Phase I Autopsy Beam Specimens**

All Phase I beams have TxDOT Class C concrete. The results of the chloride analysis for the Phase I autopsy beams and blocks (shown again for comparison) after fifty-four months of exposure are shown in Figures 4.32 and 4.33 and listed in Table 4.6. The samples of greatest interest are those taken at the two-inch depth because these samples give the chloride content in the concrete at the bar and top-of-duct level of the beams. Figure 4.34 shows the results for each sample at this critical level for the specimens. Additional plots showing chloride content at all offsets and depths for each individual beam can be found in Appendix D.

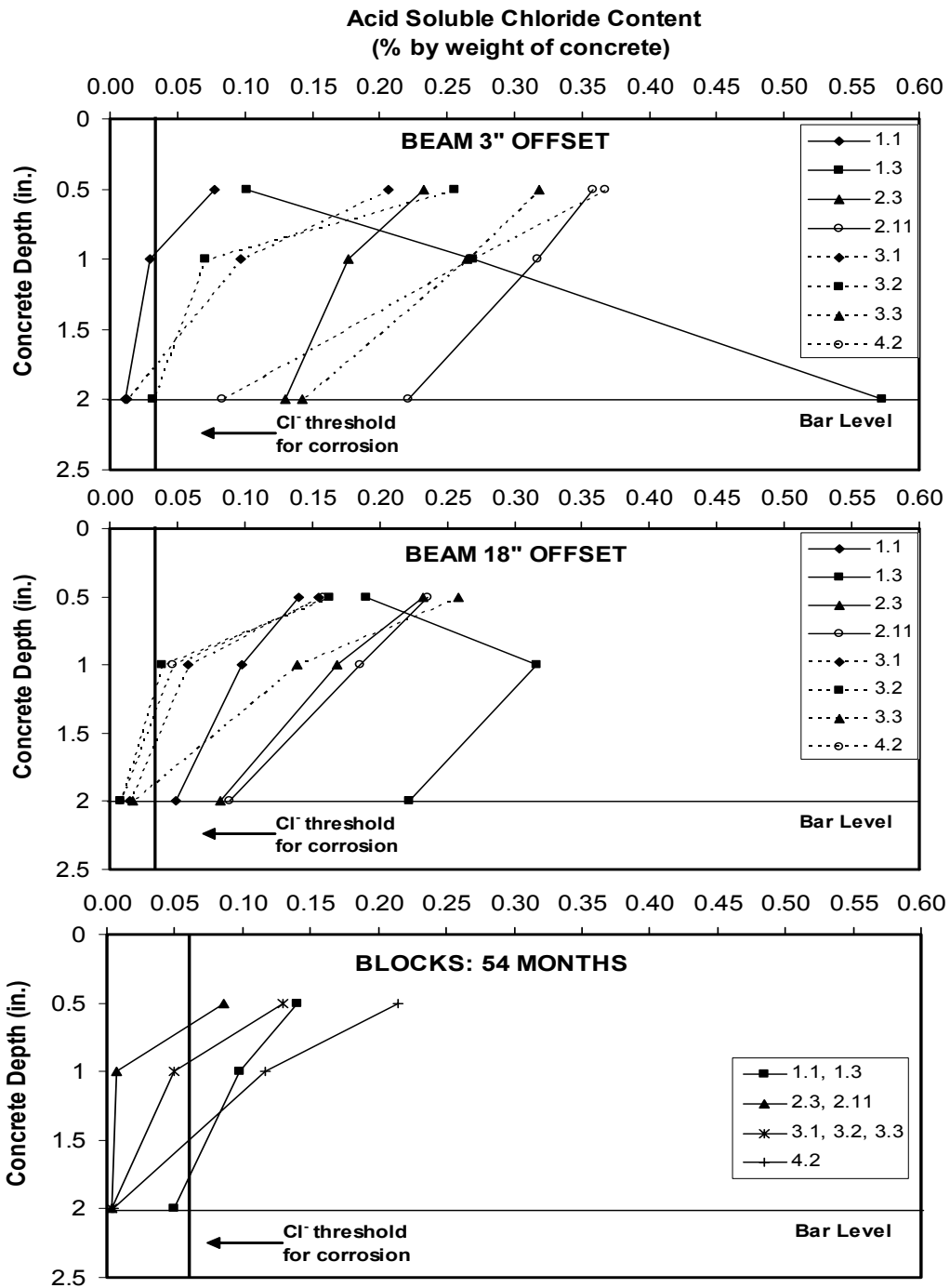


**Figure 4.32: Beam and Block Chloride Penetration at 54 Months  
(Phase I – Ponded Region on Beams)**



The plots above in Figure 4.32 show the chloride content at all three depths for the two sample locations inside the ponded region (3-inch and 18-inch offset) and corresponding blocks. Again, all Phase I beams and blocks are TxDOT Class C. Therefore, higher chloride content in a beam, in comparison to its corresponding block, is most likely due to the presence of cracking, which would allow ease of chloride ingress. This is true of Specimen 1.3 whose chloride content at the bar level is noticeably larger than the rest of the beams and its corresponding block. This is due to samples at both locations being taken at crack locations. The three-inch offset samples for Specimens 2.11 and 4.2 were also taken at crack locations, which would explain their high values at the bar level since the values of their blocks is essentially zero.

The beam samples shown in Figure 4.33 are those taken at locations outside of the ponded region of the Phase I beams. Most measurements at the bar level at both locations are at or below the threshold, with the exception of Specimen 1.3 whose 32-inch sample was taken at a crack location. Generally, chloride levels at the one-inch depth of the Non-PS and 2/3 PS beams are significantly higher at the 27-inch offset (immediately outside the ponded region) in comparison with those from the 32-inch offset. This is not true of the 100% PS beams, suggesting that a lower prestress level (lower compressive stresses in the concrete) allows more horizontal chloride penetration.

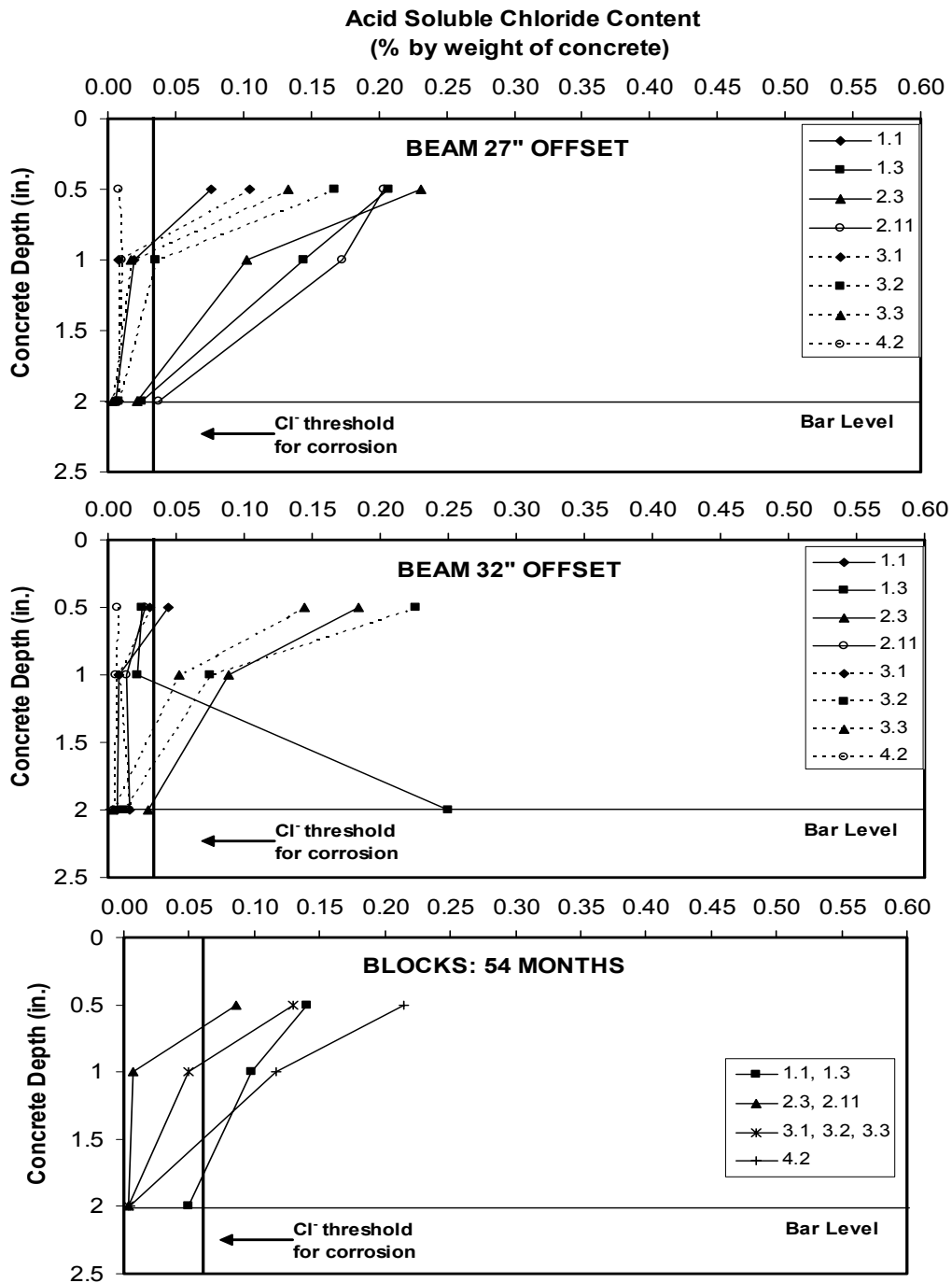


**Figure 4.33: Beam and Block Chloride Penetration at 54 Months  
(Phase I – Unponded Region on Beams)**

Figure 4.34 illustrates that samples taken in the ponded region consistently have higher chloride contents at the bar level. Unloaded and therefore uncracked Specimens 1.1 and 3.1 show very low measurements at all locations. The significantly larger values for Specimens 1.3 and 2.3 at the three-inch offset are due to the fact that the samples were taken at crack locations. As expected, an increase in the level of prestress results in lower chloride contents due to fewer cracks and higher compressive stresses in the concrete which decrease its permeability. There appears to be minimal difference in the performance of the 100%S and U PS beams. The noticeably larger value from the 100%U PS beam at the three-inch offset location is due to the small crack at the sample location.

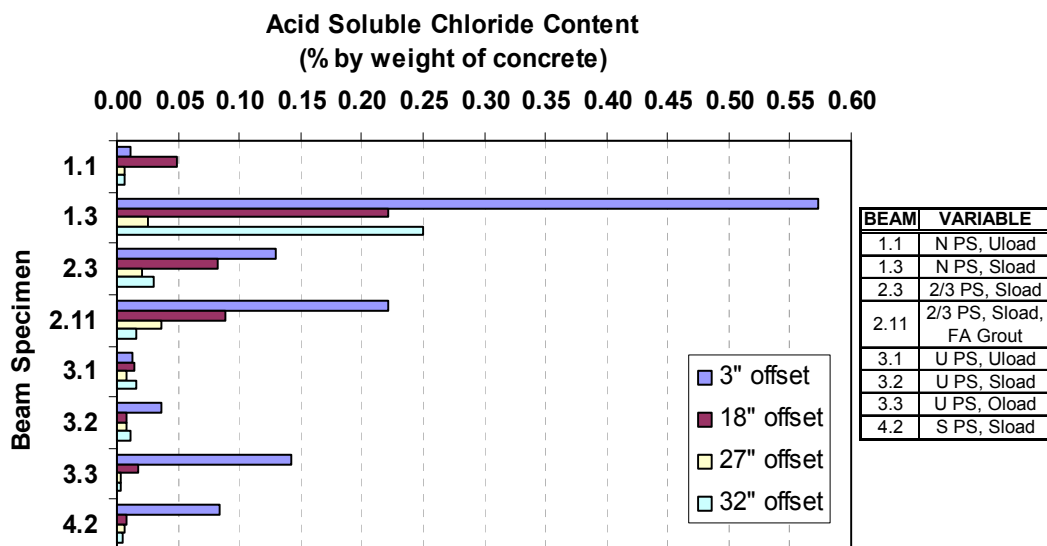


***Figure 4.34: Chloride Content at Bar and Top-of-Duct Level  
(Phase I Beams)***

**Table 4.6: Phase I Autopsy Beam Chloride Penetration Measurements**

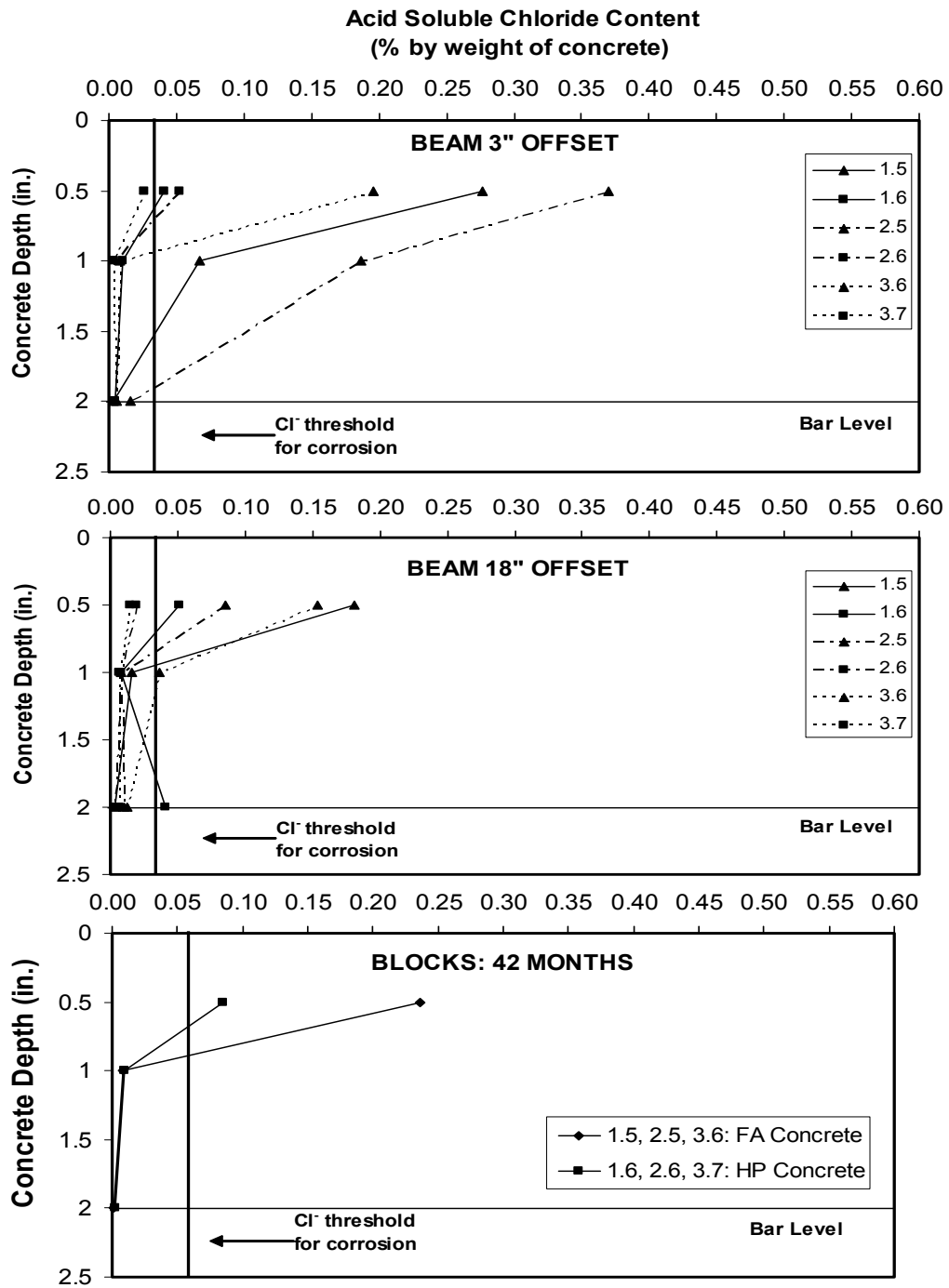
Beam	Depth (inches)	Chloride Content (% by weight of concrete)			
		3" Offset	18" Offset	27" Offset	32" Offset
1.1	0.5	0.0774	0.1399	0.0757	0.0448
	1.0	0.0300	0.0982	0.0199	0.0080
	2.0	0.112	0.0490	0.0058	0.0064
1.3	0.5	0.1020	0.1901	0.2070	0.0250
	1.0	0.2695	0.3169	0.1447	0.0219
	2.0	0.5729	0.2216	0.0250	0.2496
2.3	0.5	0.2326	0.2326	0.2306	0.1836
	1.0	0.1765	0.1689	0.1025	0.0883
	2.0	0.1299	0.0820	0.0214	0.0296
2.11	0.5	0.3583	0.2352	0.2038	0.0277
	1.0	0.3173	0.1852	0.1735	0.0138
	2.0	0.2213	0.0890	0.0373	0.0157
3.1	0.5	0.2064	0.1547	0.1047	0.0307
	1.0	0.0965	0.0583	0.0082	0.0079
	2.0	0.0120	0.0150	0.0076	0.0154
3.2	0.5	0.2557	0.1626	0.1676	0.2258
	1.0	0.0712	0.0384	0.0355	0.0746
	2.0	0.0317	0.0079	0.0084	0.0116
3.3	0.5	0.3182	0.2581	0.1330	0.1445
	1.0	0.2641	0.1389	0.0171	0.0520
	2.0	0.1424	0.0169	0.0030	0.0031
4.2	0.5	0.3675	0.1583	0.0082	0.0064
	1.0	0.2668	0.0464	0.0097	0.0054
	2.0	0.0837	0.0084	0.0064	0.0050

#### **4.4.4 Phase II Autopsy Beam Specimens**

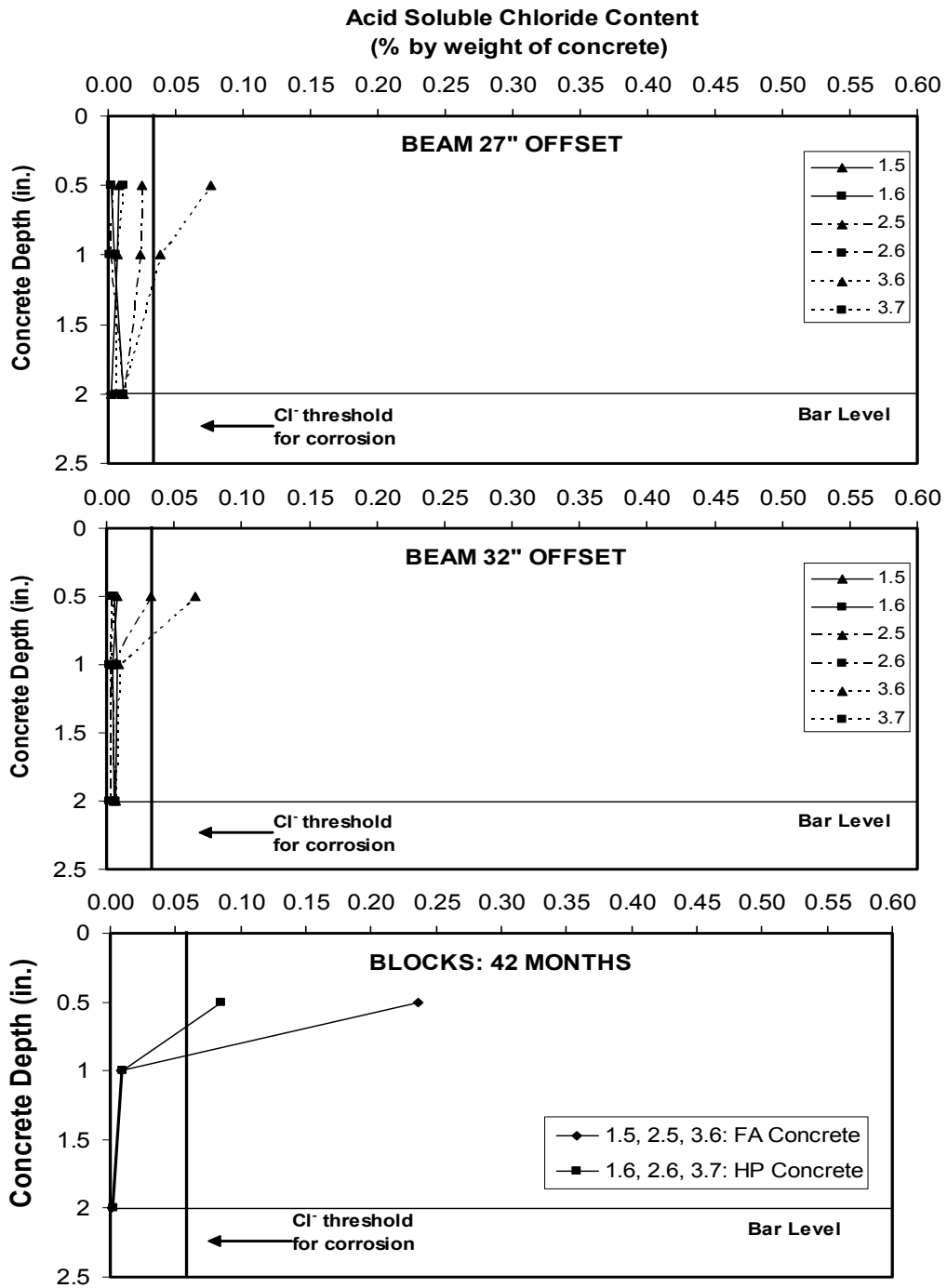
All of the Phase II specimens are service loaded, therefore the variable of interest when analyzing the chloride content results of the Phase II beams is the concrete type of each specimen. The results of the chloride analysis for the Phase II autopsy beams and blocks (shown again for comparison) after forty-two months of exposure are shown in Figures 4.35 and 4.36 and listed in Table 4.7. Figure 4.37 shows the results for each sample at the critical two-inch depth for the specimens. Additional plots showing the chloride content at all offsets and depths for each individual beam can be found in Appendix D.

Figure 4.35 consistently shows the high performance concrete as the superior concrete type in both the beam and block specimens at the first two depths. All samples from inside the ponded region at the bar level show negligible chloride contents, implying that both types of concrete are effective in limiting chloride penetration.

The majority of the measurements from samples taken outside the ponded region of the Phase II specimens show negligible chloride contents, as seen in Figure 4.36. The only notable measurements were found in the fly ash concrete specimens. This supports the conclusion drawn above that high performance concrete is superior to fly ash concrete in limiting chloride penetration.



**Figure 4.35: Beam and Block Chloride Penetration at 42 Months  
(Phase II Autopsy Beams – Ponded Region on Beams)**



*Figure 4.36: Beam and Block Chloride Penetration at 42 Months  
(Phase II Autopsy Beams – Unponded Region on Beams)*

Figure 4.37 confirms that the chloride contents at the bar level of the Phase II specimens are very low. This again implies that both concrete types are effective in minimizing the penetration of chlorides to the reinforcement through the concrete.

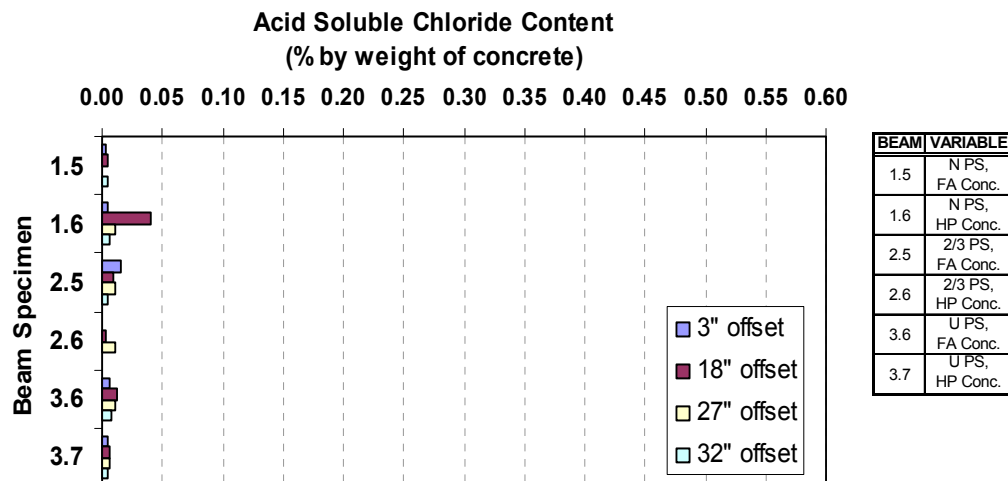


*Figure 4.37: Chloride Content at Bar and Top-of-Duct Level  
(Phase II Beams)*



**Table 4.7: Phase II Autopsy Beam Chloride Penetration Measurements**

Beam	Depth (inches)	Chloride Content (% by weight of concrete)			
		3" Offset	18" Offset	27" Offset	32" Offset
1.5	0.5	0.2770	0.1810	0.0076	0.0077
	1.0	0.0674	0.0163	0.0067	0.0043
	2.0	0.0034	0.0039	0.0021	0.0052
1.6	0.5	0.0410	0.0515	0.0019	0.0057
	1.0	0.0108	0.0082	0.0048	0.0076
	2.0	0.0046	0.0409	0.0111	0.0066
2.5	0.5	0.3700	0.0854	0.0250	0.0333
	1.0	0.1868	0.0077	0.0236	0.0039
	2.0	0.0156	0.0099	0.0109	0.0051
2.6	0.5	0.0525	0.0196	0.0018	0.0029
	1.0	0.0030	0.0076	0.0015	0.0019
	2.0	no reading	0.0033	0.0114	0.0021
3.6	0.5	0.1959	0.1540	0.0766	0.0652
	1.0	0.0081	0.0366	0.0381	0.0089
	2.0	0.0058	0.0120	0.0103	0.0070
3.7	0.5	0.0263	0.0144	0.0116	0.0045
	1.0	0.0035	0.0066	0.0057	0.0040
	2.0	0.0040	0.0064	0.0056	0.0051

## **CHAPTER 5**

### **Forensic Examination**

#### **5.1 FORENSIC EXAMINATION**

After four and a half years of exposure testing for the Phase I beam specimens and three and a half years for the Phase II beams, a detailed visual inspection of the exterior condition was performed on all 27 specimens, and exposure testing data were thoroughly analyzed. Based on this evaluation, it was decided to perform a forensic examination that includes full or partial autopsies of approximately half of the beams. The forensic examination procedure was developed based on the main objective of the experimental program, to evaluate the effect of post-tensioning on durability. To accomplish this, an evaluation of the relative performance of a large number of corrosion protection variables had to be conducted. The variables included prestress level and crack width, applied load, concrete type, duct type, duct splice type, grout type, strand type and end anchorage protection.

Specific forensic examination objectives were as follows:

1. Obtain visual evaluation of the overall exterior condition of beam specimens.
2. Determine chloride ion penetration through the concrete.
3. Obtain visual evaluation of corrosion damage on duct, duct splice, prestressing strand and mild steel reinforcement.
4. Determine chloride ion content in the grout.
5. Determine most effective variables in corrosion protection.

## 5.2 SELECTION OF AUTOPSY BEAMS

Originally, all beam specimens were scheduled for full autopsy in May 2002. This date marked four and a half or three and a half years of exposure testing for the Phase I and Phase II beams, respectively. Results from the portion of this project that tested macrocell specimens<sup>22</sup> indicated that a substantial extension of exposure testing for select specimens would produce valuable and informative results. Half of the duplicated macrocell specimens were autopsied after four and a half years of very aggressive exposure. The remaining duplicates were autopsied after eight years of exposure. When the results from the later autopsy were compared with the preliminary conclusions reported after four and a half years of exposure testing, it was found that a number of significant changes had occurred due to the extension of the exposure duration. For example, no corrosion had been found in the epoxy jointed specimens after four and a half years. The later autopsy found that there was some corrosion (away from the joint) in the epoxy jointed specimens. Additionally, after eight years there was extremely substantial deterioration of the galvanized ducts due to corrosion and a clear indication of the superiority of plastic ducts in corrosion protection. This was not so evident after the first autopsy. If all exposure testing had been halted after four and a half years in the macrocell specimens, a great deal of important information would have been missed.

Because of this experience, it was decided to select approximately half of the beam specimens for autopsy in May 2002. Twelve out of the total of twenty-seven beam specimens in Phase I and Phase II were selected for full autopsy, while two specimens were selected for partial autopsy. The remaining specimens were left under continuous exposure testing for future autopsy. Figures 5.1 and Tables 5.1 and 5.2 show the beam specimens selected for full and partial forensic examination and their corresponding test variables. The autopsy specimen

selection was made based on visual inspection, measurements taken during exposure testing and the necessity for comparison of test variables.

It was determined that Beams 1.1 and 3.1 would be needed for both the present and future autopsies because they were the only uncracked and unloaded specimens. Thus they served as control specimens for comparison. Since these beams were not loaded or cracked, a portion of the specimen could be removed while the remainder was returned to the exposure testing. Thus, it was decided that a partial autopsy would be performed on these two specimens. The partial autopsy consisted of exposing and removing half of the mild steel/duct/strand section that was removed for each fully autopsied beam, leaving the other half for continued exposure testing.

Main Variable		Section Type			
		Non-PS	2/3 PS	100%U	100%S
Phase I	Unloaded	1.1		3.1	
	Very Small Crack		2.1	3.2	
	Constant Service Load	1.2	2.2	3.3	4.1
	Constant Service Load (duplicate)	1.3	2.3	3.4	4.2
	Overload and Return to Service	1.4	2.4	3.5	
	High Performance Fly Ash Grout		2.11		
Phase II	Standard Concrete with 25% Fly Ash	1.5	2.5	3.6	
	High Performance Fly Ash Concrete	1.6	2.6	3.7	
	Epoxy Coated Strands		2.7		
	Galvanized Strands		2.8		
	Poor Grouting Procedures		2.9		
	High Performance Anti-Bleed Grout		2.10		
	Encapsulated System w/ Plastic Duct		2.12		

	Full autopsy		Partial Autopsy		Exposure ongoing
--	--------------	--	-----------------	--	------------------

**Figure 5.1: Beam Specimens Selected for Forensic Examination**

**Table 5.1: Phase I Beams Selected for Forensic Examination**

<b>Specimen</b>	<b>Prestress Level</b>	<b>Cracking (mm)</b>	<b>Applied Load</b>	<b>Concrete Type</b>	<b>Splice Type</b>	<b>Damage to Duct</b>	<b>Grout type</b>	<b>Strand</b>	<b>PT Anchorage</b>
1.1	Non-PS	Uncracked	Unloaded	(1)	--	--	--	--	--
1.3	Non-PS	0.3	Constant Service	(1)	--	--	--	--	--
2.3	2/3 PS	0.2	Constant Service	(1)	(2)	(3)	(4)	(7)	(8)
2.11	2/3 PS	0.2	Constant Service	(1)	(2)	None	Fly Ash (5)	(7)	(8)
3.1	100% U PS	Uncracked	Unloaded	(1)	(2)	None	(4)	(7)	(9)
3.2	100% U PS	Uncracked	Constant Service	(1)	(2)	None	(4)	(7)	(9)
3.3	100% U PS	Cracked	124% - Return to Service	(1)	(6)	None	(4)	(7)	(9)
4.2	100% S PS	Uncracked	Constant Service	(1)	(2)	(3)	(4)	(7)	(10)
(1) TxDOT Class C (0.45 w/c, cement Type I, retarder, air entrainment agent) (2) Industry Standard (IS) and Heat Shrink (HS) (3) IS with damage and HS with damage (4) TxDOT Class C (0.44 w/c, cement Type I, expanding admixture) (5) 0.33 w/c, 30% Fly Ash replacement. (6) Industry Standard (IS) (7) 7-wire 0.5 in. low relaxation (270 ksi) strand (8) VSL Type E5-3 (with third strand opening unused) (9) VSL Type E5-3 (10) VSL Type E5-4									

**Table 5.2: Phase II Beams Selected for Forensic Examination**

Specimen	Prestress Level	Cracking (mm)	Applied Load	Concrete Type	Splice Type	Damage to Duct	Grout type	Strand	PT Anchorage
1.5	Non-PS	0.3	Constant Service	(11)	--	--	--	--	--
1.6	Non-PS	0.3	Constant Service	(12)	--	--	--	--	--
2.5	2/3 PS	0.2	Constant Service	(11)	(13)	None	(14)	(15)	(16)
2.6	2/3 PS	0.2	Constant Service	(12)	(13)	None	(14)	(15)	(16)
3.6	100% U PS	0.1	Unloaded	(11)	(13)	None	(14)	(15)	(17)
3.7	100% U PS	0.1	Constant Service	(1)	(13)	None	(14)	(15)	(17)
(11) TxDOT Class C with Fly Ash (0.44 w/c, with 25% Class F Fly Ash) (12) High Performance (0.29 w/c, 25% Fly Ash, superplasticizer) (13) Industry Standard Splice (IS) and Heat Shrink Splice (HS) (14) TxDOT Class C (0.44 w/c, cement Type I, expanding admixture) (15) 7-wire 0.5 in. low relaxation (270 ksi) strand (16) VSL Type E5-3 (with third strand opening unused) (17) VSL Type E5-3									

### **5.3 BEAM AUTOPSY PROCEDURE**

The beam autopsy procedure described in this section was conducted for the specimens chosen for forensic examination only. Any full autopsy procedure conducted resulted in complete destruction of the specimen.

#### **5.3.1 Visual Inspection**

The appearance of the specimens can indicate corrosion activity. The exterior surface of each beam specimen was examined for signs of additional cracking, rust staining and concrete spalling.

#### **5.3.2 Crack Width Measurements**

One of the main objectives of the forensic examination was to determine the influence of cracking on specimen performance and reinforcement corrosion (onset of corrosion and propagation) due to chloride and moisture ingress. Crack widths were measured at the beginning of exposure (after post-tensioning and first loading) and at the end of exposure. The crack width measurement procedure is described in Section 3.2.2 and the results are given in Section 4.1.

#### **5.3.3 Concrete Samples for Chloride Analysis**

Another procedure conducted to assess the chloride penetration through the concrete involved obtaining concrete powder samples and testing their acid soluble chloride content. The procedure for obtaining the samples is explained in Section 3.2.5 and the results of the chloride content analysis performed immediately prior to the autopsy are given in Section 4.4.3.

#### **5.3.4 Saw Cuts**

Analysis of the post-tensioning system and mild steel reinforcement was limited to a total length of 72 inches. The section analyzed extended 42 inches

from the centerline of the beams to one side and 30 inches to the other side. Figure 5.2 shows a diagram of the section removed for observation. The section included the entire 48-inch ponded region, and extended six inches outside the ponded region on one side and 18 inches on the other side. It was decided that this section would sufficiently provide the following information:

1. Reinforcement corrosion performance from the area in the ponded region
2. Possible horizontal ingress of chlorides through the concrete from the area immediately outside of the ponded region
3. A section of reinforcement not exposed to a corrosive environment for comparison

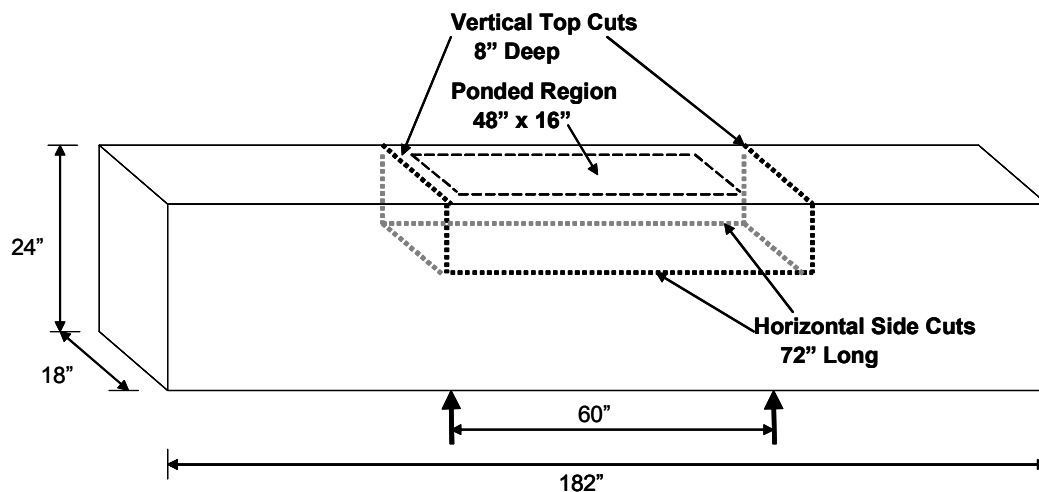


**Figure 5.2: Section Removed from Beams for Analysis**

The concrete saw with a 27-inch circular blade shown in Figure 5.5 was used to make all the cuts in the specimens. Two eight-inch deep vertical cuts were made on the top of the beam, and a horizontal cut was made on each side of the beam, below the duct line. These cuts separated the portion of the beam to be



analyzed from the rest of the beam, allowing the area of interest to be removed with a forklift.



*Figure 5.3: Concrete Saw Used in Autopsy*

### **5.3.5 Exposure and Removal of Post-Tensioning System**

After the section was removed, it was placed on the ground with the cut surface facing up. Each section was examined and existing cracks were measured and recorded. Jackhammers and chipping hammers were used to carefully remove all existing concrete around post-tensioning ducts and mild steel reinforcement, as illustrated in Figure 5.4. The post-tensioning system was then removed from the concrete. Immediately after removing the ducts, the concrete surface was examined for rust staining, salt deposits and damage.



*Figure 5.4: Concrete Removal and Reinforcement Exposure*

### **5.3.6 Exposure and Removal of Mild Steel**

After the ducts were removed, the mild steel bars and stirrups were exposed, using the jackhammers and chipping hammers, and removed for analysis. Figure 5.5 shows a portion of a rebar cage after removal. Each rebar cage was disassembled prior to the condition analysis of each longitudinal bar and stirrup.



*Figure 5.5: Mild Steel Reinforcement Cage*

### **5.3.7 Exposure, Examination and Removal of Grout**

After the external surface of each duct splice was examined, the splices were removed from the duct for further analysis by making longitudinal cuts along each side of the splice. All metal cuts were made using a small air grinder. Once the splices were removed, the duct was opened in the same manner, exposing the grout. Post-tensioning grout was evaluated for bleed water voids, incomplete duct filling and excessive porosity. Since grout is injected after the stressing of post-tensioning steel, it is unstressed. Therefore the hardened grout is susceptible to service cracking due to deflections and vibrations. Just as cracks in concrete serve as direct paths to the reinforcement for moisture and chlorides, this is also true of cracks in grout. For this reason, it was important to identify cracking in the grout and examine grout cracks for indication of moisture and chloride ingress.

Grout Samples were collected from every duct at six-inch intervals over the entire length of 72 in. The grout pieces were crushed between two steel plates and ground into powder using a mortar and pestle. The grout powder samples were analyzed for acid-soluble chlorides following the same procedure

used for the concrete samples described in Section 3.2.5. After the desired samples were removed, the remainder of the grout was carefully removed, exposing the prestressing strand for examination.

### **5.3.8 Examination of Elements**

After all elements of the mild steel reinforcement and post-tensioning system were exposed and removed, they were thoroughly examined and rated following the procedures in Section 5.4.

## **5.4 CORROSION RATING SYSTEM**

The rating system selected for evaluation was created by West.<sup>1</sup> The procedure was developed in a universal form with the intention of applying the same rating system to various situations. The basis for the system is to divide the element under examination into uniform intervals and assign a systematic rating to each interval depending on the severity of corrosion. For the beam specimens in this testing program, the length (72 inches) of longitudinal mild steel, duct and strand was divided into 36, two-inch intervals. Using such small intervals assured the determination of both the extent and severity of corrosion.

As described in West<sup>1</sup>, the rating system is essentially the same for the prestressing strand, mild steel reinforcement and galvanized steel duct and splice, with some modifications to reflect unique corrosion aspects of each type of steel. In general, the evaluation system doubles the severity rating for each category of increasing corrosion damage.

#### 5.4.1 Mild Steel Reinforcement

The longitudinal mild steel bars were examined at 36 two-inch intervals, as indicated in Figure 5.6. Because there was frequently a significant difference in the severity of corrosion on the top and bottom bar surface, a separate rating for each was assigned at every interval. The same procedure was applied to the stirrups, except the interval division varied slightly. As with the longitudinal bars, the top portion of stirrup was divided into 7 two-inch intervals. Due to the dimensions of the section removed from each beam for forensic examination, there were 2 three-inch sections (legs) from the sides of the stirrup to be analyzed. (See Figure 5.6) Each three-inch leg was considered one interval, for a total of nine intervals per stirrup. One rating was assigned to the inside and outside surfaces of each leg.

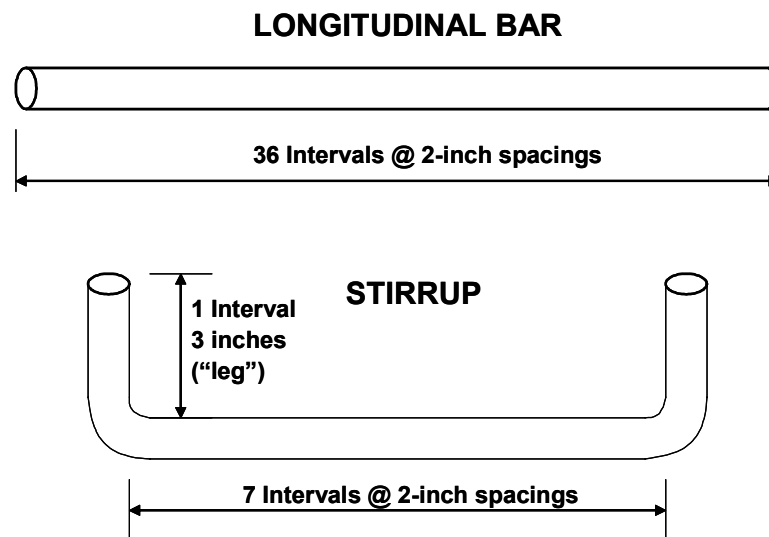


*Figure 5.6: Intervals for Corrosion Ratings on Mild Steel*

The total bar corrosion rating was calculated as follows:

$$R_{Bar} = \sum_{i=1}^{36} (R_{Top\ i} + R_{Bot\ i}) \quad \text{Eq. 5.1}$$

$$\text{Total Bar Corrosion Rating} = \sum_{n=1}^m R_{Bar\ n} \quad \text{Eq. 5.2}$$

where,

- $R_{Top\ i}$  = corrosion rating on top bar surface, interval  $i$
- $R_{Bot\ i}$  = corrosion rating on bottom bar surface, interval  $i$
- $R_{Bar\ n}$  = total bar corrosion rating, bar  $n$
- $i$  = interval, 1 to 36
- $n$  = bar number, 1 to  $m$
- $m$  = total number of bars on each specimen (2 or 8)

The corrosion rating system is described in Table 5.3. Each beam design had a different number of mild steel bars ( $m$ ), depending on the post-tensioning level. The Non-PS beams had 6#6 and 2#4 bars as the tensile steel reinforcement ( $m=8$ ). The mixed reinforced beams (2/3 PS) had 4#3 and 4#4 bars ( $m=8$ ). The 100% PS specimens, designed either with the strength design method or the allowable stress design method, had 2#3 mild steel bars ( $m=2$ ). These bars were not required by design, but were included for construction purposes. The variation in number of longitudinal bars is accounted for in the analysis of the data. (See Section 6.1)

The stirrups were also rated using Table 5.3. However, a different equation was used to calculate the total stirrup rating. As with the longitudinal mild steel, the ratings for the top and bottom bar surface of each interval were summed to give a total corrosion rating for the stirrup.

The total stirrup rating was calculated as follows:

$$R_{Stirrup} = \sum_{i=1}^9 (R_{Top\ i} + R_{Bot\ i}) \quad Eq. 5.3$$

$$Total\ Stirrup\ Corrosion\ Rating = \sum_{n=1}^6 R_{Stirrup\ n} \quad Eq. 5.4$$

where,

- $R_{Top\ i}$  = corrosion rating on top bar surface, interval  $i$
- $R_{Bot\ i}$  = corrosion rating on bottom bar surface, interval  $i$
- $R_{Stirrup\ n}$  = total stirrup corrosion rating, stirrup  $i$
- $i$  = interval, 1 to 9
- $n$  = stirrup number, 1 to 6

**Table 5.3: Evaluation and Rating System for Corrosion Found on Mild Steel Bars<sup>1</sup>**

Code	Meaning	Description	Rating
NC	No Corrosion	No evidence of corrosion	0
D	Discoloration	No evidence of corrosion, but some discoloration from original color	1
L	Light	Surface corrosion on less than one half of the interval, no pitting. Surface corrosion can be removed using cleaning pad.	2
M	Moderate	Surface corrosion on more than one half of the interval, no pitting. <b>and/or</b> Corrosion cannot be completely removed using cleaning pad.	4
P	Pitting	Pits visible to unaided eye.	8
AR	Area Reduction	Measurable reduction in bar cross-sectional area due to corrosion	R <sup>2</sup>

R = Estimated cross-sectional area reduction in percent

#### 5.4.2 Galvanized Steel Duct/Duct Splice

The galvanized steel ducts were examined at 36 two-inch intervals, and the duct splices at 6 two-inch intervals as indicated in Figure 5.7. At each interval, a corrosion rating was assigned to the inside and outside surfaces of the top and bottom of each duct. The rating system for the galvanized steel ducts and duct splices is described in Table 5.4.

The total duct corrosion rating was calculated as follows:

$$\text{Duct Corrosion Rating} = \sum_{i=1}^{36} R_{\text{TopOuter},i} + R_{\text{BotOuter},i} + R_{\text{TopInner},i} + R_{\text{BotInner},i} \quad \text{Eq. 5.5}$$

where,  $R_{\text{TopOuter},i}$  = corrosion rating on top outer surface, interval  $i$   
 $R_{\text{BotOuter},i}$  = corrosion rating on bottom outer surface,  
interval  $i$   
 $R_{\text{TopInner},i}$  = corrosion rating on top inner surface, interval  $i$   
 $R_{\text{BotInner},i}$  = corrosion rating on bottom inner surface,  
interval  $i$   
 $i$  = interval, 1 to 36



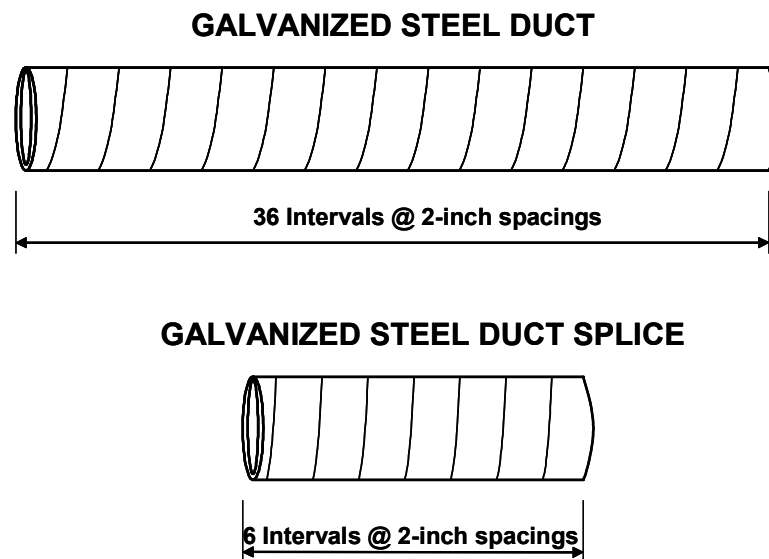


*Figure 5.7: Intervals for Corrosion Ratings on Galvanized Steel Duct/Splice*

**Table 5.4: Evaluation and Rating System for Corrosion Found on Galvanized Steel Duct/Duct Splice<sup>1</sup>**

<b>Code</b>	<b>Meaning</b>	<b>Description</b>	<b>Rating</b>
NC	No Corrosion	No evidence of corrosion	0
D	Discoloration	No evidence of corrosion, but some discoloration from original color	1
L	Light	Surface corrosion on less than one half of the interval, no pitting.	2
M	Moderate	Surface corrosion on more than one half of the interval, no pitting.	4
S	Severe	Corrosion completely covers the interval. <b>and/or</b> Presence of pitting.	8
H	Hole Through Duct	Hole corroded through duct.  Used in conjunction with ratings D, L, M and S.	32 + A <sub>h</sub>

A<sub>h</sub> = Area of hole(s) in mm<sup>2</sup>

### 5.4.3 Prestressing Strand

The strands were examined at 36 two-inch intervals, just like the longitudinal bars. Corrosion ratings were assigned to the outer six wires of the strand and the center wire (after de-stranding) at each interval. This was done to address the possibility of different corrosion activity on the interior and exterior of the strand, and the interstices between wires. The corrosion rating system for the prestressing strands is described in Table 5.5. The total strand corrosion rating was calculated as follows:

$$\text{Strand Corrosion Rating} = \sum_{i=1}^{36} R_{Outer,i} \times n_i + R_{Center,i} \quad \text{Eq. 5.6}$$

where,

- $R_{Outer,i}$  = corrosion rating on outer wires, interval  $i$
- $n_i$  = number of corroded outer wires, interval  $i$
- $R_{Center,i}$  = corrosion rating on center wire, interval  $i$
- $i$  = interval, 1 to 36

***Table 5.5: Evaluation and Rating System for Corrosion Found on Prestressing Strand<sup>1</sup>***

<b>Code</b>	<b>Meaning</b>	<b>Description</b>	<b>Rating</b>
NC	No Corrosion	No evidence of corrosion.	0
D	Discoloration	No evidence of corrosion, but some discoloration from original color.	1
L	Light	Surface corrosion on less than one half of the interval, no pitting. Surface corrosion can be removed using cleaning pad.	2
M	Moderate	Surface corrosion on more than one half of the interval, no pitting. <b>and/or</b> Corrosion cannot be completely removed using cleaning pad.	4
P1	Mild Pitting	Broad shallow pits with a maximum pit depth not greater than 0.02 in.	8
P2	Moderate Pitting	Pitting where the maximum pit depth ranged between 0.02 and 0.04 in.	16
P3	Severe Pitting	Pitting where the maximum pit depth is greater than 0.04 in.	32

As reported by West,<sup>1</sup> the use of a cleaning pad to assess corrosion severity and classify the degree of rusting on a prestressing strand for new construction was used in this rating system. The recommended cleaning pad is a 3M Scotch Brite Cleaning Pad. The pad is held by hand and rubbed longitudinally along the strand axis with a pressure similar to that used when cleaning pots and pans. The classification of pitting severity was based on tensile tests performed on corroded prestressing strands. The tests were used to assign a reduced tensile capacity of 97% GUTS to pitting damage at the level of P1. Moderate pitting (P2) was assigned a capacity of 90% GUTS, and severe pitting

(P3) a capacity of 77% GUTS. In general, the presence of any pitting visible to the unaided eye is deemed cause for rejection in new construction.

#### **5.4.4 Duct Splice**

All Industry Standard and Heat-Shrink duct splices were thoroughly inspected for corrosion, salt deposits, zinc corrosion products, rust staining and damage. Additionally, all Industry Standard duct splices were galvanized steel and were rated using the procedure in Section 5.4.2.

## 5.5 SPECIMEN EXAMINATION AND DATA – PHASE I SPECIMENS

It was determined that the best way to examine the performance of the individual elements of the specimens was to assign each element a total corrosion rating. The procedure followed for assigning the ratings is described in Section 5.4. Like many of the measurements taken during exposure testing, the purpose of the corrosion ratings was to compare the corrosion severity among the specimens and to identify trends. The general and local corrosion ratings calculated for each specimen are summarized in a small table located in each of the following sections. (See Section 5.7 for an explanation of the determination of the generalized and localized corrosion ratings.)

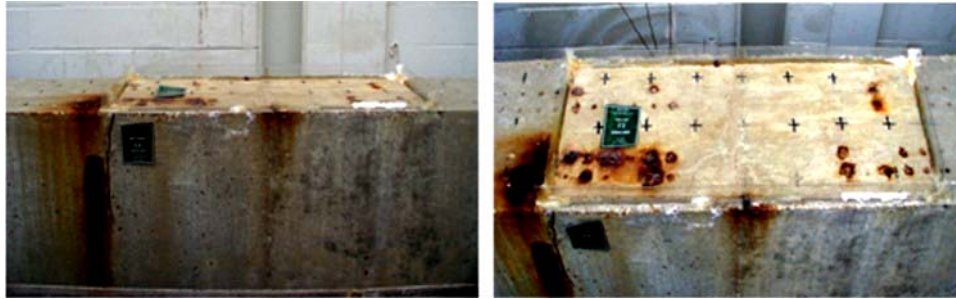
### 5.5.1 Beam Specimen 1.1 – Non-PS, Unloaded

At the end of exposure, rust stains were visible on the north side of the specimen, as shown in Figure 5.8. On the south side, only two small rust spots were visible. In most cases, corrosion stains were attributed to

Specimen	Corrosion Rating:	
	Generalized Rating	Localized Rating
Stirrups	101	295
Long. Mild Steel	1	8
Duct	NA	NA
Strand	NA	NA

corrosion of the bolster strips used to support the reinforcement during construction. This was evident due to the concrete spalling around the “feet” of many of the strips. The bolster strips were plastic tipped, but still corroded very early during testing, as reported by West.<sup>1</sup> The spots of rust were aligned and at regular intervals.

A 0.003-inch maximum width crack extended from the northeast corner of the ponded region, down the beam a distance of 11 inches. Hairline cracks were visible in the northeast corner of the ponded region between the corroded bolster tips.



*Lateral (North) View*

*Top View (from North Side)*

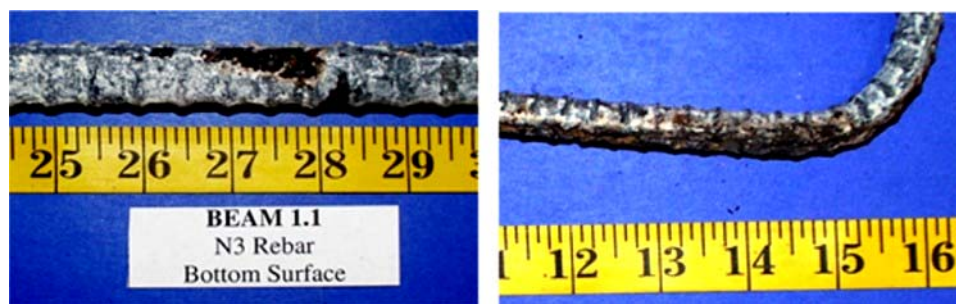
***Figure 5.8: Specimen 1.1 – Condition Prior to Autopsy***

This specimen was partially autopsied as explained in Section 4.3.2. Forty-two inches of the mild steel bars west of the centerline and four stirrups were exposed and removed. The analysis length included half of the ponded region (24 inches) and an additional foot and a half (18 inches) outside the ponded region.

After removing all mild steel bars in the autopsy region, severe corrosion was found on three out of eight longitudinal bars. The corrosion was very localized, at approximately 14 inches from the beam centerline. These localized corrosion areas coincided with the rust stains found on the top of the specimen in the northeast corner of the ponded region. In Figure 5.9, the measurement tape indicates the localized corrosion at 28 inches from the left end of the mild steel bar. This location corresponds to 14 inches from the beam centerline.

Stirrups were placed at 12-inch spacings in all specimens. Therefore, four stirrups were included in the partial autopsy region. After a detailed visual inspection, severe localized corrosion was found in the stirrup located 14 inches from the beam centerline. (The actual location of the center stirrup was two inches

from the beam centerline) The most severe corrosion was found in the north top corner of the stirrup, as shown in Figure 5.9. The stirrups located at 26 and 38 inches from the beam centerline had moderate to light corrosion in the top section, with no section loss. These stirrups were located outside the ponded region. The center stirrup, located 2 inches from the beam centerline, had only minor discoloration and light corrosion in localized areas.



*Longitudinal Bar*

*Stirrup*

*Figure 5.9: Specimen 1.1 – Mild Steel Bar and Stirrup*

Figure 5.10 shows the longitudinal bar and stirrup corrosion rating graphs. Corrosion rating values for the east side of the beam were extrapolated from the west side, due to the partial autopsy procedure. This was done to compare results of the partial autopsy beams with those of the full autopsy beams. By doing so, it was assumed that the bars and stirrups to the east side of the beam centerline performed similarly to those west of the centerline.

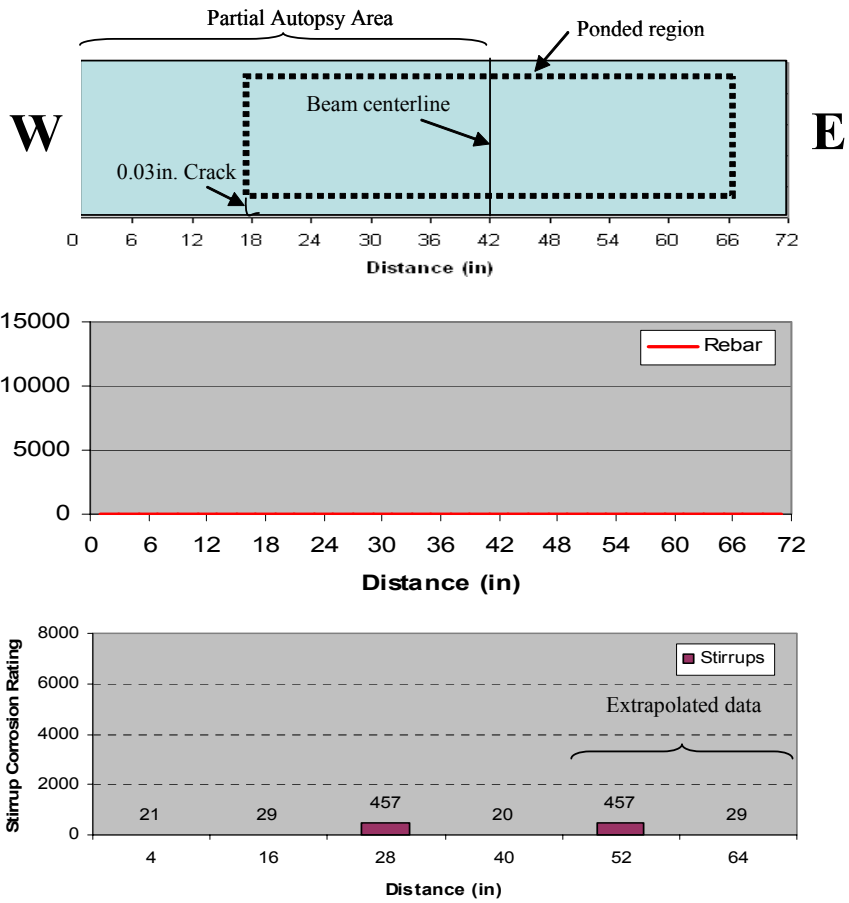


**Figure 5.10: Specimen 1.1 – Crack Pattern and Specimen Corrosion Rating Graphs**



### 5.5.2 Beam Specimen 1.3 – Non-PS, Service Load

Specimen condition after testing included nine transverse cracks in the constant moment region (seven in the ponded region), with a maximum crack width of 0.020 inches. Longitudinal cracks were also visible at 4.5 inches

from the sides of the beam. Heavy rust stains and salt deposits were visible in the top of the cracks in localized areas, as shown in Figure 5.11.

Specimen	Corrosion Rating:	
	Generalized Rating	Localized Rating
Stirrups	1231	770
Long. mild steel	91	261
Duct	NA	NA
Strand	NA	NA



*Lateral (South) View*



*Top View (from South Side)*

**Figure 5.11: Specimen 1.3 – Condition Prior to Autopsy**

Very severe corrosion, pitting and section loss were observed for all longitudinal bars, corresponding with crack locations. All the stirrups were also severely corroded, with large pits and section loss. Crack locations coincided with the stirrup locations. Therefore, the stirrups were severely damaged, especially under the ponded region. Figure 5.12 shows examples of the typical longitudinal bar and stirrup corrosion in Specimen 1.3. Figure 5.13 shows the crack pattern in the top of the specimen after exposure and the rebar and stirrup corrosion ratings across the analyzed section.



*Longitudinal Bar*

*Stirrup*

*Figure 5.12: Specimen 1.3 – Mild Steel Bar and Stirrup*

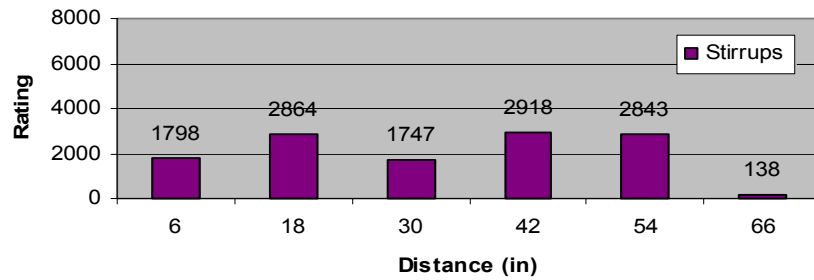
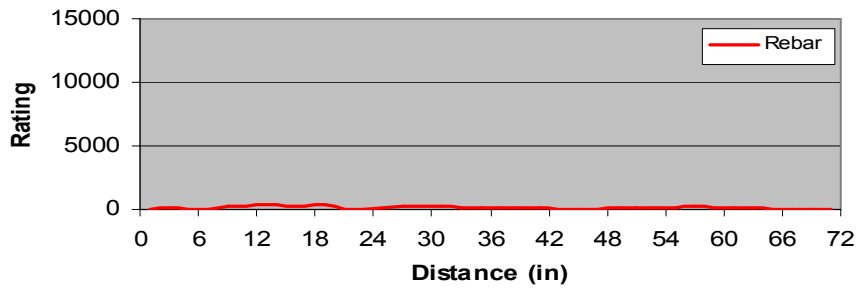
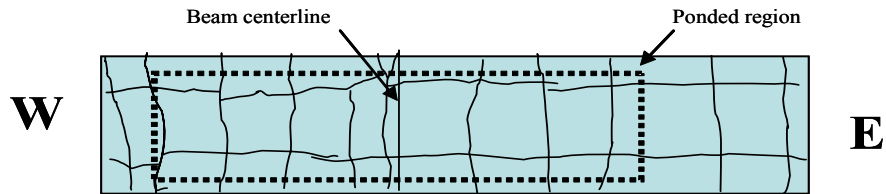


*Figure 5.13: Specimen 1.3 – Crack Pattern and Specimen Corrosion Rating Graphs*

### 5.5.3 Beam Specimen 2.3 – 2/3 PS, Service Load

Three main transverse cracks, with a maximum crack width of 0.02 inches, and two longitudinal cracks, with a maximum crack width of 0.05 inches, were found at the end of exposure. These cracks were located on the top of the specimen in the ponded region. Salt deposits and large rust stains were visible on the sides of the beam, as shown in Figure 5.14.

Specimen	Corrosion Rating:	
	Generalized Rating	Localized Rating
Stirrups	1359	2236
Long. mild steel	467	6241
North Duct	4299	2107
South Duct	5069	6248
North Strands	96	20
South Strands	122	56

Very severe pitting and section loss was found on the mild steel bars in the northeast corner of the ponded region. (See Figure 5.16) The corrosion was located 24 inches from the beam centerline, which corresponded with the border of the ponded region. The stirrups were also severely corroded, as seen in Figure 5.16. It was found that severely corroded stirrups coincided with crack locations. (See graphs in Figure 5.17)



*Lateral (South) View*

*Top View (from South Side)*

**Figure 5.14: Specimen 2.3 – Condition Prior to Autopsy**

Extremely severe corrosion and area loss, corresponding to crack locations, was found in both post-tensioning ducts. (See Figure 5.16 and graphs in Figure 5.17) Corrosion was aggravated at locations where large grout voids existed, as shown in Figure 5.15. A large accumulation of corrosion products from the ducts was found attached to the grout.

Moderate localized corrosion and pitting in a few wires was found on the south strands. The north strands show only moderate to light uniform corrosion. As with the mild steel bars, stirrups and ducts, localized corrosion in the strands corresponded to crack locations in the ponded region.

The acid soluble chloride content in the grout reached a maximum value of 0.3% by weight of grout inside the south duct, and 0.18% inside the north duct. These values are much higher than the critical chloride threshold value of 0.033% by weight of grout (corresponding to 0.2% by weight of cement). Chloride samples were taken at 6-inch intervals within the forensic analysis length and chloride content plots were obtained, as observed in Figure 5.17.

Beam specimen 2.3 had four duct splices. The north duct had two industry standard splices, and the south duct had two heat-shrink splices. Figure 5.15 shows the condition of the duct splices at the end of exposure testing. Severe area loss and extremely severe corrosion were found on the oversized piece of both industry standard splices in the north duct. As shown in the photographs, moisture was able to enter the sides of the splice at the duct tape locations. This accelerated the corrosion by allowing corrosive attack from the inside of the splice as well as the outside. Voids in the grout at the splice locations also aggravated the corrosion in the galvanized steel pieces. The west duct splice on the north duct had been intentionally damaged during construction. The role the damage played with respect to the splice corrosion protection is not clear due to the effect of the other contributing factors, such as splice locations, crack locations, moisture ingress

and chloride contents. The heat-shrink splices in the south duct also performed poorly. As can be seen from Figure 5.15, the east heat-shrink splice trapped moisture from the grout bleed water and accelerated the galvanized duct deterioration. The west side splice was intentionally damaged during construction, with a small cut (less than 1 inch) in the center. The generalized duct corrosion under the splice and the uniform rust stains on the inside of the heat-shrink splice indicate that the damage was not the main cause of duct corrosion. Nevertheless, the damage is considered as one of the duct deterioration contributing factors.

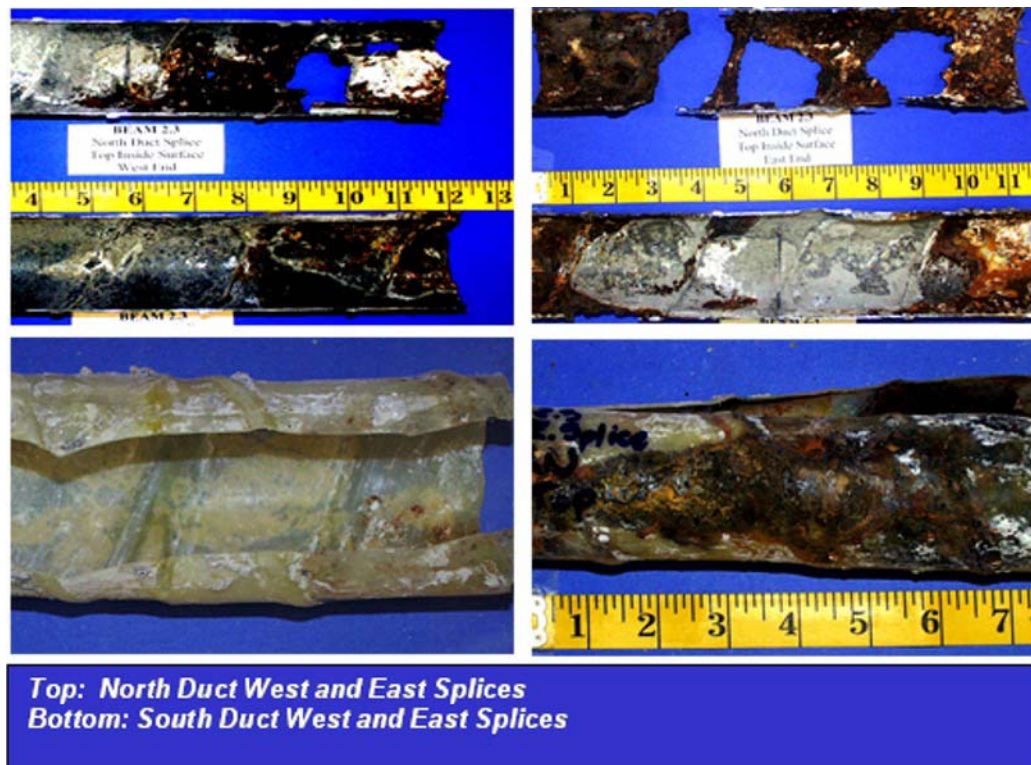


*Figure 5.15: Specimen 2.3 – Duct Splices*

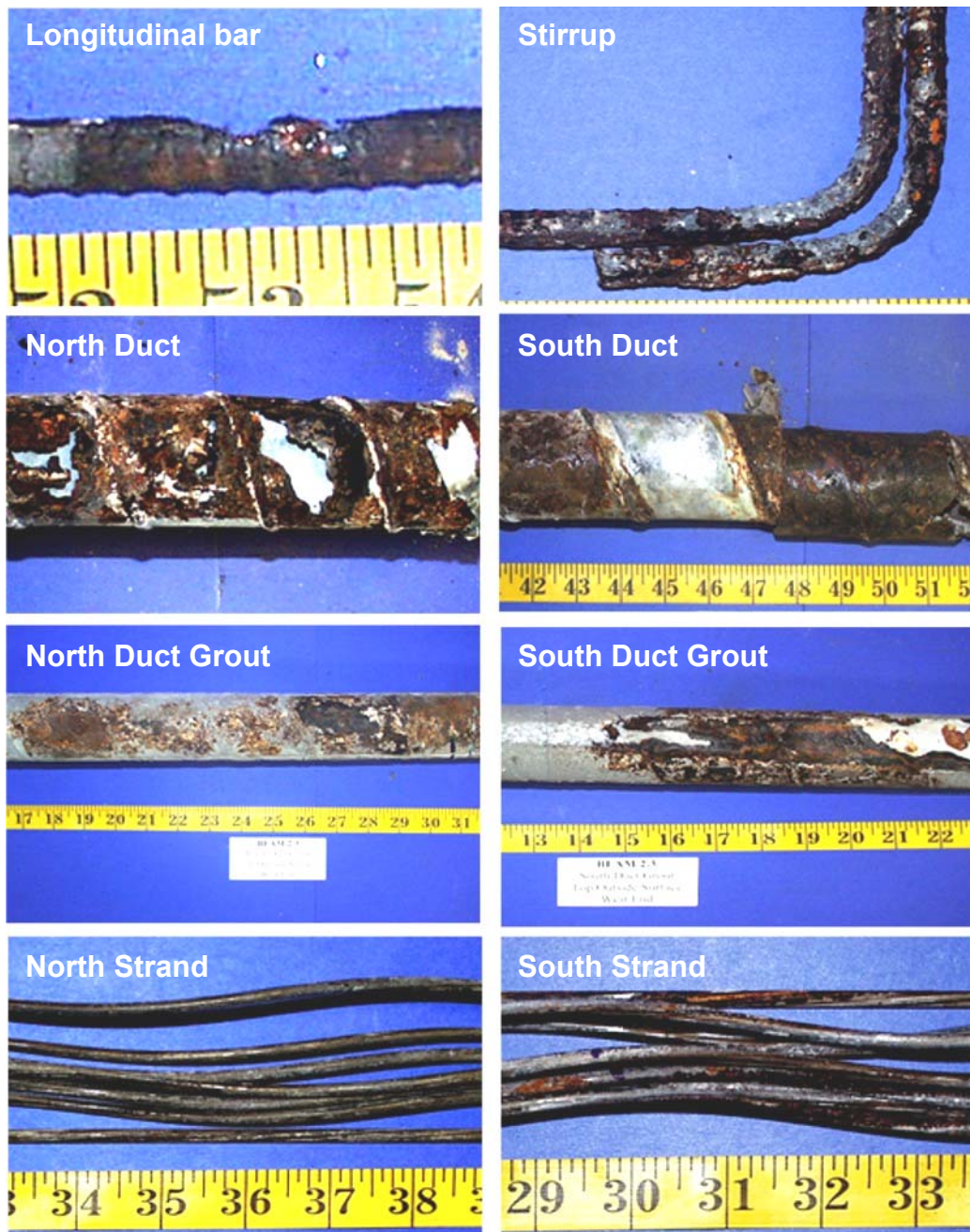


**Figure 5.16: Specimen 2.3 – Reinforcing Elements**

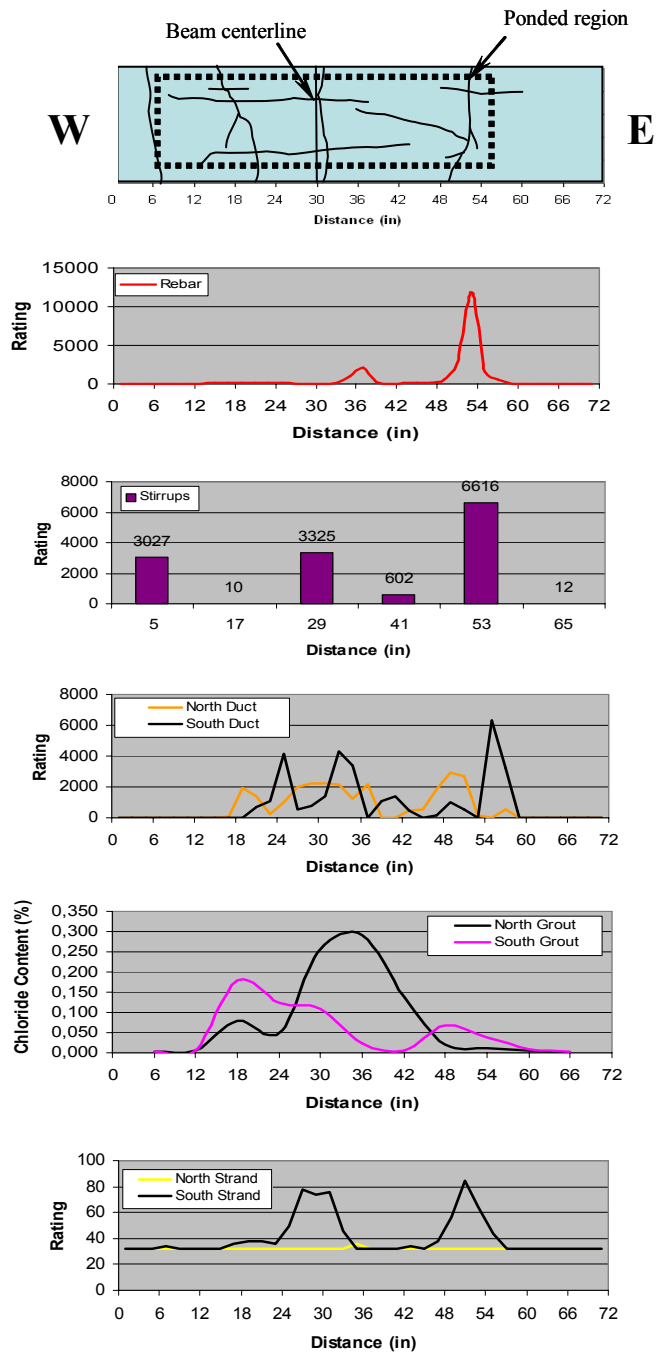


**Figure 5.17: Specimen 2.3 – Crack Pattern and Specimen Corrosion Rating Graphs**

#### 5.5.4 Beam Specimen 2.11 – 2/3 PS, Service Load, Fly Ash Grout

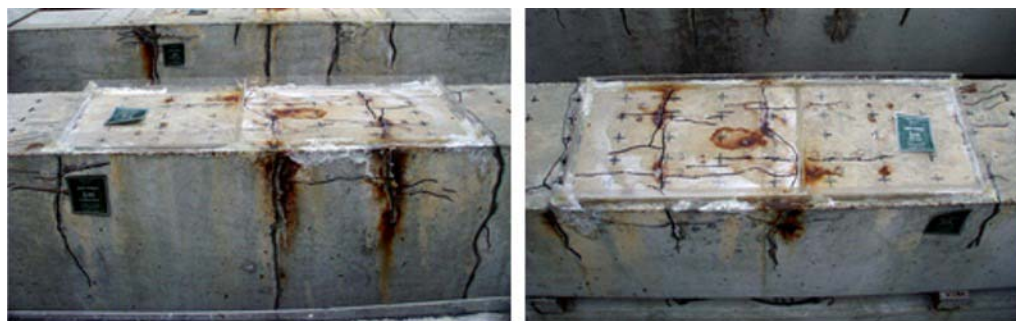
As shown in Figure 5.18, four main transverse cracks and several small longitudinal cracks were visible on the top of Specimen 2.11 in the constant moment region at the end of exposure. A maximum crack width of 0.03 inches was found in the southwest area of the ponded region. Heavy rust stains were

visible on the top of the specimen in localized areas extending out of the cracks, as shown in Figure 5.18. The additional rust stains corresponded to the location of the “legs” of the bolster strips, used to support the reinforcement.

A full autopsy of Specimen 2.11 was performed, providing a total length of 72 inches of the longitudinal bars, ducts, grout and strands and six stirrups to be analyzed. Thirty inches of the analysis length extended to the west of the centerline of the beam and the remaining 42 inches extended to the east.

#### Corrosion Rating:

Specimen	Generalized Rating	Localized Rating
Stirrups	1923	2978
Long. mild steel	476	7757
North Duct	1504	2440
South Duct	1413	1673
North Strands	97	20
South Strands	92	26



*Lateral (North) View*

*Top View (from South Side)*

**Figure 5.18: Specimen 2.11 – Condition Prior to Autopsy**



Very severe section loss and pitting was observed in all longitudinal mild steel bars corresponding to all crack locations. (See Figure 5.20) The most severe corrosion was found at the beam centerline crack. Similar results were found on the stirrups, where the beam centerline stirrup had extensive corrosion and section loss.

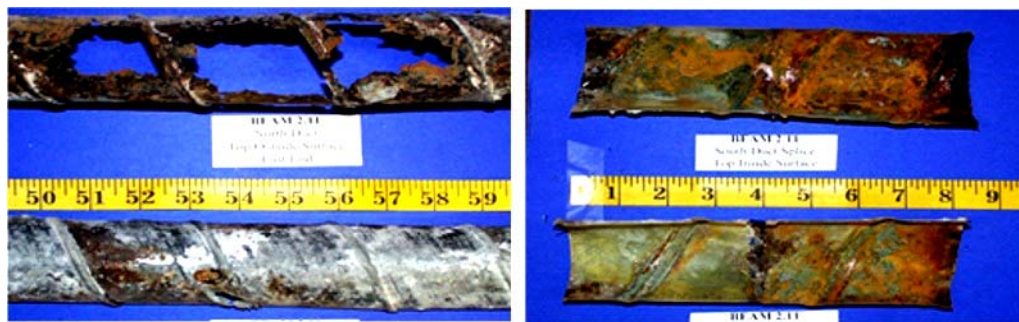
Figure 5.20 shows the severe corrosion and area loss found in the south duct. Extensive duct deterioration was mostly located to the west of the centerline. Zinc and steel corrosion products covered the remaining areas on the top of the duct. The bottom of the duct was found to be in better condition, with some areas of zinc and steel corrosion products. Corrosion on the north duct was less severe than on the south duct. It was also found to have a few areas of severe localized corrosion, section loss, and build up of zinc and steel corrosion products. The corrosion on the north duct was significant at the centerline of the beam, under the industry standard splice.

The south duct grout had several transverse cracks, with a maximum crack width of 0.060 inches. This crack coincided with the location of the heavy duct corrosion and area loss. Duct corrosion stains were found inside the grout cracks, where moisture had traveled down from the grout surface. (See Figure 5.20) The north duct grout had one large void due to bleed water that was 22 inches in length and 0.013 inches deep. Corrosion products were found attached to the grout in the void. This location corresponded with the splice location at the centerline of the beam. Three transverse cracks, with a maximum crack width of 0.010 inches, were found on the east side of the grout. The cracks coincided with the area where severe duct corrosion and duct area loss were found. The acid soluble chloride content in the grout reached a maximum value of 0.31% by weight of grout inside the north duct, and 0.033% inside the south duct. The content in the north duct was from the sample taken at the centerline of the beam,

under the industry standard splice. It was much higher than the critical chloride threshold value of 0.033% by weight of grout. Chloride samples were taken at 6-inch intervals within the forensic analysis length and chloride content plots were obtained, as observed in Figure 5.21.

Light to moderate corrosion was found on the outer wires of the strands in both ducts, with the center wires presenting a slight increase in corrosion severity.

Specimen 2.11 had two duct splices. The north duct had an industry standard splice, and the south duct had a heat-shrink splice. Both splices were located at the centerline of the beam. Figure 5.19 shows the condition of the duct splices at the end of exposure testing. The top of the north duct splice was found to be severely deteriorated. The heat-shrink splice showed severe signs of rust staining from the duct corrosion.



*North Duct Splice*

*South Duct Splice*

**Figure 5.19: Specimen 2.11 – Duct Splices**

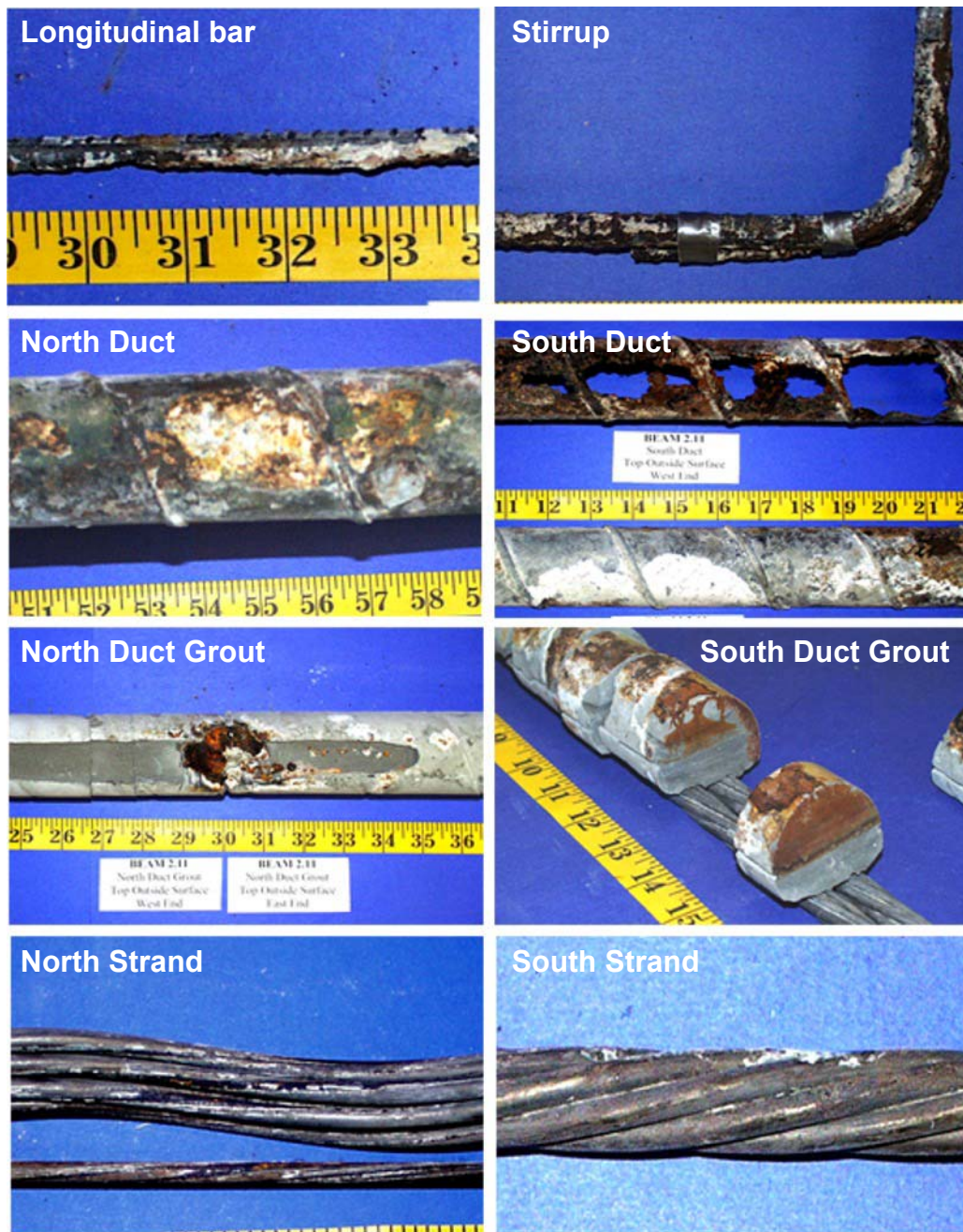


*Figure 5.20: Specimen 2.11 – Reinforcing Elements*

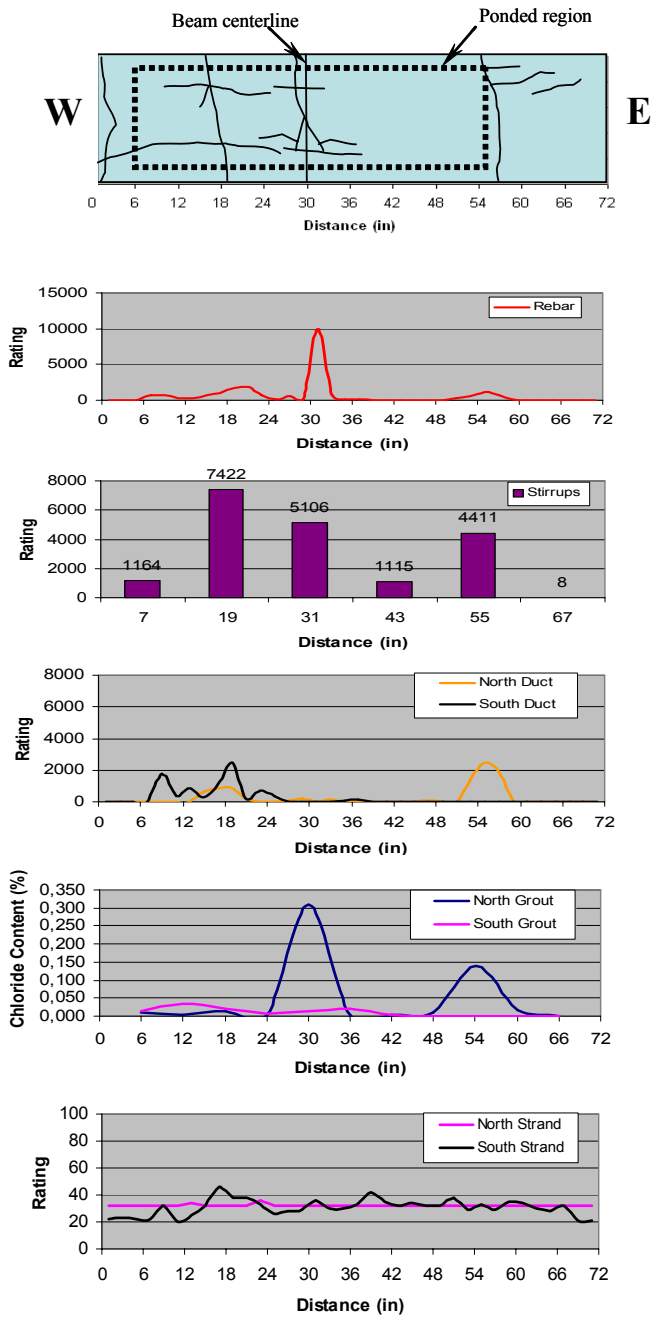


**Figure 5.21: Specimen 2.11 – Crack Pattern and Specimen Corrosion Rating Graphs**

### 5.5.5 Beam Specimen 3.1 – 100%U PS, Unloaded

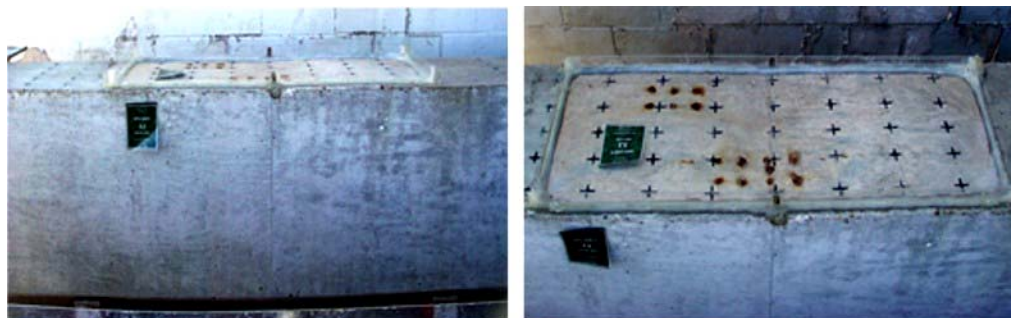
As seen in Figure 5.22, a visual inspection of Specimen 3.1 at the end of exposure found that it remained uncracked. Any rust staining on Specimen 3.1 was due to the bolster strips.

This specimen was partially autopsied, as explained in Section 4.3.2.

The analysis length included half of the ponded region (24 inches) and an additional foot and a half (18 inches) outside the ponded region. Forty-two inches of the mild steel bars, ducts, grout and strands west of the centerline were exposed and removed. The section autopsied only included three stirrups for analysis.

**Corrosion Rating:**

<b>Specimen</b>	<b>Generalized Rating</b>	<b>Localized Rating</b>
Stirrups	15	4
Long. mild steel	0	0
North Duct	0	0
South Duct	0	0
North Strands	119	20
South Strands	96	22



*Lateral (North) View*

*Top View (from North Side)*

**Figure 5.22: Specimen 3.1 – Condition Prior to Autopsy**

As shown in Figure 5.24, there was no corrosion found on either of the mild steel bars in Specimen 3.1.

Light uniform corrosion was found on the three stirrups included in the partial autopsy. The centerline stirrup was intended to be included in the partial

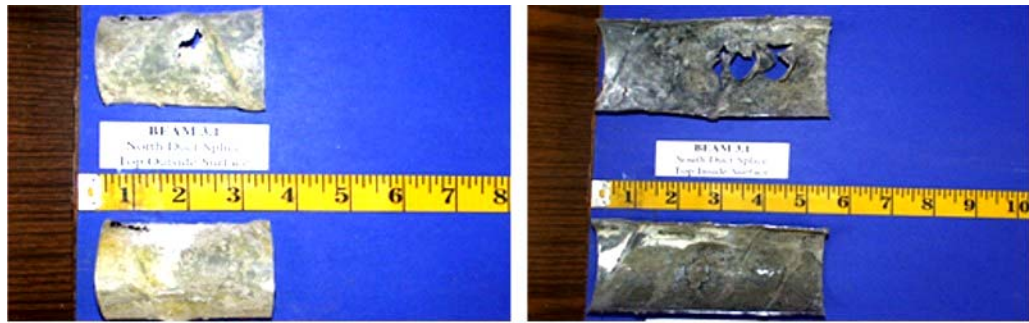
autopsy, but its actual location was outside of the section removed. This is why there is no analysis or rating for the centerline stirrup

There were no signs of corrosion on either of the ducts.

The grout in the north and south ducts showed multiple small voids over the entire length. Neither of the duct grouts had significantly large voids. The acid soluble chloride content in the north duct grout was negligible. The chloride content in the south duct grout was also negligible, except for the single measurement of 0.021% by weight of grout. The sample yielding this value was taken 36 inches to the west of the centerline. It was determined that this value was due to an error in the equipment and considered an outlier. Chloride samples were taken at 6-inch intervals within the forensic analysis length and chloride content plots were obtained, as shown in Figure 5.25.

Moderate uniform corrosion was found on the strands in the north duct, and light uniform corrosion was found on those located in the south duct. (See Figure 5.24)

Specimen 3.1 had two duct splices. The south duct had an industry standard splice and the north duct had a heat-shrink splice. Both splices were located at the centerline of the beam. Therefore, only half of each splice was included in the section autopsied. Figure 5.23 shows the condition of the duct splices at the end of exposure testing. No signs of corrosion were found on either splice.

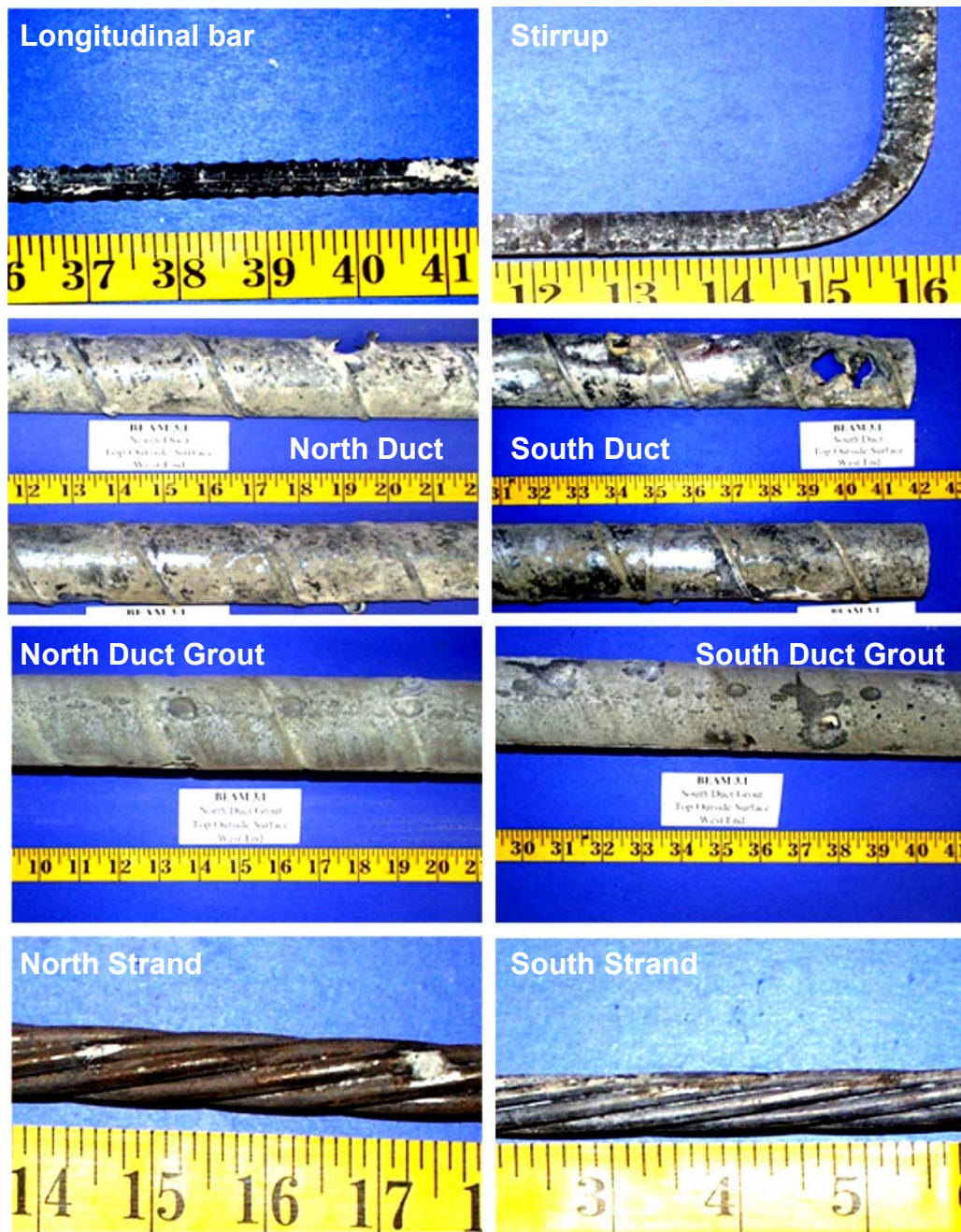


*North Duct Splice*

*South Duct Splice*

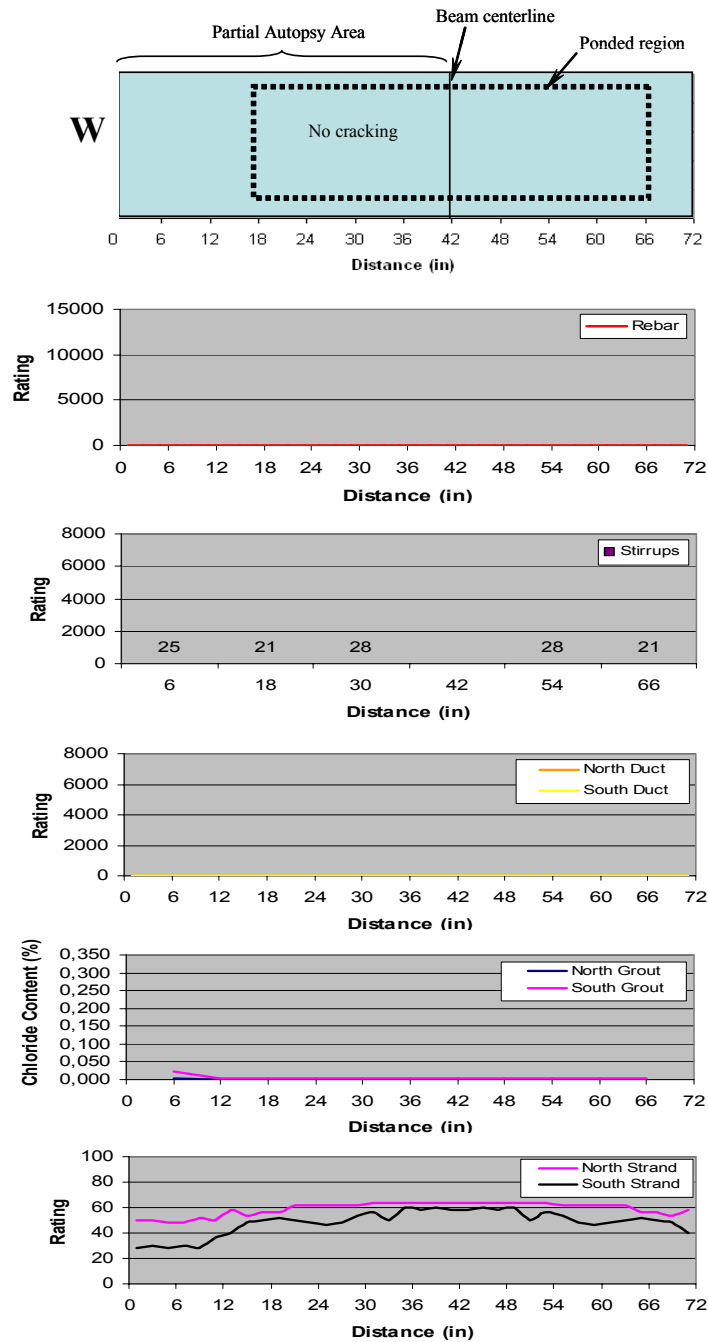
*Figure 5.23: Specimen 3.1 – Duct Splices*

Figure 5.25 shows the chloride content and corrosion rating graphs for each reinforcing element. Corrosion rating values for the east side of the beam were extrapolated from the west side, due to the partial autopsy procedure. This was done to compare results of the partial autopsy beam with those of the full autopsy beams. By doing so, it was assumed that the reinforcing elements to the east side of the beam centerline performed similarly to those west of the centerline.



*Figure 5.24: Specimen 3.1 – Reinforcing Elements*





**Figure 5.25: Specimen 3.1 – Crack Pattern and Specimen Corrosion Rating Graphs**

### 5.5.6 Beam Specimen 3.2 – 100%U PS, Service Load

A visual inspection found that Specimen 3.2 had one transverse crack (See Figure 5.26) across the top of the beam at the end of exposure even though this specimen was designed to remain uncracked. The crack had a maximum width of 0.01 inches and was located 12 inches to the west of the centerline of the

beam. This location was directly above a stirrup. As seen in Figure 5.26, any rust staining was due to the bolster strips.

A full autopsy of Specimen 3.2 was performed, providing a total length of 72 inches of the longitudinal bars, ducts, grout and strands and six stirrups to be analyzed. (See Figure 5.29) Forty-two inches of the analysis length extended to the west of the centerline of the beam and the remaining 30 inches extended to the east.

Specimen	Corrosion Rating:	
	Generalized Rating	Localized Rating
Stirrups	95	462
Long. mild steel	1	4
North Duct	1	2
South Duct	0	2
North Strands	168	28
South Strands	168	28



*Lateral (North) View*



*Top View (from South Side)*

**Figure 5.26: Specimen 3.2 – Condition Prior to Autopsy**

The only corrosion found on the mild steel bars was a small localized area of light corrosion. It was located 10 inches to the east of the centerline.

Two localized areas of severe corrosion and area loss were found on the stirrups. These areas were found on the stirrups located 13 and 25 inches to the west of the centerline. The stirrup 13 inches to the west corresponds to the crack described above. The remaining stirrups showed light uniform corrosion.

The only corrosion found on the north duct was located under the heat-shrink splice at the centerline of the beam. It showed two very light spots of corrosion. The south duct showed no signs of corrosion. (See Figure 5.29)

The grout in the north duct showed multiple small voids over the entire length. The south duct grout had three large voids. A 14-inch long void was located at the centerline, as shown in Figure 5.29. Two six-inch long voids were found 24 inches to the east and to the west of the centerline. Figure 5.27 was included to illustrate the good grouting quality of both ducts in Specimen 3.2. The acid soluble chloride content in the north and south duct grout was negligible. Chloride samples were taken at 6-inch intervals within the forensic analysis length and chloride content plots were obtained, as shown in Figure 5.30.

Light uniform corrosion was found on all of the strands located in the north and south ducts.

Specimen 3.2 had two duct splices. The south duct had an industry standard splice and the north duct had a heat-shrink splice. Both splices were located at the centerline of the beam. Figure 5.28 shows the condition of the duct splices at the end of exposure. Both splices showed no signs of corrosion, with only a minor salt stain on the industry standard splice.

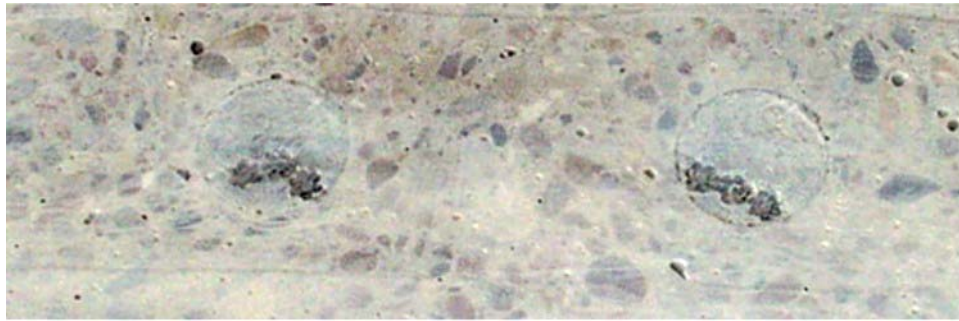


*Figure 5.27: Specimen 3.2 – Grouted Duct*



*North Duct Splice*

*South Duct Splice*

*Figure 5.28: Specimen 3.2 – Duct Splices*

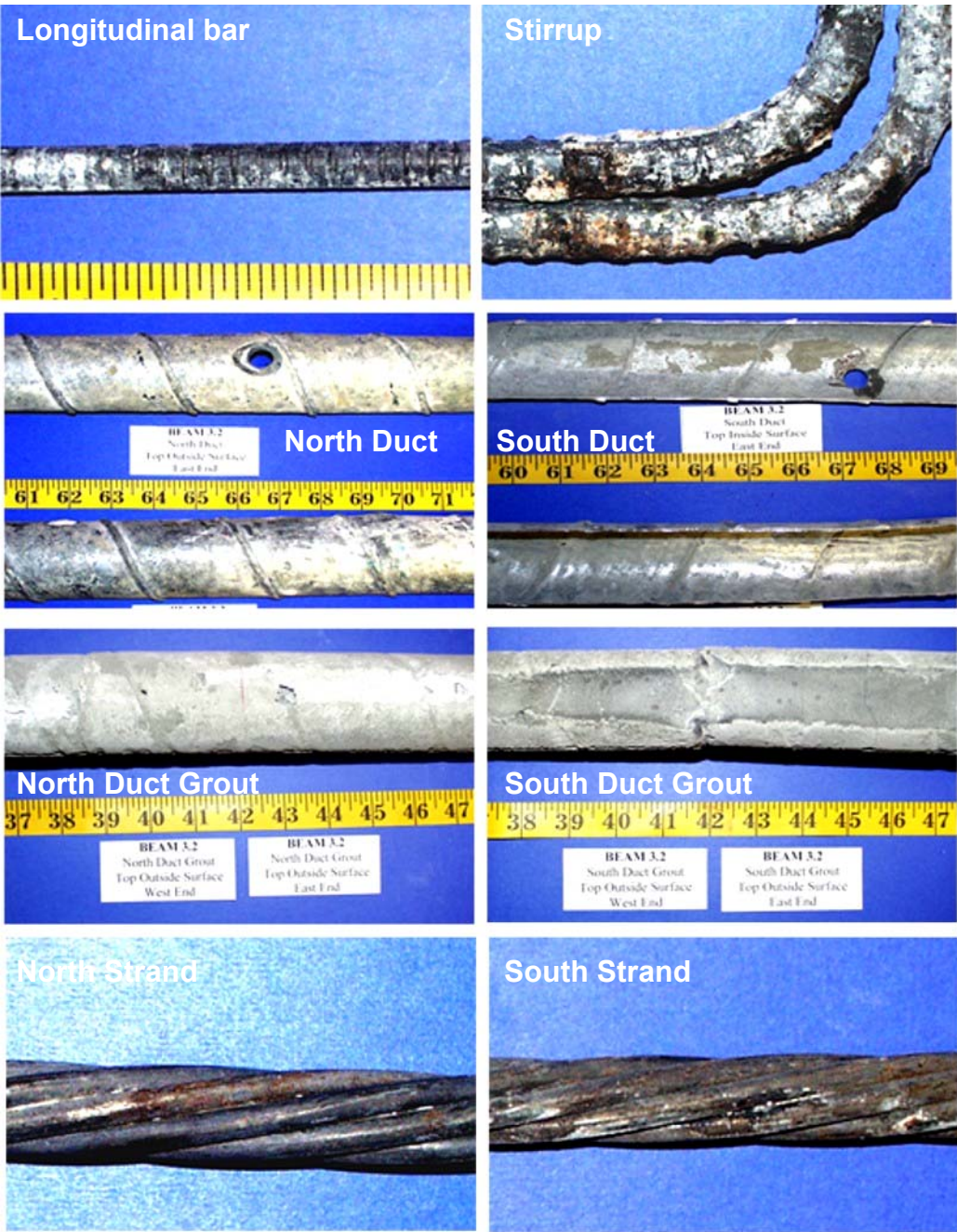


**Figure 5.29: Specimen 3.2 – Reinforcing Elements**

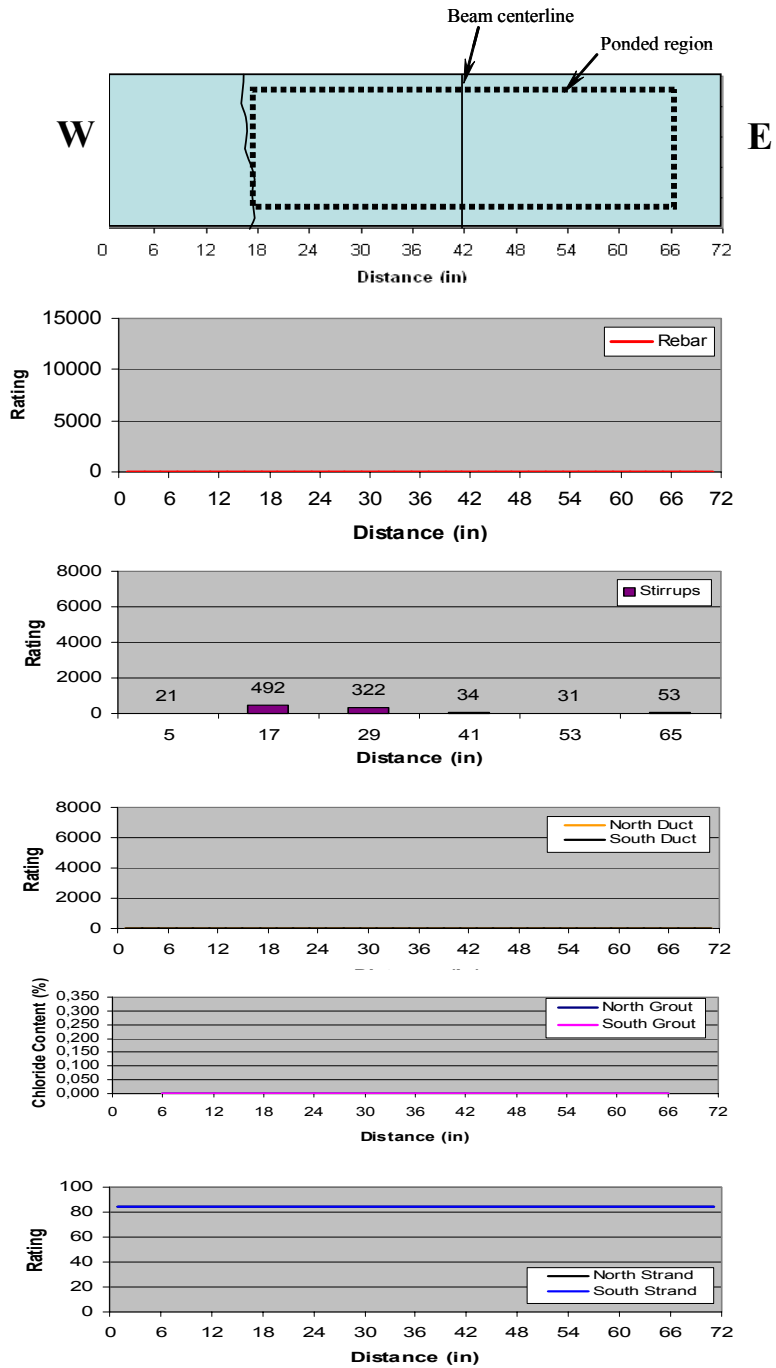


**Figure 5.30: Specimen 3.2 – Crack Pattern and Specimen Corrosion Rating Graphs**

### 5.5.7 Beam Specimen 3.3 – 100%U PS, Overload

As shown in Figure 5.31, specimen 3.3 had three transverse cracks across the top of the beam at the end of exposure. The largest crack had a maximum width of 0.013 inches and was located at the centerline of the beam. This location was directly above a stirrup. The other two cracks had a

maximum width of 0.01 inches. They were located 24 inches to the east and west of the centerline. Both of these cracks also coincided with stirrup locations. As seen in Figure 5.31, there was minor rust staining around the cracks on the sides of the beam. A majority of the rust spots on the top were from the bolster strips.

A full autopsy of Specimen 3.3 was performed, providing a total length of 72 inches of the longitudinal bars, ducts, grout, and strands and six stirrups to be analyzed. Forty-two inches of the analysis length extended to the west of the centerline of the beam and the remaining 30 inches extended to the east. (See Figure 5.33)

Specimen	Corrosion Rating:	
	Generalized Rating	Localized Rating
Stirrups	423	867
Long. mild steel	36	294
North Duct	429	924
South Duct	220	685
North Strands	161	64
South Strands	118	32



*Lateral (North) View*

*Top View (from North Side)*

**Figure 5.31: Specimen 3.3 – Condition Prior to Autopsy**

Two areas with severe corrosion with area loss were found on one of the mild steel bars. They coincided with the stirrups located at the centerline and 24 inches to the west.

Severe uniform corrosion and section loss was found on the three stirrups located under the cracks described above. The remaining stirrups showed light uniform corrosion.

Severe corrosion and area loss corresponding to the three crack locations was found on the north duct. The south duct also showed signs of severe corrosion and area loss at the centerline, and moderate corrosion under the other two cracks. (See Figure 5.33) The remainder of the ducts showed no signs of corrosion.

The grout in the north duct had two voids located at the centerline and 24 inches to the east. Corrosion products from the duct were found coinciding with the three crack locations. Two voids were also present in the south duct grout. They were located 30 inches to the west and 14 inches to the east of the centerline. Neither of these voids coincided with any duct corrosion or crack locations. Corrosion products from the south duct were found coinciding with three crack locations. The acid soluble chloride content in the grout reached a maximum value of 0.0423% by weight of grout inside the north duct at the centerline. The maximum chloride content in the south duct grout was 0.0457% by weight of grout. This sample was located 24 inches to the east of the centerline, which is the same location as one of the cracks and severe duct corrosion. These values are higher than the critical chloride threshold value of 0.033% by weight of grout. Chloride samples were taken at 6-inch intervals within the forensic analysis length and chloride content plots were obtained, as shown in Figure 5.34.



Moderate to severe uniform corrosion was found on all three prestressing strands in the north duct. As shown in Figure 5.33, severe localized corrosion was found 24 inches to the west of the centerline, which again coincides with a crack location. Moderate to severe uniform corrosion was also found on all three prestressing strands in the south duct.

Specimen 3.3 had one duct splice. It was an industry standard splice located on the north duct at the centerline. Figure 5.32 shows the condition of the duct splice at the end of exposure testing. The top of the north duct splice was found to be severely corroded with significant section loss.



***Figure 5.32: Specimen 3.3 – North Duct Splice***

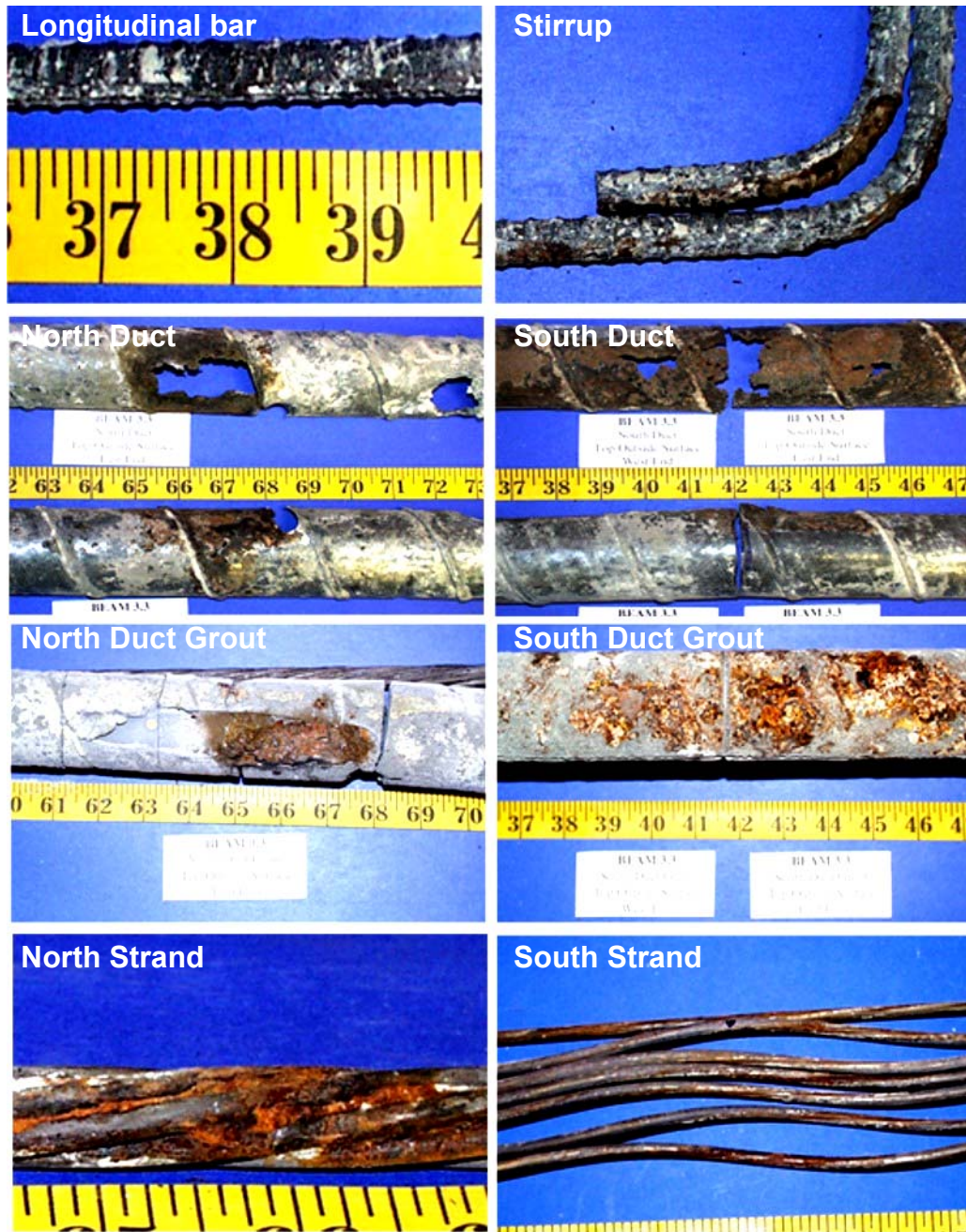


*Figure 5.33: Specimen 3.3 – Reinforcing Elements*

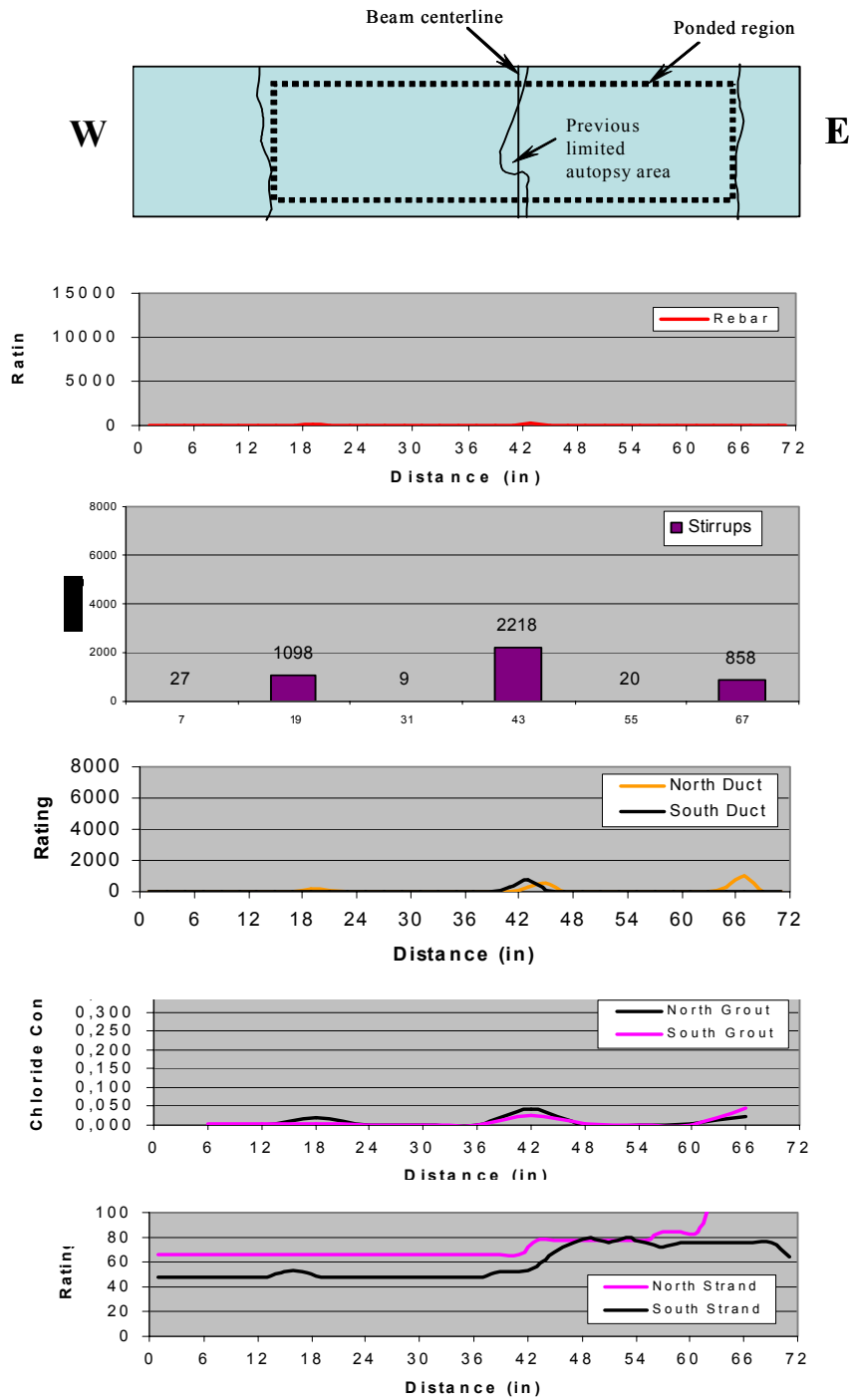


Figure 5.34: Specimen 3.3 – Crack Pattern and Specimen Corrosion Rating Graphs

### 5.5.8 Beam Specimen 4.2 – 100%S PS, Service Load

As shown in Figure 5.35, a visual inspection found that Specimen 4.2 had two transverse cracks across the top of the beam at the end of exposure. This specimen was designed to remain uncracked. The first crack had a maximum width of 0.013 inches and was located one inch to the west of

the centerline of the beam. This location was directly above a stirrup. The second crack had a maximum width of 0.01 inches. It was located 22 inches to the east of the centerline, also above a stirrup. As seen in Figure 5.35, there was no rust staining around the cracks. Any rust spots were again from the bolster strips.

A full autopsy of Specimen 4.2 was performed, providing a total length of 72 inches of the longitudinal bars, ducts, grout and strands and six stirrups to be analyzed. Thirty inches of the analysis length extended to the west of the centerline of the beam and the remaining 42 inches extended to the east. (See Figure 5.38)

Specimen	Corrosion Rating:	
	Generalized Rating	Localized Rating
Stirrups	189	236
Long. mild steel	15	169
North Duct	7	8
South Duct	4	4
North Strands	96	22
South Strands	96	16



*Lateral (South) View*

*Top View (from East Side)*

**Figure 5.35: Specimen 4.2 – Condition Prior to Autopsy**

Signs of corrosion were only found on one of the mild steel bars. It was severe localized corrosion with minor section loss at the centerline. (See Figure 5.37)

Severe localized corrosion and section loss were found on the two stirrups located under the cracks described before. The remaining stirrups showed light uniform corrosion with a few areas of moderate localized corrosion.

Severe corrosion corresponding to the maximum crack location at the centerline was found on the north duct. The south duct showed signs of light to moderate corrosion corresponding with the two cracks on the specimen. The remainder of the ducts showed no signs of corrosion. (See Figure 5.37)

The grout in the north duct had a large void approximately 12 inches long. It was located under the smaller crack to the east of the centerline. Corrosion stains from the duct were found a few inches to the east of the centerline. As seen in Figure 5.37, a large crack in the grout was also present at this location, showing rust stains on the face of the crack. Two large voids were present in the south duct grout. One began six inches to the west of the centerline, extending 18 inches. (See Figure 5.37) The second void was 14 inches in length and began 20 inches to the east. The acid soluble chloride content in the grout reached a maximum value of 0.0023% by weight of grout inside the north and south ducts. This value is much lower than the critical chloride threshold value of 0.033%. Chloride samples were taken at 6-inch intervals within the forensic analysis length and chloride content plots were obtained, as shown in Figure 5.38.

Light uniform corrosion was found on all of the strands located in the north and south ducts.

Specimen 4.2 had four duct splices. The south duct had two industry standard splices, one beginning 12 inches to the east of the centerline and the other 12 inches to the west. The north duct had two heat-shrink splices at the same

locations. Figure 5.36 shows the condition of the duct splices at the end of exposure testing. The only corrosion found on the industry standard splices was very light and located on the end of the splice. Both heat-shrink splices showed no signs of rust staining.

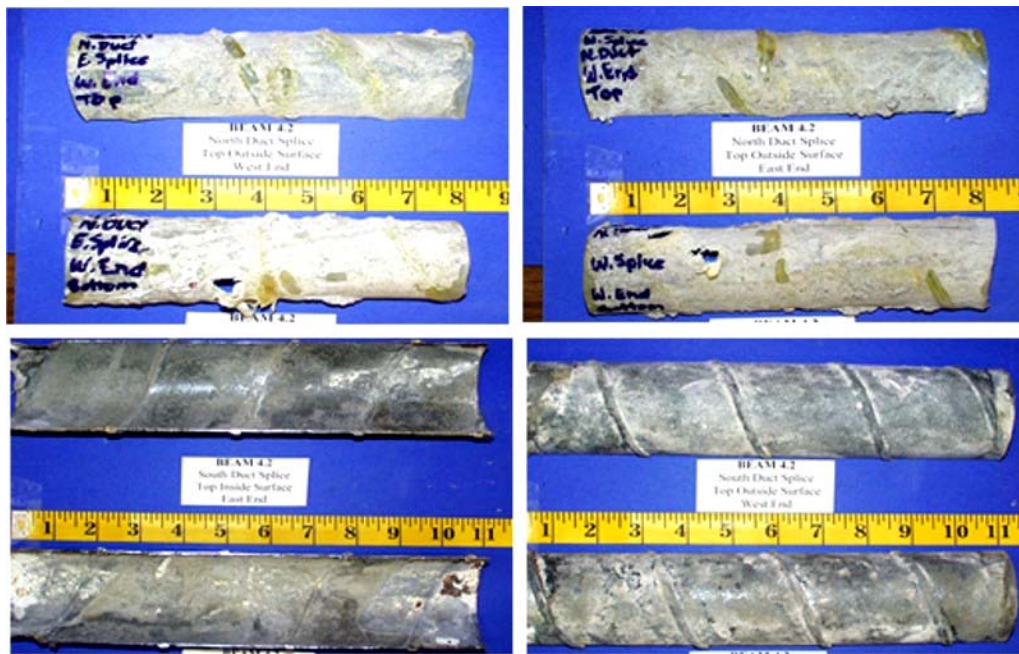


*Figure 5.36: Specimen 4.2 – Duct Splices*

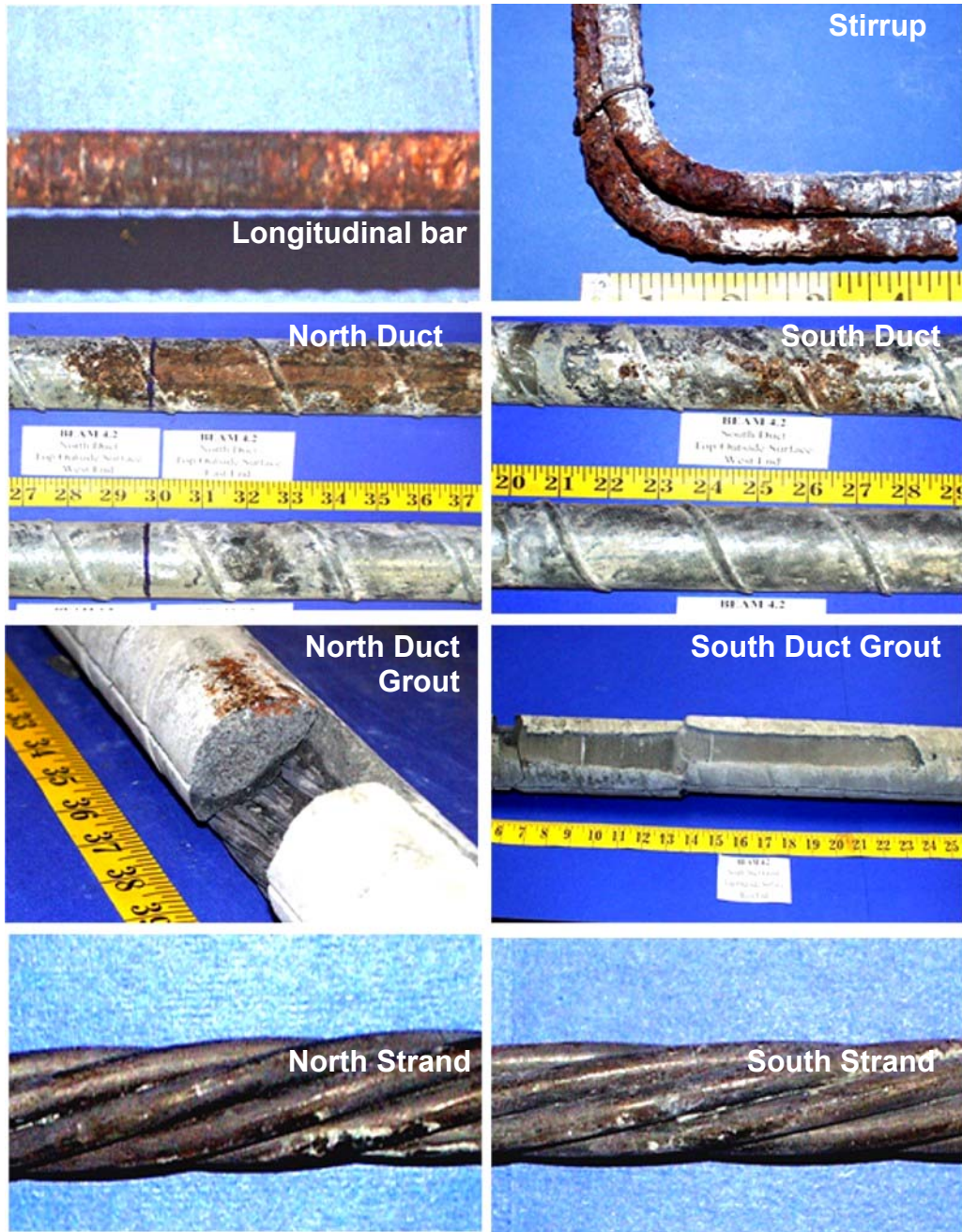


**Figure 5.37: Specimen 4.2 – Reinforcing Elements**

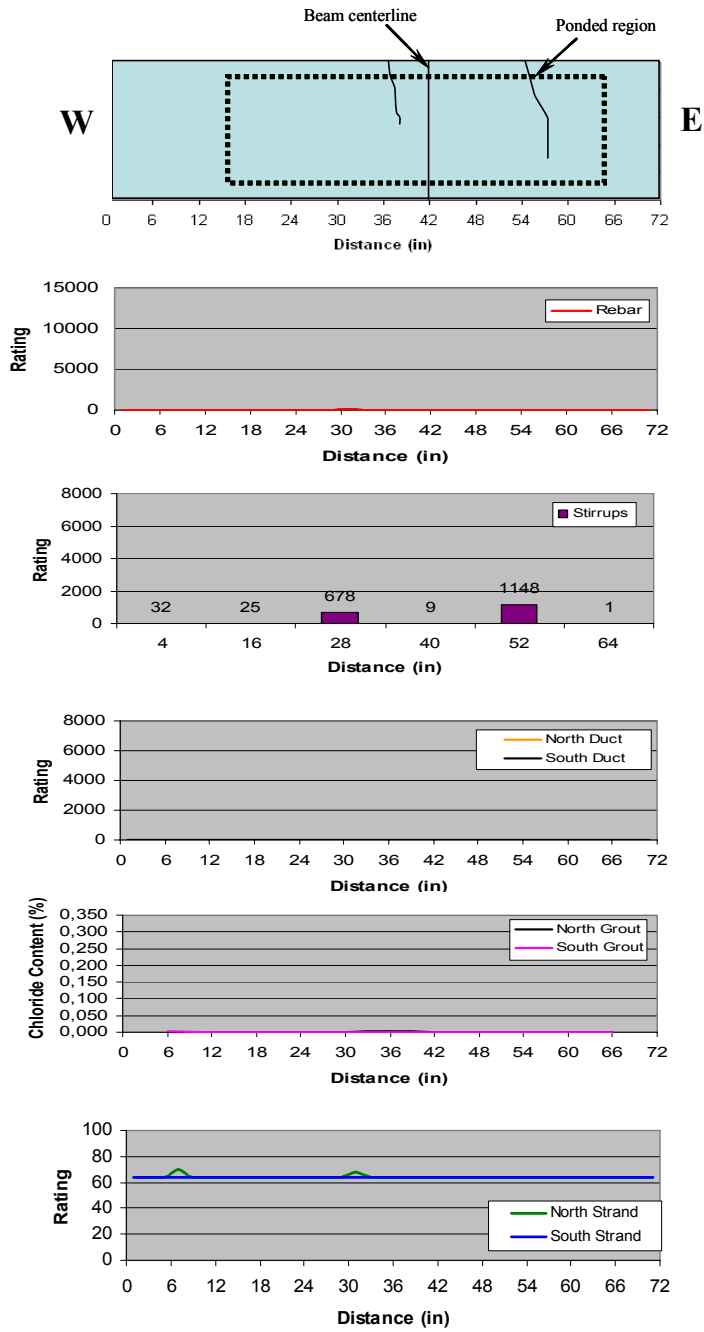


**Figure 5.38: Specimen 4.2 – Crack Pattern and Specimen Corrosion Rating Graphs**



## 5.6 SPECIMEN EXAMINATION AND DATA – PHASE II SPECIMENS

### 5.6.1 Beam Specimen 1.5 – Non-PS, Fly Ash Concrete

At the end of exposure, Specimen 1.5 had a large number of cracks on the top face and both sides. (See Figure 5.39) A majority of the cracks were confined to the constant maximum moment region. There was a large amount of rust staining, corresponding to the cracks, on both

sides of the specimen. Rust stains did not surround the cracks located outside the ponded region. Specimen 1.5 had a maximum crack width of 0.02 inches located 14 inches to the west and 11 inches to the east of the centerline.

#### Corrosion Rating:

Specimen	Generalized Rating	Localized Rating
Stirrups	224	296
Long. mild steel	6	8
North Duct	NA	NA
South Duct	NA	NA
North Strands	NA	NA
South Strands	NA	NA

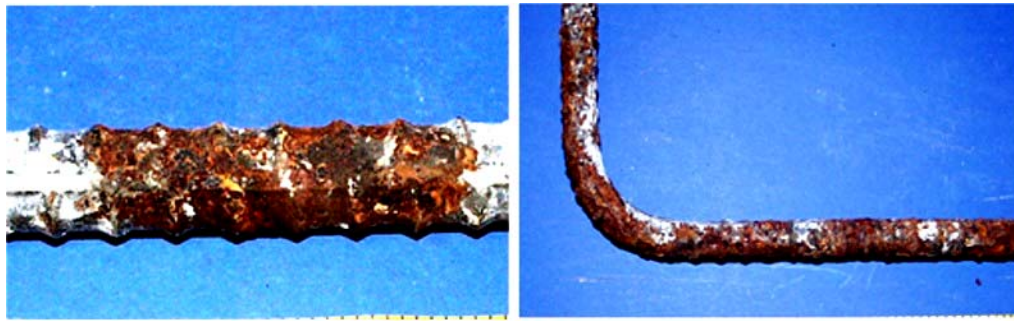


*Lateral (North) View*



*Top View (from South Side)*

*Figure 5.39: Specimen 1.5 – Condition Prior to Autopsy*



*Longitudinal Bar*

*Stirrup*

*Figure 5.40: Specimen 1.5 – Mild Steel Bar and Stirrup*

A full autopsy of Specimen 1.5 was performed, providing a total length of 72 inches of the longitudinal bars and six stirrups to be analyzed. Forty-two inches of the analysis length extended to the west of the centerline of the beam and the remaining 30 inches extended to the east.

After removing all mild steel bars in the autopsy region, very mild corrosion was found on the eight longitudinal bars, with only a few locations showing moderate to severe corrosion. Five of the eight bars showed localized corrosion (See Figure 5.40) 14 inches to the west of the beam centerline. This location coincides with one of the maximum crack width locations.

The actual location of the centerline stirrup was offset one inch to the east of the centerline of the beam. After a detailed visual inspection, pitting and severe corrosion was found on the top portion of four out of the six stirrups. The two remaining stirrups also showed moderate to severe corrosion. All of the severely corroded stirrups were located inside the ponded region, with the exception of one, which was only one inch outside the ponded region. Figure 5.41 shows the longitudinal bar and stirrup corrosion rating graphs across the analysis length.

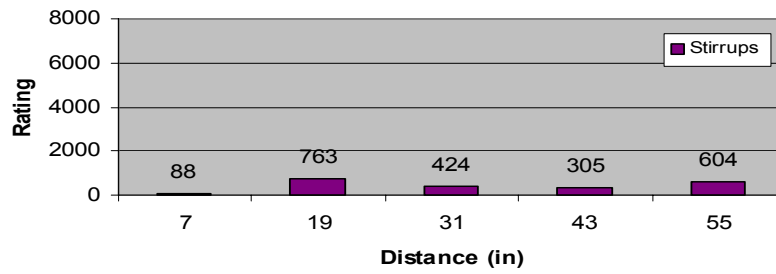
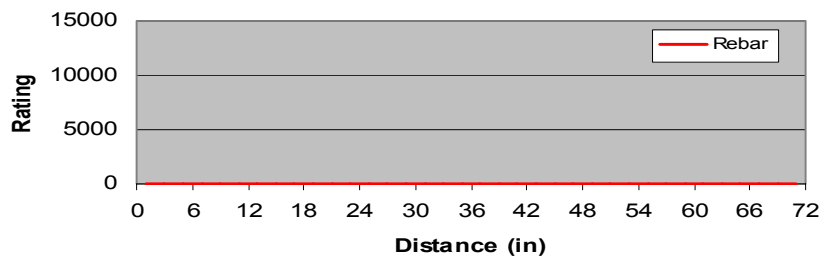
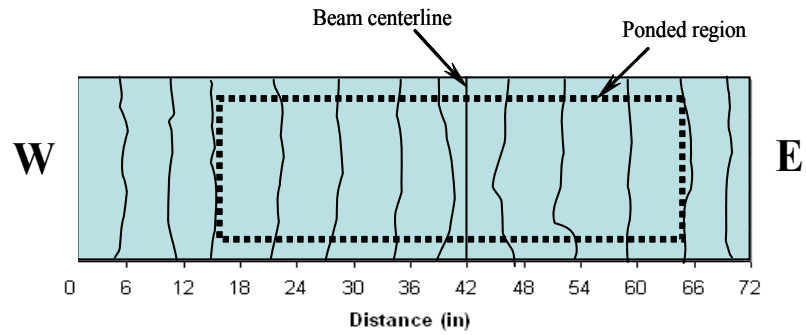


**Figure 5.41: Specimen 1.5 – Crack Pattern and Specimen Corrosion Rating Graphs**

### 5.6.2 Beam Specimen 1.6 – Non-PS, High Performance Concrete

Specimen 1.6 had a large number of cracks on the top face and both sides at the end of exposure. (See Figure 5.42) A majority of the cracks were confined to the constant maximum moment region. There was minimal rust staining around a few of the cracks. Figure 5.42 shows moisture surrounding the cracks, indicating that the chlorides are traveling through the cracks. Specimen 1.6 had a maximum crack width of 0.016 inches on the crack located 13 inches to the west of the centerline.

**Corrosion Rating:**

Specimen	Generalized Rating	Localized Rating
Stirrups	92	361
Long. mild steel	7	15
North Duct	NA	NA
South Duct	NA	NA
North Strands	NA	NA
South Strands	NA	NA

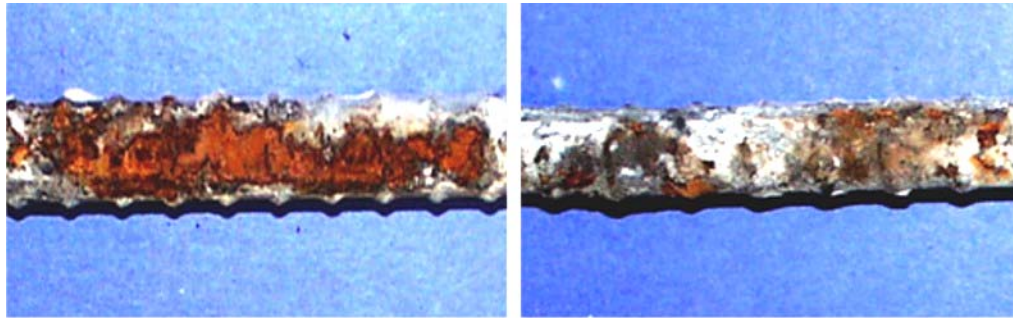


*Lateral (North) view*



*Top view (from North side)*

**Figure 5.42: Specimen 1.6 – Condition Prior to Autopsy**



*Longitudinal Bar*

*Stirrup*

***Figure 5.43: Specimen 1.6 – Mild Steel Bar and Stirrup***

A full autopsy of Specimen 1.6 was performed, providing a total length of 72 inches of the longitudinal bars, ducts, grout and strands and six stirrups to be analyzed. Forty-two inches of the analysis length extended to the west of the centerline of the beam and the remaining 30 inches extended to the east.

After removing all mild steel bars in the autopsy region, spots of moderate to severe corrosion were found on all eight longitudinal bars. (See Figure 5.43) The most severe corrosion was found on all the bars in the same location as the maximum crack width. Other spots of corrosion on the bars were consistently located in the same areas, all of which coincided with crack locations

The actual location of the centerline stirrup was offset one inch to the west of the centerline of the beam. After a detailed visual inspection, severe pitting and section loss were found on the top portion of the stirrup located 23 inches to the east of the centerline. Cracks were located two inches to each side of the stirrup. Pitting was also found on the stirrup located 25 inches to the west of the centerline, which was one inch from a crack. These two stirrups were included in the ponded region. The remaining stirrup showed light corrosion. Figure 5.44 shows a plot of the longitudinal bar and stirrup corrosion ratings across the analysis length.

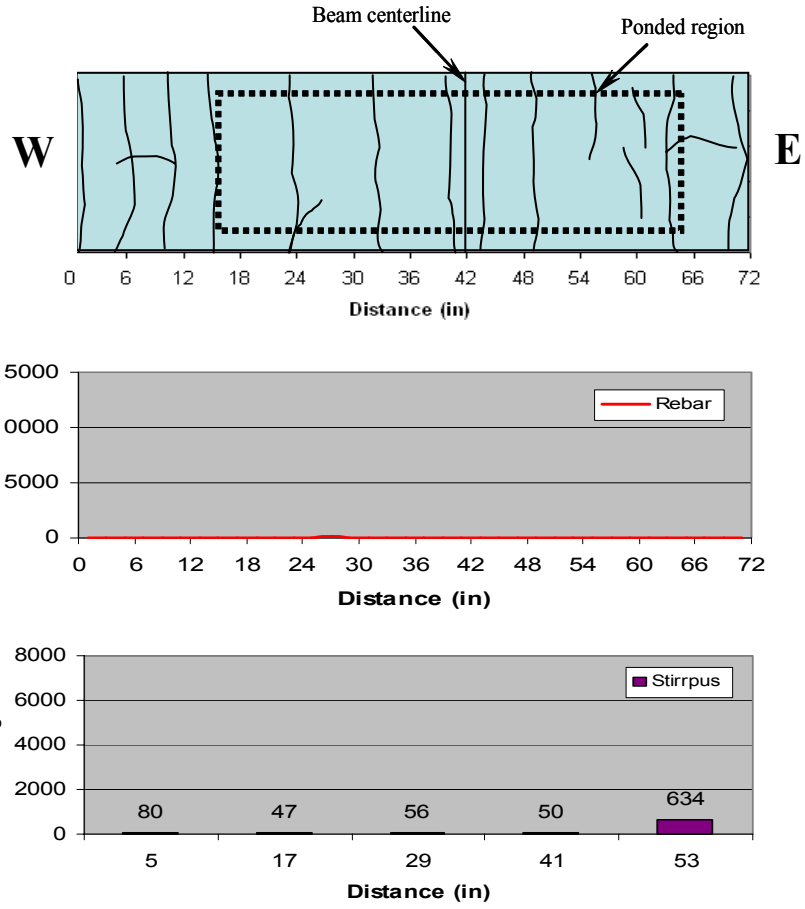


**Figure 5.44: Specimen 1.6 – Crack Pattern and Specimen Corrosion Rating Graphs**

### 5.6.3 Beam Specimen 2.5 – 2/3 PS, Fly Ash Concrete

As seen in Figure 5.45, Specimen 2.5 had five major transverse cracks at the end of exposure. Each of these cracks coincided with the stirrup locations. (See graphs in Figure 5.48) The maximum crack widths were 0.016 and 0.013 inches, located 13 inches

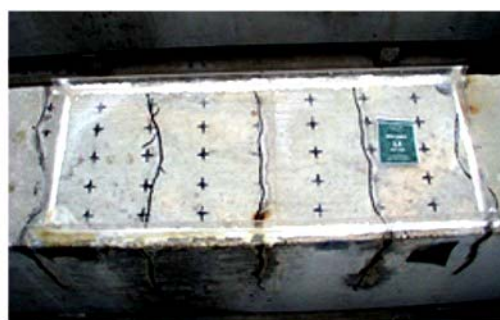
Specimen	Corrosion Rating:	
	Generalized Rating	Localized Rating
Stirrups	356	866
Long. mild steel	4	20
North Duct	21	8
South Duct	309	1776
North Strands	168	32
South Strands	168	28

to the east and 12 inches to the west of the beam centerline, respectively. Rust staining on the concrete was minimal for this specimen.

A full autopsy of Specimen 2.5 was performed, providing a total length of 72 inches of the longitudinal bars, duct, grout and strands, and six stirrups for analysis. (See Figure 5.47) Forty-two inches of the analysis length extended to the west of the centerline of the beam and the remaining 30 inches extended to the east.



*Lateral (North) view*



*Top view (from South side)*

**Figure 5.45: Specimen 2.5 – Condition Prior to Autopsy**

Any corrosion found on the mild steel bars was moderate to severe and very localized. No bars had any section loss. Seven of the eight bars had localized corrosion that corresponded to the maximum crack width. Four of the eight bars

experienced moderate corrosion that corresponded to the second maximum crack width of 0.013 inches. No corrosion was found anywhere on any of the bars, except in these two previously described locations.

After a thorough visual inspection, severe uniform corrosion, pitting and section loss were found covering the stirrups located under the largest crack and at the centerline of the beam. The stirrup coinciding with the second largest crack was completely covered with uniform corrosion and pitting. The stirrup 20 inches to the east of the centerline did not show signs of uniform corrosion, but did have one large area of severe corrosion and section loss. This stirrup was also located beneath a crack. The remaining two stirrups showed few signs of corrosion.

Extremely severe corrosion and area loss, corresponding to the second maximum crack location, were found on the south duct. (See Figure 5.47 and graphs in Figure 5.48) Both ducts showed signs of light corrosion at the centerline.

The grout in both ducts showed large voids in the top due to bleed water. The void did not affect the north duct; however it appears to have contributed to the consumption of the south duct. A large accumulation of corrosion products from the south duct was found attached to the grout. (See Figure 5.47) The corrosion rating of the south duct and the chloride content of the south duct are significantly higher at the second maximum crack location. The acid soluble chloride content in the grout reached a maximum value of 0.0036% by weight of grout inside the south duct, and 0.0013% by weight of grout inside the north duct. These values are much lower than the critical chloride threshold value of 0.033% by weight of grout. Chloride samples were taken at 6-inch intervals within the forensic analysis length and chloride content plots were obtained, as shown in Figure 5.48.



Light uniform corrosion was found on all of the strands located in the north and south ducts.

Specimen 2.5 had two duct splices. The south duct had an industry standard splice, and the north duct had a heat-shrink splice. Both splices were located at the centerline of the beam. Figure 5.46 shows the condition of the duct splices at the end of exposure. Severe corrosion and minor section loss were found on the center half of the top of the oversized piece of the industry standard splice. The heat-shrink splice on the north duct showed signs of rust staining on one side. This is due to the lack of sufficient adhesion between the steel duct and splice, allowing moisture to be trapped under the splice.



*Figure 5.46: Specimen 2.5 – Duct Splices*

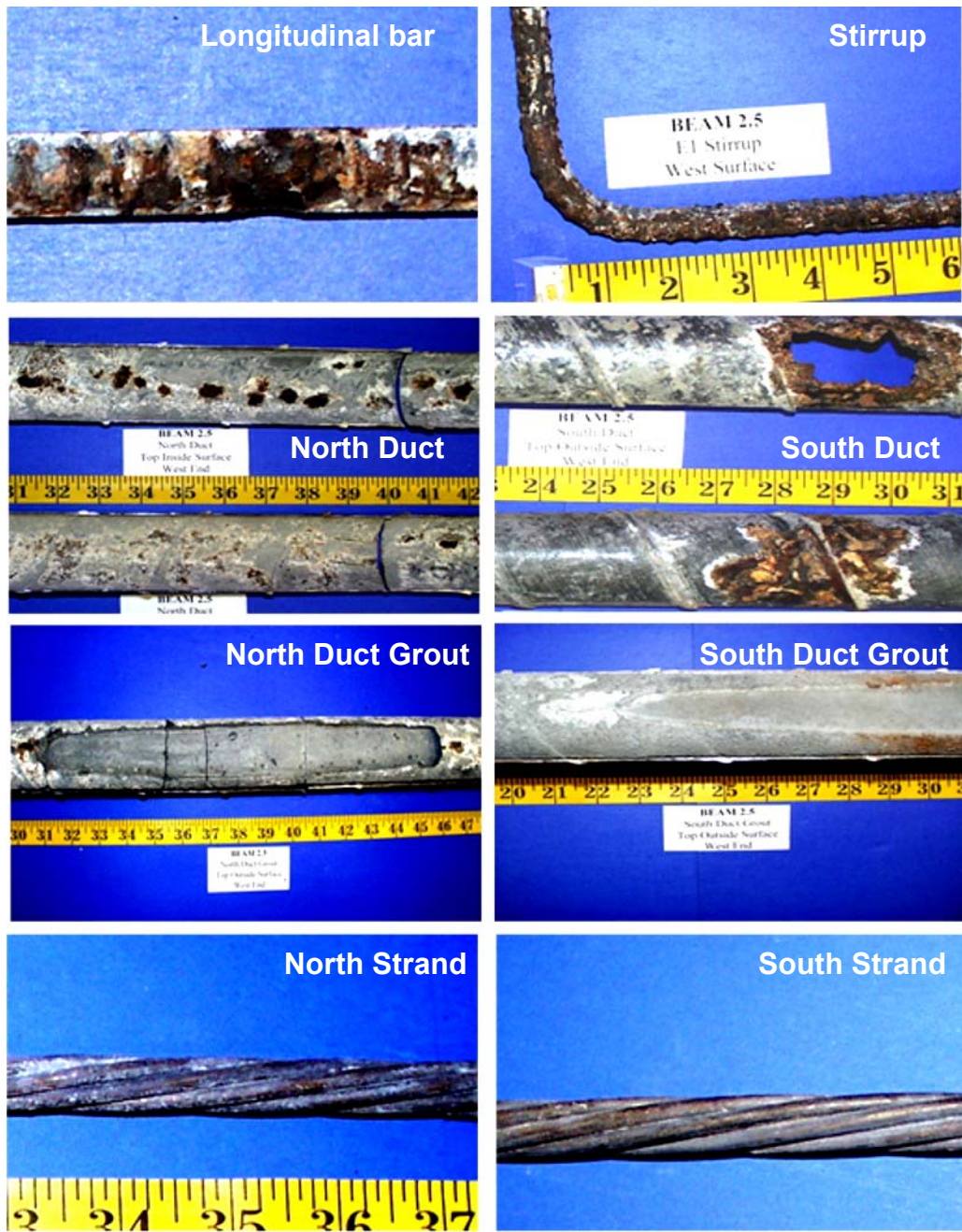


*Figure 5.47: Specimen 2.5 – Reinforcing Elements*

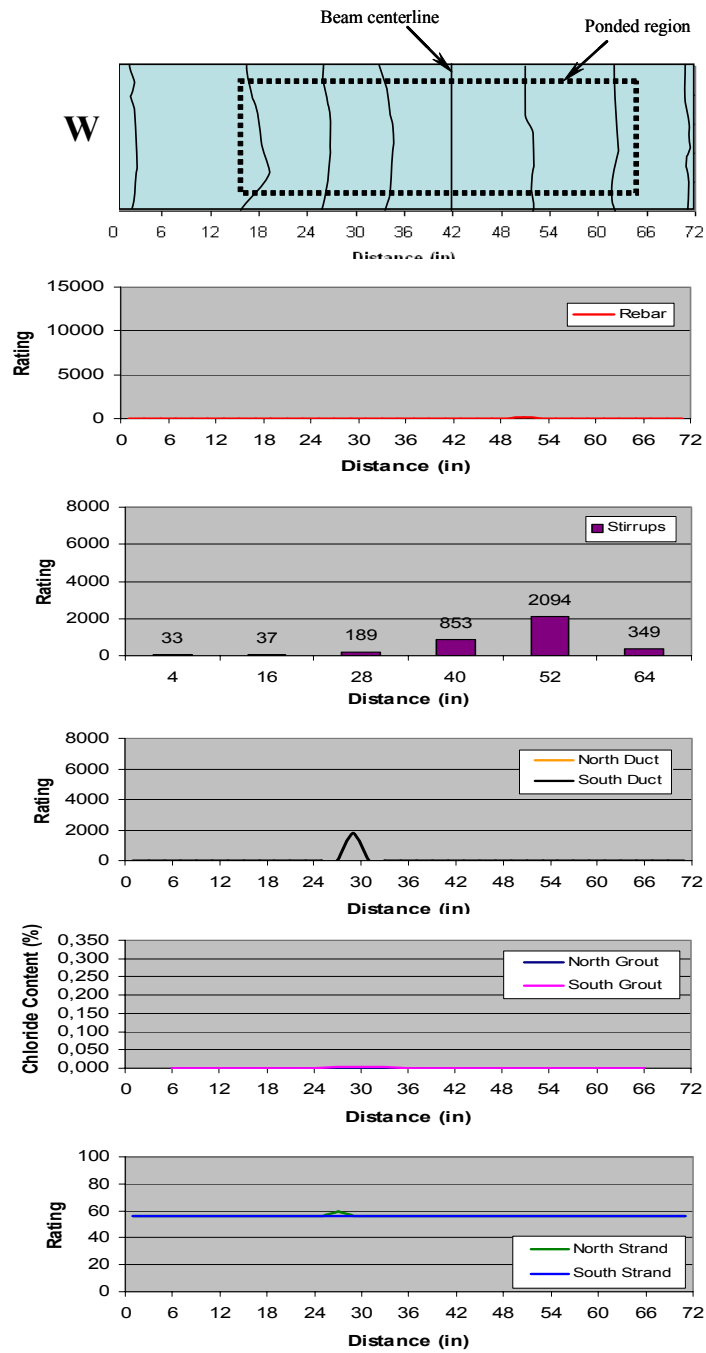


**Figure 5.48: Specimen 2.5 Crack Pattern and Specimen Corrosion Rating Graphs**

#### 5.6.4 Beam Specimen 2.6 – 2/3 PS, High Performance Concrete

Figure 5.49 shows Specimen 2.6 as having five major cracks at the end of exposure. Each of these cracks coincided with the stirrup locations. (See graphs in Figure 5.52) The maximum crack width was 0.016 inches, located 26 inches to the east and 23 inches to the west of the beam

Specimen	Corrosion Rating:	
	Generalized Rating	Localized Rating
Stirrups	41	88
Long. mild steel	7	190
North Duct	2	4
South Duct	10	34
North Strands	95	16
South Strands	96	16

centerline. As seen in Figure 5.49, rust staining on the concrete was present around a few of the cracks.

A full autopsy of Specimen 2.6 was performed, providing a total length of 72 inches of the longitudinal bars, duct, grout and strands, and six stirrups for analysis. Forty-two inches of the analysis length extended to the west of the centerline of the beam and the remaining 30 inches extended to the east. (See Figure 5.51)



*Lateral (North) view*



*Top view (from South side)*

**Figure 5.49: Specimen 2.6 – Condition Prior to Autopsy**

The only corrosion found on the mild steel bars was confined to one bar. It was severe corrosion with significant section loss. This area was located 22 inches

to the west of the centerline. It was found to be due to its contact with cross bars that were present for construction purposes only.

The only significant corrosion found on the stirrups was present on those located 14 and two inches to the west of the centerline. These two stirrups had minor section loss in very localized areas. The remaining stirrups showed little signs of corrosion.

Few signs of corrosion were found on both ducts in Specimen 2.6. One area of localized corrosion was found 11 inches to the east of the centerline, as shown in Figure 5.51. The only corrosion found on the south duct was at the centerline, located under the industry standard splice. This area showed severe corrosion with minor area loss.

The grout in both ducts showed large voids in the top due to bleed water. The void in the north duct extended from about 22 to 32 inches west of the centerline, as shown in Figure 5.51. This void did not appear to affect the corrosion protection of the duct. The void in the south duct grout extended from 20 inches west of the centerline to 22 inches to the east, also pictured in Figure 5.51. It is likely that this void contributed to the corrosion of the south duct at the centerline, as it trapped the bleed water under the duct. The acid soluble chloride content in the grout reached a maximum value of 0.0016% by weight of grout inside the north duct, and 0.005% inside the south duct. These values are much lower than the critical chloride threshold value of 0.033% by weight of grout. Chloride samples were taken at 6-inch intervals within the forensic analysis length and chloride content plots were obtained, as shown in Figure 5.52.

Light uniform corrosion was found on all the strands located in the north and south ducts.

Specimen 2.6 had two duct splices. The south duct had an industry standard splice, and the north duct had a heat-shrink splice. Both splices were

located at the centerline of the beam. Figure 5.50 shows the condition of the duct splices at the end of exposure testing. Severe corrosion and minor section loss was found on the center two inches of the top of the oversized piece of the industry standard splice. The heat-shrink splice, pictured with the north duct, showed minor signs of rust staining on the inside only.



*Figure 5.50: Specimen 2.6 – Duct Splices*

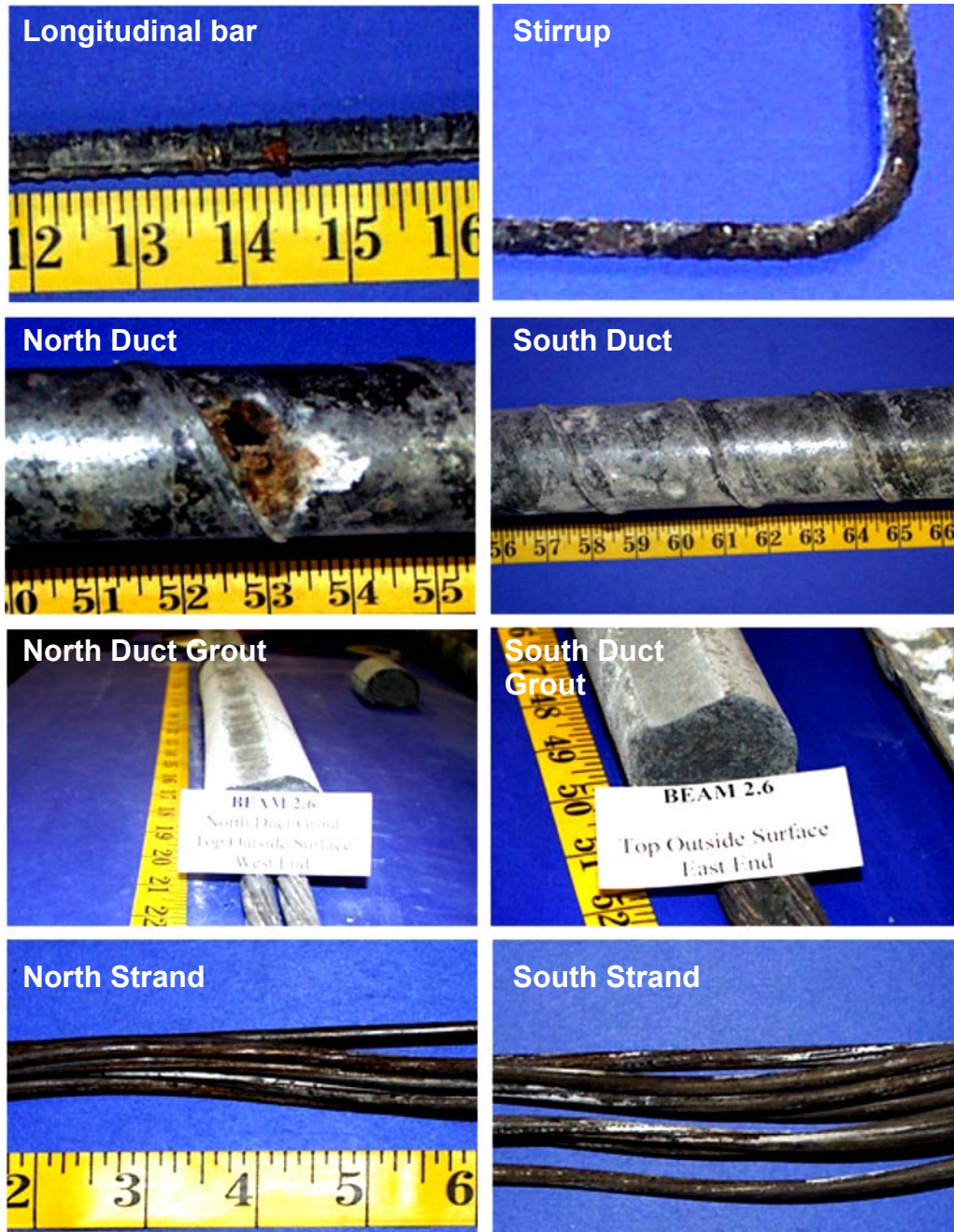


**Figure 5.51: Specimen 2.6 – Reinforcing Elements**

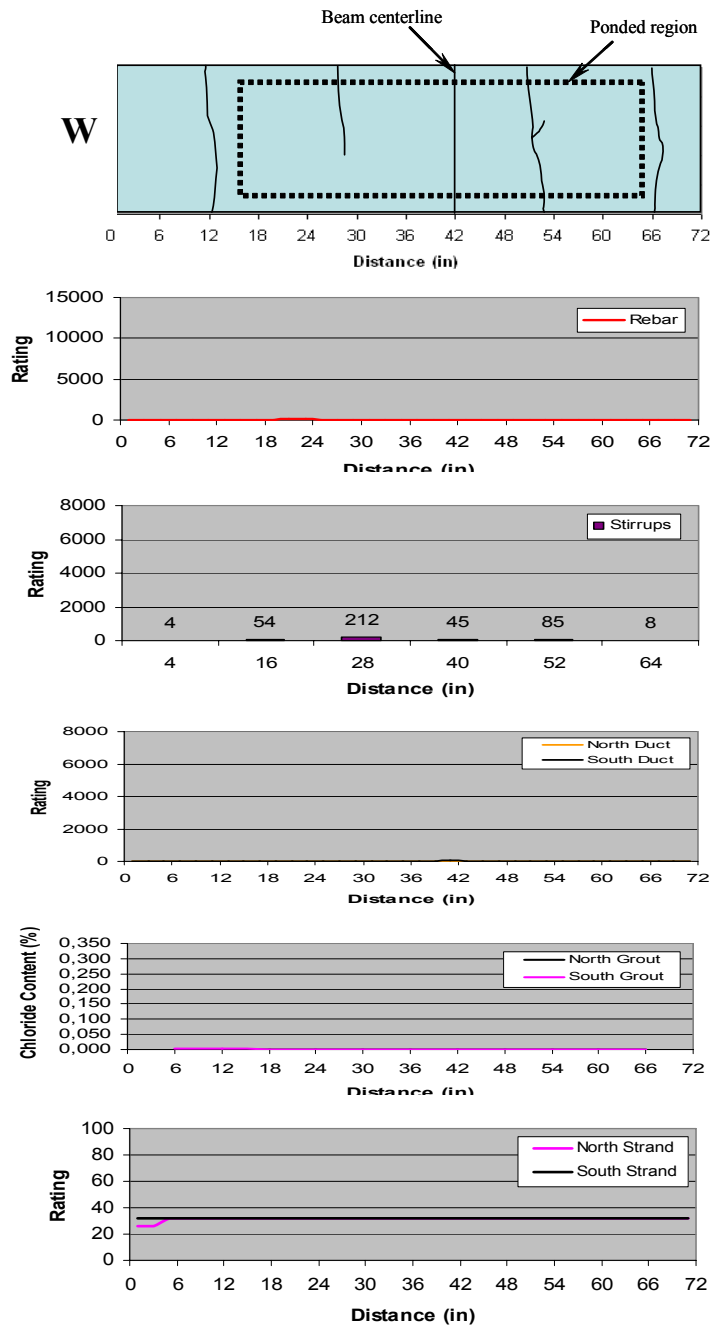


**Figure 5.52: Specimen 2.6 – Crack Pattern and Specimen Corrosion Rating Graphs**



### 5.6.5 Beam Specimen 3.6 – 100%U PS, Fly Ash Concrete

Specimen 3.6 had only two major transverse cracks across the top of the beam, as shown in Figure 5.53. The location of both of these cracks coincided with a stirrup. (See Figure 5.56) The maximum crack width was 0.016 inches, located 13 inches to the east. The second crack,

located 11 inches to the west of the centerline, had a maximum width of 0.013 inches. As shown in Figure 5.53, rust staining around the cracks was minimal. A majority of the rust spots were again from the bolster strips.

A full autopsy of Specimen 3.6 was performed, providing a total length of 72 inches of the longitudinal bars, duct, grout and strands, and six stirrups for analysis. (See Figure 5.55) Forty-two inches of the analysis length extended to the west of the centerline of the beam and the remaining 30 inches extended to the east.

Specimen	Corrosion Rating:	
	Generalized Rating	Localized Rating
Stirrups	78	245
Long. mild steel	4	4
North Duct	24	44
South Duct	6	8
North Strands	91	16
South Strands	96	16



*Lateral (North) view*

*Top view (from South side)*

**Figure 5.53: Specimen 3.6 – Condition Prior to Autopsy**

The only corrosion found on the two mild steel bars was light to moderate, and coincided with the two cracks.

Uniform light to moderate corrosion was found on all the stirrups, except the two located directly under the cracks. These stirrups were severely corroded in many areas, with some section loss.

Corrosion in the north duct was found at the centerline and directly under the larger crack. The centerline corrosion was a result of the industry standard splice on the outside and the large void in the grout on the inside. There was minor area loss at the location, which was due to the alignment with the larger crack and the void in the grout. The only corrosion found on the south duct was moderate to severe corrosion with no area loss, located under the larger crack. (See Figure 5.55)

The grout in the north duct showed a large void in the top due to bleed water. The void extended from the centerline across the entire east side. The effect of the void in the corrosion of the duct is apparent in Figure 5.55. The corrosion on the north duct and the corrosion products on the north grout are confined to the area above the void. A few small voids were present on the south duct grout, with the most significant one located 13 inches to the east of the centerline. This location is again directly under the larger crack. The acid soluble chloride content in the north duct grout reached a maximum value of 0.0022% by weight of grout at the location under the larger crack. The grout in the south duct reached 0.0021%. These values are much lower than the critical chloride threshold value of 0.033% by weight of grout. Chloride samples were taken at 6-inch intervals within the forensic analysis length and chloride content plots were obtained, as shown in Figure 5.56.

Light uniform corrosion was found on all the strands located in the north and south ducts.

Specimen 3.6 had two duct splices. The north duct had an industry standard splice, and the south duct had a heat-shrink splice. Both splices were located at the centerline of the beam. Figure 5.54 shows the condition of the duct splices at the end of exposure. Minor corrosion and salt staining was found on the center of the oversized piece of the industry standard splice. The heat-shrink splice showed no signs of rust staining or corrosion.



**Figure 5.54: Specimen 3.6 – Duct Splices**

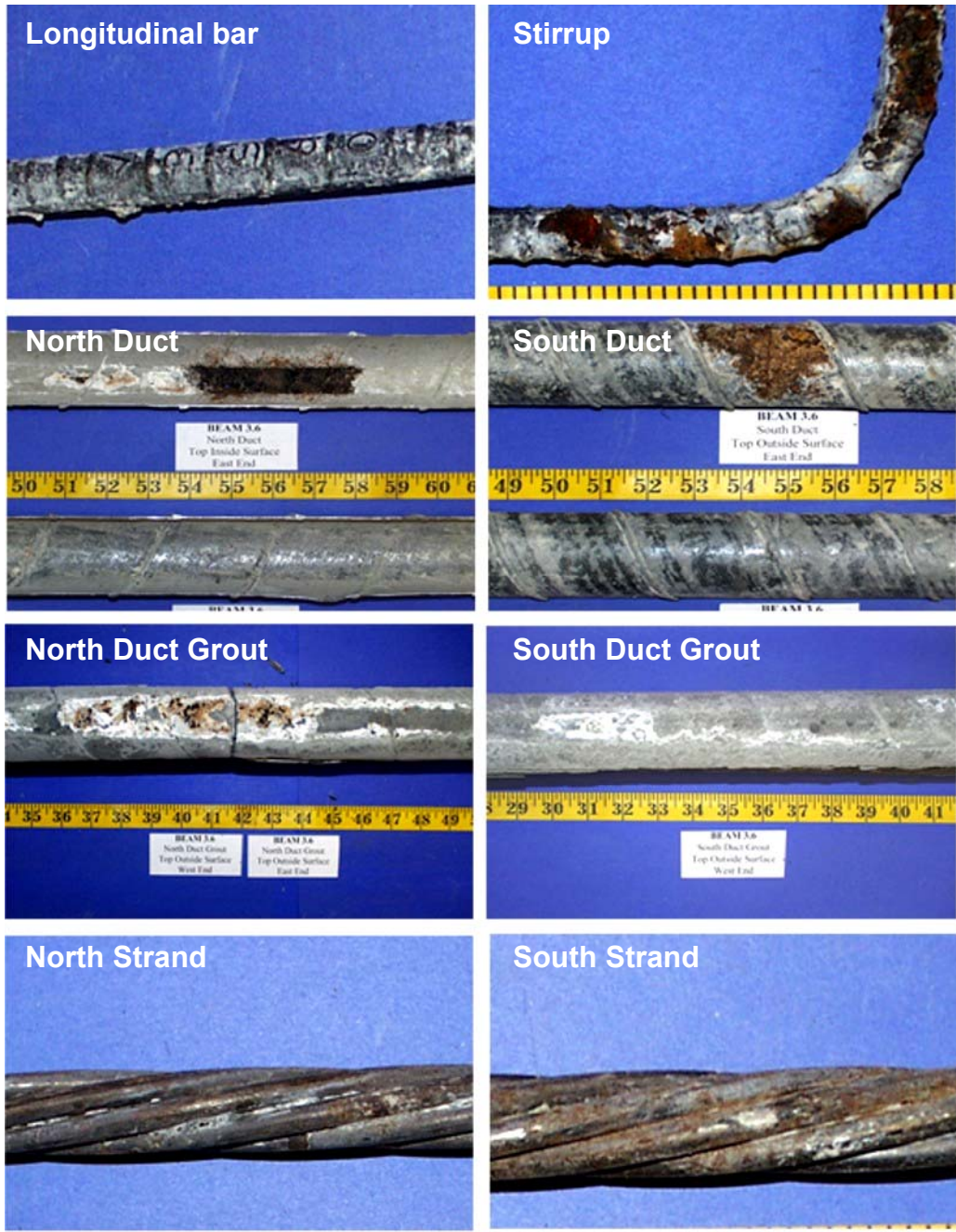


*Figure 5.55: Specimen 3.6 – Reinforcing Elements*

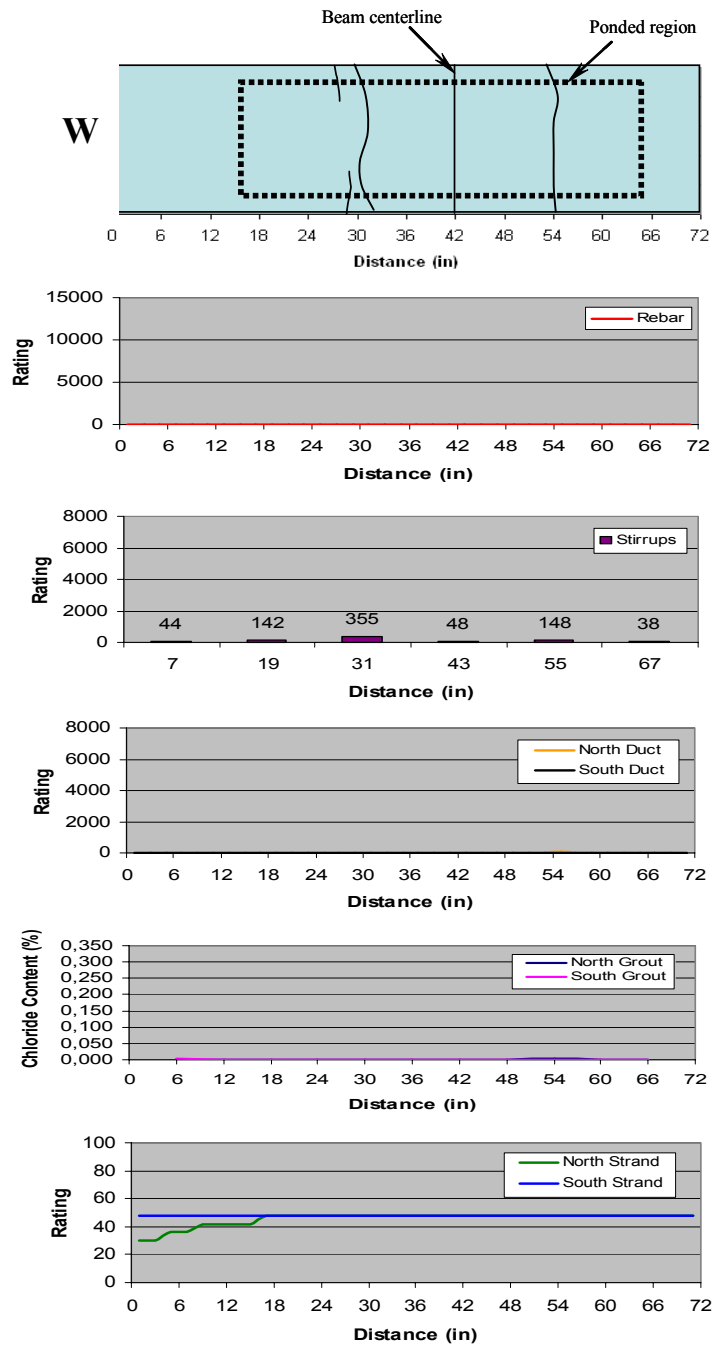


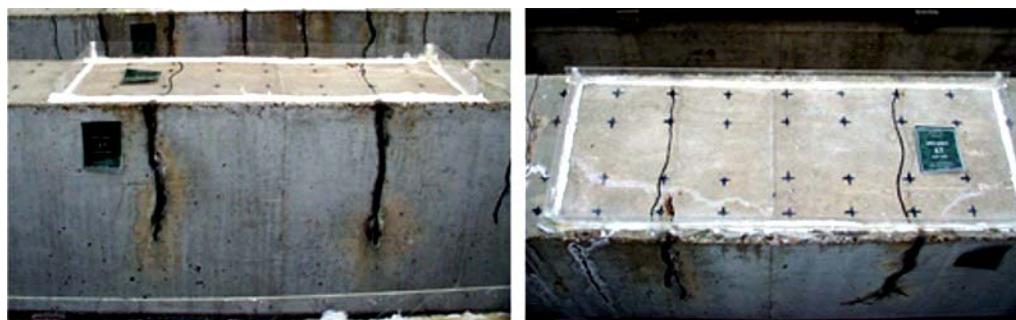
**Figure 5.56: Specimen 3.6 – Crack Pattern and Specimen Corrosion Rating Graphs**

### 5.6.6 Beam Specimen 3.7 – 100%U PS, High Performance Concrete

Specimen 3.7 had four major transverse cracks across the top of the beam, two of which were located outside the ponded region (See Figure 5.57) The maximum crack width was 0.04 inches, located outside the ponded region at 26 inches to the west of the centerline. The second largest crack, located 13 inches to the east of the centerline, had a maximum width of 0.016 inches. As seen in Figure 5.57, rust staining around the cracks was present on the sides of the beam.

Specimen	Corrosion Rating:	
	Generalized Rating	Localized Rating
Stirrups	27	16
Long. mild steel	0	2
North Duct	214	1164
South Duct	12	20
North Strands	168	28
South Strands	168	28

A full autopsy of Specimen 3.7 was performed, providing a total length of 72 inches of the longitudinal bars, duct, grout and strands, and six stirrups for analysis. (See Figure 5.59) Forty-two inches of the analysis length extended to the west of the centerline of the beam and the remaining 30 inches extended to the east.



*Lateral (North) view*

*Top view (from South side)*

**Figure 5.57: Specimen 3.7 – Condition Prior to Autopsy**

No corrosion was found on the two mild steel bars in Specimen 3.7.

Moderate to severe uniform corrosion was found on the stirrups 10 inches to the west and 14 inches to the east. Both of these stirrups were located directly under cracks. The remaining stirrups showed light uniform corrosion.

A significant amount of area loss was found on the north duct, as shown in Figure 5.59. This location was very close to a 0.013-inch crack. There was severe corrosion and minor area loss at this same location on the south duct. (See Figure 5.59) These were the only significant areas of corrosion found on the ducts in Specimen 3.7.

The grout in the north duct showed a large void in the top due to bleed water. The void extended from 30 inches west of the centerline to six inches west. Corrosion products from the north duct at the location of area loss were found on the grout. (See Figure 5.59) A few small voids were present on the south duct grout, with the most significant one located under the location of minor area loss in the south duct. The acid soluble chloride content in the north duct grout reached a maximum value of 0.004% by weight of grout. A value of 0.0199% in the south duct was found in the region of the duct area loss. These values are much lower than the critical chloride threshold value of 0.033% by weight of grout. Chloride samples were taken at 6-inch intervals within the forensic analysis length and chloride content plots were obtained, as shown in Figure 5.60.

Light uniform corrosion was found on all the strands located in the north and south ducts.

Specimen 3.7 had two duct splices. The north duct had an industry standard splice, and the south duct had a heat-shrink splice. Both splices were located at the centerline of the beam. Figure 5.58 shows the condition of the duct splices at the end of exposure. The only corrosion found on the industry standard

splice was located under the duct tape. The heat-shrink splice showed no signs of rust staining or corrosion.



*Figure 5.58: Specimen 3.7 – Duct Splices*



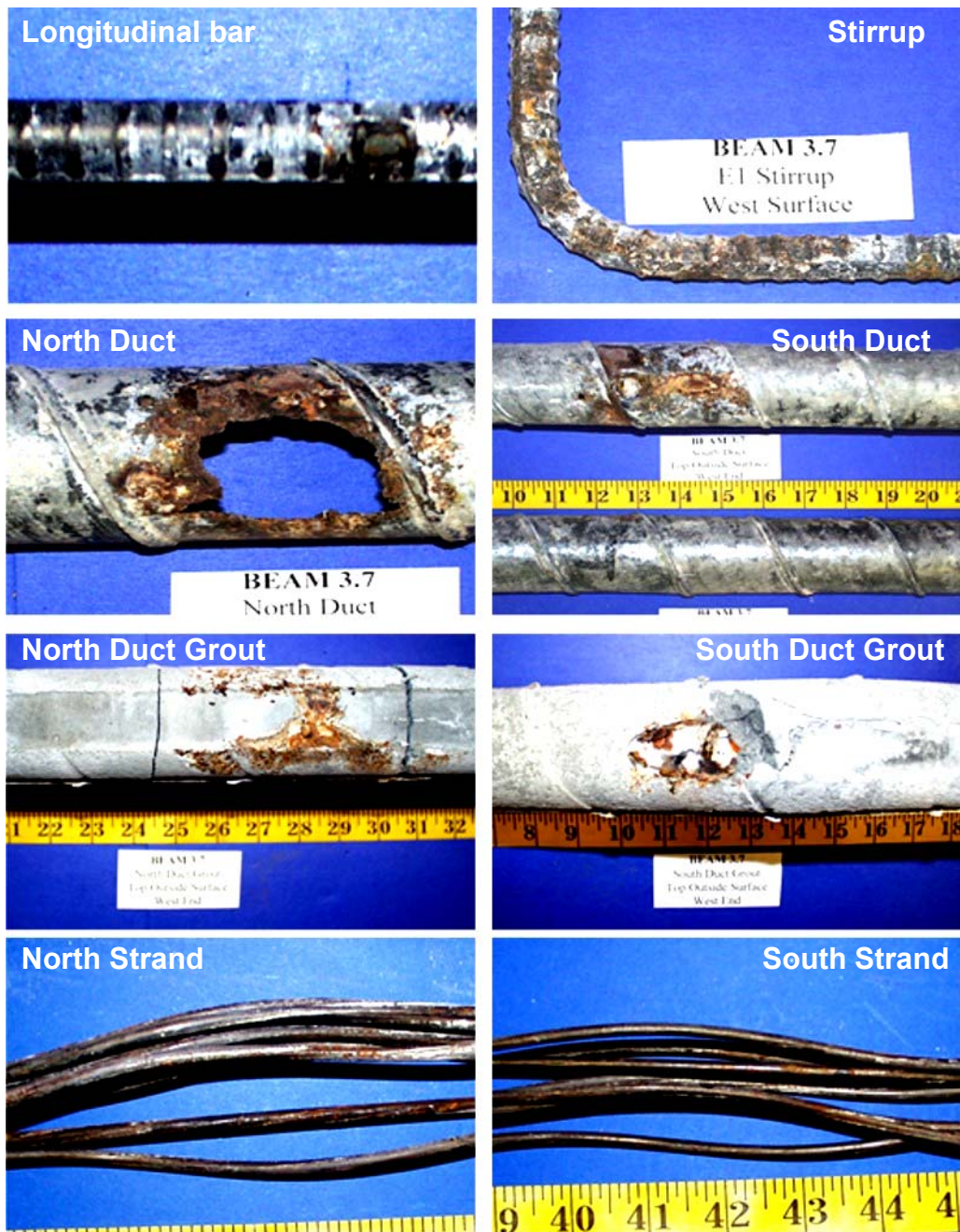


*Figure 5.59: Specimen 3.7 – Reinforcing Elements*

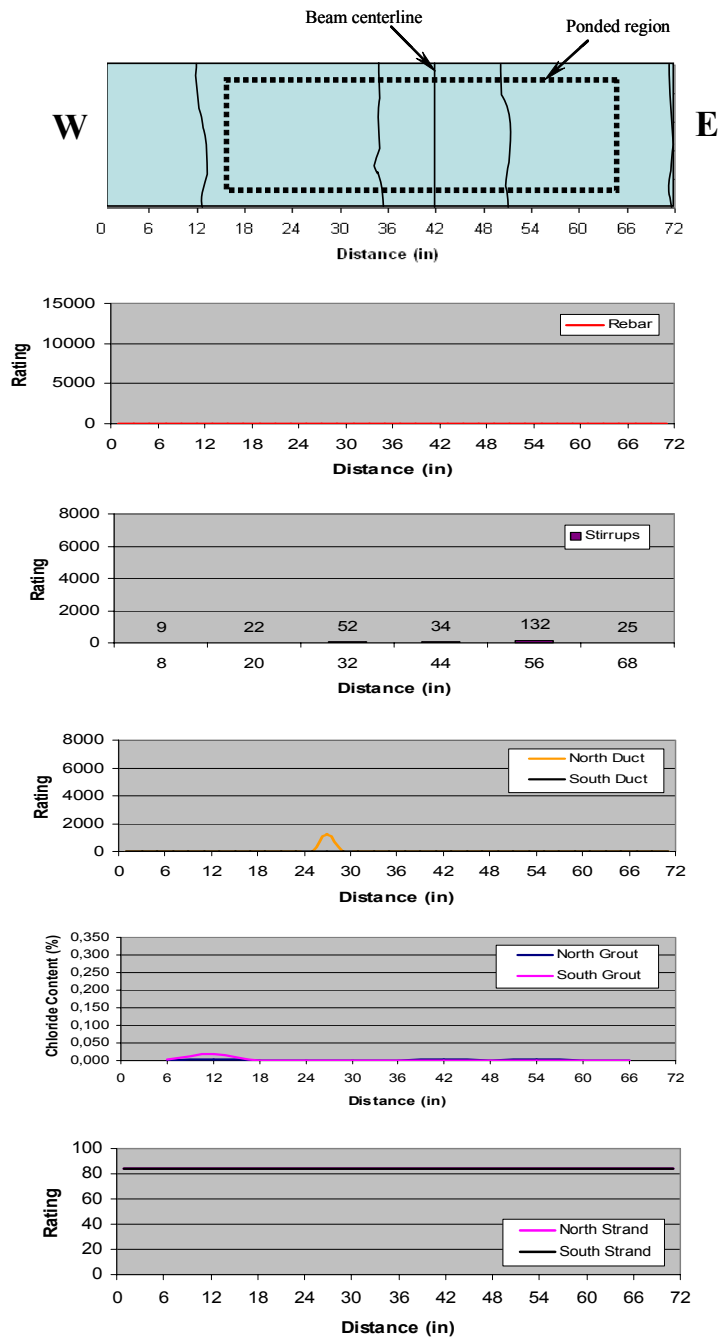


**Figure 5.60: Specimen 3.7 – Crack Pattern and Specimen Corrosion Rating Graphs**

## 5.7 CORROSION RATING SUMMARY

Once the total corrosion ratings were determined, two different methods were developed to modify them so they could be used to compare the element performance among all the specimens. Each modification method is described below, and summarized in Table 5.6.

The first method was developed to compare the severity of generalized corrosion among the specimens. This was accomplished by dividing the total rating by the total length of each element. The result was a rating per unit foot of each element. The detailing of the stirrups and the ducts was identical for each specimen, assuming the specimen was prestressed and had a duct. Therefore, the same modification was made to the stirrup or duct ratings. The modification included dividing the total stirrup/duct corrosion rating by the total stirrup/duct length to get an average rating per foot of the element. The number of reinforcing bars in each specimen type varied. Therefore, the total rebar rating for each beam was divided by the total length of rebar being evaluated. For example, all the Non-PS and 2/3 PS beams had eight reinforcing bars that were each six feet in length. So, the total rebar rating for either of these section types was divided by 48 feet to get an average rating per foot. The number of strands per duct in each type of prestressed specimen also varied. Therefore, the total strand rating for each duct was divided by the total length of prestressing strand being evaluated. For example, all of the 100%U PS beams had three prestressing strands per duct that were each six feet in length. The total strand rating for a 100%U PS specimen was divided by 18 feet to adjust the rating to an average rating per foot of strand. The generalized corrosion ratings are more useful in determining the performance of the concrete in limiting chloride penetration.

The second method for comparison among the specimens was developed to evaluate the severity of localized corrosion in each element. Localized

corrosion is of great interest in this experimental program since this is the type of corrosion that will ultimately result in failure of the structural element, and possibly the structure. To evaluate localized corrosion, the maximum rating recorded for any 2-inch interval for each element was plotted. The localized corrosion ratings are useful in determining the effects of cracking when compared to the crack locations on the specimen. A table showing all of the data for each plot can be found in Appendix E.

**Table 5.6: Corrosion Rating Scenarios for Analysis**

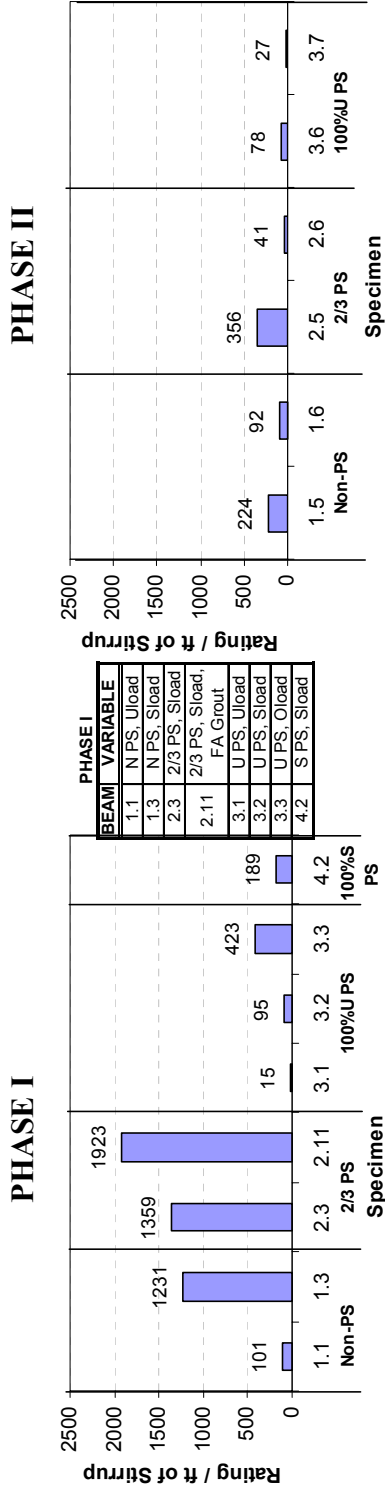
METHOD	MODIFICATION			
	Stirrups	Rebar	Ducts	Strands
1: Non-PS	$R_{Tot} \div 10.5 \text{ ft.}$	$R_{Tot} \div 48 \text{ ft.}$	N.A.	N.A.
2/3 PS	$R_{Tot} \div 10.5 \text{ ft.}$	$R_{Tot} \div 48 \text{ ft.}$	$R_{Tot} \div 6 \text{ ft.}$	$R_{Tot} \div 12 \text{ ft.}$
100%U PS	$R_{Tot} \div 10.5 \text{ ft.}$	$R_{Tot} \div 12 \text{ ft.}$	$R_{Tot} \div 6 \text{ ft.}$	$R_{Tot} \div 18 \text{ ft.}$
100% S PS	$R_{Tot} \div 10.5 \text{ ft.}$	$R_{Tot} \div 12 \text{ ft.}$	$R_{Tot} \div 6 \text{ ft.}$	$R_{Tot} \div 24 \text{ ft.}$
2: Non-PS	$R_{Max}$	$R_{Max}$	$R_{Max}$	$R_{Max}$
2/3 PS	$R_{Max}$	$R_{Max}$	$R_{Max}$	$R_{Max}$
100%U PS	$R_{Max}$	$R_{Max}$	$R_{Max}$	$R_{Max}$
100% S PS	$R_{Max}$	$R_{Max}$	$R_{Max}$	$R_{Max}$

$R_{Tot}$  = total element rating

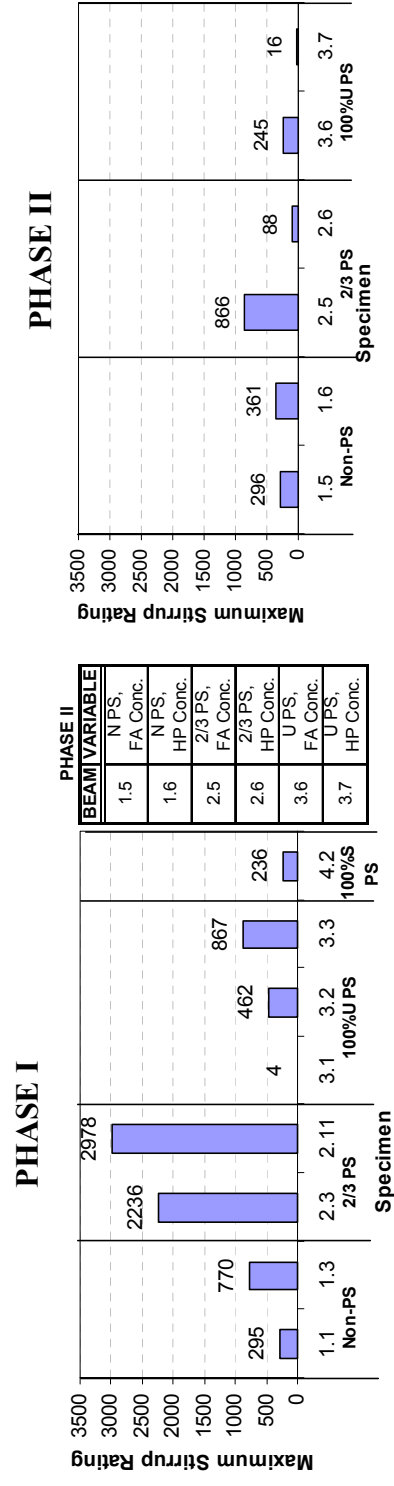
$R_{Max}$  = maximum rating over 2-inch interval

### 5.7.1 Stirrup Ratings

Figure 5.61 includes a graph of the generalized stirrup corrosion ratings for the Phase I and Phase II beams. These graphs show that the specimen performance increases as the level of prestress increases from 2/3 PS to 100% PS. The performance of the 2/3 PS beams appears to be much more similar to that of the Non-PS beams as opposed to that of the 100% PS beams. Figure 5.61 also shows that the specimen corrosion index increases as the loading, and thus cracking, increases. Comparison among the Phase II beams indicates high performance concrete as the superior concrete type.



**Figure 5.61: Generalized Stirrup Corrosion Ratings**



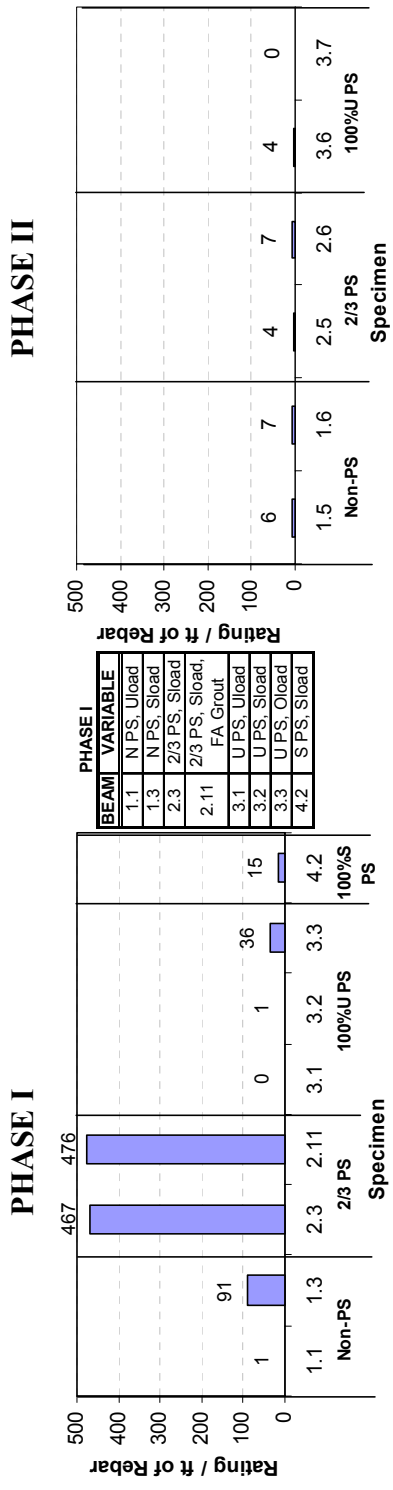
**Figure 5.62: Localized Stirrup Corrosion Ratings**

Figure 5.62 includes a graph of the localized stirrup corrosion ratings for the Phase I and Phase II beams. These graphs show the same trends as Figure 5.61. However, the increase in corrosion index as the crack width increases is much more apparent as the localized ratings significantly increase from Specimen 1.3 to Specimens 2.3 and 2.11. The increase from Specimen 3.1 (uncracked) to Specimens 3.2 (designed as uncracked, but became cracked) and 3.3 (cracked) is also significant.

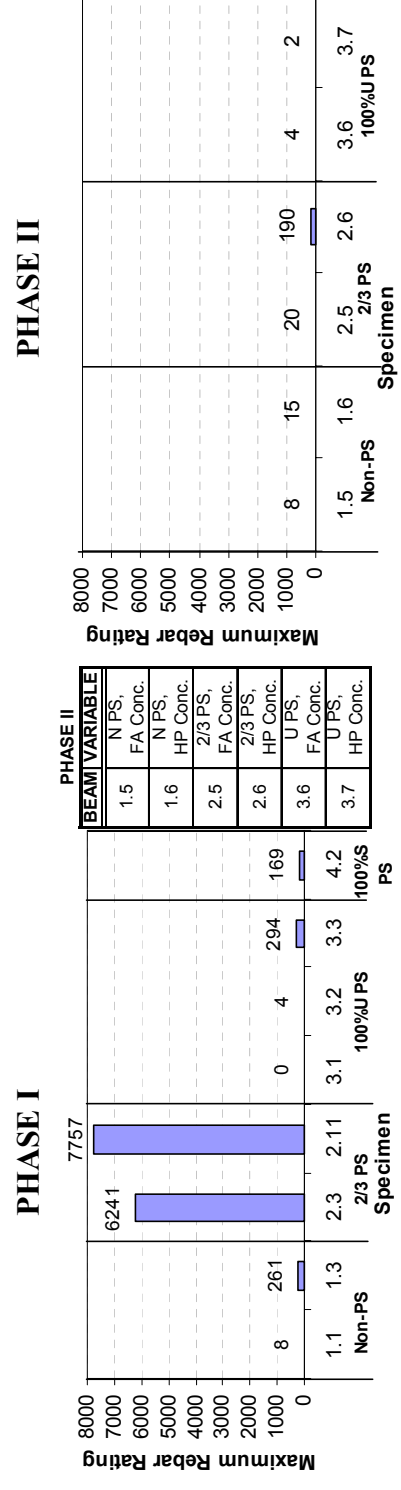
### **5.7.2 Longitudinal Bar Ratings**

Figure 5.63 includes a graph of the generalized bar corrosion ratings for the Phase I and Phase II beams. The Phase I graph shows a significant increase in corrosion index of the 2/3 PS beams in comparison to all other prestress levels, including the Non-PS beams. The negative effects of cracking are also evident from the comparison of Specimen 1.1 (uncracked) and 1.3 (cracked). All ratings in the Phase II beams are very low, indicating that the high performance and fly ash concrete are aiding in the prevention of chloride ingress. However, this could be a result of the Phase II beams being exposed for one less year.

Figure 5.64 includes a graph of the localized bar corrosion ratings for the Phase I and Phase II beams. These graphs show the same trends as those in Figure 5.63. Therefore the same conclusions can be drawn from the localized corrosion ratings.



*Figure 5.63: Generalized Bar Corrosion Ratings*



*Figure 5.64: Localized Bar Corrosion Ratings*

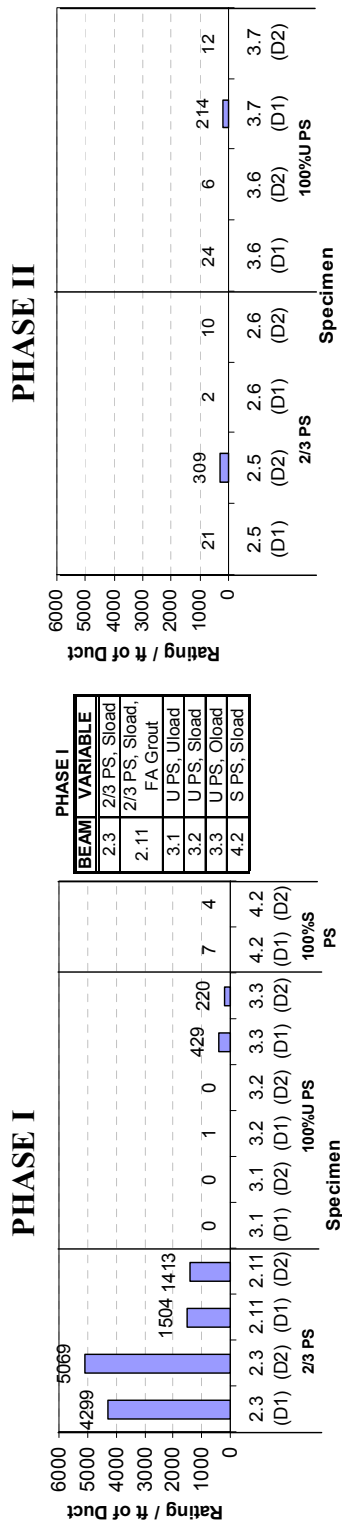
### 5.7.3 Galvanized Steel Duct Ratings

Because there are two ducts in each beam, it was necessary to reference each one separately. To do so, the designation of D1 and D2 was used to differentiate between the two ducts.

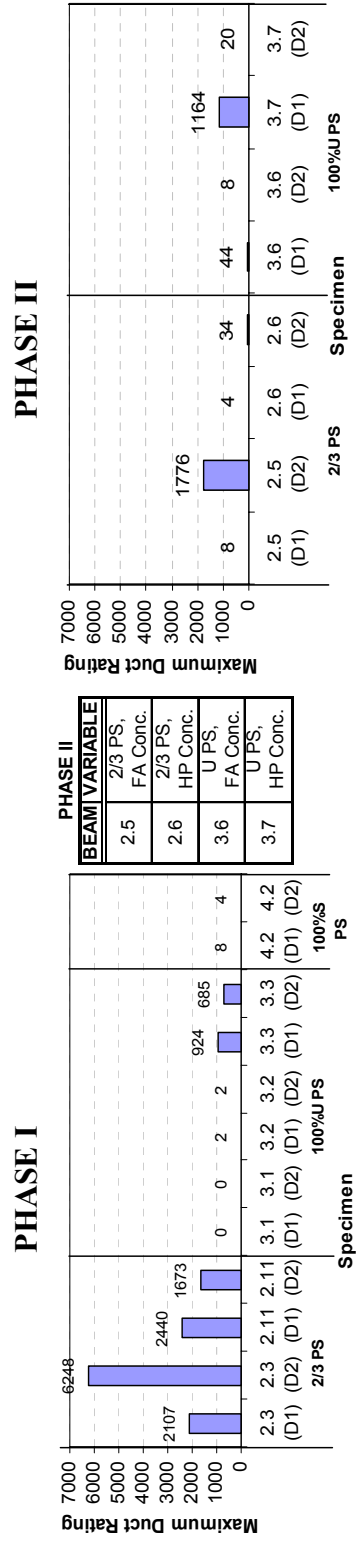
Figure 5.65 includes a graph of the generalized duct corrosion ratings for the Phase I and Phase II beams. The Phase I graph shows a significantly worse performance of the 2/3 PS beams in comparison to the 100% PS beams. The harmful effects of cracking are also evident from the comparison of Specimen 3.1 (uncracked) and 3.3 (cracked). The difference between Specimen 2.3 (normal grout) and 2.11 (fly ash grout) indicates that the addition of fly ash to the grout aids in the corrosion protection of the duct. The large rating of Specimen 3.7 in the Phase II beams does not follow the trend of an increase in corrosion resistance with an increase of prestressing. This is most likely due to the significantly large cracking present in the specimen. The Phase II specimens do not show a consistent difference between the concrete types. They both appear to be performing well.

Figure 5.66 includes a graph of the localized duct corrosion ratings for the Phase I and Phase II beams. These graphs show the same trends as those in Figure 5.65, therefore the same conclusions can be drawn from the localized corrosion ratings.





**Figure 5.65: Generalized Duct Corrosion Ratings**

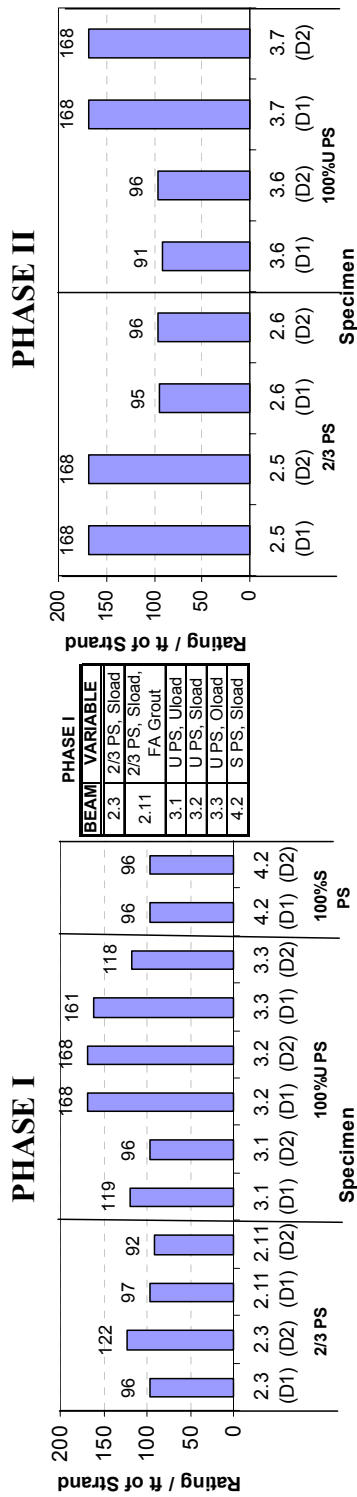


**Figure 5.66: Localized Duct Corrosion Ratings**

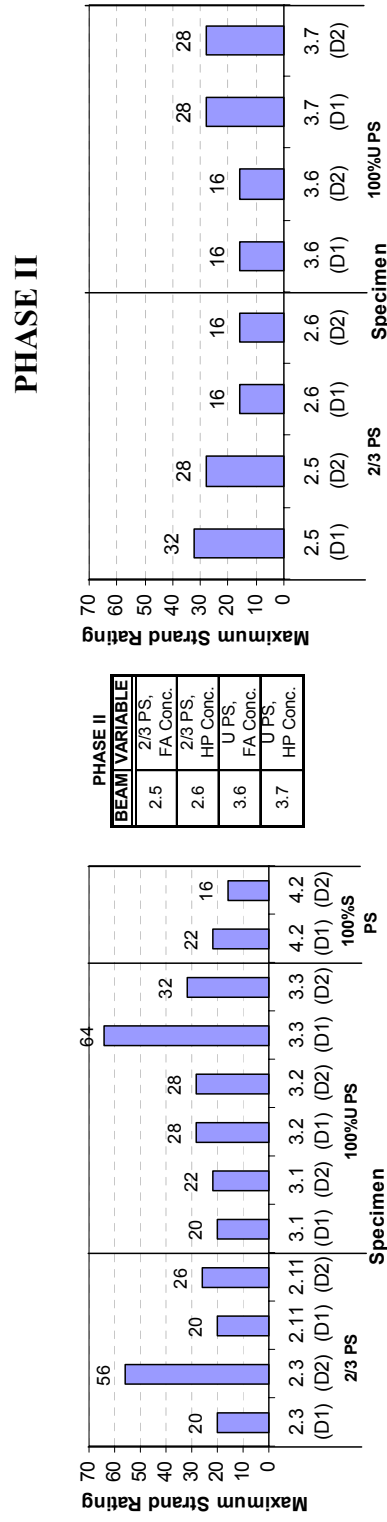
#### **5.7.4 Prestressing Strand Ratings**

Figure 5.67 includes a graph of the generalized strand corrosion ratings for the Phase I and Phase II beams. All strands appear to be performing similarly. The differences in the values on the graphs appear to be significant. However, this is misleading due to the large increase in the corrosion index when the increase in corrosion severity is minimal. A detailed visual inspection indicated minimal variation in the performance of the strands. Because this is not true of all other reinforcing elements, it is possible that the specimens required more exposure so that more chlorides could reach the strands. The difference between Specimen 2.3 (normal grout) and 2.11 (fly ash grout) indicates that the addition of fly ash to the grout does not have a large effect on the protection of the strand.

Figure 5.68 includes a graph of the localized strand corrosion ratings for the Phase I and Phase II beams. The Phase II beams show the same trends as those in Figure 5.67. Therefore the same conclusions can be drawn from the localized corrosion ratings. Specimens 2.3 (D1) and 3.3 (D1) show noticeably larger localized ratings. The rating graphs of these specimens, which were presented in the previous section, show that the high ratings coincide with crack locations.



**Figure 5.67: Generalized Strand Corrosion Ratings**



**Figure 5.68: Localized Strand Corrosion Ratings**

## CHAPTER 6

# Analysis of Exposure Test Measurements and Forensic Examination Findings

### 6.1 FORENSIC EXAMINATION VS. EXPOSURE TESTING MEASUREMENTS

The purpose of comparing the results from the forensic examination with those from the exposure testing measurements is to determine the reliability of each form of non-destructive corrosion measurement used in this experimental program. It was determined that it is more realistic to use the generalized, as opposed to the localized, corrosion ratings in these comparisons. It was necessary to create two separate graphs of the total corrosion ratings due to the fact that the Non-PS beams did not have duct or strand ratings. The first graph is the summation of all the element ratings, with the intention of showing the overall corrosion resistance of each beam. The Non-PS beams were left out of this graph for the previously mentioned reason. The second graph shows the corrosion rating of the longitudinal bars only in order to provide a way of including the Non-PS beams in the comparison. All graphs are arranged in order of increasing corrosion resistance for ease of comparison.

#### 6.1.1 Forensic Examination vs. Half-Cell Potential Readings

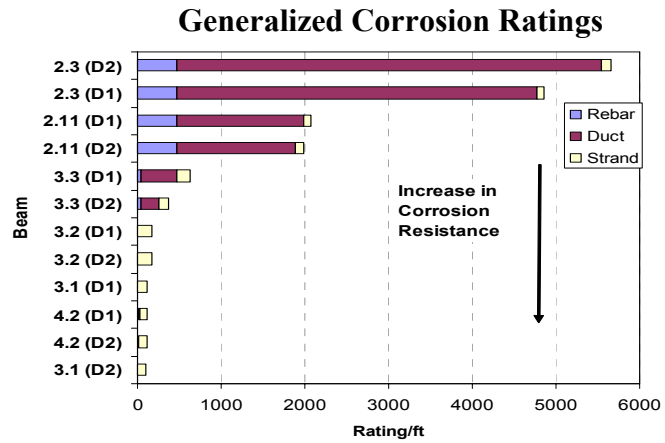
Determination of the specimen corrosion resistance based on half-cell potential readings can be accomplished through comparison of the highest half-cell potential reading and the time to initiation of corrosion. For this reason, a graph of each has been included in Figures 6.1 and 6.2.

Figure 6.1 includes graphs of the Phase I beams. They show an exact correlation in the order of corrosion resistance between the highest potential and

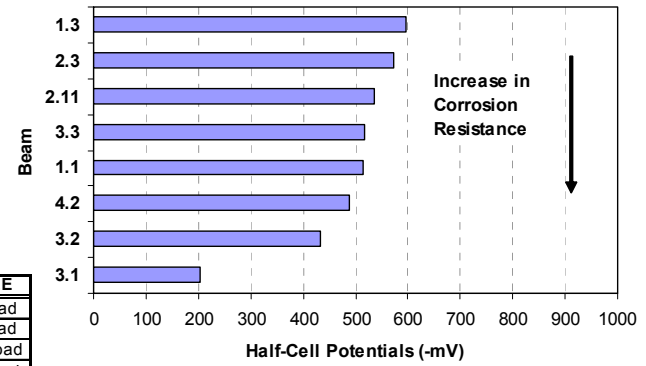
time to corrosion. Both show the loaded Non-PS and 2/3 PS beams as being the most corroded, which is in perfect agreement with the corrosion rating graphs.

Figure 6.2 includes graphs of the Phase II beams. They show an almost exact correlation in the order of corrosion resistance between the highest potential and time to corrosion. The relationship between the half-cell and bar corrosion rating graphs is not similar, but this is due to all the bar ratings being very low and close in value. Both half-cell graphs show good accuracy with the corrosion rating graphs.

Overall, half-cell potential readings appear to be a good form of non-destructive corrosion measurement when determining the relative comparison among specimens.

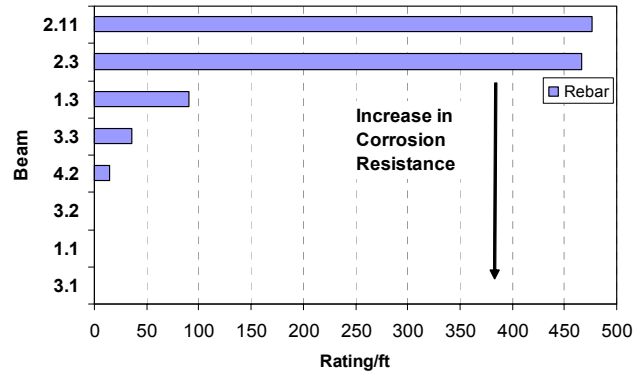


### Highest Half-Cell Potential at 1594 Days



BEAM	VARIABLE
1.1	N PS, Uload
1.3	N PS, Sload
2.3	2/3 PS, Sload
2.11	2/3 PS, Sload, FA Grout
3.1	U PS, Uload
3.2	U PS, Sload
3.3	U PS, Oload
4.2	S PS, Sload

### Generalized Rebar Corrosion Ratings



### Time to Initiation of Corrosion

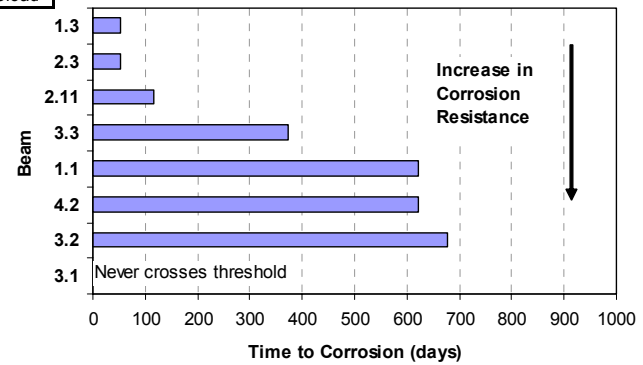


Figure 6.1: Corrosion Ratings vs. Half-Cell Potential Readings – Phase I Beams

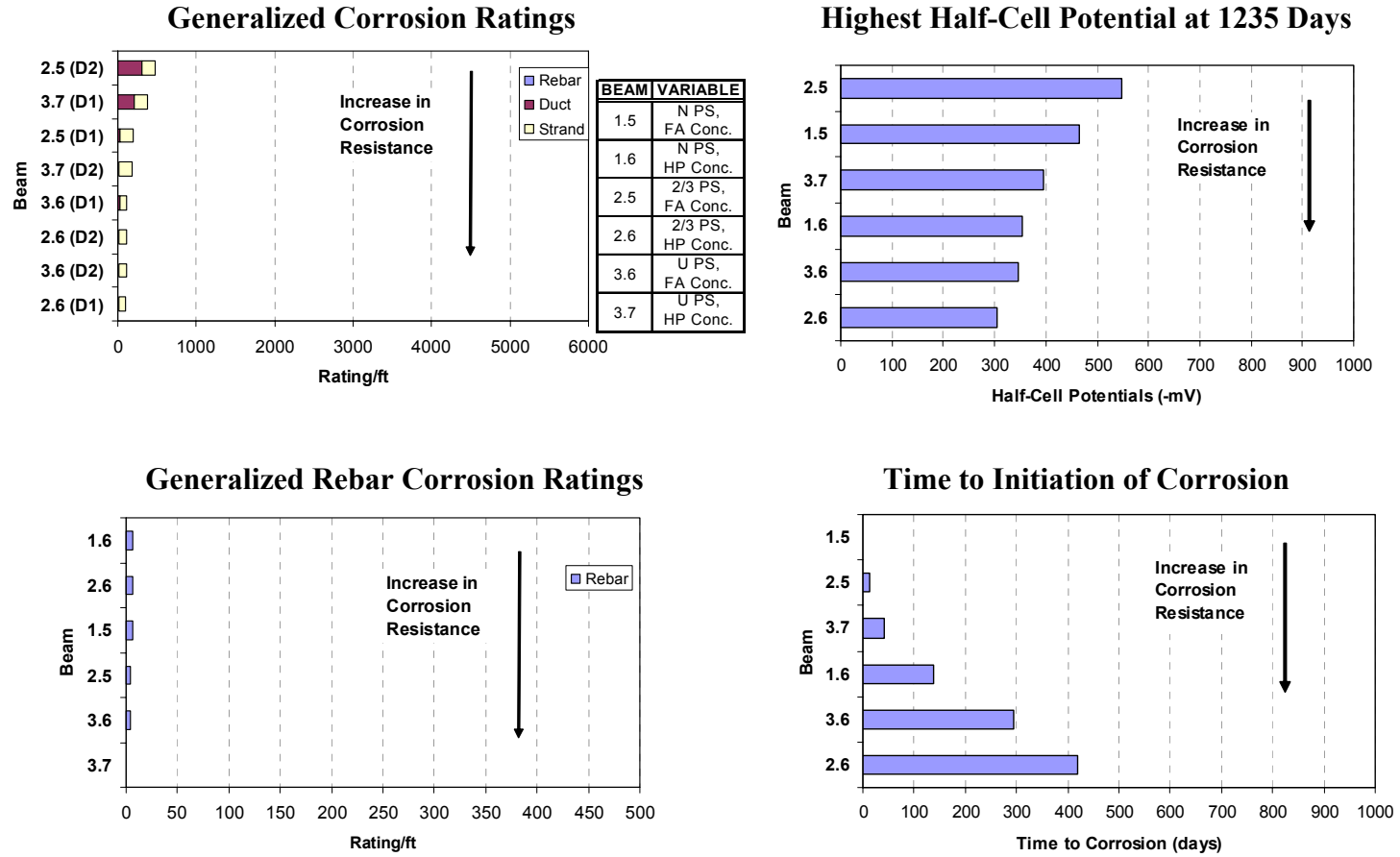


Figure 6.2: Corrosion Ratings vs. Half-Cell Potential Readings – Phase II Beams

### **6.1.2 Forensic Examination vs. Corrosion Rate Readings**

For the most accurate comparison, it was decided to compare the corrosion ratings with the final corrosion rate readings taken. Figures 6.3 and 6.4 compare the readings of the Phase I and Phase II beams, respectively.

Both Figures 6.3 and 6.4 show very poor agreement between the corrosion rate readings and the corrosion ratings. This is not very surprising since both final corrosion rate measurements were taken using the 3LP equipment, which has frequently been reported as producing inaccurate results.



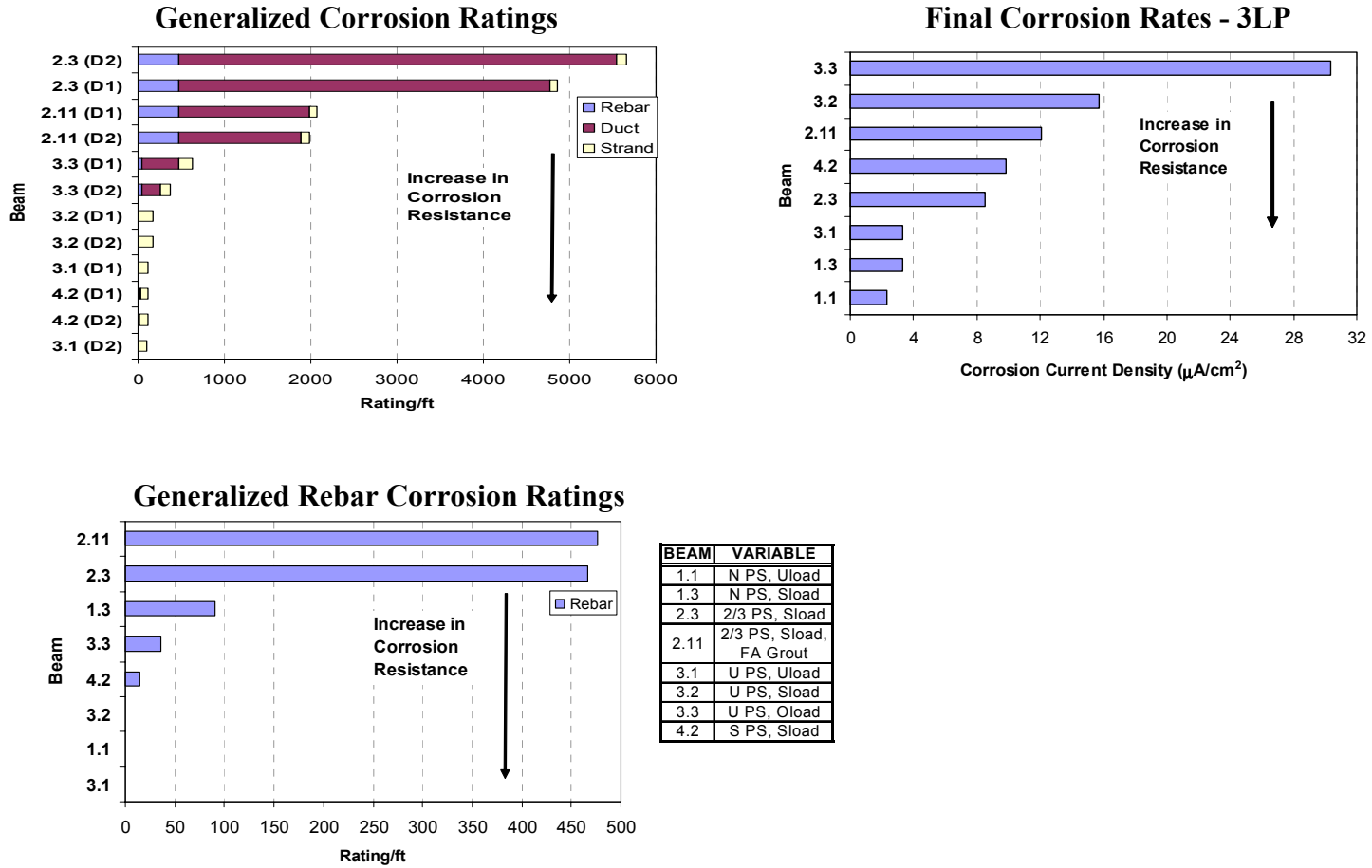
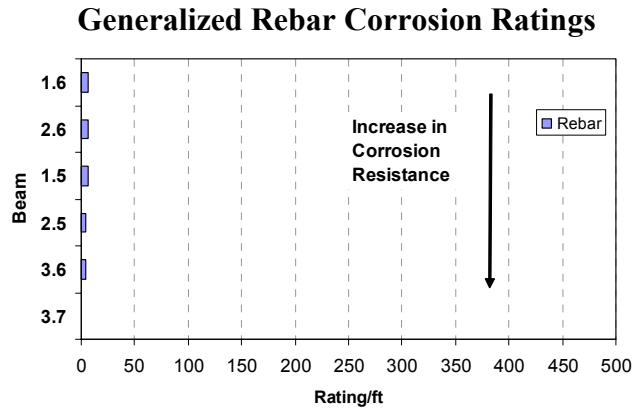
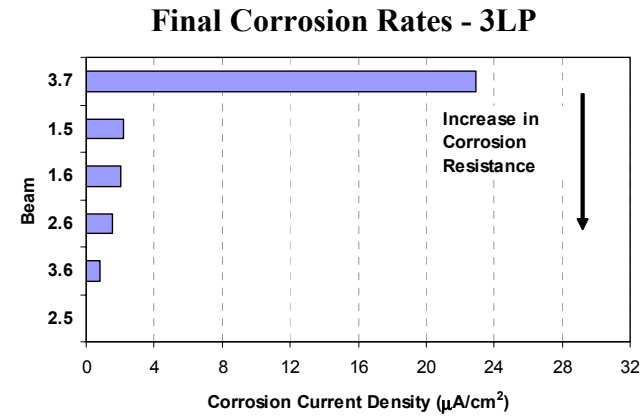
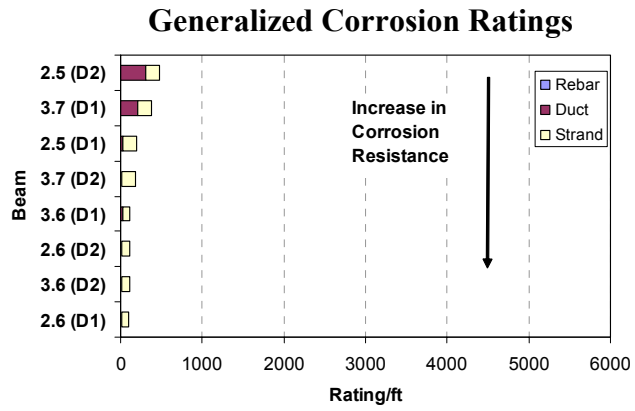


Figure 6.3: Corrosion Ratings vs. Corrosion Rate Readings – Phase I Beams



BEAM	VARIABLE
1.5	N PS, FA Conc.
1.6	N PS, HP Conc.
2.5	2/3 PS, FA Conc.
2.6	2/3 PS, HP Conc.
3.6	U PS, FA Conc.
3.7	U PS, HP Conc.

Figure 6.4: Corrosion Ratings vs. Corrosion Rate Readings – Phase II Beams

### **6.1.3 Forensic Examination vs. Chloride Penetration Measurements**

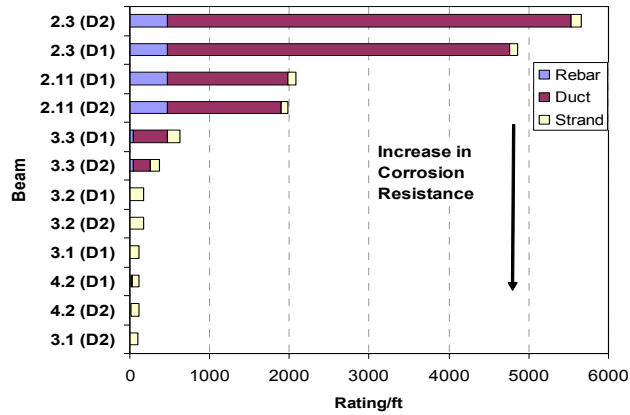
The concrete samples taken for chloride analysis that were of greatest interest were those taken within the ponded region (3-inch and 18-inch offsets from centerline of beam) at the bar/duct level. Therefore, it was decided to use these graphs in comparing the corrosion ratings from the forensic examination with the chloride penetration measurement taken immediately prior to the forensic examination.

Figure 6.5 shows the comparison of the Phase I beams. There is good consistency between the chloride content graphs of the two different offsets, with only minor discrepancies. The chloride content graphs show a strong agreement in order of performance with both corrosion rating graphs.

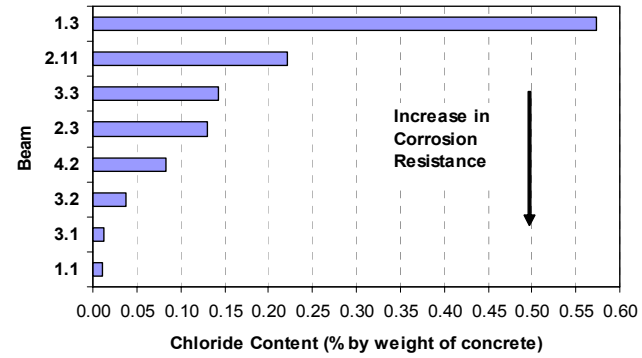
Figure 6.6 shows the comparison of the Phase II beams. As with the Phase I beams, Figure 6.6 indicates a good consistency between the chloride content graphs of the two different offsets, with only minor discrepancies. The relationship between the chloride content and bar corrosion rating graphs is not similar, but this is due to all the bar ratings being very low and close in value. The same is true of the comparison of the chloride contents with the corrosion ratings of the prestressed beams. However, this is due to the minor differences in chloride content among the Phase II beams.

Overall, the chloride content measurements are a good way of determining when the chloride content in the concrete reaches the threshold limit for corrosion to initiate. However, after corrosion has begun, there is no definite correlation between the chloride content and corrosion severity.

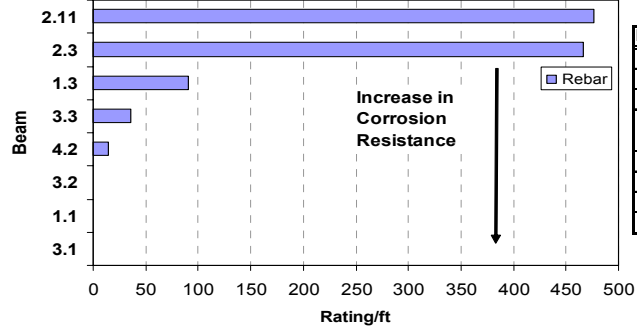
**Generalized Corrosion Ratings**



**Beam Chloride Content at Bar Level-3" Offset**



**Generalized Rebar Corrosion Ratings**



BEAM	VARIABLE
1.1	N PS, Uload
1.3	N PS, Sload
2.3	2/3 PS, Sload
2.11	2/3 PS, Sload, FA Grout
3.1	U PS, Uload
3.2	U PS, Sload
3.3	U PS, Oload
4.2	S PS, Sload

**Beam Chloride Content at Bar Level-18" Offset**

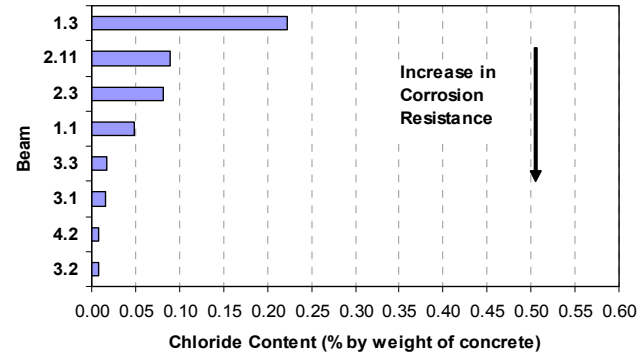
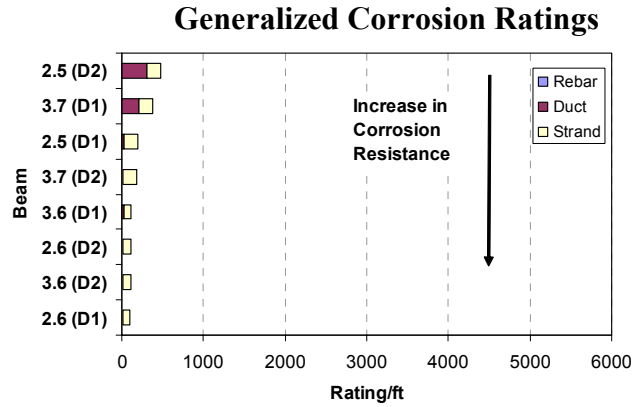


**Figure 6.5: Corrosion Ratings vs. Chloride Content Measurements – Phase I Beams**



BEAM	VARIABLE
1.5	N PS, FA Conc.
1.6	N PS, HP Conc.
2.5	2/3 PS, FA Conc.
2.6	2/3 PS, HP Conc.
3.6	U PS, FA Conc.
3.7	U PS, HP Conc.

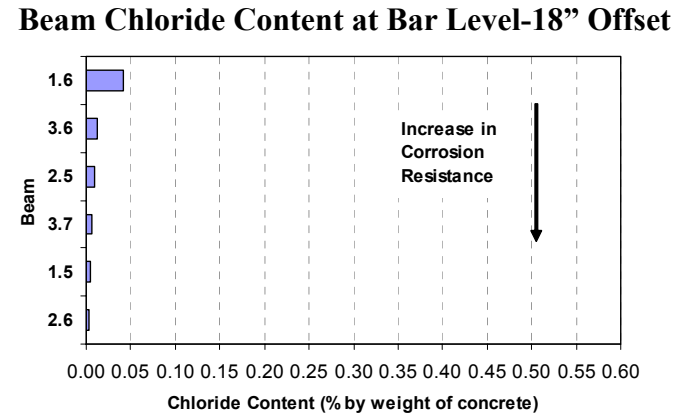
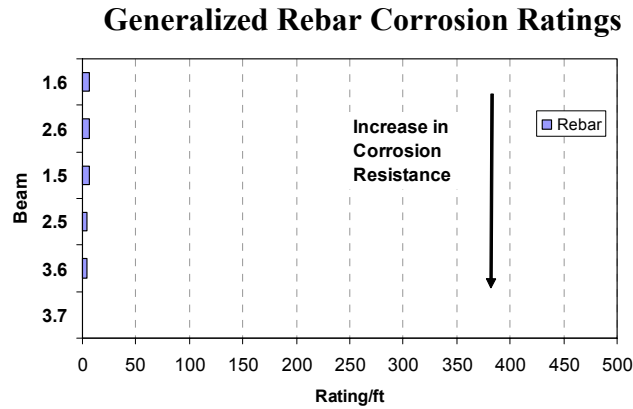
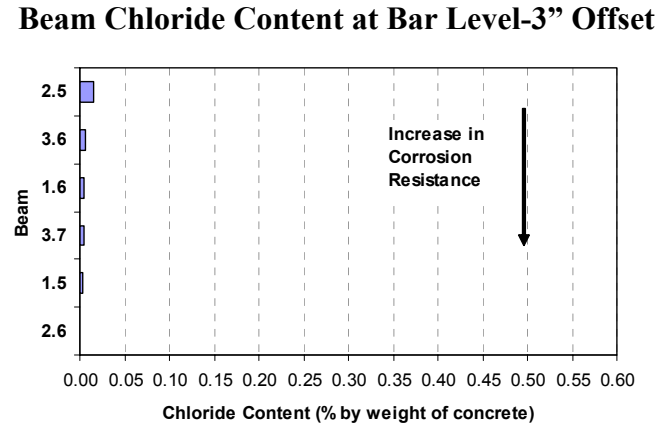


Figure 6.6: Corrosion Ratings vs. Chloride Content Measurements – Phase II Beams

# **CHAPTER 7**

## **Summary of Results, Conclusions and Recommendations**

### **7.1 SUMMARY OF RESULTS**

The following tables summarize all the results found in Chapters 4 and 5. Table 7.1 is a summary of the results presented in Chapter 4, which were based on the measurements taken during exposure testing only. Table 7.2 summarizes the results in Chapter 5, based on the forensic examination only.

**Table 7.1: Summary of Exposure Test Results**

<b>Method of Comparison</b>	<b>Beams Compared</b>	<b>Variable Analyzed</b>	<b>Result</b>
Half-Cell	1.1, 3.1	Prestress	<ul style="list-style-type: none"> <li>• 2/3 PS worse than 100%U PS</li> </ul>
Half-Cell	1.3, 2.3, 3.2, 4.2	Prestress	<ul style="list-style-type: none"> <li>• Increase in corrosion protection with increase in PS</li> <li>• 2/3 PS corrosion protection much more similar to Non-PS than 100% PS</li> <li>• No significant difference between 100%U and 100%S PS</li> </ul>
Half-Cell	1.5, 2.5, 3.6	Prestress	<ul style="list-style-type: none"> <li>• Increase in corrosion protection with increase in PS</li> <li>• 2/3 PS corrosion protection almost identical to Non-PS</li> </ul>
Half-Cell	1.6, 2.6, 3.7	Prestress	<ul style="list-style-type: none"> <li>• All levels of PS similar (due to very large crack in 100%U PS beam)</li> </ul>
Corr. Rate	1.5, 2.5, 3.6	Prestress	<ul style="list-style-type: none"> <li>• Increase in corrosion protection with increase in PS</li> </ul>
Cl <sup>-</sup> Content	All Phase I Beams	Prestress	<ul style="list-style-type: none"> <li>• Increase in horizontal chloride penetration with decrease in PS</li> <li>• Increase in corrosion protection with increase in PS</li> </ul>
Half-Cell	1.1, 1.3	Load/Cracking	<ul style="list-style-type: none"> <li>• Decrease in corrosion protection with increase in loading</li> </ul>
Half-Cell	3.1, 3.2, 3.3	Load/Cracking	<ul style="list-style-type: none"> <li>• Decrease in corrosion protection with increase in loading</li> <li>• Significant decrease in corrosion protection with cracking present</li> </ul>
Corr. Rate	3.1, 3.2, 3.3	Load/Cracking	<ul style="list-style-type: none"> <li>• Decrease in corrosion protection with increase in loading and cracking</li> </ul>
Cl <sup>-</sup> Content	1.3, 2.11, 4.2	Load/Cracking	<ul style="list-style-type: none"> <li>• Significantly higher chloride content at bar level when samples taken at crack location</li> </ul>
Half-Cell	1.5, 1.6 2.5, 2.6	Concrete Type	<ul style="list-style-type: none"> <li>• HP concrete corrosion protection better than FA</li> </ul>
Half-Cell	3.6, 3.7	Concrete Type	<ul style="list-style-type: none"> <li>• FA concrete corrosion protection better than HP (this HP beam is the one with a very large crack)</li> </ul>
Half-Cell	All Phase II Beams	Concrete Type	<ul style="list-style-type: none"> <li>• HP concrete corrosion protection better than FA</li> </ul>
Corr. Rate	1.5, 1.6 2.5, 2.6 3.6, 3.7	Concrete Type	<ul style="list-style-type: none"> <li>• No significant difference in corrosion protection of HP and FA concrete</li> </ul>
Cl <sup>-</sup> Content	Blocks	Concrete Type	<ul style="list-style-type: none"> <li>• HP concrete corrosion protection better than FA</li> </ul>
Cl <sup>-</sup> Content	1.5, 1.6 2.5, 2.6 3.6, 3.7	Concrete Type	<ul style="list-style-type: none"> <li>• HP concrete better at preventing chloride penetration</li> <li>• Both concrete types minimize chloride penetration to bar level</li> </ul>
Half-Cell	2.3, 2.11	Grout Type	<ul style="list-style-type: none"> <li>• No difference in corrosion protection between normal and FA grout</li> </ul>

**Table 7.2: Summary of Forensic Examination Corrosion Rating Results**

<b>Method of Comparison</b>	<b>Beams Compared</b>	<b>Variable Analyzed</b>	<b>Result</b>
Gen. Stirrup	1.3, 2.3, 3.2, 4.2	Prestress	<ul style="list-style-type: none"> <li>• Non and 2/3 PS much worse corrosion protection than 100%S and U PS</li> </ul>
Loc. Stirrup	1.3, 2.3, 3.2, 4.2	Prestress	<ul style="list-style-type: none"> <li>• 2/3 PS is much worse corrosion protection than all others, including Non-PS</li> </ul>
Gen. and Loc. Duct	2.3, 3.2, 4.2	Prestress	<ul style="list-style-type: none"> <li>• 2/3 PS the worst corrosion protection by a significant amount</li> </ul>
Gen. and Loc. Strand	2.3, 3.2, 4.2	Prestress	<ul style="list-style-type: none"> <li>• All corrosion protections about the same, with 100%U PS a little worse</li> </ul>
Gen. Stirrup	1.5, 2.5, 3.6 1.6, 2.6, 3.7	Prestress	<ul style="list-style-type: none"> <li>• 100%U PS consistently best corrosion protection</li> <li>• corrosion protection of Non and 2/3 PS similar, no consistent superiority</li> </ul>
Gen. and Loc. Bar	1.5, 2.5, 3.6 1.6, 2.6, 3.7	Prestress	<ul style="list-style-type: none"> <li>• 2/3 PS shows worst corrosion protection by a significant amount</li> </ul>
Gen. and Loc. Duct	2.5, 3.6	Prestress	<ul style="list-style-type: none"> <li>• 2/3 and 100%U PS corrosion protection similar, no consistent superior PS</li> </ul>
Gen. and Loc. Strand	2.5, 3.6	Prestress	<ul style="list-style-type: none"> <li>• 2/3 and 100%U PS corrosion protection similar, no consistent superior PS</li> </ul>
Gen. Stirrup	1.1, 1.3 3.1, 3.2, 3.3	Load/Cracking	<ul style="list-style-type: none"> <li>• Much worse corrosion protection when cracking is present</li> <li>• Corrosion protection decreases as loading increases</li> </ul>
Loc. Stirrup	1.1, 1.3 3.1, 3.2, 3.3	Load/Cracking	<ul style="list-style-type: none"> <li>• Much worse corrosion protection when cracking is present</li> <li>• Corrosion protection decreases as loading increases</li> </ul>
Gen. and Loc. Bar	1.1, 1.3 3.1, 3.2, 3.3	Load/Cracking	<ul style="list-style-type: none"> <li>• Cracked beams show a little worse corrosion protection</li> </ul>
Gen. and Loc. Duct	3.1, 3.2, 3.3	Load/Cracking	<ul style="list-style-type: none"> <li>• Much worse corrosion protection when cracking is present</li> </ul>
Gen. and Loc. Stirrup	1.5, 1.6 2.5, 2.6 3.6, 3.7	Concrete Type	<ul style="list-style-type: none"> <li>• HP concrete consistently better corrosion protection</li> </ul>
Gen. and Loc. Bar	1.5, 1.6 2.5, 2.6 3.6, 3.7	Concrete Type	<ul style="list-style-type: none"> <li>• All similar corrosion protection and all low ratings...both concretes provide good corrosion protection</li> </ul>
Gen. and Loc. Duct	1.5, 1.6 2.5, 2.6 3.6, 3.7	Concrete Type	<ul style="list-style-type: none"> <li>• All corrosion protections similar, no consistent superior concrete</li> </ul>
Gen. and Loc. Strand	1.5, 1.6 2.5, 2.6 3.6, 3.7	Concrete Type	<ul style="list-style-type: none"> <li>• All corrosion protections similar, no consistent superior concrete</li> </ul>
Gen. Duct	2.3, 2.11	Grout Type	<ul style="list-style-type: none"> <li>• Fly ash grout shows much better corrosion protection</li> </ul>
Gen. and Loc. Strand	2.3, 2.11	Grout Type	<ul style="list-style-type: none"> <li>• No difference in corrosion protection between grout types</li> </ul>



## 7.2 CONCLUSIONS

### 7.2.1 Variable Corrosion protection

The following conclusions have been made with respect to the effects of varying applied loads and crack widths on the corrosion protection of the specimens:

- The specimen corrosion protection decreases as the applied load increases.
- There is a consistent decrease in corrosion protection when cracking is present.
- An increase in crack width produces a large decrease in corrosion protection.
- The chloride content in the concrete is significantly higher at crack locations, and increases as the crack width increases.

The following conclusions have been made with respect to the effects of varying levels of prestress on the corrosion protection of the specimens:

- The specimen corrosion protection increases as the level of prestress increases.
- There is a significant increase in corrosion protection when increasing the level of prestress from 2/3 to 100%U or 100%S.
- The corrosion protection of the 2/3 PS beam is much more similar to that of the Non-PS as opposed to the 100% PS beams. The 2/3 PS beams frequently show worse corrosion protection than the Non-PS due to the increase in crack width.
- There was no consistently superior design between the 100%U and 100%S PS beams.

- There was a noticeable increase in the horizontal chloride penetration as the level of prestress decreased. This can be attributed to the decrease in compressive stresses, which allows the concrete to be more permeable.

The following conclusions have been made with respect to the effects of varying concrete types on the corrosion protection of the specimens:

- Both the high performance concrete and the fly ash concrete beams show good corrosion protection by minimizing the chloride penetration through the concrete.
- The high performance concrete tends to show a little better corrosion protection than the fly ash concrete, but the difference is not significant.
- No conclusions can be drawn on corrosion protection of the high performance and the fly ash concrete with respect to the standard TxDOT concrete due to lack of comparable specimens.

The following conclusions have been made with respect to the effects of varying grout types on the corrosion protection of the specimens:

- The fly ash grout, in comparison to the normal grout, aided in the corrosion protection of the galvanized steel ducts.
- The fly ash grout, in comparison to the normal grout, did not show an increase in corrosion protection of the prestressing strands.

The following conclusions have been made with respect to the corrosion protection of the different duct splice types:

- The industry standard splice allows moisture to enter through the sides of the splice and get trapped between the duct and the splice due to

inefficiency of duct tape. This results in moisture and chlorides attacking the splice from both sides.

- The heat-shrink splice also allows moisture to enter through the sides and get trapped due to insufficient adhesion between the splice and the duct. It also traps bleed water from the grout.
- Intentional damage inflicted on the duct splices does not show a direct correlation with the severity of corrosion. It is logical that any imperfection in splicing should produce worse results. However, the intentionally damaged splices did not appear to perform worse than those without damage.
- Neither the industry standard nor the heat-shrink splice appears to be a satisfactory duct splice for the corrosion protection of a galvanized steel duct.

### **7.2.2 Exposure Test Measurements**

Results from this experimental program show a strong correlation between half-cell potential readings and the results from the forensic examination. Half-cell potential readings are inadequate in determining the severity of corrosion activity, but prove to be useful for relative comparison of specimens.

Corrosion rate readings are not an adequate form of non-destructive corrosion measurements for a post-tensioning system. The readings from this experimental program showed no correlation with the results from the forensic examination. The procedure and equipment for taking corrosion rate readings was intended for measuring the corrosion rate of the mild steel. It is possible that the erroneous results are due to the equipment reading the corrosion rate of the zinc on galvanized ducts, which is expected to corrode for protection. (This could also

be true of half-cell potential readings, but that was not apparent in this experiment.)

Chloride penetration measurements are useful in monitoring the chloride content in the concrete and determining when the content has reached the corrosion threshold. However, after the onset of corrosion, there is not a direct relationship between the chloride content percentage and severity of corrosion.

### **7.3 FUTURE TESTING RECOMMENDATIONS**

Should it be decided to conduct an experimental program similar to that described in this document, the following recommendations are made based on experience and results from this experimental program:

- Use a smaller concrete clear cover in the beam specimens to accelerate the time to initiation of corrosion.
- Use epoxy coated longitudinal bars and stirrups to eliminate the possibility of corrosion of the mild steel, isolating testing to the post-tensioning system.
- Develop a form of protection for the wires connected to the reinforcement that are used to take half-cell potential and corrosion rate readings. These wires were continuously exposed to the outdoor environment and began to deteriorate, resulting in possible erroneous readings.

## **APPENDIX A**

### **Beam Specimen Variables**

Figures A1 and A2 contain tables of each beam specimen and the corresponding variables. A notation key and details of the variables can be found in Section 2.7 of this document. The specimens in Figure A1 are from Phase I of the experimental program, and those in Figure A2 are from Phase II.

Specimen	Prestress Level				Applied Load			Concrete Type			Duct Type		Splice Type				Grout Type			Strand Type			
	X	P	U	S	XL	SL	OL	C	F	H	SD	PD	IS	ISD	HS	HSD	NG	FA	AB	NS	GS	ES	
1.1	■				■			■															
1.2	■					■		■															
1.3	■							■															
1.4	■							■															
2.1		■						■			■		■		■		■			■			■
2.2		■						■			■		■		■		■			■			■
2.3		■						■			■		■	■	■	■	■			■			■
2.4		■						■			■		■		■		■			■			■
2.11		■						■			■		■		■		■	■		■			■
3.1			■			■		■			■		■		■		■			■			■
3.2			■				■	■			■		■		■		■			■			■
3.3			■					■			■		■		■		■			■			■
3.4			■					■			■		■	■	■	■	■			■			■
3.5			■					■			■		■		■		■			■			■
4.1				■		■		■			■		■		■		■			■			■
4.2				■		■		■			■		■	■	■	■	■			■			■

\* See Section 2.7 for notation key

*Figure A1: Phase I Beam Specimens and Variables*

Specimen	Prestress Level				Applied Load			Concrete Type			Duct Type		Splice Type				Grout Type			Strand Type			
	X	P	U	S	XL	SL	OL	C	F	H	SD	PD	IS	ISD	HS	HSD	NG	FA	AB	NS	GS	ES	
1.5	■					■			■														
1.6	■					■			■														
2.5		■				■			■		■		■		■		■			■			
2.6		■				■			■		■		■		■		■			■			
2.7		■				■		■	■		■		■		■		■			■			■
2.8		■				■		■	■		■		■		■		■			■		■	
2.9		■				■		■	■		■		■		■		■			■			
2.10		■				■		■	■		■		■		■		■		■	■			
2.12		■				■		■	■		■	■		■		■		■		■			
3.6			■			■		■	■		■		■		■		■			■			
3.7			■			■		■	■		■		■		■		■			■			

\* See Section 2.7 for notation key

*Figure A2: Phase II Beam Specimens and Variables*

## **APPENDIX B**

### **Beam Specimen Timeline**

Figure B1 contains a timeline for all of the beam specimens. Information shown on the timeline includes:

- date of exposure testing initiation
- dates corrosion rate readings were taken
- dates chloride penetration measurements were taken
- dates beams were reloaded
- date of partial autopsy of select beams
- date of final autopsy of select beams



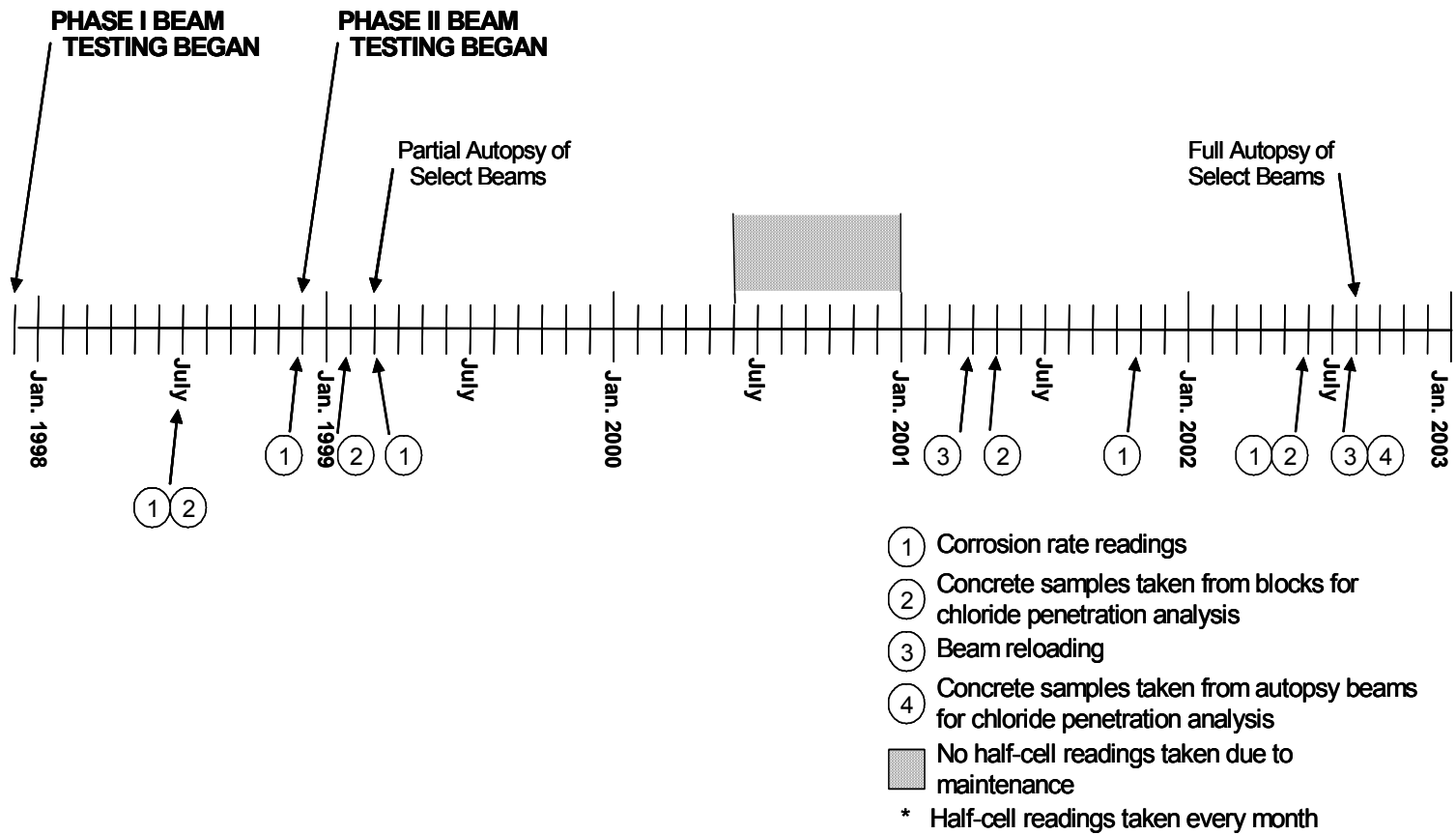
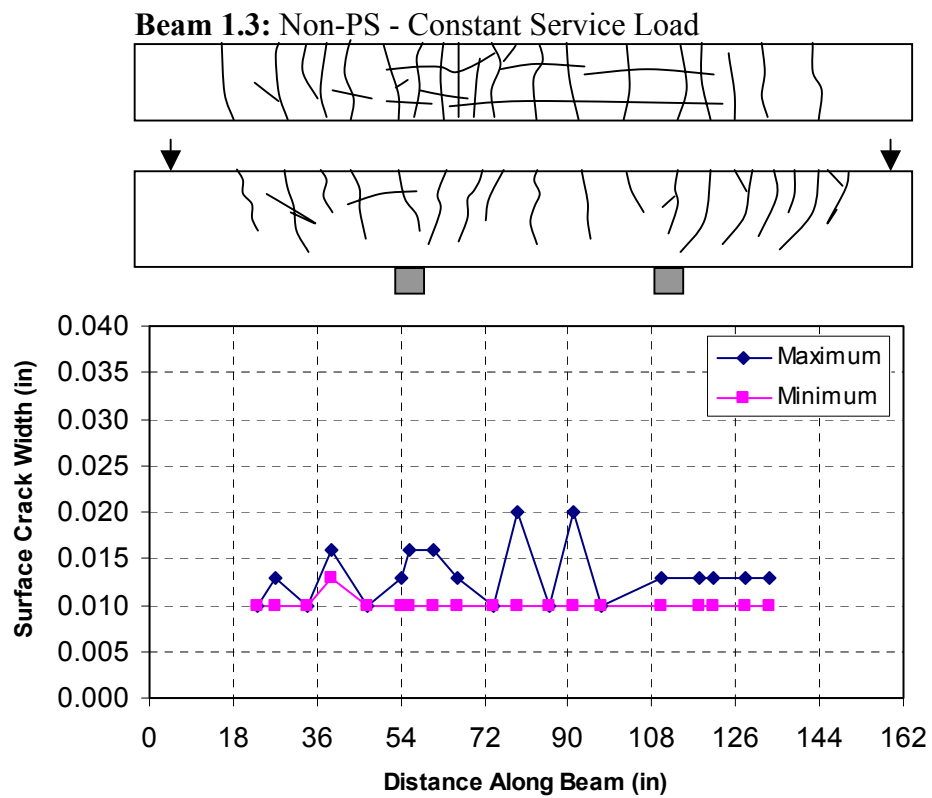


Figure B1: Beam Specimen Timeline

## APPENDIX C

### Final Surface Crack Patterns and Measurements of Autopsy Beams



*Figure C1: Final Crack Pattern and Measurements – Beam 1.3*

**Beam 2.3: 2/3 PS - Constant Service Load**

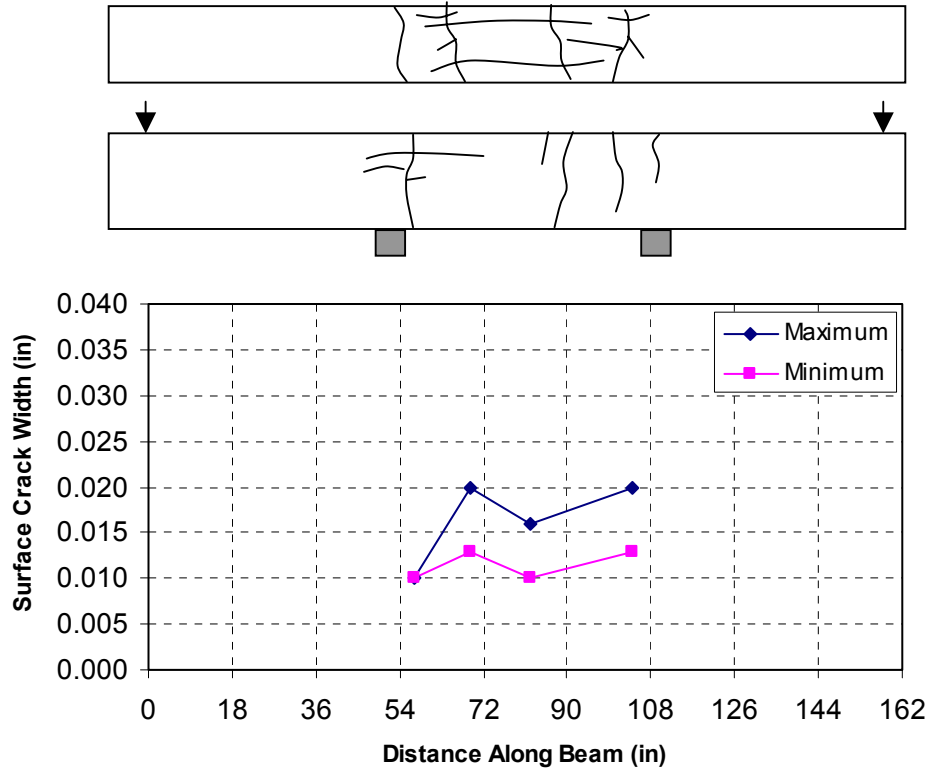


**Figure C2: Final Crack Pattern and Measurements – Beam 2.3**

**Beam 2.11: 2/3 PS - Constant Service Load**

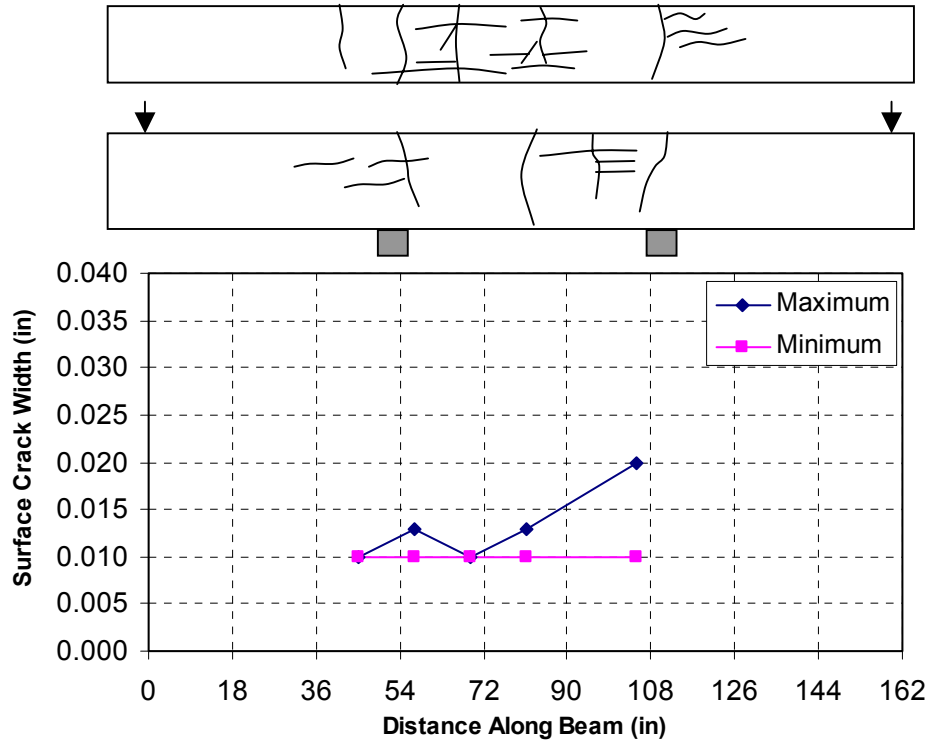


**Figure C3: Final Crack Pattern and Measurements – Beam 2.11**

**Beam 3.2: 100%U PS - Constant Service Load**

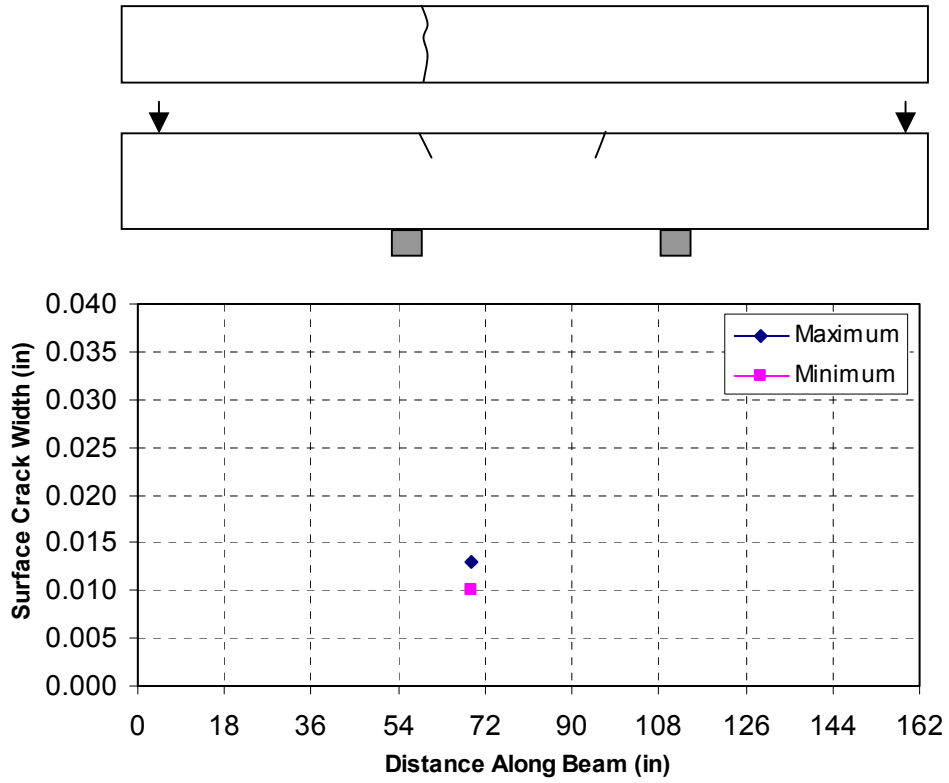


*Figure C4: Final Crack Pattern and Measurements – Beam 3.2*

**Beam 3.3: 100%U PS - 124% Overload**

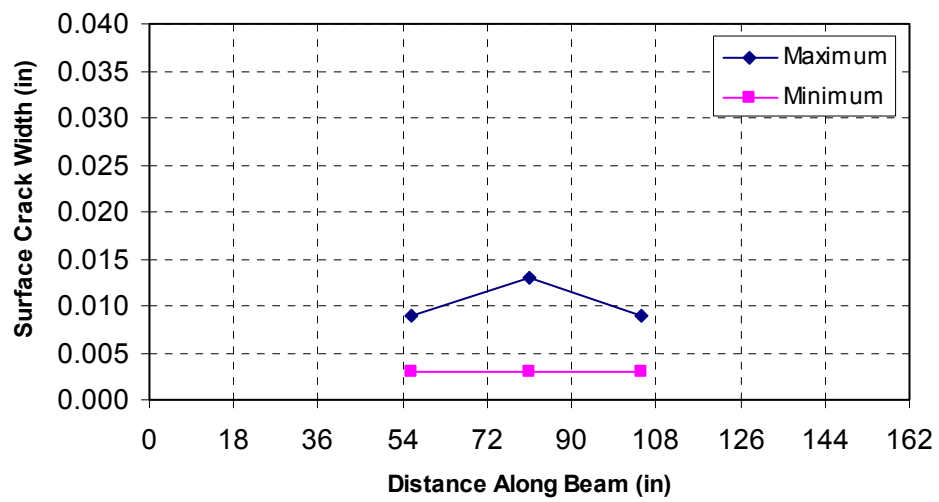
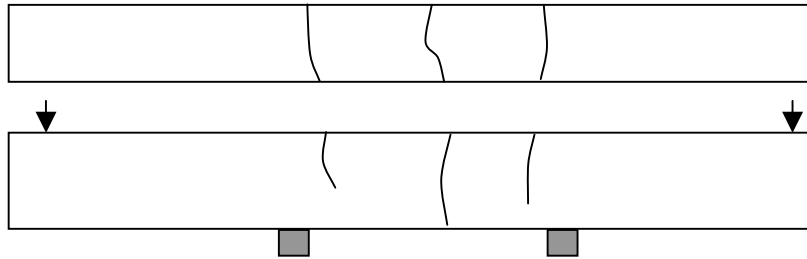


**Figure C5: Final Crack Pattern and Measurements – Beam 3.3**

**Beam 4.2: 100%S PS - Constant Service Load**

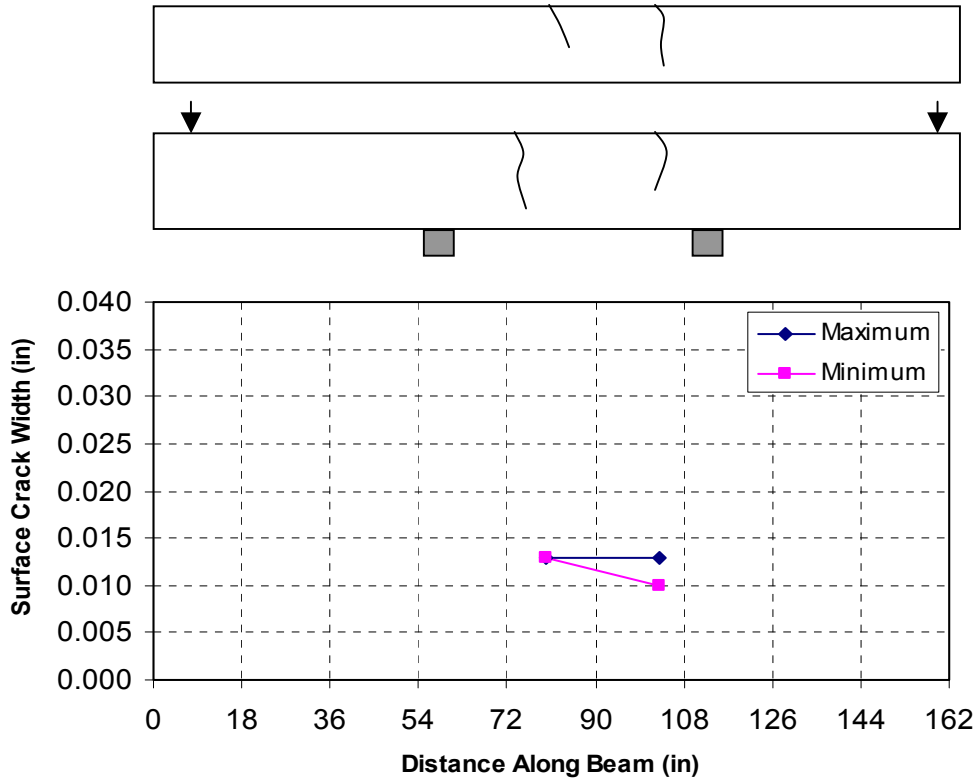


**Figure C6: Final Crack Pattern and Measurements – Beam 4.2**

**Beam 1.5: Non-PS - Constant Service Load**

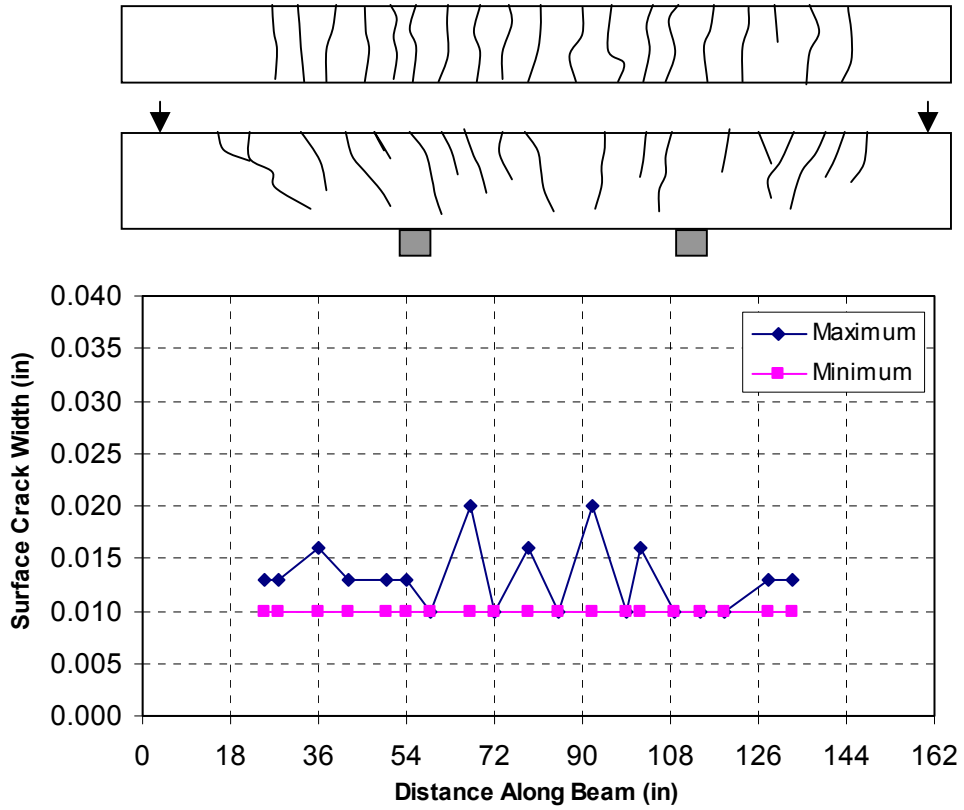


**Figure C7: Final Crack Pattern and Measurements – Beam 1.5**



**Beam 1.6: Non-PS - Constant Service Load**

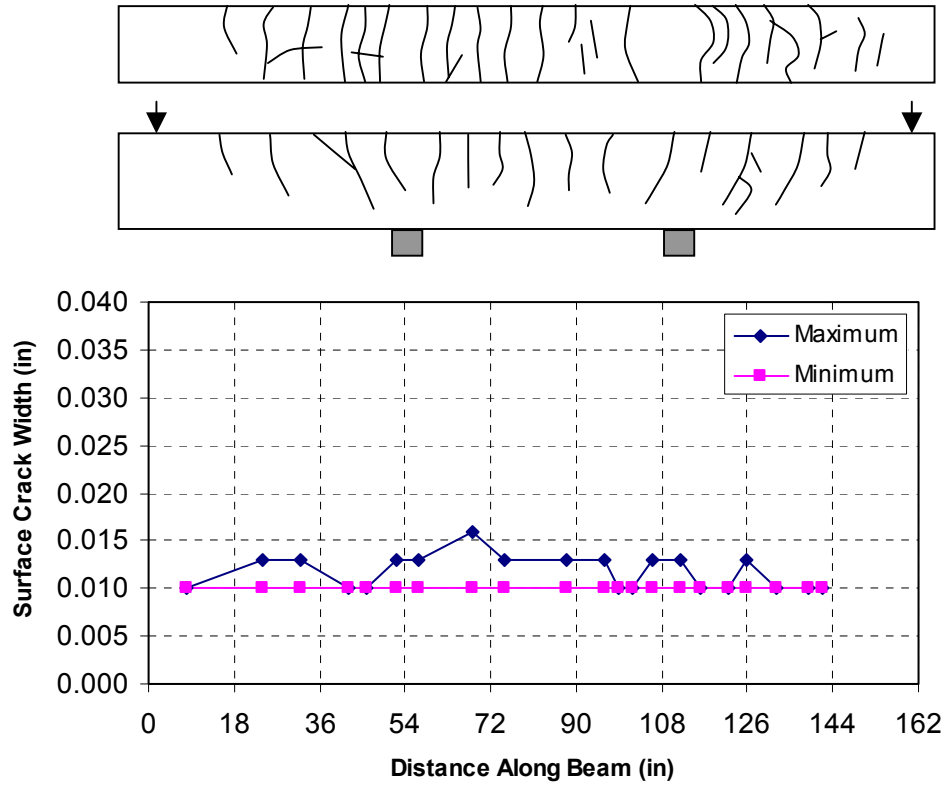


**Figure C8: Final Crack Pattern and Measurements – Beam 1.6**

**Beam 2.5: 2/3 PS - Constant Service Load**

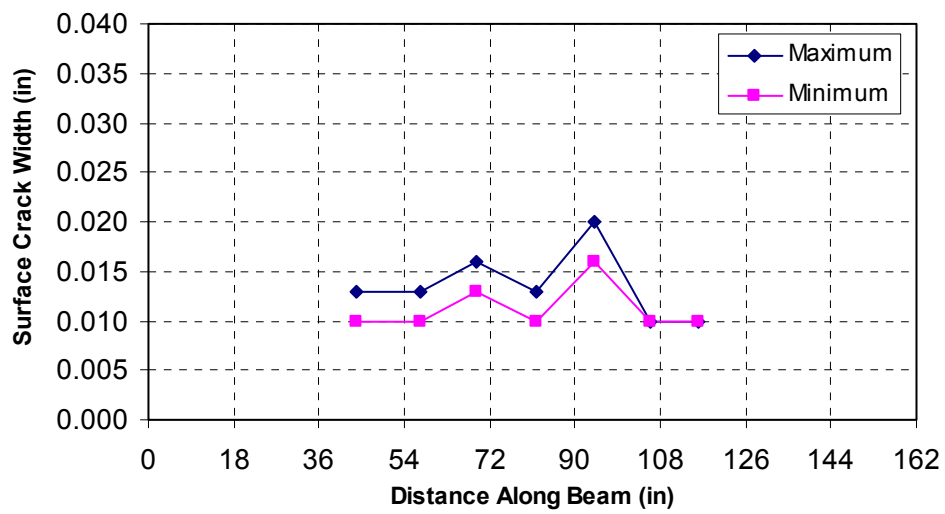
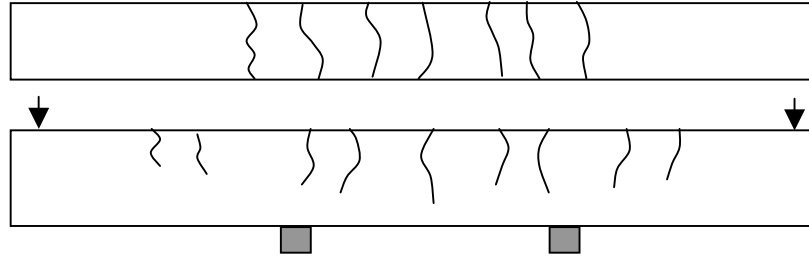


**Figure C9: Final Crack Pattern and Measurements – Beam 2.5**

**Beam 2.6: 2/3 PS - Constant Service Load**

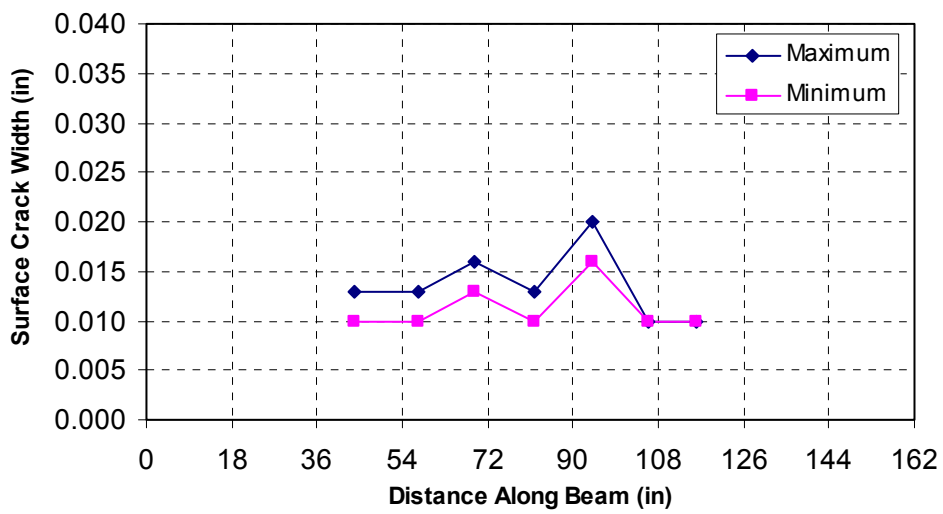
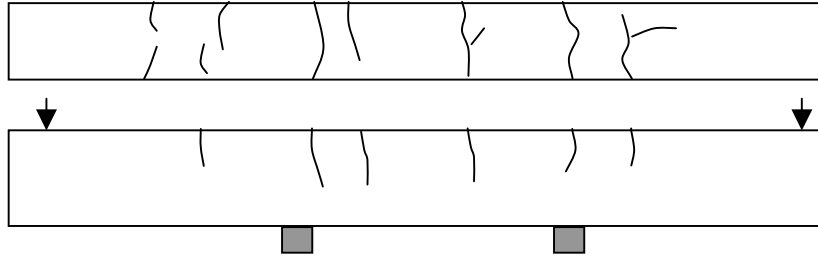


**Figure C10: Final Crack Pattern and Measurements – Beam 2.6**

**Beam 3.6: 100%U PS - Constant Service Load**

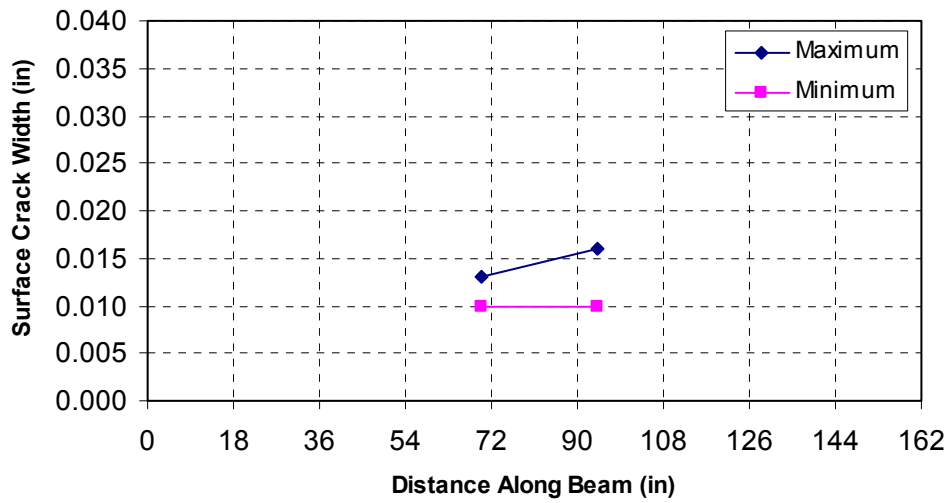
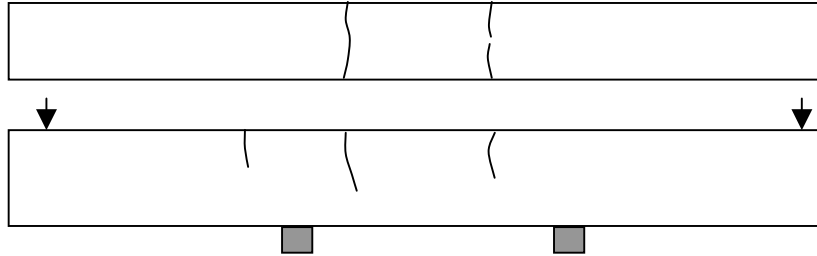


**Figure C11: Final Crack Pattern and Measurements – Beam 3.6**

**Beam 3.7: 100%U PS - Constant Service Load**

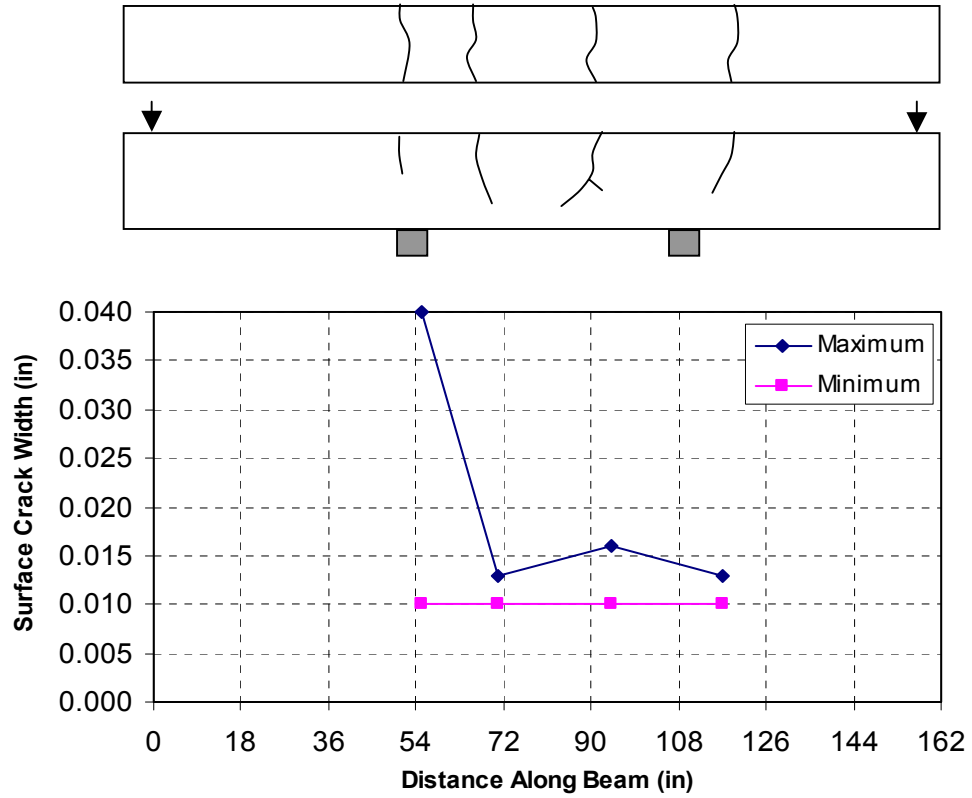


**Figure C12: Final Crack Pattern and Measurements – Beam 3.7**

# APPENDIX D

## Additional Exposure Test Beam Data

### D.1 HALF-CELL POTENTIAL READINGS

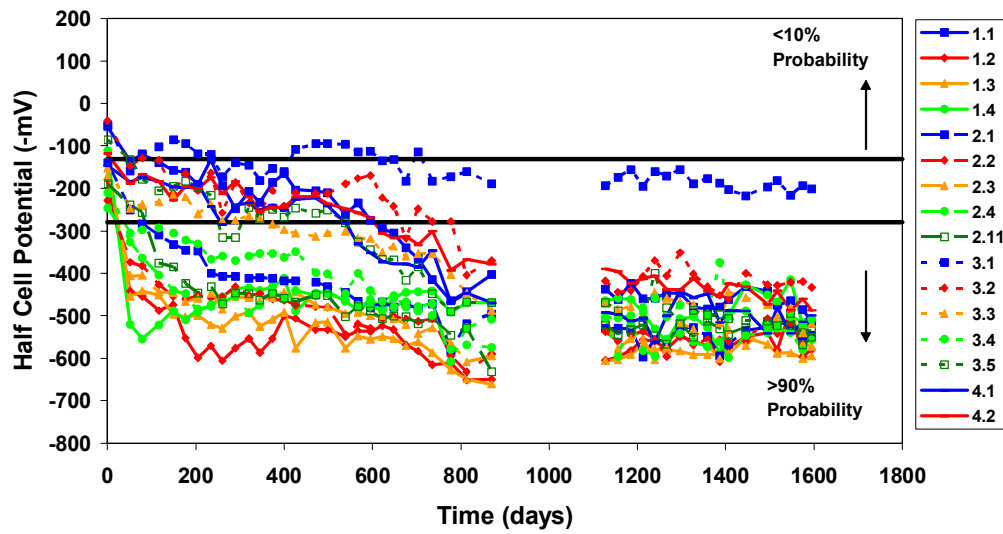


*Figure D1: Half-Cell Potential Readings  
(All Phase I Beams)*

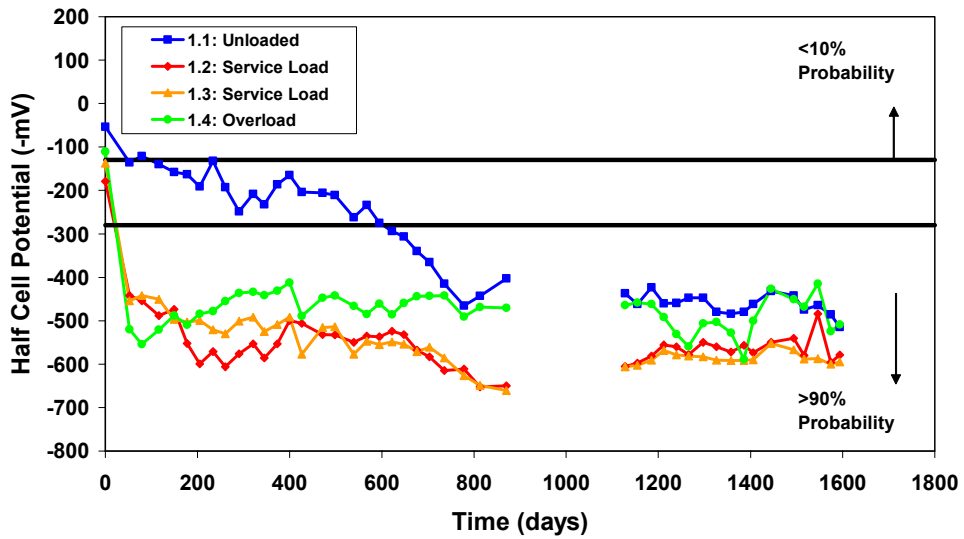


**Figure D2: Half-Cell Potential Readings  
(All Phase I Beams - Non-PS)**

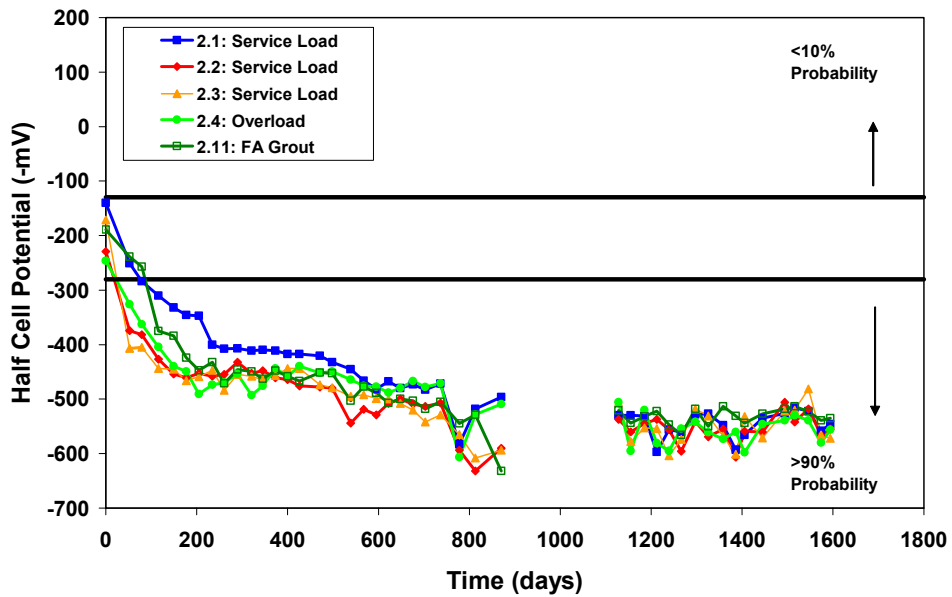


**Figure D3: Half-Cell Potential Readings  
(All Phase I Beams - 2/3 PS)**

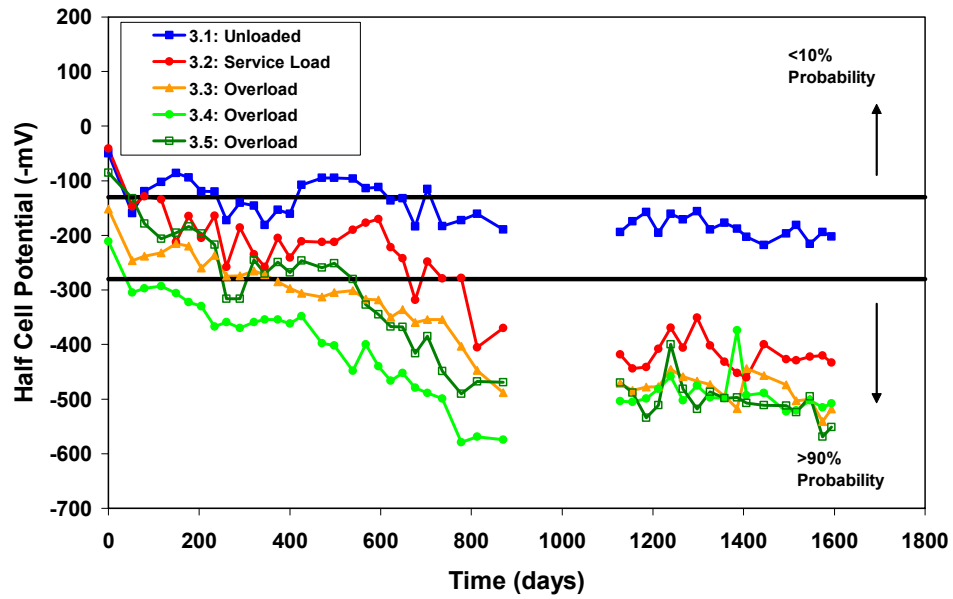


**Figure D4: Half-Cell Potential Readings  
(All Phase I Beams - 100%U PS)**

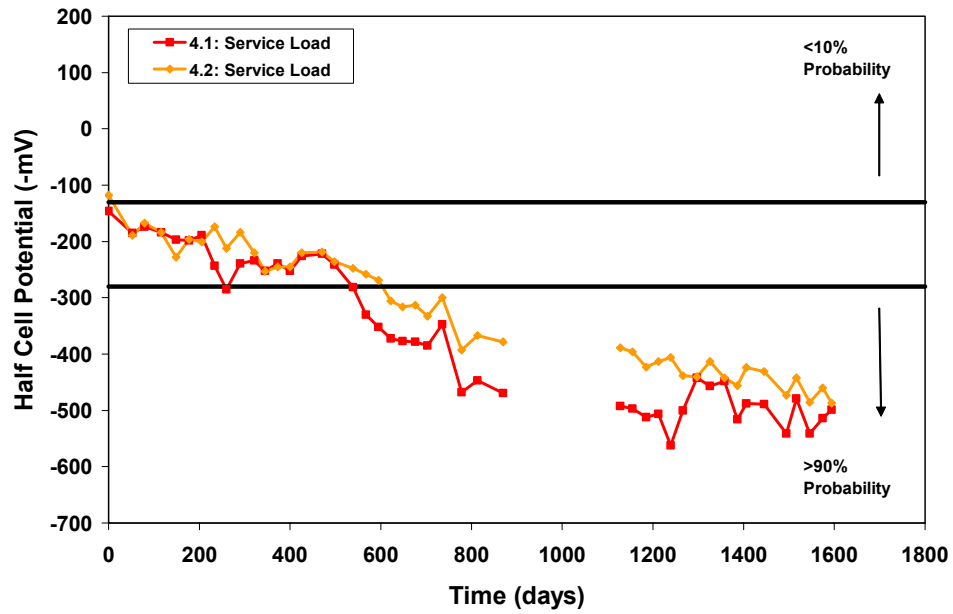


**Figure D5: Half-Cell Potential Readings  
(All Phase I Beams - 100%S PS)**



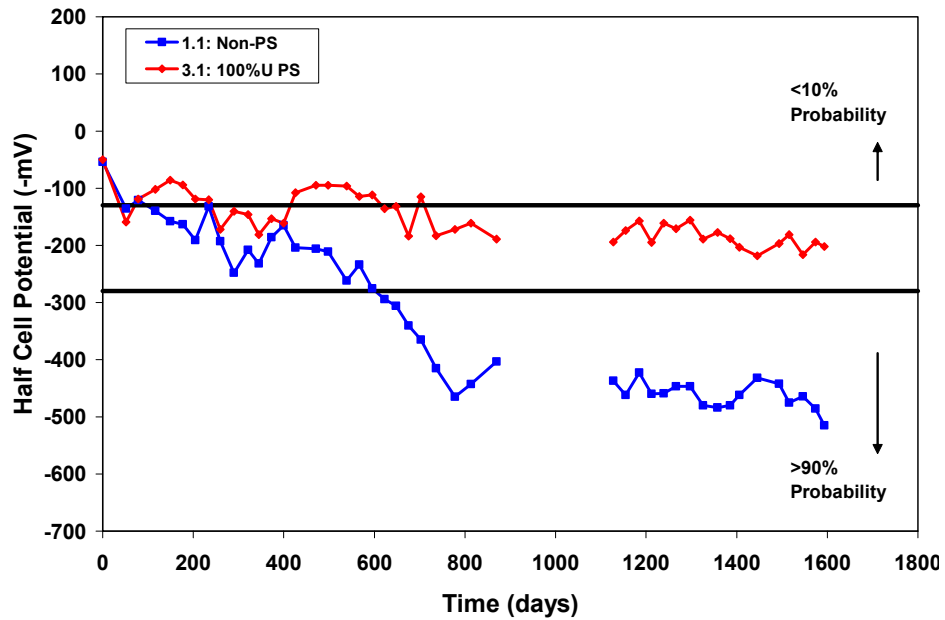


**Figure D6: Half-Cell Potential Readings  
(All Phase I Beams – Unloaded)**

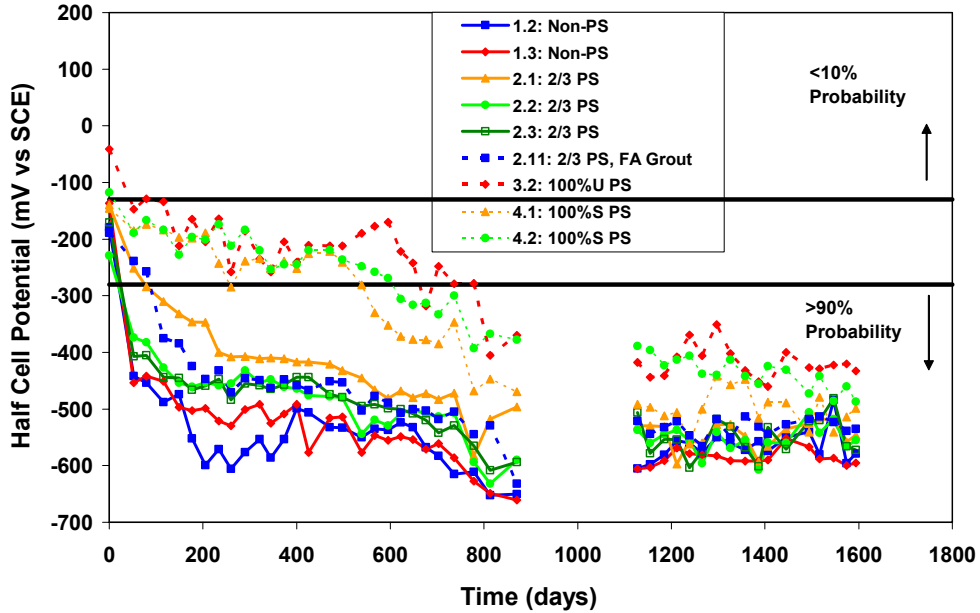


**Figure D7: Half-Cell Potential Readings  
(All Phase I Beams – Service Load)**

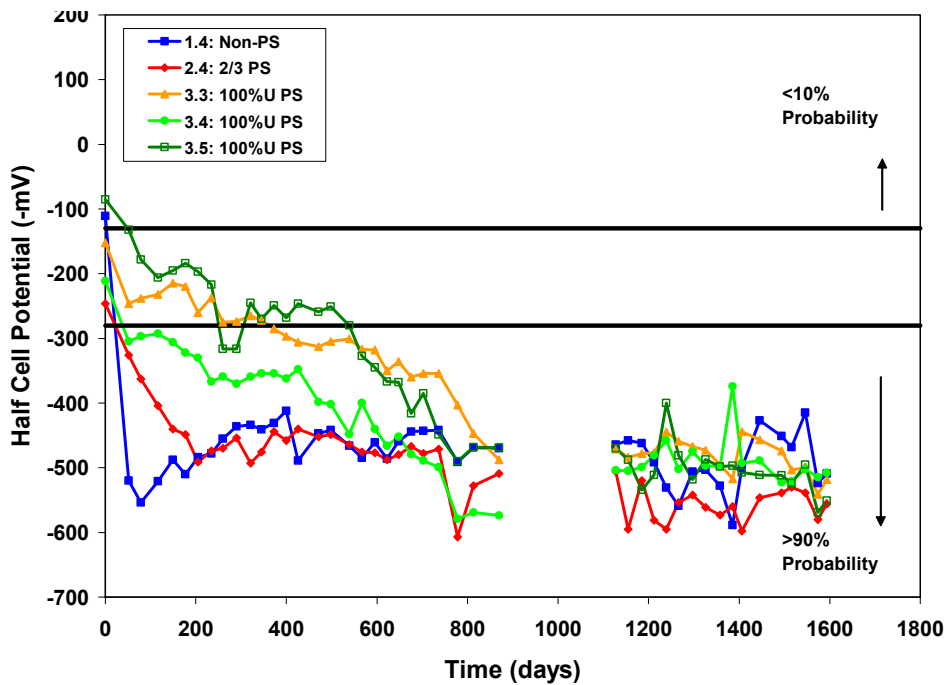


**Figure D8: Half-Cell Potential Readings  
(All Phase I Beams – Overload)**

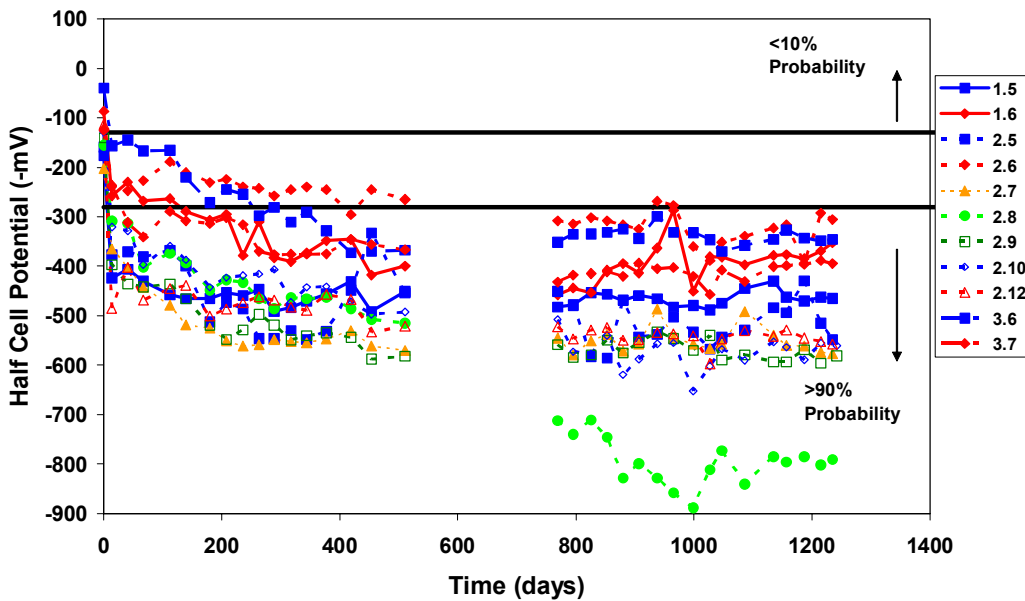


**Figure D9: Half-Cell Potential Readings  
(All Phase II Beams)**

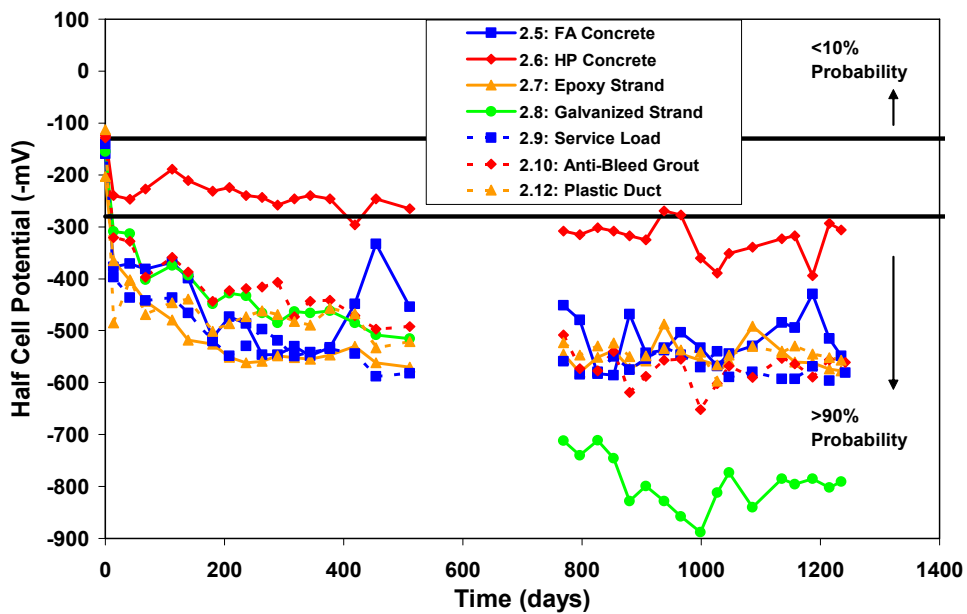


**Figure D10: Half-Cell Potential Readings  
(All Phase II Beams - 2/3 PS)**

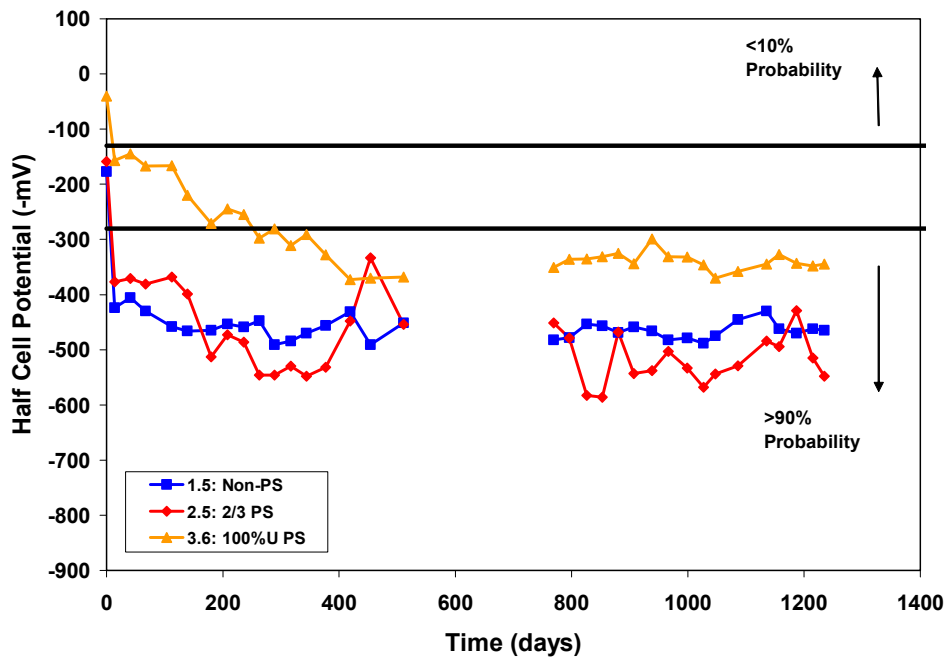


**Figure D11: Half-Cell Potential Readings  
(All Phase II Beams – Fly Ash Concrete)**

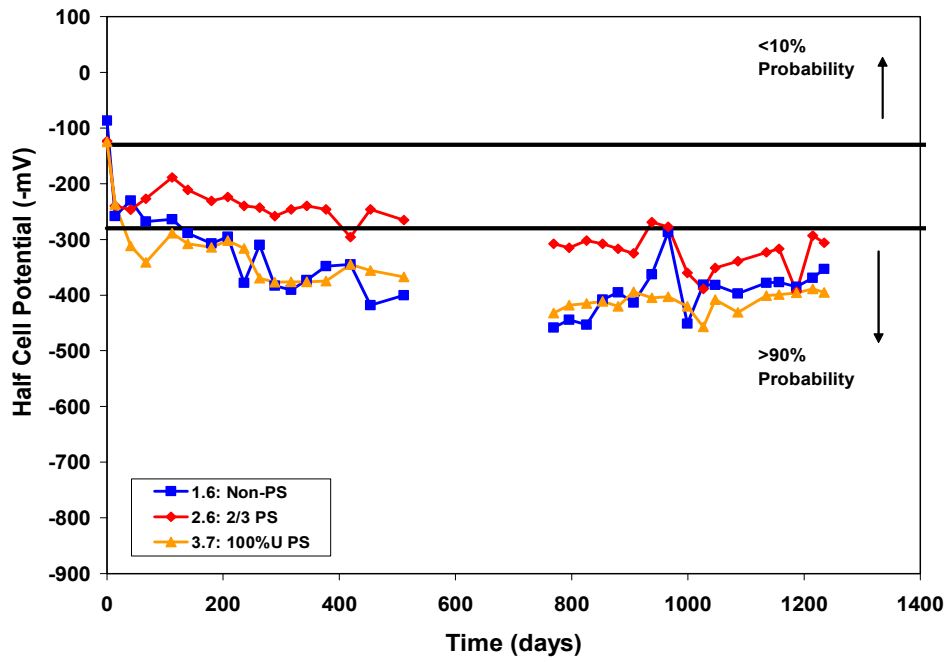


**Figure D12: Half-Cell Potential Readings  
(All Phase II Beams – High Performance Concrete)**

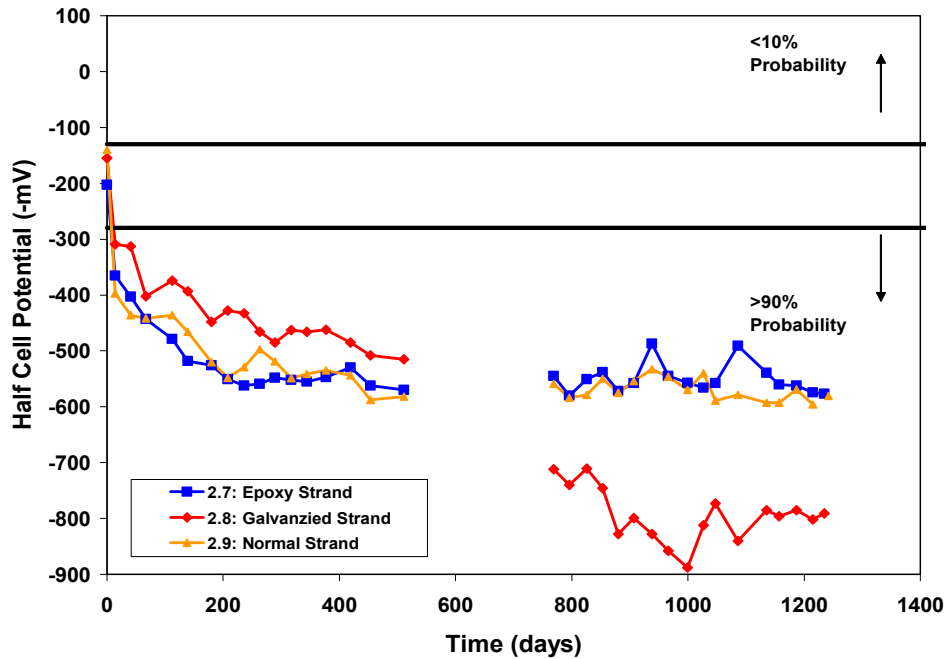


**Figure D13: Half-Cell Potential Readings  
(All Phase II Beams – Varying Strand Type)**

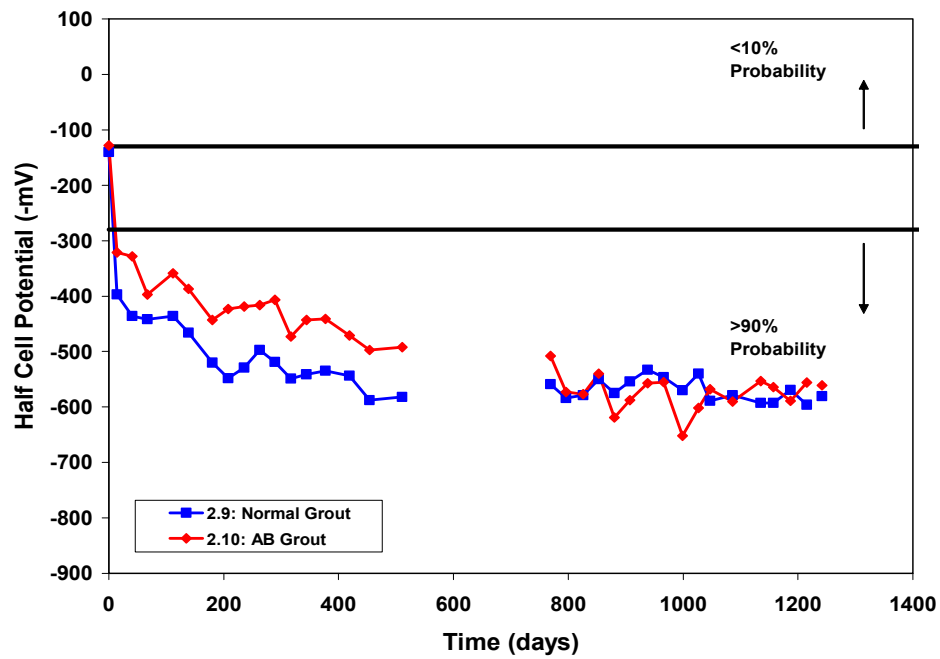


*Figure D14: Half-Cell Potential Readings  
(All Phase II Beams – Varying Grout Type)*

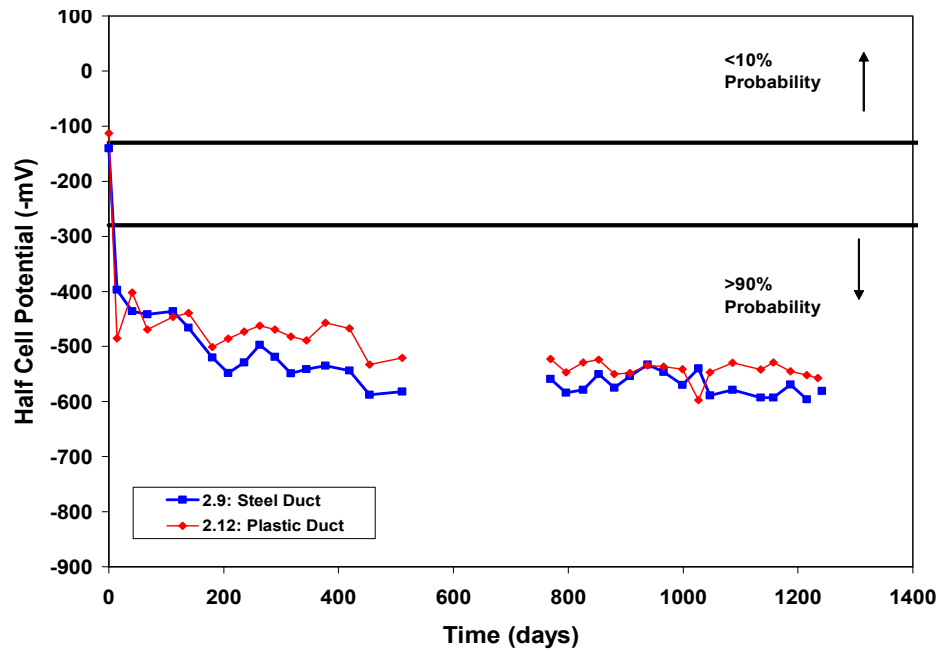
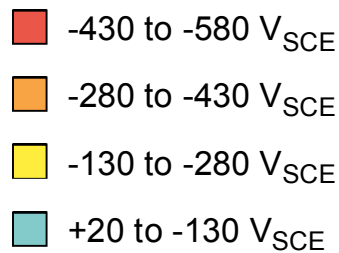
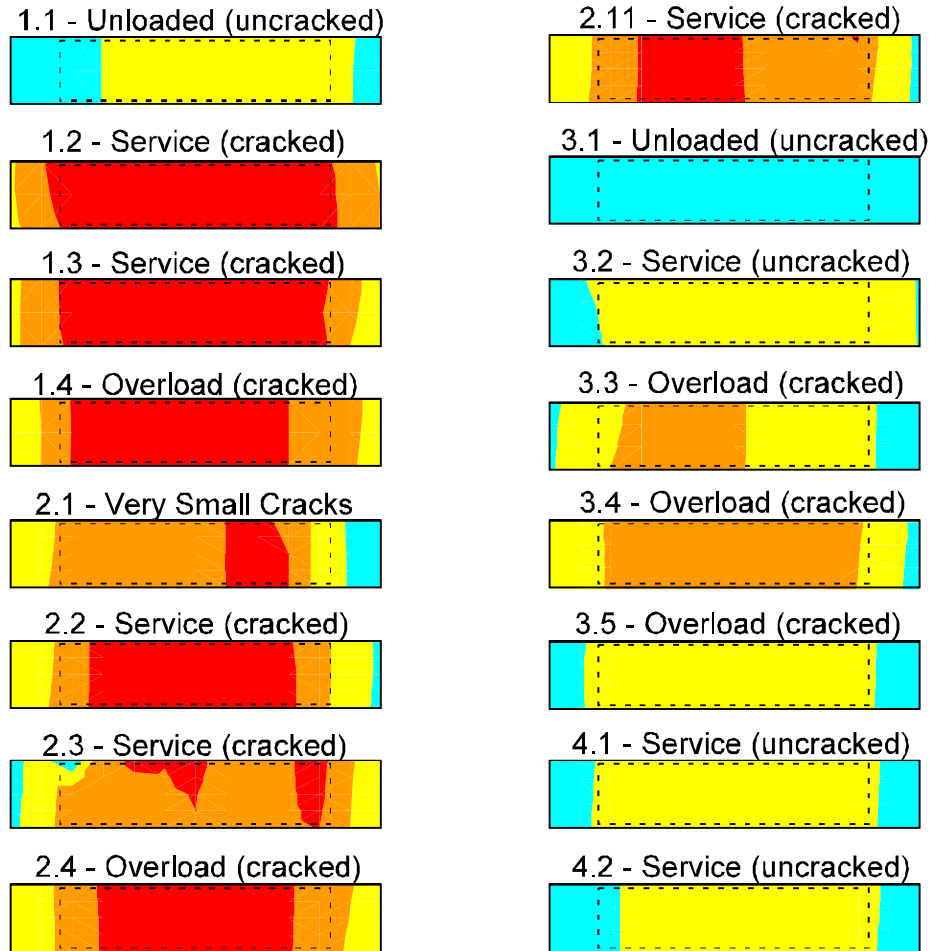


*Figure D15: Half-Cell Potential Readings  
(All Phase II Beams – Varying Duct Type)*

## D.2 HALF-CELL POTENTIAL READING CONTOUR MAPS



*D16: Contour Plots of Half-Cell Potential Readings at 498 Days<sup>2</sup>*

### D.3 HALF-CELL POTENTIAL READING OUTLIERS

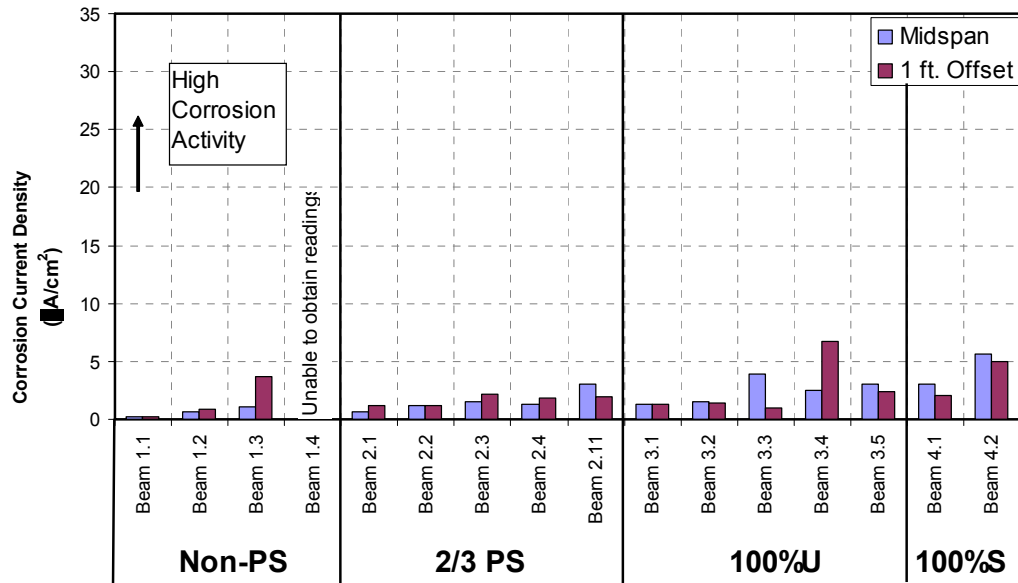
*Table D1: Half-Cell Outliers – Phase I Beams*

<b>Beam</b>	<b>Day of Reading</b>	<b>Initial Reading</b>	<b>Altered Reading</b>
1.1	736	-269	-415
	1297	-199	-447
	1326	-171	-480
1.2	1297	-255	-550
	1326	-261	-560
	1445	-312	-550
2.2	212	-304	-537
3.1	778	-403	-172
3.2	1297	-205	-351
	1326	-173	-402
4.1	1546	-791	-541

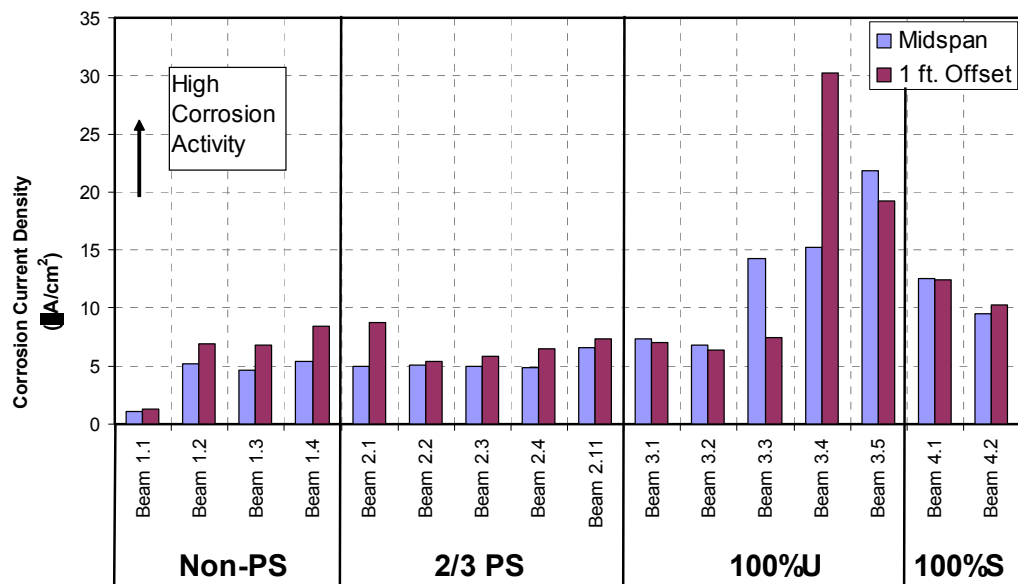
*Table D2: Half-Cell Outliers – Phase II Beams*

<b>Beam</b>	<b>Day of Reading</b>	<b>Initial Reading</b>	<b>Altered Reading</b>
2.8	938	-402	-828
	966	-389	-858
3.6	454	-262	-370
	1086	-515	-358
3.7	344	-470	-376

## D.4 CORROSION RATE READINGS

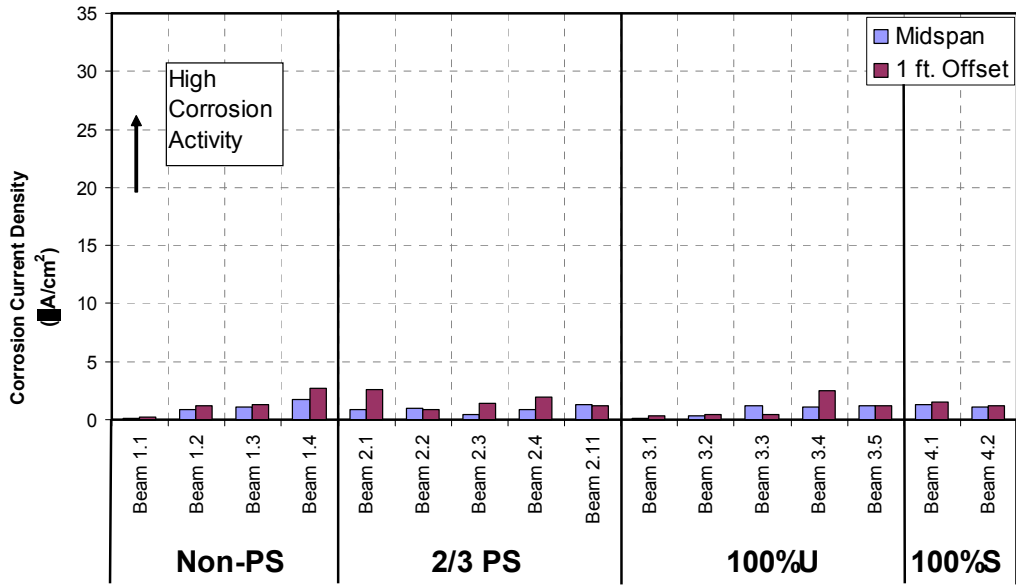


***D17: Phase I Beams - Measured Corrosion Rates  
(Seven Month Exposure Duration - PR Monitor Equipment)***

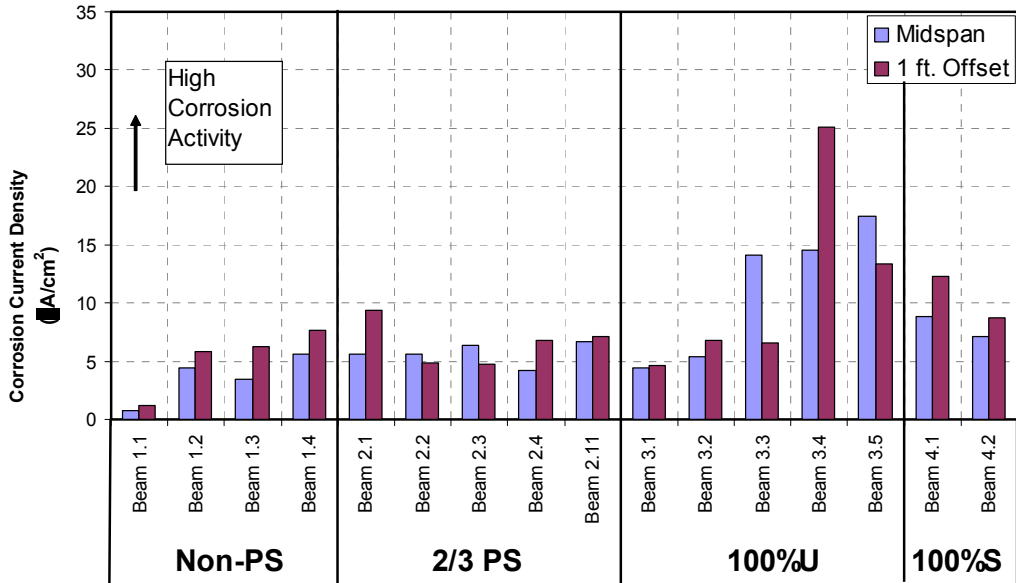


***D18: Phase I Beams - Measured Corrosion Rates  
(Twelve Month Exposure Duration - 3LP Equipment)***

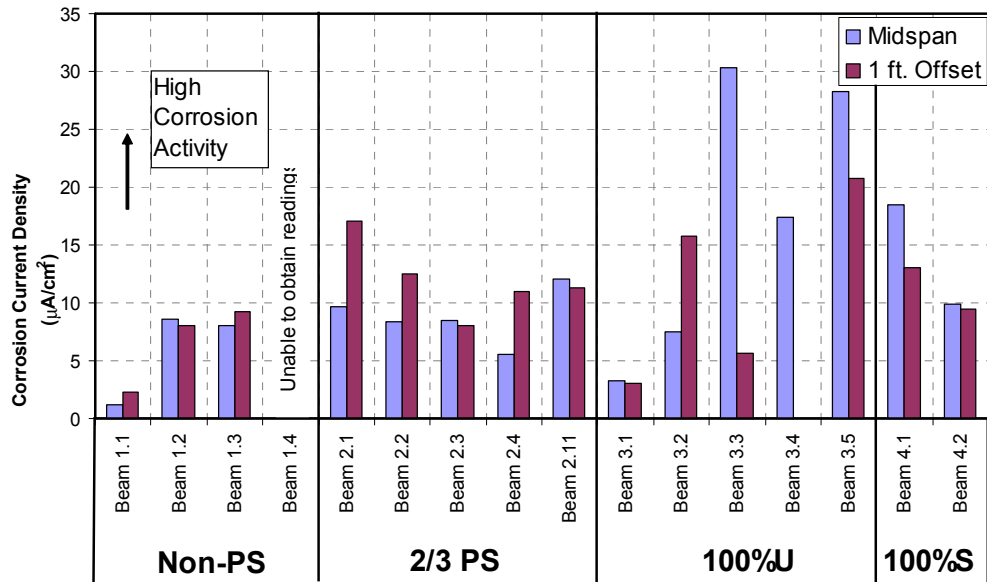




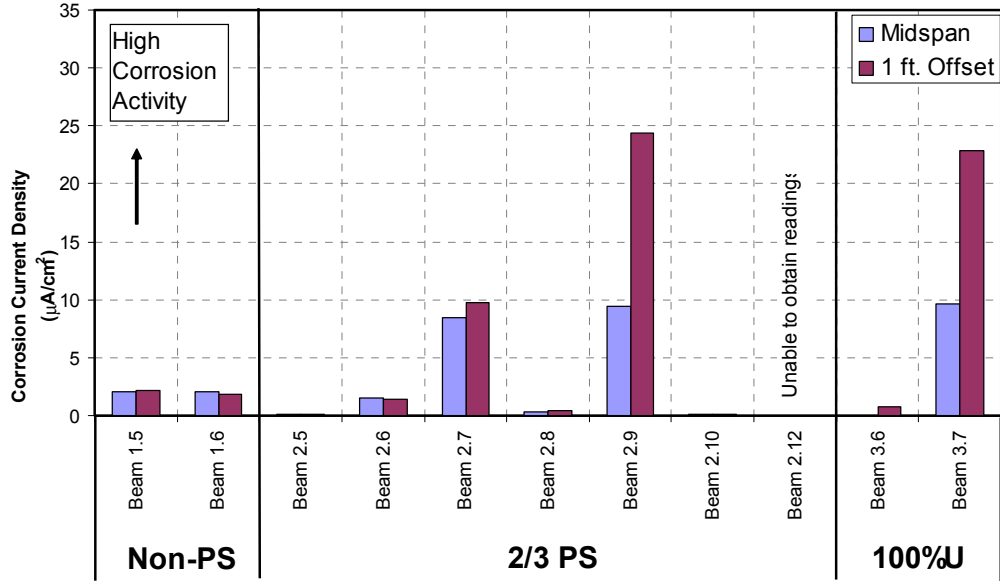
***D19: Phase I Beams - Measured Corrosion Rates  
(Fifteen Month Exposure Duration - PR Monitor Equipment)***



***D20: Phase I Beams - Measured Corrosion Rates  
(Fifteen Month Exposure Duration - 3LP Equipment)***



***D21: Phase I Beams - Measured Corrosion Rates  
(47 Month Exposure Duration – 3LP Equipment)***



***D22: Phase II Beams - Measured Corrosion Rates  
(35 Month Exposure Duration – 3LP Equipment)***

## D.5 BLOCK CHLORIDE PENETRATION

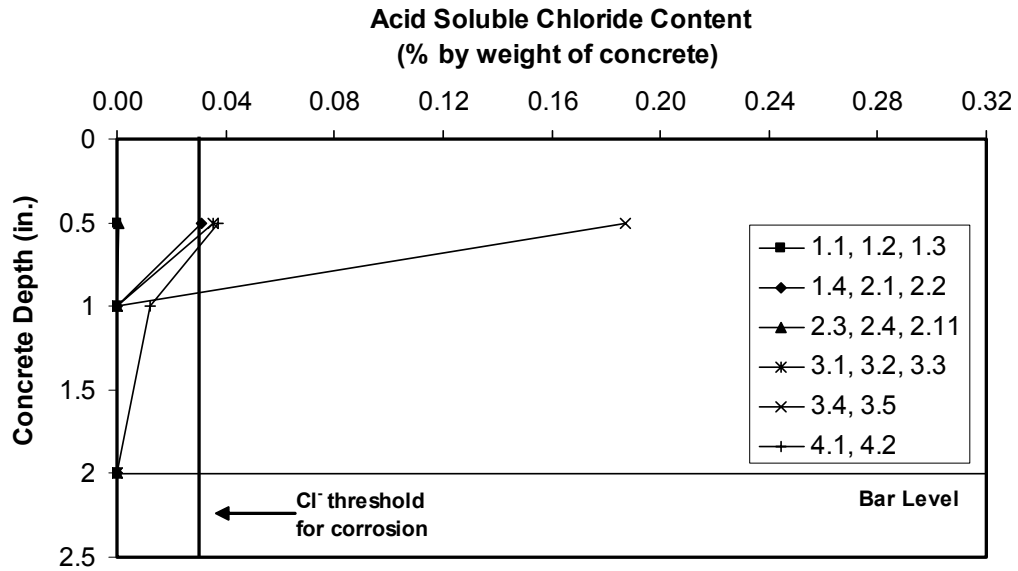


*Figure D23: Block Chloride Penetration at 7 Months  
(Phase I Ponded Block Specimens)*

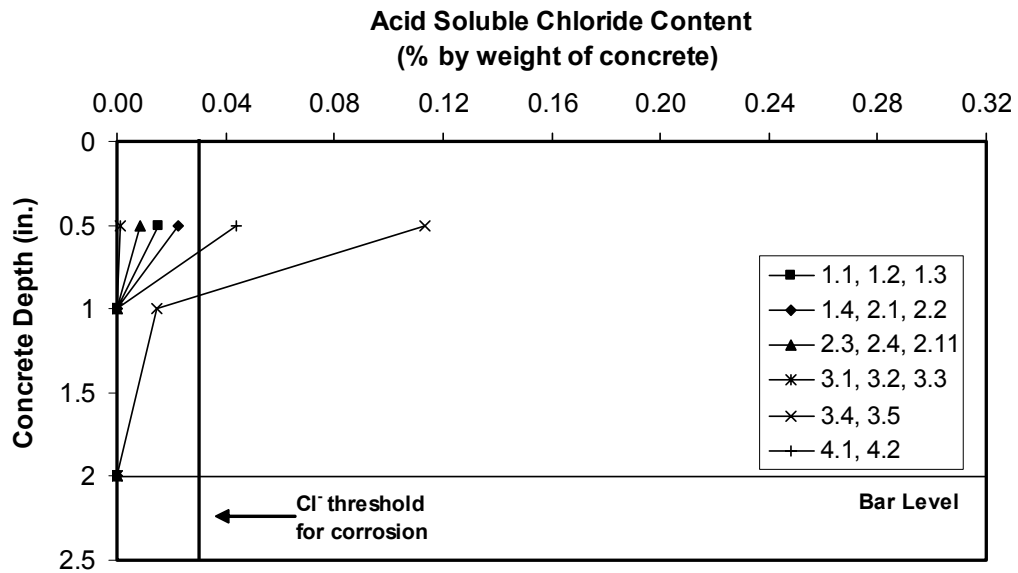


*Figure D24: Block Chloride Penetration at 14 Months  
(Phase I Ponded Block Specimens)*

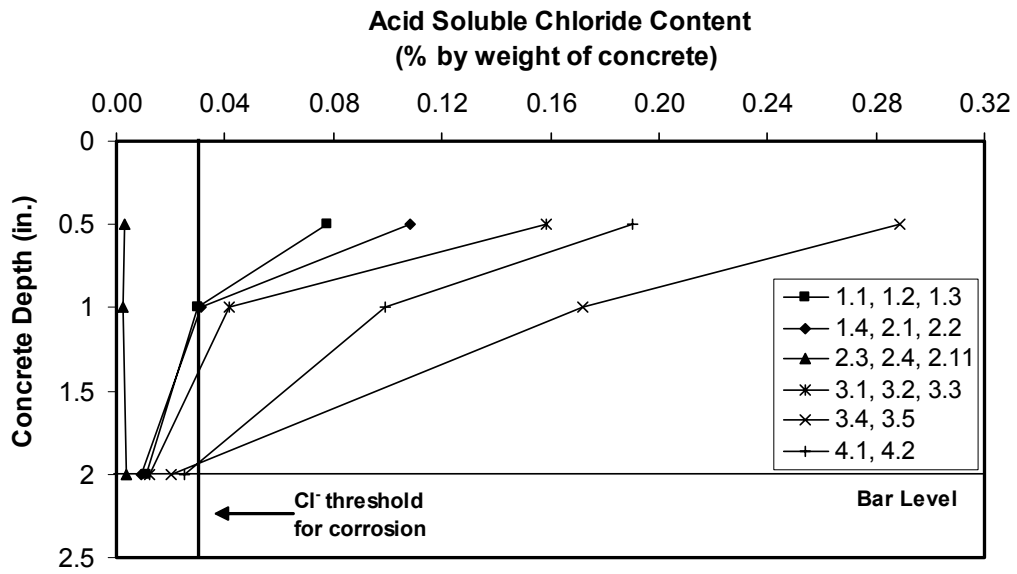


**Figure D25: Block Chloride Penetration at 41 Months  
(Phase I Ponded Block Specimens)**

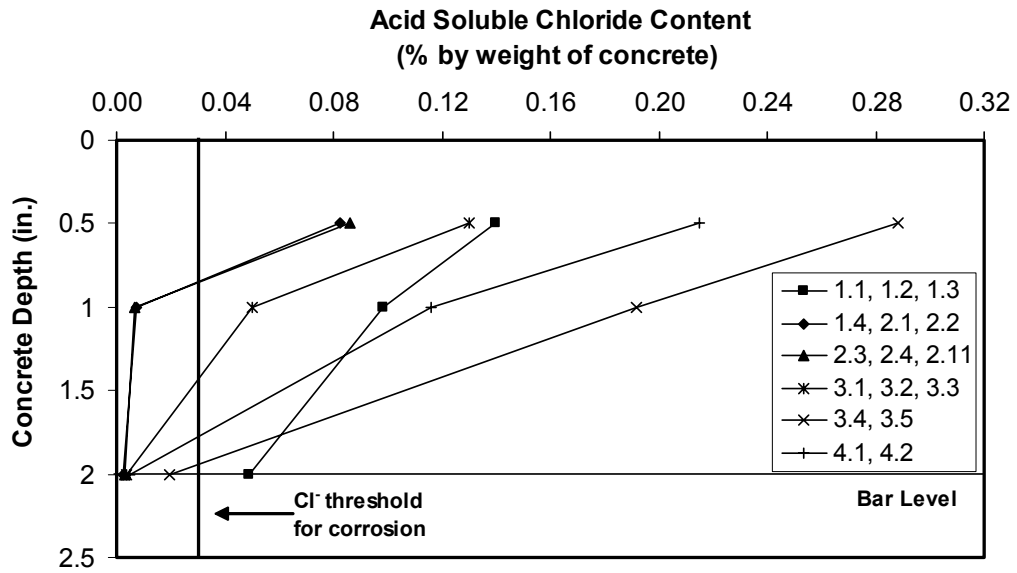


**Figure D26: Block Chloride Penetration at 54 Months  
(Phase I Ponded Block Specimens)**

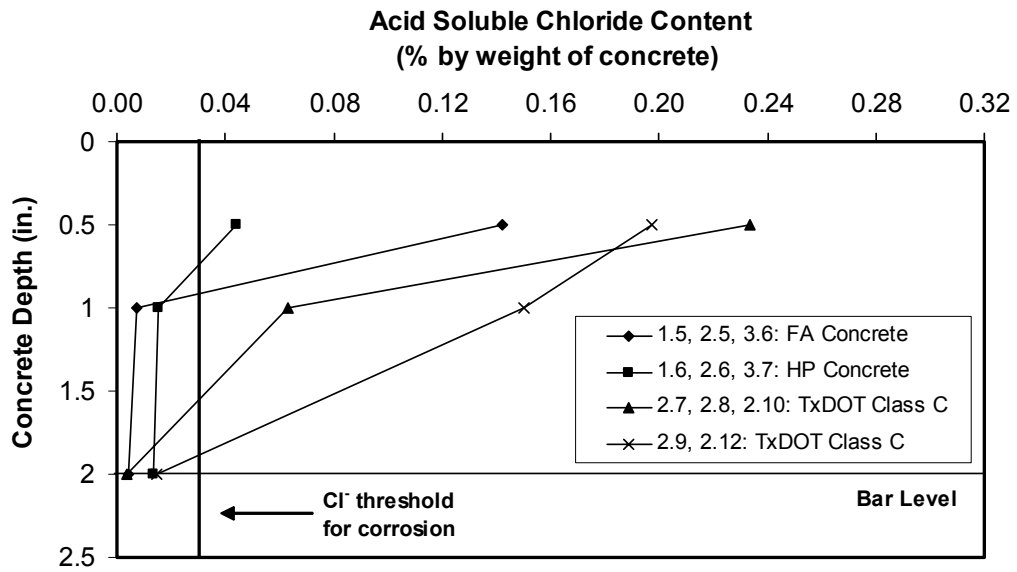


**Figure D27: Block Chloride Penetration at 29 Months  
(Phase II Ponded Block Specimens)**

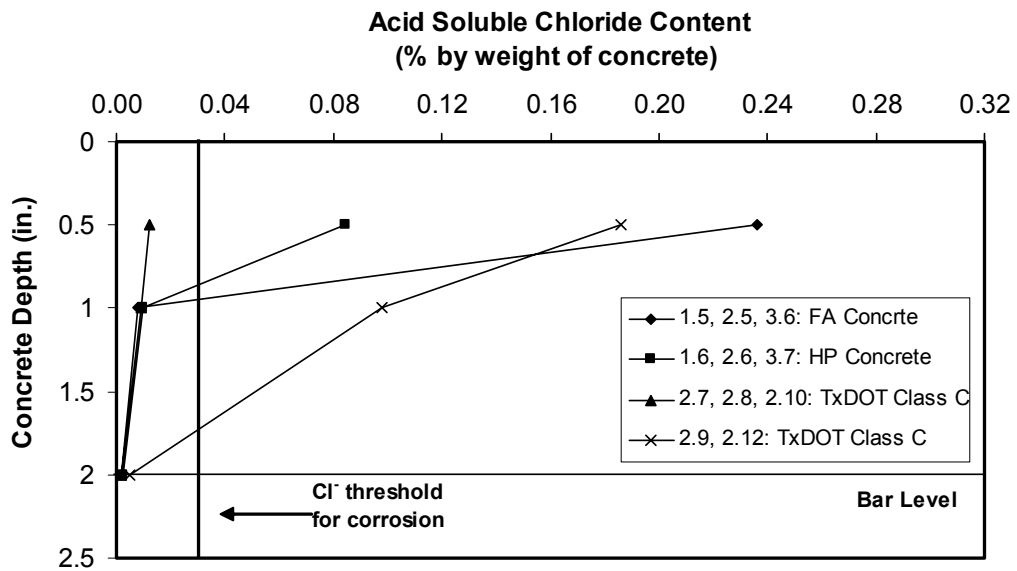


**Figure D28: Block Chloride Penetration at 42 Months  
(Phase II Ponded Block Specimens)**

## D.6 BEAM CHLORIDE PENETRATION

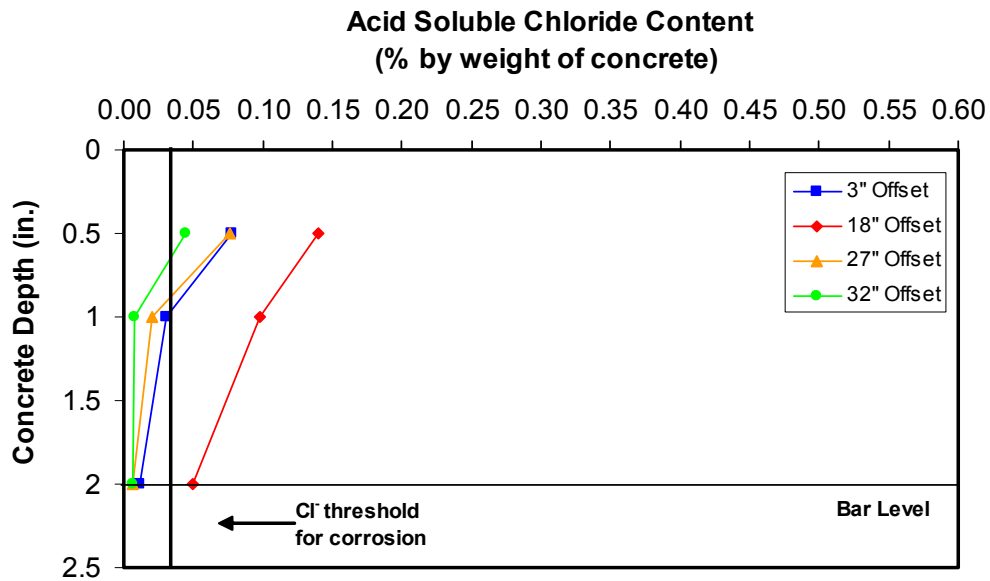


*Figure D29: Chloride Penetration at 54 Months – Beam 1.1*

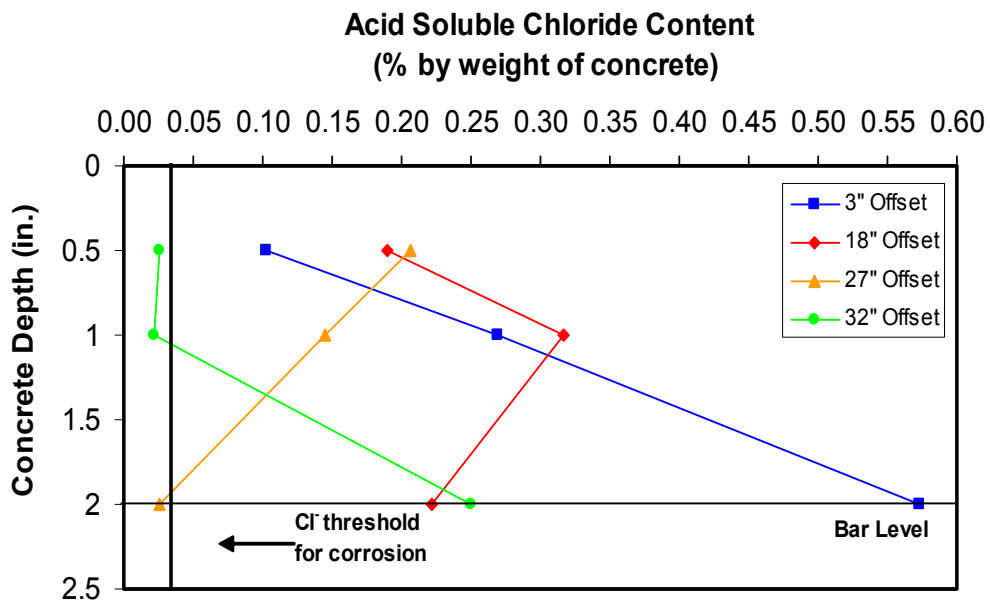


*Figure D30: Chloride Penetration at 54 Months – Beam 1.3*

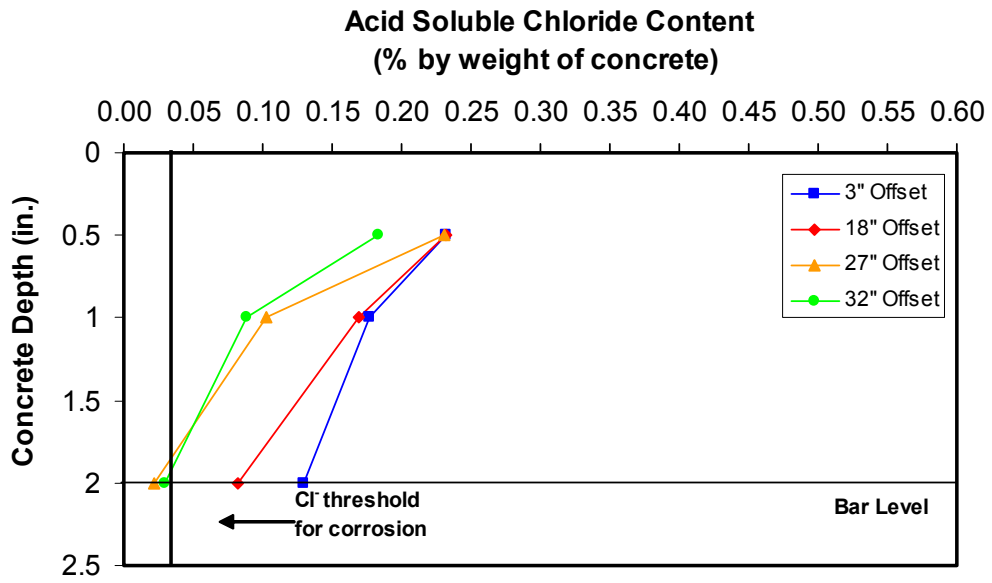


*Figure D31: Chloride Penetration at 54 Months – Beam 2.3*

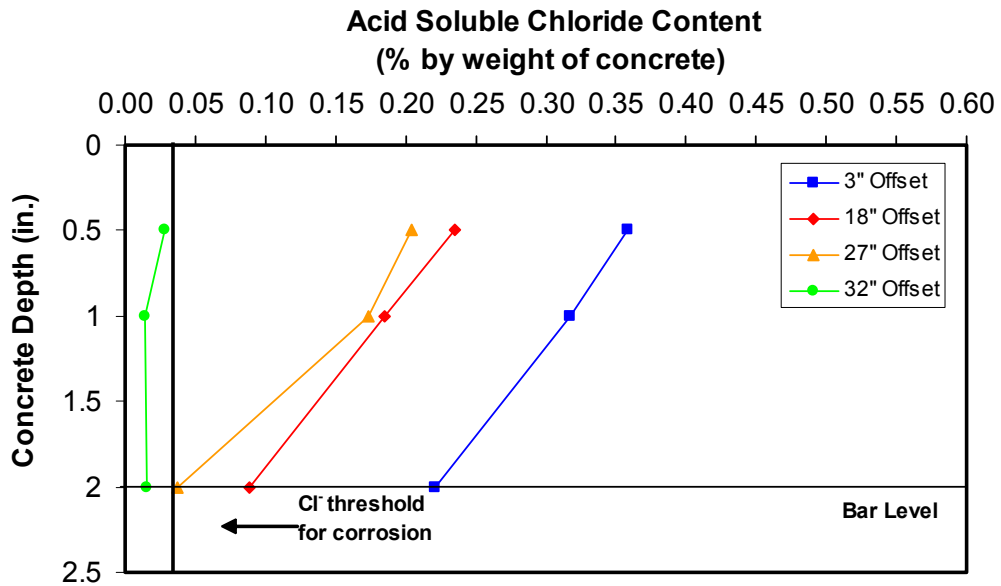


*Figure D32: Chloride Penetration at 54 Months – Beam 2.11*

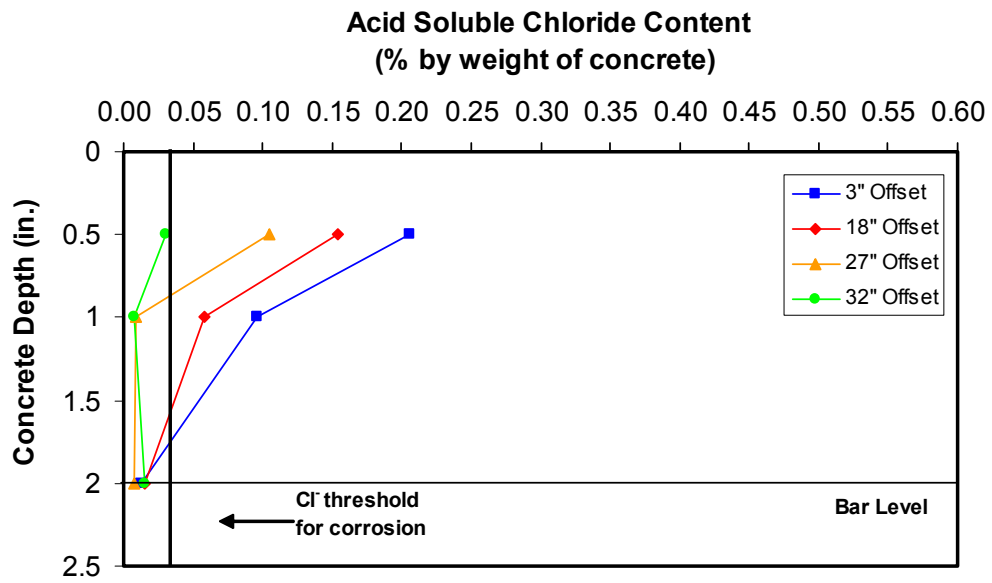


*Figure D33: Chloride Penetration at 54 Months – Beam 3.1*

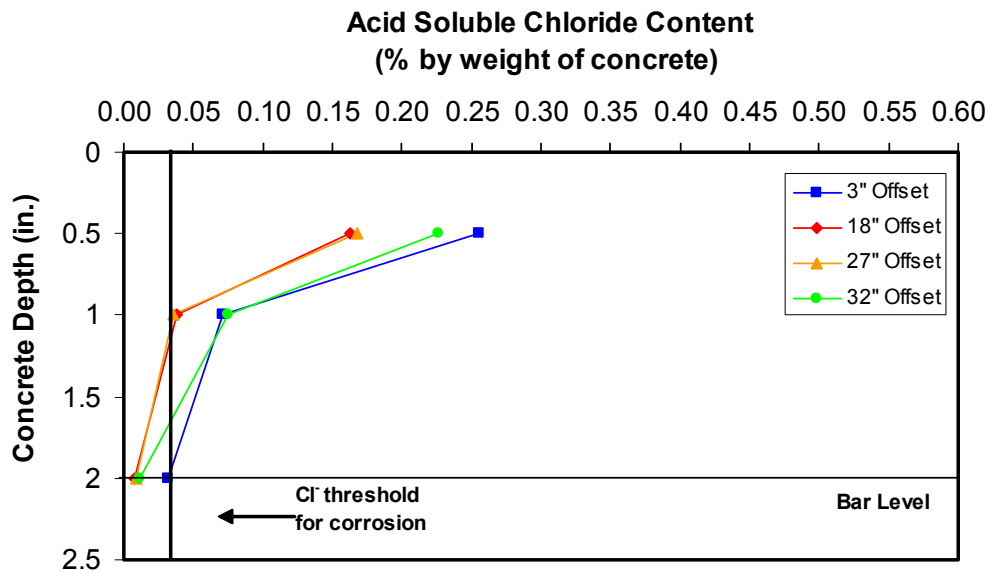


*Figure D34: Chloride Penetration at 54 Months – Beam 3.2*



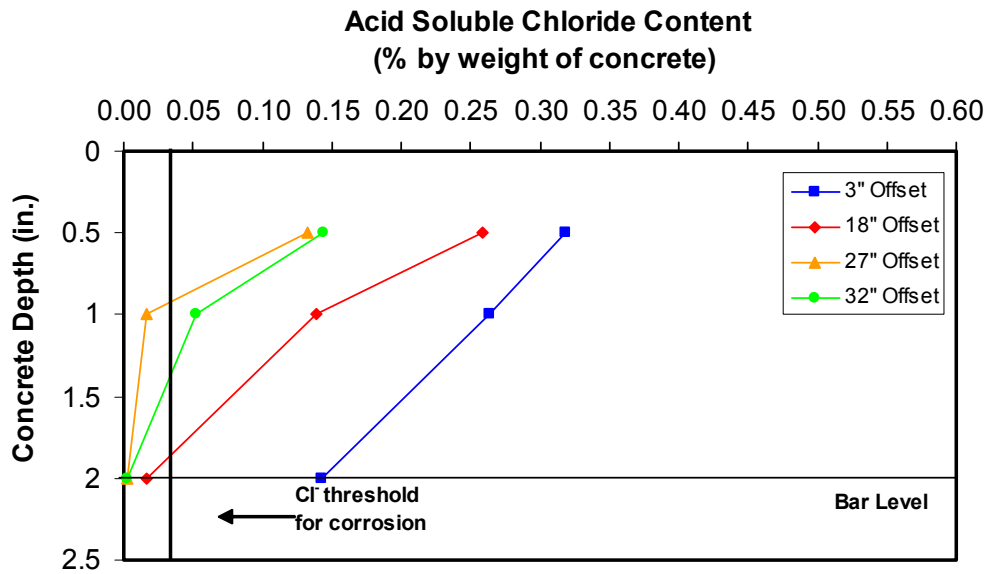


*Figure D35: Chloride Penetration at 54 Months – Beam 3.3*

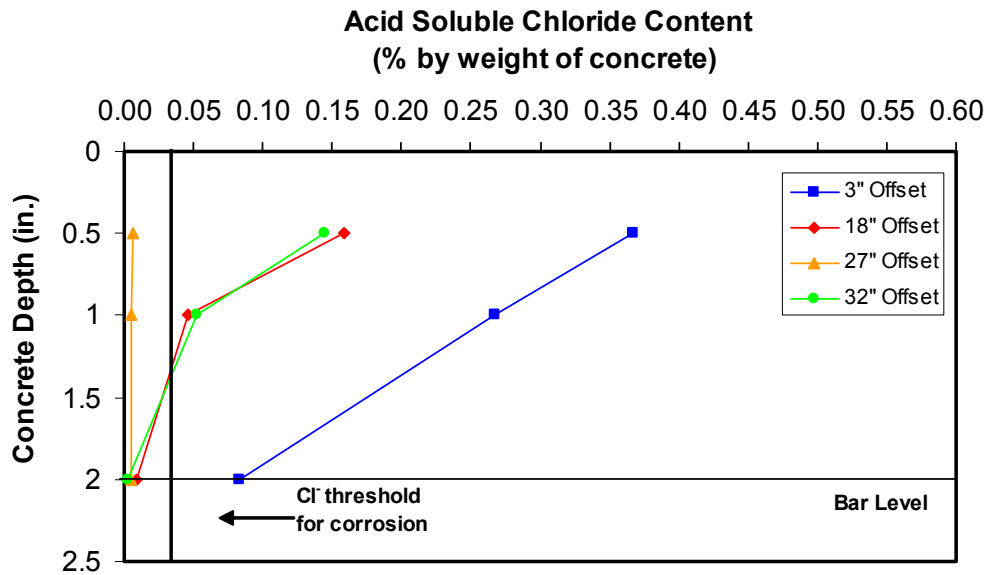


*Figure D36: Chloride Penetration at 54 Months – Beam 4.2*

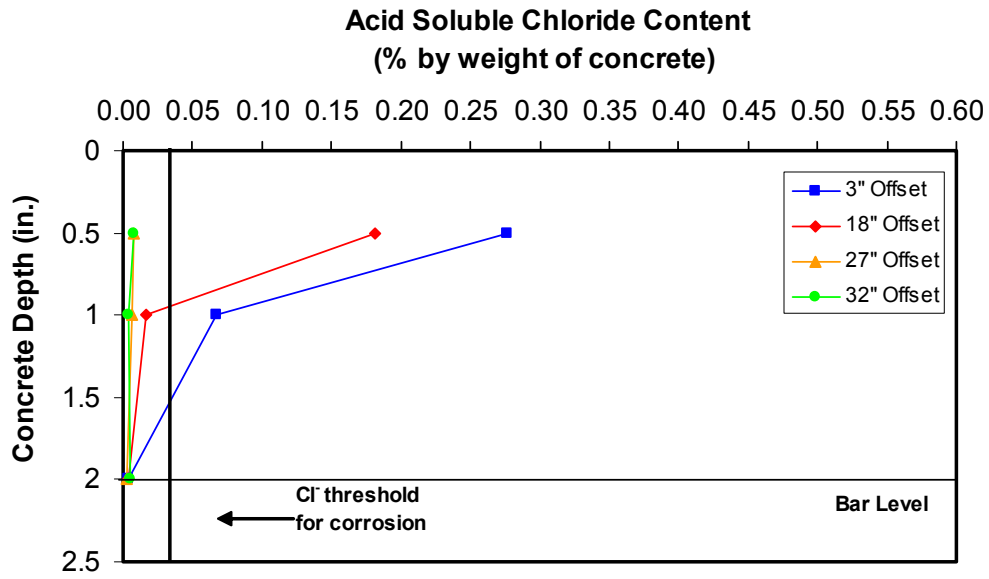


*Figure D37: Chloride Penetration at 42 Months – Beam 1.5*

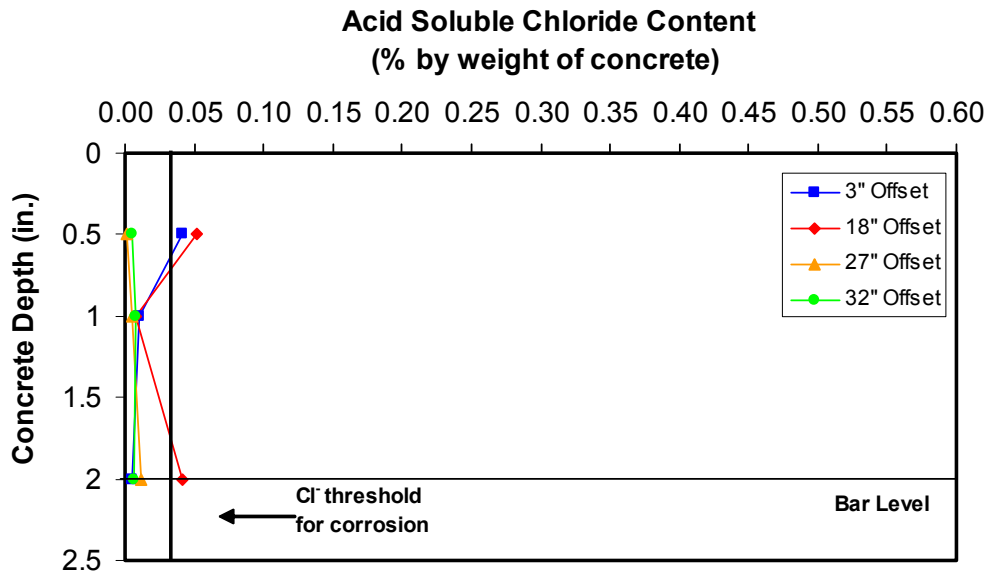


*Figure D38: Chloride Penetration at 42 Months – Beam 1.6*

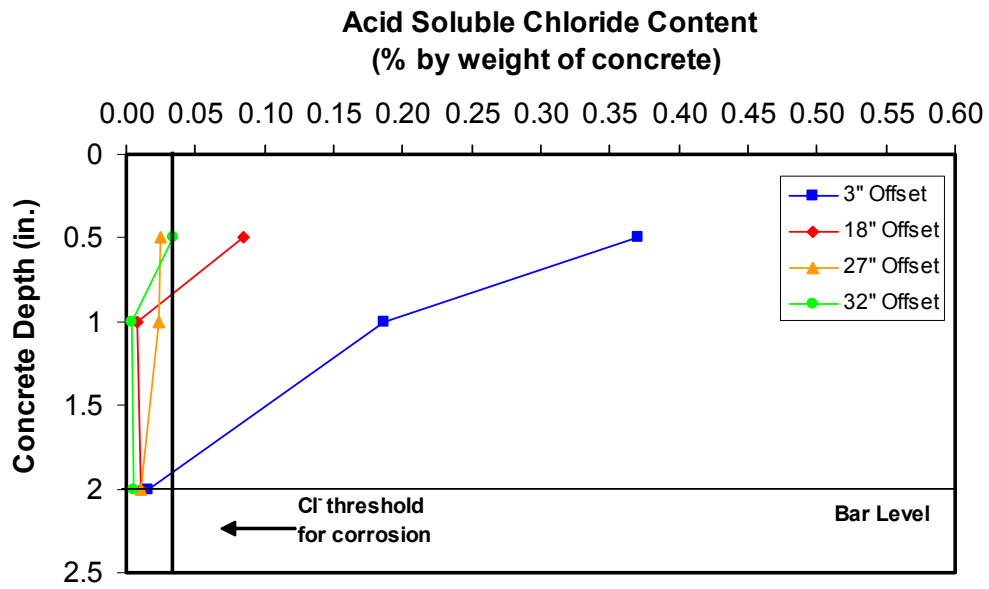


*Figure D39: Chloride Penetration at 42 Months – Beam 2.5*

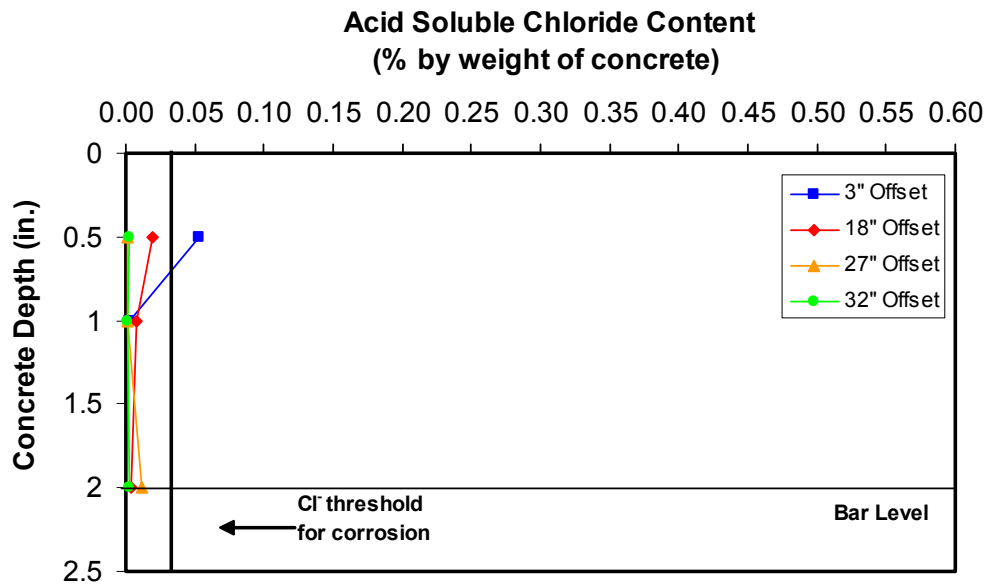


*Figure D40: Chloride Penetration at 42 Months – Beam 2.6*

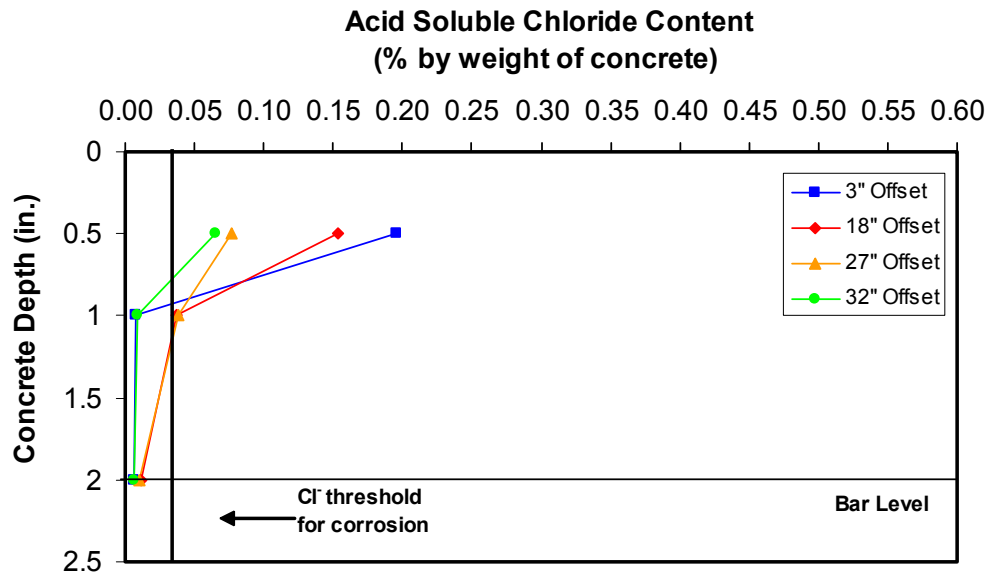


*Figure D41: Chloride Penetration at 42 Months – Beam 3.6*

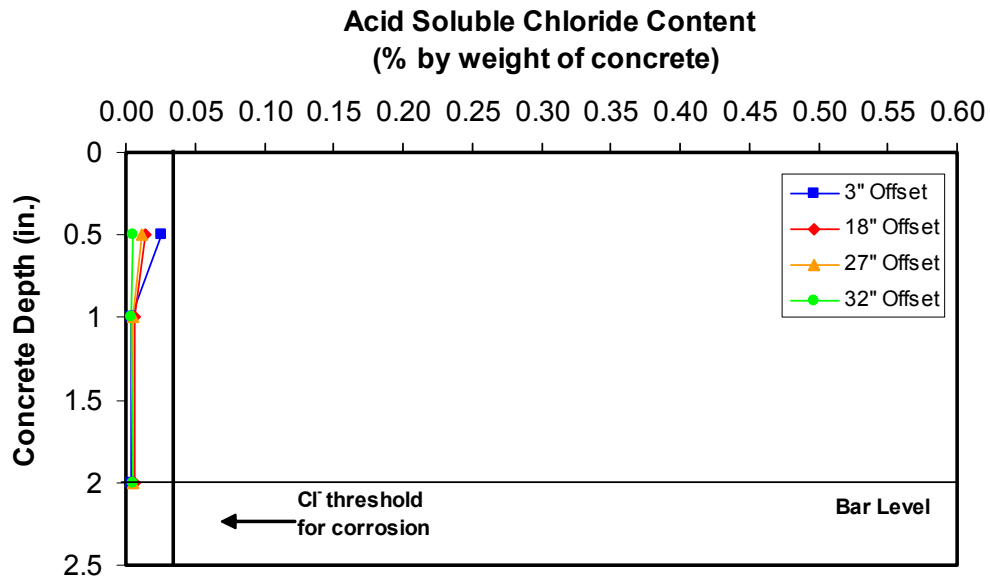


*Figure D42: Chloride Penetration at 42 Months – Beam 3.7*

## **APPENDIX E**

### **Beam Specimen Ratings**

Tables E1 and E2 contain the total, generalized and localized corrosion rating for each element of the autopsy beam specimens from Phase I and Phase II, respectively.

**Table E1: Phase I Beam Ratings**

BEAM	TOTAL RATING						RATING PER FOOT						MAXIMUM RATING					
	Stirrup	Rebar	Duct	Strand	Splice 1	Splice 2	Stirrup	Rebar	Duct	Strand	Splice 1	Splice 2	Stirrup	Rebar	Duct	Strand	Splice 1	Splice 2
1.1	1013	31					96	1					295	8				
1.3	12308	4357					1172	91					770	261				
2.3 (D1)	13592	22422	25794	1156	10103	2951	1294	467	4299	96	10103	2951	2236	6241	2107	20	2745	1615
2.3 (D2)	13592	22422	30412	1466			1294	467	5069	122			2236	6241	6248	56		
2.11 (D1)	19226	22835	9021	1158	1367		1831	476	1504	97	1367		2978	7757	2440	20	407	
2.11 (D2)	19226	22835	8479	1102			1831	476	1413	92			2978	7757	1673	26		
3.1 (D1)	151	0	0	2134	2		14	0	0	119	2		4	0	0	20	2	
3.1 (D2)	151	0	0	1736			14	0	0	96			4	0	0	22		
3.2 (D1)	953	6	4	3024			91	1	1	168			462	4	2	28		
3.2 (D2)	953	6	2	3024	2		91	1	0	168	2		462	4	2	28	2	
3.3 (D1)	4230	432	2571	2892	1894		403	36	429	161	1894		867	294	924	64	795	
3.3 (D2)	4230	432	1322	2128			403	36	220	118			867	294	685	32		
4.2 (D1)	1893	181	42	2314			180	15	7	96			236	169	8	22		
4.2 (D2)	1893	181	26	2304	0	2	180	15	4	96	0	2	236	169	4	16	0	2

263

**Table E2: Phase II Beam Ratings**

BEAM	TOTAL RATING						RATING PER FOOT						MAXIMUM RATING					
	Stirrup	Rebar	Duct	Strand	Splice 1	Splice 2	Stirrup	Rebar	Duct	Strand	Splice 1	Splice 2	Stirrup	Rebar	Duct	Strand	Splice 1	Splice 2
1.5	2244	264					214	6					296	8				
1.6	923	339					88	7					361	15				
2.5 (D1)	3555	190	125	2020			339	4	21	168			866	20	8	32		
2.5 (D2)	3555	190	1854	2016	63		339	4	309	168	63		866	20	1776	28	32	
2.6 (D1)	408	330	14	1140			39	7	2	95			88	190	4	16		
2.6 (D2)	408	330	59	1152	55		39	7	10	96	55		88	190	34	16	34	
3.6 (D1)	775	46	144	1644	20		74	4	24	91	20		245	4	44	16	4	
3.6 (D2)	775	46	38	1728			74	4	6	96			245	4	8	16		
3.7 (D1)	274	2	1284	3024	13		26	0	214	168	13		16	2	1164	28	4	
3.7 (D2)	274	2	71	3024			26	0	12	168			16	2	20	28		

## REFERENCES

1. **West, J.S.**, “Durability Design of Post-Tensioned Bridge Substructures,” Doctor of Philosophy Dissertation, The University of Texas at Austin, May 1999.
2. **Schokker, A.J.**, “Improving Corrosion Resistance of Post-Tensioned Substructures Emphasizing High Performance Grouts.” Doctor of Philosophy Dissertation, The University of Texas at Austin, May 1999.
3. **Billington, S.L.**, “Behavior of Two-Span Continuous Pier Caps With Varying Levels of Prestress,” Masters of Science Thesis, The University of Texas at Austin, December 1994.
4. **Thurlimann, Bruno**, “Considerations to the Design of Prestressed Concrete Bridges,” *IABSE Proceedings*, No. 70, 1983, pp.237-?
5. **Vignos, R.P.**, “Test Method for Evaluating the Corrosion Protection of Internal Tendons Across Segmental Bridge Joints.” Master of Science Thesis, The University of Texas at Austin, May 1994.
6. Standard Specifications for Construction of Highways, Streets and Bridges, Texas Department of Transportation, March 1995.
7. Standard Specifications for Construction of Highways, Streets and Bridges, Special Provision to Item 426 (Prestressing), Sub-Section: Construction Methods, Texas Department of Transportation, 1995. (also, personal communication with Dean Van Landuyt, Texas Department of Transportation, April 1997.)
8. **PTI Committee on Grouting Specifications**, “Guide Specification for Grouting of Post-Tensioned Structures,” 5<sup>th</sup> Draft, Post-Tensioning Institute, Phoenix, AZ, November 1997, 37 pp.
9. **ASTM**, “Standard Test Method for Determining the Effects of Chemical Admixtures on the Corrosion of Embedded Steel Reinforcement in Concrete Exposed to Chloride Environments,” ASTM G109-92, American Society for Testing and Materials, Philadelphia, PA, 1992.

10. **AASHTO**, Standard Method of Test for Resistance of Concrete to Chloride Ion Penetration," AASHTO Designation T 259-80, American Association of State Highway and Transportation Officials, Washington, D.C., 1980.
11. **Jones, D.A.**, *Principles and Prevention of Corrosion*, Mac Millan Publishing Company, New York, 1992.
12. **ASTM**, "Standard Test Method for Half-Cell Potentials of Uncoated Reinforcing Steel in Concrete," ASTM C876-91, American Society for Testing and Materials, Philadelphia, Pa., 1991.
13. **Fontana, M.G.**, Corrosion Engineering, 3<sup>rd</sup> Edition, McGraw-Hill, Inc., New York, New York, 1986.
14. **Jones, D.A.**, Principles and Prevention of Corrosion, 2<sup>nd</sup> Edition, Prentice Hall, Inc., Upper Saddle River, NJ, 1996.
15. **Flis, J., Sehgal, A., Li, D., Kho, Y., Sabol, S., Pickering, H., Osseo-Asare, K, and Cady, P.D.**, "Condition Evaluation of Concrete Bridges Relative to Reinforcement Corrosion, Volume 2: Method for Measuring the Corrosion Rate of Reinforcing Steel," SHRP-S/FR-92-104, Strategic Highway Research Program, Washington, D.C., 1992, 105 pp.
16. **Clear, K.**, "Measuring the Rate of Corrosion of Steel in Field Concrete Structures," Transportation Research Record 1211, pp. 28-37, 1989.
17. **Andrade, C., Castelo, V., Alonso, C. and Gonzalez, J.A.**, "The Determination of Corrosion Rate of Steel Embedded in Concrete by the Polarization Resistance and AC Impedance Methods," Corrosion Effect of Stray Currents and the Techniques for Evaluating Corrosion of Rebars in Concrete, ASTM STP 906, V. Chaker, Editor, American Society for Testing and Materials, Philadelphia, PA, 1986, pp. 43-63.
18. **CONCORR, Inc.**, "FHWA-SHRP Showcase: Assessment of Physical Condition of Concrete Bridge Components," Federal Highway Administration, Washington, D.C., July 1996.
19. **Cady, P., and Gannon, E.**, "Condition Evaluation of Concrete Bridges Relative to Reinforcement Corrosion, Volume 8: Procedure Manual," SHRP-S/FR-92-330, Strategic Highway Research Program, Washington, D.C., 1992, 124 pp.



20. **AASHTO**, "Standard Method of Test for Sampling and Testing for Chloride Ion in Concrete Ram Materials," AASHTO Designation T 260-94, American Association of State Highway and Transportation Officials, Washington, D.C., 1994.
21. **ACI Committee 222**, "Corrosion of Metals in Concrete," ACI 222R-96, American Concrete Institute, Detroit, Michigan, 1996.
22. **Salas, R.M., Kotys, A.L, West, J.S., Breen, J.E. and Kreger, M.E.**, "Final Evaluation of Corrosion Protection for Bonded Internal Tendons in Precast Segmental Construction," Texas Department of Transportation Research Report 1405-6, Not Published Yet.

## VITA

Andrea Lynn Kotys was born on January 30, 1979 in St. Louis, Missouri to Gregory and Susan Kotys. After completing her studies at Triad High School in 1997, Andrea attended Vanderbilt University in Nashville, Tennessee where she studied civil engineering. She received her Bachelor of Engineering Degree in Civil Engineering from Vanderbilt University in May of 2001. In the fall of 2001, she entered the graduate program in the Department of Civil Engineering at the University of Texas at Austin to pursue her Master of Science in Civil (Structural) Engineering.

Permanent Address: 525 Coventry Rd.  
Troy, IL 62294

This thesis was typed by the author.